

# Final Report

Cryogenic H<sub>2</sub> and O<sub>2</sub> propellant refuelling & transfer infrastructure in space

AE3200: Design Synthesis Exercise  
Group 08

# Final Report

## Cryogenic H<sub>2</sub> and O<sub>2</sub> propellant refuelling & transfer infrastructure in space

by

### Group 08

Student Name	Student Number
Matas Venčkauskas	4838815
Neil Richez	4816617
Augustas Barysas	5048621
Adrian Ehrenberger	5025648
Jonah Pedra	5003768
Teun Blom	4793021
Marcel Kwapień	5063744
Jarek Gierulski	4785967
Mattias ten Voorde	5104068
Luc du Chatinier	5082218

Tutor: Dr. B.V.S. Jyoti  
Assistant Tutors: A.O. Başkaya, Dr. A. Heidebrecht  
Teaching Assistant: K.I. Janisch  
Institution: Delft University of Technology  
Place: Faculty of Aerospace Engineering, Delft  
Project Duration: April, 2022 - June, 2022

Cover Image: Blender Model of UCM, own work

# Contents

<b>Nomenclature</b> .....	<b>ii</b>
<b>1 Executive Overview</b> .....	<b>1</b>
<b>2 Introduction</b> .....	<b>5</b>
<b>3 Market Analysis</b> .....	<b>6</b>
3.1 Motivation .....	6
3.2 Market Identification .....	7
3.3 Cislunar Markets .....	7
3.4 Interplanetary Markets .....	10
3.5 Customer Summary .....	11
<b>4 System Description &amp; Optimisation Method</b> .....	<b>12</b>
4.1 Concept .....	12
4.2 Sizing Process .....	14
4.3 Sustainable Optimisation Method ....	17
<b>5 Cryogenic Storage System</b> .....	<b>18</b>
5.1 Trade-off Summary & Requirements .	18
5.2 Composite Structural Layer .....	19
5.3 Insulation Layer .....	22
5.4 Heat Flow Calculation Method .....	23
5.5 Cryocoolers .....	24
5.6 Propellant Transfer Mechanism .....	25
5.7 Complete Sizing Method .....	27
<b>6 Electrical Power System</b> .....	<b>29</b>
6.1 Requirements & Trade-off Summary .	29
6.2 Power Consumption Profiles .....	29
6.3 EPS System Profiles .....	30
6.4 Solar Panel Selection, Configuration, & Sizing .....	30
6.5 Fuel Cell Sizing .....	31
6.6 System Overview .....	32
6.7 EPS Budget Analysis .....	32
<b>7 Propulsion System</b> .....	<b>37</b>
7.1 Requirements & Trade-off Summary .	37
7.2 Engine Selection & Tank Design .....	38
7.3 $\Delta V$ Budget & Thrust Level .....	38
7.4 Operations Profile .....	40
7.5 Engine Ignition .....	41
7.6 Plumbing .....	44
<b>8 Attitude Determination &amp; Control System</b>	<b>46</b>
8.1 Requirements & Trade-off Summary .	46
8.2 Attitude Determination .....	46
8.3 Reaction Control System .....	48
<b>9 Telemetry, Tracking, &amp; Command</b> .....	<b>55</b>
9.1 Requirements .....	55
9.2 Concept .....	55
9.3 Antenna Selection .....	58
<b>10 Command &amp; Data Handling</b> .....	<b>59</b>
10.1 Functionality & Software .....	59
10.2 Configuration and Data Handling ....	61
10.3 Power consumption estimation .....	61
<b>11 Thermal Management System</b> .....	<b>64</b>
11.1 Requirements .....	64
11.2 Mission Profiles .....	64
11.3 Thermal Control System .....	65
<b>12 Structural Design &amp; Layout</b> .....	<b>73</b>
12.1 Landing Gear Design .....	73
12.2 Landing Gear in UCM sizing .....	82
12.3 Architecture .....	83
<b>13 Sustainable Optimisation Results</b> .....	<b>88</b>
13.1 Result .....	88
13.2 Sensitivity Analysis .....	90
<b>14 Universal Cryogenic Module Lifespan ..</b>	<b>92</b>
14.1 Manufacturing, Integration & Testing .	92
14.2 Operations & End-of-life .....	97
14.3 Risk Management .....	101
<b>15 Maintenance &amp; Supportability</b> .....	<b>105</b>
15.1 Maintenance Philosophy .....	105
15.2 Digital Twin Technology .....	105
15.3 Health Monitoring .....	105
15.4 Replacement .....	106
15.5 Threat of Lunar Dust .....	107
15.6 Possible Manned Intervention .....	108
15.7 Discarded Cleaning & Maintenance Rover .....	108
<b>16 Business Case</b> .....	<b>109</b>
16.1 Analysis Approach .....	109
16.2 Cost Breakdown .....	109
16.3 Propellant Pricing .....	114
16.4 Economic Analysis .....	115
16.5 Financial Analysis Results .....	120
16.6 Sensitivity Analysis .....	121
<b>17 Design Evaluation</b> .....	<b>123</b>
17.1 Requirement Compliance .....	123
17.2 Recommendations .....	124
<b>18 Conclusion</b> .....	<b>126</b>
<b>Task Division</b> .....	<b>128</b>
<b>References</b> .....	<b>135</b>

# Nomenclature

## Abbreviations

Abbreviation	Definition
DSE	Design Synthesis Exercise
LEO	Low Earth Orbit
LLO	Low Lunar Orbit
TLI	Trans-Lunar Injection
UCM	Universal Cryogenic Module
CSS	Cryogenic Storage Subsystem
OPS	Operational Module
ECSS	European Cooperation for Space Standardization
TBD	To Be Determined
DTT	Digital Twin Technology
OC-SVM	One-Class Support Vector Machine
PROP	Propulsion Subsystem
STR	Structural
EPS	Electrical Power Subsystem
TMS	Thermal Management Subsystem
TT&C	Tracking, Telemetry and Communication
ADCS	Attitude Determination & Control Subsystem
C&DH	Command and Data Handling
PAY	Payload
INT	Interfacing Mechanism
LNT	Launch and Transportation
PAS	Production and assembly
BUD	Budget
SUS	Sustainability
SAR	Safety and Reliability
ISO	In-situ Operations
BOL	Beginning of life
EOL	End of Life
RCS	Reaction control system
MLI	Multi-layer insulation
S/C	Spacecraft
TRL	Technology Readiness Level
FDIR	Fault, Detection, Recovery and Isolation
COTS	Commercial Of The Shelf
$LO_2$ , LOX	Liquid Oxygen
$LH_2$	Liquid Hydrogen
$GH_2$	Gaseous Hydrogen
$GO_2$	Gaseous Oxygen
$LCH_4$	Liquid Methane
$H_2O_2$	Hydrogen Peroxide
RP - 1	Rocket Propellant - 1
IMU	Inertial Measurement Unit
VCHP	Variable Conductance Heat Pipes
NGC	Non Condensable Gas
RAFP	Robotic Automated Fiber Placement
MMOI	Mass Moment of Inertia
CG	Center of Gravity
LIDAR	Laser Imaging Detection and Ranging
COPV	Composite Overwrapped Pressure Vessel
PID	Proportional Integral Derivative

# 1 Executive Overview

In recent years the space industry has been striving towards higher sustainability. However, the focus has mainly been on launch vehicles operating from Earth and few attempts have been undertaken to make the space industry more sustainable outside of the atmosphere as well. Nevertheless, NASA sees an opportunity to transform frozen water on the moon into rocket propellant for the use of interplanetary missions through electrolysis [50]. Having the ability to refuel in low Lunar orbit will greatly reduce the fuel required to launch from Earth into orbit. This in turn will reduce launch vehicle emissions within Earth's atmosphere and ensure interplanetary missions will use green propellants (hydrogen and oxygen propellant as well as hydrogen peroxide in this case), greatly contributing to the sustainability of the space industry. Also, the cost of interplanetary missions will be reduced in doing this. Accordingly, the mission need statement of this project will be as follows:

*"Provide a Lunar ecosystem design to facilitate reduced interplanetary mission costs and increased transportation capacity."*

The project objective statement is then defined as follows:

*"Design an in-orbit Lunar refueling station with support from a surface depot for  $LH_2$  and  $LO_2$ , in 10 weeks with a team of 10 students."*

The system will be able to deliver up to 50 tonnes of hydrolox in orbit during an operation cycle as well as constantly storing 50 tonnes of hydrolox on the Lunar surface at all times, with the propellant being purchased from NASA's Artemis mission [50]. In addition, the entire system should be able to process 250 tonnes of propellant per year as required by the contractor.

A market analysis was conducted in order to assess the feasibility and the demand for such a system. With NASA's Artemis mission being announced to launch in this decade [50], cislunar economy needs and in-situ resource utilization methods and missions will increase swiftly. Setting up a Lunar base able to launch rockets to deep space is the long-term goal which will propel humanity into its next phase. One of the first steps is to have a system able to refuel other spacecraft in Lunar orbit, greatly reducing the propellant required to be carried onboard from Earth by the customer, greatly reducing cost of those missions. This is the gap in the market COLD is aiming to fill. A crucial aspect is to find the optimal value of propellant price such that it is still economically reasonable for the partnered entity to pass by the Moon before continuing its operations. For deep space missions, this is not really a problem as the  $\Delta V$  required to go to the Moon is most likely way lower than its mission  $\Delta V$ , but for missions such as GEO satellites it might be a tight range of profitability. Knowing the undeniable potential of a cislunar ecosystem, COLD has great future if it can perform its tasks consistently and for an acceptable price. COLD would be just one unit in the greater ecosystem, but its function is crucial to enable such ecosystems to thrive.

The system description and the optimisation methods were proposed next. The main stakeholder requirements were *REQ-SH-02*, *REQ-SH-03*, *REQ-SH-12*, *REQ-SH-13* *REQ-SH-18*. This translates into the following statements: the project cost can not exceed \$7B. The launch vehicle and the spacecraft shall use  $LH_2/LO_2$  as a propellant. The system shall be able to facilitate 250 tonnes of propellant to customers per year. The system shall be able to store 50 tonnes of propellant on the Lunar surface. Last, the system shall be remotely controllable from Earth. From intensive trade-offs performed in the last phases of the design [5], the system concept was chosen based on these stakeholder requirements. This concept consists of four UCM's that will have to fulfill all stakeholder requirements. This removes the idea of having a surface station, an orbital station, and a refueling spacecraft between these two. In this concept, each spacecraft acts as all of these three segments. Two UCM's will be on the Lunar surface at all times to comply with the requirement of propellant stored on the Lunar surface. From the concept, the sizing process was already decided. The CSS, TT&C and C&DH subsystems were designed statically as they were assumed to be independent from the other subsystems. The only real inputs were the allowed boil-off and the number of MLI layers in the CSS system. From there, an iterative process began for every other subsystem, which attempted to maximize the P2P ratio. This ratio is the ratio of propellant sold over propellant bought, the higher, the more efficient the whole system is, and the more sustainable as well. Then, orbital calculations were performed to be able to have an idea of the eclipse and sunlit period times. This led to 0.774 h of eclipse per orbit and 1.189 h of sunlit period per orbit. The propellant to be delivered to the customer will be stored in the cryogenic storage subsystem. This subsystem has two tanks each equipped with a structural layer, an insulation layer, cryocoolers, and a propellant transfer mechanism. The structural layer is responsible for containing the pressure of the cryogenic liquids,

it is made from a composite sandwich structure with an aluminium honeycomb core. The insulation layer is responsible to control the heat inflow and limit the boil-off, it is made from multi-layer insulation. The cryocoolers are responsible for removing heat from the tanks and were sized using empirical data from literature. The propellant transfer mechanism makes use of a pair of counter-rotating centrifugal pumps for each tank resulting in a short propellant transfer time of approximately four hours. The liquid hydrogen storage tank and liquid oxygen storage tank had a total mass of 1640 kg and 379 kg respectively. The total power consumption of the cryogenic storage system varies from 0 kW to 2.4 kW throughout each mission cycle.

Two electrical power generation concepts were considered for the UCM; placing a solar array on the continuously sunlit Lunar crater and beaming/using a power cable to transport the power down to the lander or use a fuel cell and buy the fuel from NASA's Artemis mission. After an in-depth economic analysis, the latter concept was chosen. The UCM will use hydrogen fuel cells in the permanently shaded crater and solar cells while in sunlight. A highly weight optimised fuel cell and triple junction solar cells will be used. The solar panels will be body mounted to avoid high cycled counts on deployment mechanisms. The highest power consumption of the spacecraft will be equal to 9343 W for the fuel cell, and 3524 W for the solar cell, and as such have been sized accordingly. Purchasing power directly from the Artemis mission should be further considered as a more cost-effective alternative to self-sufficient power generation.

Moreover, the propulsive system was considered. For this system liquid hydrogen & liquid oxygen were selected as propellant. Reasoning being the ease of access on with the provided mission profile, competitive performance in relation to alternatives and it being sustainable. Further, the 5 different stages were defined for the mission cycle which were: Ascent & Circularisation, Docking, Descent, Hover and Touchdown, which resulted in a total  $\Delta V$  budget of 4092 m/s. Next, a configuration with 2 Vinci engines outboard of a RL-10 CECE engine was selected. The Vinci engines produce 180 kN each and the RL-10 CECE 66.7 kN. Based on the operational profile, the engines are to ignite 50 times individually, and for this a spark-plug hydrogen oxygen ignition system was selected with defined ignition sequences. For the plumbing system, the fuel cell, the gaseous tank, the engines were connected from the main propellant tanks. Additionally, an emergency feed from the payload tank was included in case of customer aborting mission, to recuperate as much propellant as possible.

The attitude determination and control system considered the selection of attitude sensors and the design of the reaction control system. The chosen sensors consisted of two pairs of a star and sun sensor, an Inertial Measurement Unit (IMU), an altimeter and a docking sensor based on LIDAR. With these devices, the desired pointing accuracy of  $\pm 0.2^\circ$  could be reached that is needed to dock with the customer spacecraft. The most critical power phase was additionally found to be during docking when 99 W of power is required by the sensors. Additionally, for the reaction control system, 24 thrusters were placed onto the UCM in clusters of 3 with each thruster providing a thrust of 220 N. In such a way, rendezvous and docking with the customer can be performed in 6 min, after which the propellant transfer can start by slewing the UCM to a rate of  $140^\circ/\text{min}$  in just under 6 s. The RCS thrusters use hydrogen peroxide ( $H_2O_2$ ) as a propellant, which can be made by the hydrogen peroxide printer that is provided by partner company SolvGE that runs on the water residue of the fuel cell. In such a way, the waste stream is minimized and resources are used up to their best extent. Finally, the storage and plumbing of the hydrogen peroxide monopropellant was considered, where the decision was made to opt for a self pressurised tank containing a teflon lining to prevent degradation of the  $H_2O_2$ . Of the latter, 1032 kg will be on board to perform all the required maneuvers.

The telemetry tracking and command system is responsible for maintaining contact with the Lunar lander vehicles. In order to assure constant communication, a net of relay satellites provided by external partners such as NASA, ESA and perhaps commercial enterprises. As for the onboard equipment, three medium gain phased array antennas placed equidistantly around the spacecraft simulate an omni-directional antenna. Its purpose is to provide emergency communications as well as serve as backup communications, as it can establish contact with targets without precise pointing. A single parabolic high gain placed near the top of the spacecraft will serve as the main point of contact, and will be capable of transmitting large data rates towards the ground control either directly or via relay.

To control the spacecraft, a command and data handling subsystem was designed. A diagram was made to show how the operations of the spacecraft are performed. This diagram shows in detail what the software shall be able to do. The actual coding of this software is out of the scope of this report. Also, per subsystem it was determined what data needs to be handled. Finally, preliminary sizing of the subsystem was performed, with as outputs the mass and the power consumption.

The TMS was considered next. Temperatures in the Lunar environment differ drastically, from  $-244^\circ\text{C}$  to  $127^\circ\text{C}$ , the spacecraft is equipped with an appropriate thermal control system. Heat pipes connected to radiators were implemented in the spacecraft design to cool the spacecraft components that generate heat waste. The spacecraft will also be coated with a low absorptivity and high emissivity coating, which will help the spacecraft to stay within operating temperature in the sunlight. Especially the fuel cell and the hydrogen peroxide printer

require intense cooling. Some of the waste heat is recycled and used to heat parts of the spacecraft when the temperature is cooler.

The last subsystem considered in the study was structures. For this department, two major elements were concentrated on the landing gear and the load-carrying framework. The landing gear configuration used for the UCM included an assembly of 4 legs of the cantilever type. Each leg had three actuators, one primary one and two secondary ones attached to it. The design was checked with a stability condition derived from inelastic impact theory and the most critical tumbling mode. However, the efforts were focused on the reusability aspect of the gear. A comprehensive study was conducted on the reusability of the absorbers, and both flight-proven and experimental technologies were considered. The study resulted in selecting pressurized metal bellows for the UCM application. For the load-carrying elements, Euler-Johnson and local buckling conditions were applied to ensure sufficient thickness. The calculated masses of the struts were as follows: the primary strut 180 kg, and secondary 16.2 kg. Lastly, a preliminary sizing of the footpad was performed. The resulting diameter of the pad was 1.6 m and the mass was approximately 77 kg. The total landing gear mass including insulation and deployment mechanism was approximated to be 1288 kg. For the primary structure a comprehensive study was performed for the best structure type. The structure had to be manufacturable from the composites, as use of this material would allow to lower mass of the system. Using former studies on the Lunar landers, a shell - truss configuration was chosen. This type is characterised by use of both trusses and shell, allowing to integrate the components extensively in the design. This solution also resulted in the lowest mass in comparison to pure truss or shell configurations. The detailed design of the structure was left out from the scope of this paper, thus the mass of the systems was assumed to be 20 % of the dry mass.

As quickly mentioned during the system description, the team followed a sustainable optimisation strategy in the design by maximizing the ratio of propellant sold to propellant bought. 6561 designs were considered, each having different  $H_2$  and  $O_2$  MLI layers. From this optimization, 77 MLI layers for the  $H_2$  tank and 29 MLI layers for the  $O_2$  tank were the best result, yielding a P2P ratio of 0.485. In order to decrease uncertainty, a thorough sensitivity analysis was performed, which in turn confirmed that the iterator functioned as desired and showed no signs of exponential growth. Before starting operations, the UCM must arrive at the  $LH_2$  and  $LO_2$  production site on the Moon. These pre-operations encompass detaching from the Starship fairing, turning telemetry on and if everything is on track and every subsystem is operational, performing the initial descent burn and landing in the desired location in Shackleton crater, after which operations begin. The operations are divided in a high number of cycles, in which each UCM begins and ends the cycle emptied of fuel on the Lunar surface, after refueling a customer in LLO. The approach towards end-of-life consists of the 3R approach as well as the possibility of extending the mission life with external help to maintain the UCM's health. During operation, all kinds of risk can occur that can endanger the mission. Therefore, a risk analysis was made that assessed the impact and likelihood of each risk and thereby determined its severity. For three risks that were deemed of an unacceptable level, mitigation measures were put in place. The following risks were mitigated: orbit insertion failure by the launch vehicle, metal fatigue occurring during operation and the presence of Lunar dust.

Furthermore, maintenance & supportability of the mission was discussed. Since the mission has high operational cycle count per UCM, in a very hazardous environment, for a long duration of time, maintenance was deemed crucial for the success of the mission. After thorough investigation and consultation with experts, telerobotic autonomous repair and/or replacement of parts was discarded as it is unfeasible as of now. Maintenance was split in two groups, software and hardware. The software consisted of intensive health monitoring systems, such as the NOSTRADAMUS method combined with NASA's ISP, RTP, MSK-view and ELOG. Also, Digital Twin Technology was selected in order to have a virtual real-time counterpart of a physical UCM, for comparison, optimization and simulation purposes. Regarding hardware, it was decided that there shall be hardware to protect from Lunar dust. Lunar dust is abrasive, electrically charged, and can deal high damage to mechanical parts of the spacecraft. To counteract this, measures were taken per subsystem. Mechanical Iris Valves were decided for parts that are very susceptible to dust such as docking ports. Indium Tin Oxide coating will be applied to the landing gear and the lower part of the spacecraft, and a shell around the propulsive system will be implemented for protection. Next, manned interventions by NASA's Artemis astronauts has been considered if the budget allows it at that point in the mission. This is in case of a failure of a part of a UCM that is repairable by the infrastructure NASA has built, as long as it is economically viable. Lastly, the maintenance rover considered in the previous report was discarded, as it would require more maintenance itself than the system it is offering maintenance to. In order to determine the value of the project in terms of its economic benefits, COLD business case was evaluated. This was done by first looking at the total costs of the mission, composed of development, production, operations, insurance testing and launch costs and their respective uncertainties. Afterwards, using Monte Carlo simulations, the total cost of the mission was evaluated based on the different cost elements, modeled using split normal distributions.

The characteristics of the business case were evaluated using multiple economic metrics, such as the net present value (NPV), internal rate of return (IRR) as well as the break-even point. While evaluating these

---

parameters, it was important to make sure that the NPV remains above 0, the IRR above the assumed 10% discount rate, and project breaks even before the end of the mission lifespan. Only then the project could be assumed to be an interesting venture, which creates value and as such can sustain itself economically without any external financial help. Thanks to the economic analysis of the project, it was determined to set at a propellant sale price of 5400 \$/kg. This price is still high enough for COLD to make a significant profit, as well as assure that the internal rate of revenue is attractive enough to attract investors. It simultaneously low enough to allow for profitable deliveries to most places in the cislunar space by potential partnered entities. The net present value, one of the main parameters used in the financial analysis, created in this scenario was around 2.5 billion dollars. The internal rate of return meanwhile, another crucial factor, remained above the discount rate in 90% of cases, meaning that potential investors could expect larger profits than by simply investing in the market. Additionally, with such pricing, the project would break even on average around the 7th year of operation.

Finally, a design evaluation was performed. A compliance matrix showed that at this stage, all stakeholder requirements were met. However, many recommendations for this design and for a continuation of it have been shown. The main recommendation regarding the general system concept lied in purchasing the power directly from Artemis rather than using a fuel cell while on the Lunar surface. Furthermore, regarding the concepts, more investigation in the prospect of repairs by NASA's Artemis that could potentially extend the UCM life by a big margin is recommended. Most importantly, the end of life procedures of the UCM should be investigated further, as 10 weeks of designing did not allow for extensive end-of-life procedures, and these could be very beneficial to the mission in terms of sustainability. From the modelling point of view, many recommendations can be done. Vibrational simulations, noise temperature models are amongst the analytical models that should be implemented. In terms of numerical simulations, FEM analysis for the structures and tanks and a numerical thermal modelling are strongly suggested. Last, a flight trajectory simulation will allow for more efficient propellant use, which will in turn increase the P2P ratio.

In the greater scope of things, the purpose of the UCM network is to become a solid member of the foundations of a thriving cislunar ecosystem that will propel mankind to the next phase of its existence.



## 2 Introduction

For the vast majority of mankind's recorded history, the moon has been an unreachable and fascinating mystery. Yet, the rapid technological advance over the last centuries has allowed humans to track, observe and even set foot on what once was seen as a deity. However, since this milestone was reached by the Apollo 11 mission in July 1969, the number of major Lunar missions has declined drastically, while the demand for LEO and Deep Space missions has been increasing ever since. As a result, the engineering sector of the industry is greatly encouraged to conceive new systems that will make such missions more economical.

There are many possible solutions to this issue, ranging from designing more efficient launcher vehicles to finding alternative ways of getting payload into orbit. Amongst these solutions lies the idea of having an in-space refuelling station in LLO which can be refilled without having to launch the propellant from Earth, but from a propellant production plant on the Lunar surface. Such a system would be a major milestone in space exploration, reducing mission costs and increasing mission maneuverability and longevity. This entire system is the core aim of the *Design Synthesis Exercise*. This Final Report presents the in-space cryogenic  $H_2$  and  $O_2$  propellant transfer & refuelling station infrastructure will be designed by a team of 10 engineering students of the TU Delft's Aerospace Faculty.

In this report the preliminary detailed design of the universal cryogenic module shall be presented. Firstly, in Chapter 3 the market analysis is presented, in which various different possible markets are considered. The size of these markets is analysed, and the current evaluations of prices and relevant customers are described. Furthermore, in Chapter 4 the system is presented and the optimisation method is discussed. After these considerations the technical aspects follow, the first subsystem covered is the cryogenic storage system Chapter 5. In this chapter, the design of the payload and propellant tanks are discussed, with the sizing and respective methodologies for the insulation and cryocoolers. Next, the electrical power system is discussed in Chapter 6. Here the sizing, power profiles, cost analysis for the EPS are discussed. This is followed by the propulsive system, which is introduced in Chapter 7. In this chapter the selection of engines is described, the  $\Delta V$  budgets are drawn and plumbing and ignition sequencing is discussed. This chapter then leads into the attitude determination and control system, described in Chapter 8. In this chapter the attitude determination is considered, with the reaction control system defined and a preliminary design drawn up and discussed. Then, in Chapter 9 the antenna selection, placement is discussed. Next, Chapter 10 discusses the command and data handling system. This chapter explains the various functions of the software using a software diagram and further, presents the data flow utilising the data block diagram. The subsequent chapter, Chapter 11 covers the thermal management system where the various methods to transfer and control heat will be discussed. This chapter describes the heat pipe design, the thermal coating selection and the radiator design. After this chapter, follows Chapter 12 where the structures of the spacecraft are presented. This chapter is to cover the landing gear design and over arching configuration of all discussed subsystems. Continuing, Chapter 13 will summarize the results of the optimisation and will present the final UCM design parameters.

After the optimisation results have been covered the final elements of the design process will be covered. In Chapter 14, the entire lifespan of the project technicalities from inception to end-of-life will be discussed. In this chapter manufacturing & production, testing, operations, end of life, risk management are discussed. This chapter is followed by Chapter 15, where the ability to maintain and support the spacecraft throughout its life is discussed. This chapter highlights the various elements of the mission that require maintenance and the methods that can be used to accomplish said maintenance. Next up, in Chapter 16 one of the most critical elements of the mission will be discussed - the business case. This covers the commercial viability of the venture and provides a financial analysis of the mission. Next, in Chapter 17 the design is evaluated. This chapter analyses the performance of the design by means of compliance matrices. Additionally, this chapter provides recommendations for future development. Finally, the findings and design are summarised in Chapter 18, also known as the conclusion.

# 3 Market Analysis

In order for the COLD project to be economically sustainable it needs to turn a profit and have its place in the economy. In order to evaluate whether that would be the case, a market analysis was performed. Its objective was to establish the competitive cost and volume of the economic environment for the propellant delivery system provided by COLD. Future industries such as orbital manufacturing and Lunar bases were also considered, as they are being currently being developed. This chapter presents the results of this economic study.

Section 3.1 further explains the motivation behind the market analysis for the COLD mission. It is followed by Section 3.2 where different characteristics of the general market are analysed. In Section 3.3 and 3.4 market segmentation is performed, and specific sectors of the space economy are described. The chapter closes off with Section 3.5 giving a general overview of the most important potential customers for COLD.

## 3.1. Motivation

Since the dawn of the space age, humanity has consistently developed a small but steadily growing presence in space. Nowadays, it seems like it is only a matter of time until it expands its reach covering interplanetary travel as well, just like Earth's orbit has been filling up exponentially over the past few decades. The Moon plays a central role in this process - it will serve as a springboard, catapulting manned and unmanned missions into interplanetary space. Earth's natural satellite will also serve to support operations in the Earth's immediate vicinity, providing propellant, oxygen and a safe haven for human presence.

The first of these, propellant, is the market gap that COLD is aiming to fill. Currently the only way to obtain additional propellant in space is to deliver it from Earth, which is expensive and extremely unsustainable. This is because delivering cargo to space requires burning exponentially more propellant, based on how much and how far it has to be delivered, due to Earth's relatively large gravitational pull and presence of dense atmosphere. Alternatively, propellant production could be outsourced to the Moon. Delivering it from there would allow for substantial increase in efficiency, as the Moon's gravitational pull is six times weaker than Earth's. Add to it savings resulting from the absence of atmospheric drag, and the ensuing increase in delivery efficiency is so large as to validate considerable research effort by NASA, SpaceX, and hundreds of other companies and research groups <sup>1</sup>.

The increased efficiency would in turn allow for propellant to be delivered to space for much lower prices and much larger quantities than should that be done from Earth. It will also allow for spacecraft to lift off from Earth, and refuel on the way, requiring less propellant on launch. The compounding effects of in space refueling can be easily seen in Figure 3.1, provided by Sowers [69]. This figure visualises the exponential growth of necessary propellant expenditure to achieve a certain  $\Delta V$ , which is the defining characteristic of space mission reach capability <sup>2</sup>.

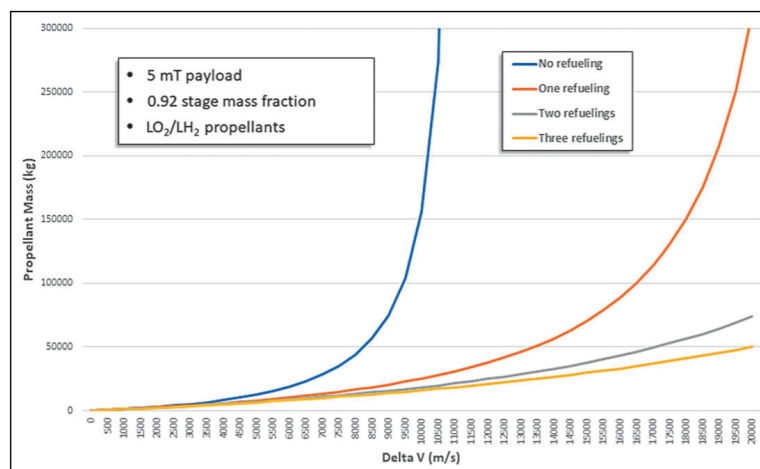


Figure 3.1: Benefits of refueling with space-sourced LO<sub>2</sub>/LH<sub>2</sub> propellants [69]

<sup>1</sup>URL:<https://www.nytimes.com/2019/07/12/science/nasa-moon-apollo-artemis.html>

<sup>2</sup>URL:[https://www.nasa.gov/mission\\_pages/station/expeditions/expedition30/tryanny.html](https://www.nasa.gov/mission_pages/station/expeditions/expedition30/tryanny.html)

## 3.2. Market Identification

In order to create a self sustaining enterprise in the lunar orbit, the COLD mission needs to be economically viable. To that end, a market identification and analysis has to be performed, as to determine the potential sources of demand for Lunar propellant, as well as possibilities for growth and cost wise self sufficiency. The space economy as a whole is currently growing at a steady pace, and via multiple estimates, is expected to reach trillions USD worth by 2040, as shown in Figure 3.2<sup>3</sup>. This compared to the budget of COLD, which is equal to around 7 billion USD, indicates vast market opportunity for profits, as almost all spacecraft require propellant, which COLD will be able to deliver at a competitive price.

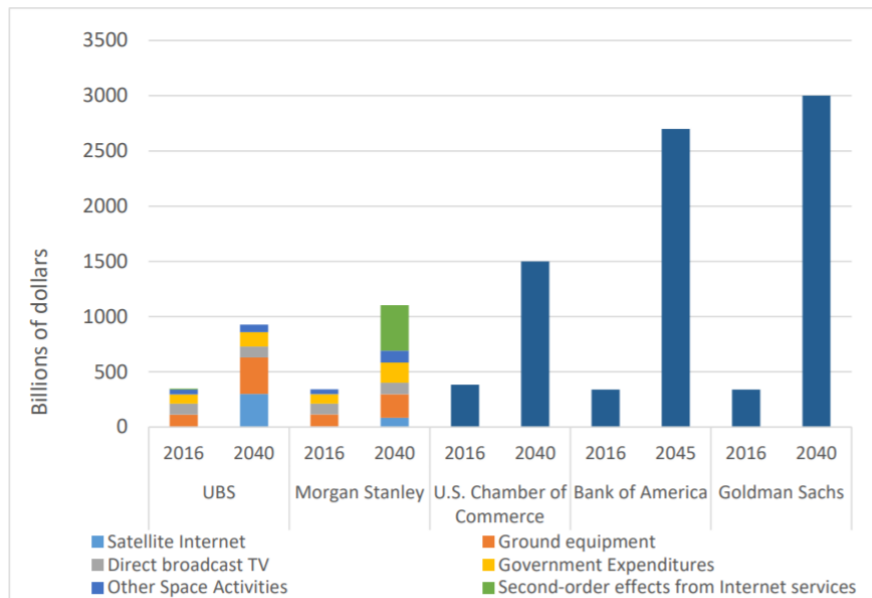


Figure 3.2: Comparisons by Category of 2016 Estimates and 2040 Projections of the Size of the Space Economy

The main possible markets that could be tapped by this mission are the markets of cislunar and interplanetary space. In this case, the former is defined as space between Earth and the orbit of the Moon, encompassing popular spacecraft operating regions such as low and geostationary Earth orbits (LEO and GEO respectively), EML1 Lagrangian point between the Moon and Earth, etc. The latter refers to anything located further from Earth than the Moon's orbit, such as EML2 Lagrangian point around which the James Webb telescope is located or most importantly, interplanetary missions. More in depth identification of potential customers will be done in sections 3.3 and 3.4.

## 3.3. Cislunar Markets

The first markets that will be considered are the cislunar markets which bounded by the Earth-Moon system. This cislunar market encompasses a relatively well developed economic ecosystem of spacecraft located between the Earth and an orbit around the Moon. Within this ecosystem there are multiple potential markets that the COLD mission can tap into. The COLD mission has the ability to refuel customer spacecraft and generate revenue in doing so. This ability could influence markets such as: scientific research, telecommunication, space stations, and more. Providing refuelling capability to these markets is valuable as it allows the spacecraft forming these markets to require less propellant during launch from Earth and thereby increase their payload capacity. This would lead to more versatile designs with larger possible design variations due to lowering of mass constraints. The refuelling possibility could also extend possible operational life of these spacecraft, which are now limited by the amount of propellant they have on board. An example, of a spacecraft whose lifetime is mainly limited by the amount of propellant it has available is the James Webb telescope<sup>4</sup>.

At this point in time, the only option for in-space refuelling is to deliver propellant from the Earth's surface to the customer. However, as already mentioned, this is very expensive and environmentally unfriendly as it requires large propellant expenditures during launch from Earth. Nonetheless, in order for COLD and for Lunar propellant to become economically viable, the propellant that COLD will sell will have to be offered at a competitive price. This competitive price would have to be cheaper than its Earth-born alternative, or launching with additional

<sup>3</sup>URL:<https://www.jstor.org/stable/pdf/resrep25331.7.pdf>

<sup>4</sup>URL:<https://webb.nasa.gov/content/about/faqs/faqLite.html>

propellant on board. The latter however is not always that easy, as the size and mass of the spacecraft is often limiting as to how far it could technically go. Adding extra mass on launch might not be feasible as perhaps the spacecraft could not be delivered to a target orbit, requiring gargantuan expenses for a new launcher and redesign of the structure to allow for a larger tank.

As far as refueling using Earth-born propellant, literature research shows that the pricing of the latter would be in order of magnitudes presented in Table 3.1. The 1 dollar per kg was based on the prices of both liquid hydrogen and oxygen (3.66 and 0.16 F2001\$/kg respectively) presented in a NASA datasheet <sup>5</sup>. Adjusted for inflation and the fuel/oxidiser ratio, it results in a price of around 1F2022\$/kg of propellant.

The values in this table are based on values presented by Kornuta [14] and Sowers [69], which were adjusted for current best market prices offered by SpaceX [33] at around 3000\$ per kg to LEO. With this information it can be easily seen that the costs become very substantial the further away one is from Earth. On the moon itself the cost is estimated to be around 16k\$/kg, which is economically unsustainable when it comes to refueling operations as no commercial enterprise would agree to such costs, especially on a larger scale. This is without even mentioning the Earth environmental impact of such operations. It is also important to note that these estimates do not include the price of the vehicle/tanker needed to transport this propellant to its destination, nor the profit margins necessary to make a hypothetical Earth refueling service profitable. This is important because were it to be included, it would further increase the delivery price, perhaps even to an unacceptably high extent, at which it would not make economic sense to perform such refuelling operations [14].

**Table 3.1:** Price of propellant brought from Earth to different locations in the cislunar region based on literature research, adjusted for current (2022) pricing to LEO [14]

Location	Cost of propellant from Earth
Earth's surface	1 \$/kg
LEO	3000 \$/kg
GTO	6000 \$/kg
GEO	12000 \$/kg
EML1	9000 \$/kg
LLO	16000 \$/kg
Lunar surface	27000 \$/kg

Nonetheless, the possibility to refuel in orbit and by extent the ability to bring more payload into orbit will allow for rapid expansion of the space customer base. In the upcoming years it is expected that the majority of new spacecraft will consist of Earth orbiting satellites <sup>6</sup>, mainly from the telecommunication/Earth observation domain. These usually have a lifespan of around 15 years <sup>7</sup> and do not require much additional propellant. However, as already mentioned, by delivering fuel after launch, these satellites could potentially have a larger payload or they would be less expensive to launch, in both cases benefiting the spacecraft operator. This type of spacecraft forms a large market share, which will however be difficult to profitably cater, as their location is often within close vicinity to Earth. There, the price of propellant delivery from the planet's surface will be the most competitive with regards to the propellant of Lunar origin, possibly limiting the economic viability of the project. However should a low enough price be achieved, COLD would immediately seize a large market opportunity, given that the customer spacecraft were to be adapted for in orbit refueling.

These satellites will however not be the only customers located in the cislunar space. Other markets could consist of propellant demand on board space stations, such as the International Space Station or the planned Artemis Gateway station. Both of these would require significant amounts of propellant due to the required station keeping  $\Delta V$  requirements [14]. Currently there are plans in motion for creation of commercial space stations <sup>8</sup>, supporting everything from scientific research efforts, orbital manufacturing facilities or even space hotels. All of these would require propellant for remaining in orbit, and the heavier these stations are, the larger the amount of required propellant would be. For this reason the propellant demand from space stations is expected to be quite substantial. Lunar propellant could fulfill this role very well, in terms of sustainable and environmentally friendly procurement, as it does not require launches from Earth. It could also fulfill this role in a beneficial way in terms of economical savings should the price be competitive in comparison to alternatives originating from Earth.

Two of the aforementioned space industries should be looked at further: orbital manufacturing and space tourism. The former is a very interesting concept which would allow for creation of very specific products that

<sup>5</sup>URL:[https://www.nasa.gov/centers/kennedy/pdf/167433main\\_Propellants08.pdf](https://www.nasa.gov/centers/kennedy/pdf/167433main_Propellants08.pdf)

<sup>6</sup>URL:<https://www.morganstanley.com/Themes/global-space-economy>

<sup>7</sup>URL:<https://www.nsr.com/satellite-eol-not-one-size-fits-all/>

<sup>8</sup>URL:<https://www.nasa.gov/press-release/nasa-selects-companies-to-develop-commercial-destinations-in-space>

could only be produced in micro gravity, such as ultra efficient optical fibre cables<sup>9</sup>. Orbital manufacturing is a rapidly developing industry with large profit capabilities and is expected to start functioning in the near future [68]. The latter is a very popular topic when it comes to space accessibility. Multiple companies such as SpaceX, Blue Origin and Virgin Galactic are at the forefront of space tourism and increasing space accessibility<sup>10</sup>. Both of these industries require vehicles which are capable of transferring cargo/passengers to and from target locations. This is regardless of whether the transported item is an orbital fibre manufacturing plant or a Lunar base. If refuelling capability was available, these spacecraft could refuel while in space, potentially allowing for large savings and increased capacity.

In general all space transfer vehicles could make use of Lunar propellant and refuelling options in Lunar orbit. For example, for NASA's Artemis mission, a commercially developed reusable Lunar lander will be used<sup>11</sup>. Other potential customers could be autonomous cargo landers bringing He3, a helium isotope found abundantly on the Moon, from Lunar mines back to Earth for use in possible fusion generators on Earth. Such vehicles could travel from Earth to the Moon, refuel in orbit, and only then land. This could allow for additional payload to be delivered to the Lunar surface from Earth, as the landing procedure is relatively intensive on the  $\Delta V$  budget at 1.9 km/s. This could be repeated each time the lander would go back to orbit, should increased payload capacity be desired.

Another rapidly developing important element of space industry is the debris removal industry, a very important space economy sector which will be responsible for keeping space easily accessible and more importantly safe to operate in. An example of such companies would be ClearSpace, expected to demonstrate their concept in 2025<sup>12</sup>. More advanced debris removal systems would remain in orbit for prolonged periods of time, collecting man made space waste. To support these operations, which would most likely involve frequent orbital altitude changes, large propellant expenditures will be necessary. These could originate from large onboard capacities, or alternatively from scheduled propellant deliveries. Lunar propellant could serve as an environmentally conscious alternative to propellant brought from Earth, as it would not involve the polluting of Earth's atmosphere.

Lastly, it is important to note that the COLD mission does not include a specialised delivery vehicle, but rather a single universal cryogenic module. As part of the mission requirements, this spacecraft operates within the immediate vicinity of the Moon, reaching only the low Lunar orbit. As such it would not be able to access all the aforementioned cislunar markets, with the exception of Lunar landers and Lunar orbiting spacecraft. In the future, it might be interesting to consider a Lunar depot located at one of the Lagrange points, as this is an interesting place from which there will be much more freedom in terms of access to the customers.

However should the orbital height of delivery remain unchanged, the cooperation with an external party which would perform a space version of "last mile delivery" would be necessary. Such endeavours would include the external entity having to operate a space tanker. Such an entity would purchase propellant in LLO in bulk, and travel to a different destination, such as the GEO or perhaps even LEO orbit and refuel customers there at a profit. This partnership would benefit both sides, as each could specialise in their own field, either the Lunar landing and ascent with the case of COLD, or intra orbit transfer for the external party. A sole venture involving both mission elements could prove too expensive for a single entity to accomplish, as speculated by different studies of the matter [14] [69].

One very crucial element of such a partnership would be the adequate propellant pricing on the side of COLD. The price cannot be too high, otherwise the markets located further away in terms of  $\Delta V$  would cease to be economically viable for the partnered entity. As visible on the  $\Delta V$  map, presented in Figure 3.3<sup>13</sup>, some of locations such as the low Earth orbit require rather large  $\Delta$  expenditures, even though these are still smaller than the one required to lift off from Earth, leaving a window for potential profitability in such a venture. Further analysis of this propellant pricing problem is presented in Chapter 16.

---

<sup>9</sup>URL:[https://www.nasa.gov/mission\\_pages/station/research/news/b4h-3rd/eds-mis-building-better-optical-fiber/](https://www.nasa.gov/mission_pages/station/research/news/b4h-3rd/eds-mis-building-better-optical-fiber/)

<sup>10</sup>URL:<https://www.nytimes.com/2022/05/07/travel/space-travel-tourism.html>

<sup>11</sup>URL:[https://www.nasa.gov/sites/default/files/atoms/files/artemis\\_plan-20200921.pdf](https://www.nasa.gov/sites/default/files/atoms/files/artemis_plan-20200921.pdf)

<sup>12</sup>URL:<https://www.wired.com/story/the-us-space-force-wants-to-clean-up-junk-in-orbit/>

<sup>13</sup>URL:[https://commons.wikimedia.org/wiki/File:Delta\\_V\\_Earth\\_Moon\\_Mars.png](https://commons.wikimedia.org/wiki/File:Delta_V_Earth_Moon_Mars.png)

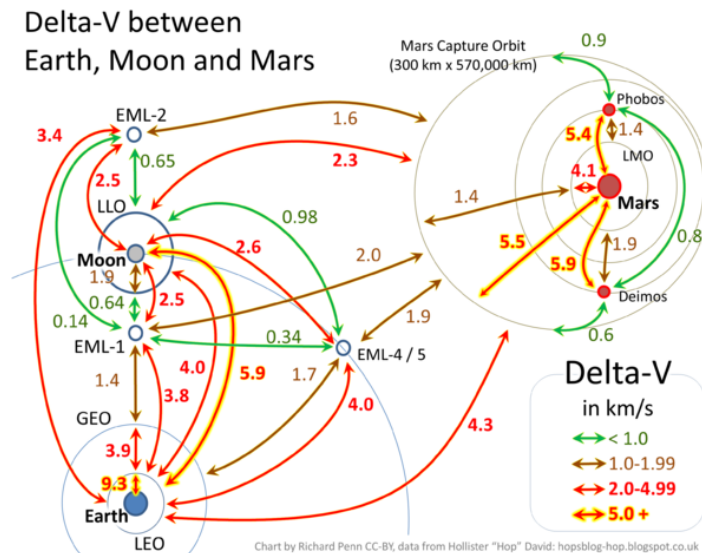


Figure 3.3:  $\Delta V$  map in the cislunar space region around Earth and towards Mars

Finally, a few companies from different space industry sectors are presented in Figure 3.4<sup>14</sup>. The sectors surrounded with a red border are those of relevance for the COLD mission. The launch vehicle industry was assumed to be of interest as it includes companies developing Lunar landers, which would be one of COLD’s principal customers.

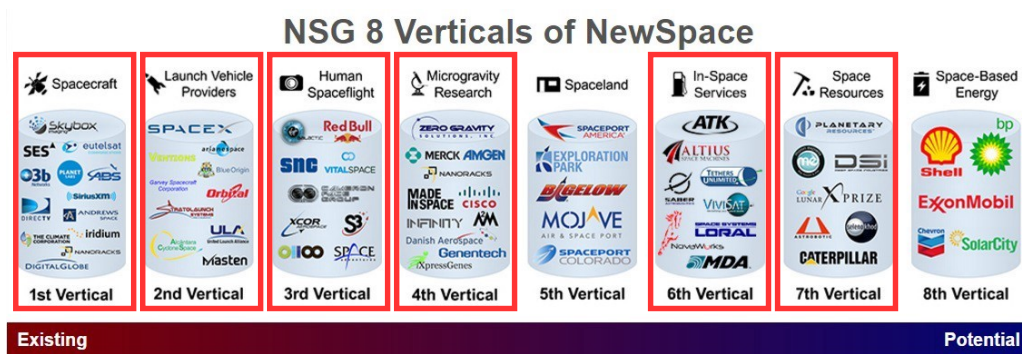


Figure 3.4: Space industry verticals. Sectors surrounded with a red border are the ones of interest for the COLD mission

### 3.4. Interplanetary Markets

The second general region space that is of great interest for the space community, and to COLD by extension, is the vast translunar and interplanetary expanse stretching out behind the orbit of the Moon. While the number of spacecraft flown in this region is rather small when compared to the number of satellites in Earth’s orbit, this is expected to change in the upcoming years. SpaceX has long held as goal reaching Mars and establishing a colony there<sup>15</sup>. Each year there are increasingly more missions to distant parts of the Solar System, such as the Parker probe studying the Sun<sup>16</sup> or the NASA’s DART mission to a nearby asteroid<sup>17</sup>. Such missions would benefit immensely from the ability to refuel on the way, as for example the  $\Delta V$  required to reach a low Mars orbit is equal to around 15 km/s based on Figure 3.3. Looking in turn at Figure 3.1, it can be easily seen that with such a high velocity requirement, the exponential nature of propellant vs payload requirement prevents the bringing of a large payload. Refueling around the Moon would increase the potential of such missions tremendously, allowing for larger payloads and in turn greater capabilities of interplanetary missions.

A specific type of interplanetary/translunar/cislunar depending on its location industry, is economy of asteroid mining. While still quite far fetched, several space missions have brought back samples from Near Earth Objects demonstrating the possibility of such endeavours. Yet multiple studies have found that such projects would be

<sup>14</sup>URL:https://newspaceglobal.com/nsg-verticals-1-spacecraft/

<sup>15</sup>URL:https://www.spacex.com/human-spaceflight/mars/

<sup>16</sup>URL:https://www.nasa.gov/content/goddard/parker-solar-probe-humanity-s-first-visit-to-a-star

<sup>17</sup>URL:https://nssdc.gsfc.nasa.gov/nmc/spacecraft/display.action?id=2021-110A

extremely expensive - 90 billion USD per one source [12]. They would also risk not being economically viable due to the current pricing of space transportation. Perhaps refuelling with Lunar propellant would prove the key factor in developing this industry. Unfortunately, asteroid mining has not yet reached the level of maturity necessary for serious economic consideration, and as such will not be the main focus of COLD.

### 3.5. Customer Summary

Market analysis and opportunity identification is arguably the most important element of any given project if its goal is to be self sustaining. For the COLD this has been done in the previous sections. The recognised markets and customers of both cisLunar and translunar/inter planetary space are summarised in Figure 3.5. Out of all these, perhaps the most important economic market in terms of its influence on price setting is the industry of propellant transfer. As COLD only delivers fuel to the low Lunar orbit, its further distribution is highly dependent on external parties. Pricing of the propellant on the side of COLD should reflect the necessity of these other parties to also turn a profit. This is because their area of operations would include locations closer to Earth, to which propellant could be brought from Earth for a reasonable cost. As such, COLD has to assure that the price is not set too high as not to turn these potential partners away. This will be evaluated in greater detail in Chapter 16.

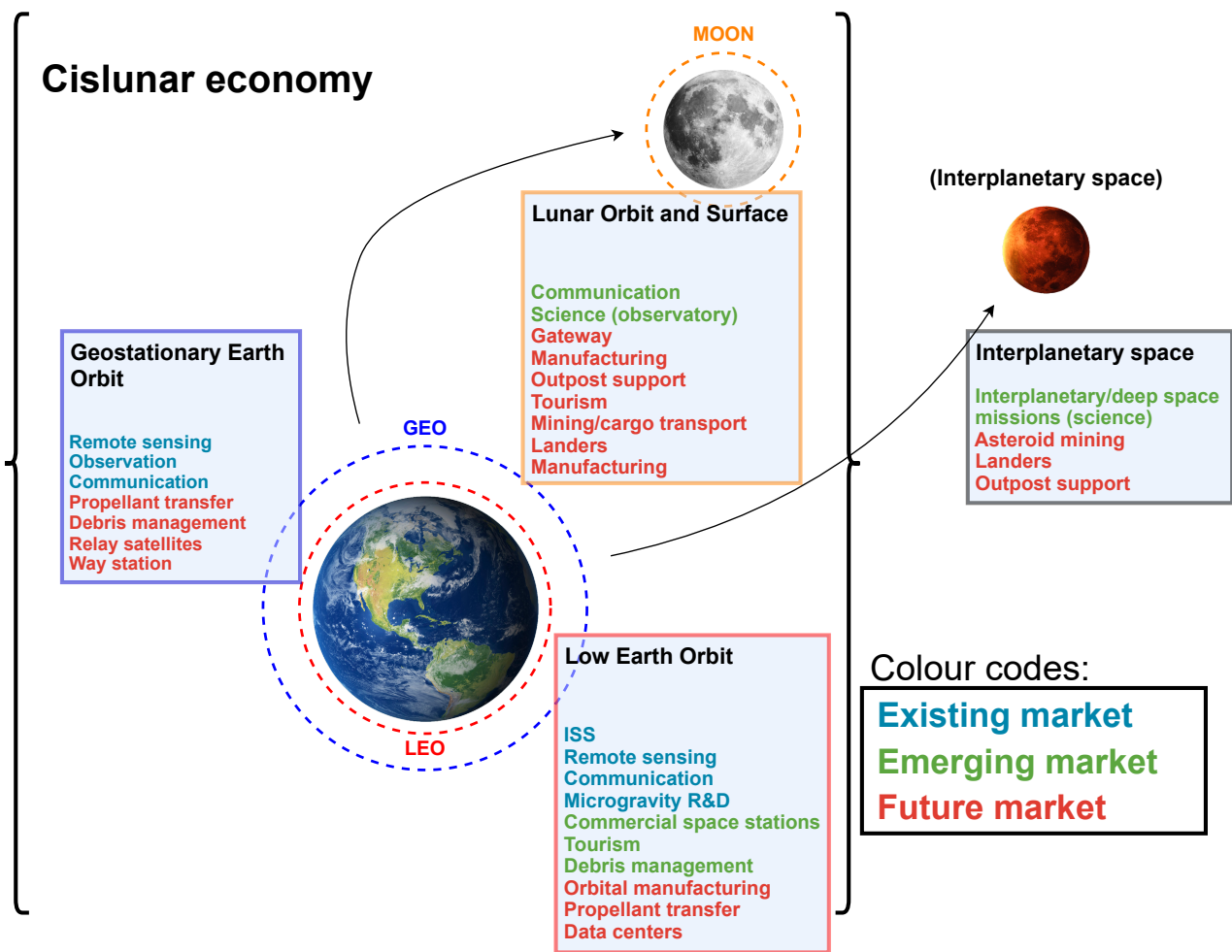


Figure 3.5: Map of space industry sectors of interest for the COLD mission. Blue markets are the already existing ones, green refers to emerging markets. while red signifies the future markets

# 4 System Description & Optimisation Method

The stakeholders of this project provided several requirements as shown in Table 4.1. One of the key requirements, *REQ-SH-12* states: "COLD shall be able to facilitate the transfer of 250 tonnes of propellant per year." This led to three mission concepts as described in the mid-term report [5]. In this mid-term report, a trade-off was performed which led to the choice of the universal cryogenic module concept. This mission concept will be described in Section 4.1 and the method of sizing it will be described globally in Section 4.2. Finally the method of optimisation used to select appropriate configuration options for the concept is described in Section 4.3.

**Table 4.1:** Stakeholder requirements

Requirement ID	Requirement
<i>REQ-SH-01</i>	The infrastructure shall be delivered at a cost of \$36 $\frac{k}{kg}$
<i>REQ-SH-02</i>	The overall project budget shall not exceed \$7B
<i>REQ-SH-03</i>	Launch vehicle that transfers spacecraft shall use green propellants for launch or $LH_2$ & $LO_2$
<i>REQ-SH-04</i>	All spacecraft infrastructure shall be transported from earth to moon through heavy launch vehicles
<i>REQ-SH-05</i>	Launch vehicle that transfers propellant storage tanks shall use green propellants for launch or $LH_2$ & $LO_2$
<i>REQ-SH-06</i>	The propellant transfer spacecraft shall be powered by solar panels while in direct sunlight in-orbit
<i>REQ-SH-07</i>	The propellant transfer system shall be powered by solar panels
<i>REQ-SH-08</i>	Propellant transfer spacecraft shall be able to transfer 25 tonnes of propellant per one trip to orbit
<i>REQ-SH-09</i>	COLD shall be able to deliver 50 tonnes of $LH_2$ and $LO_2$ propellant to a single spacecraft in LLO
<i>REQ-SH-10</i>	$LH_2$ shall be stored in a storage tank for 1 month with less than 10% boiloff
<i>REQ-SH-11</i>	$LO_2$ shall be stored in a storage tank for 1 month with less than 10% boiloff
<i>REQ-SH-12</i>	COLD shall be able to facilitate the transfer of 250 tonnes of propellant per year
<i>REQ-SH-13</i>	COLD shall be able to store 50 tonnes of $LO_2$ and $LH_2$ at the Lunar surface
<i>REQ-SH-14</i>	The propellant transfer spacecraft (Lunar surface to LLO and vice versa) shall have $\Delta V$
<i>REQ-SH-15</i>	The propellant transfer spacecraft shall use a cryogenic propulsion system
<i>REQ-SH-16</i>	The propellant transfer spacecraft shall be operable in space conditions
<i>REQ-SH-17</i>	The propellant transfer spacecraft shall be able to be re-used for multiple refuelling missions
<i>REQ-SH-18</i>	The propellant transfer spacecraft shall be remotely controllable from Earth
<i>REQ-SH-19</i>	The propellant transfer mechanism shall be remotely controllable from Earth

## 4.1. Concept

The universal cryogenic module (UCM) mission concept consists of four identical launchers as shown in Figure 4.1. Each launcher will be capable of transporting twenty-five tons of propellant from the Lunar surface to low Lunar orbit as per requirement *REQ-SH-08*. First the subsystems that belong to the UCM will be described along with the overall sizing method. Then some key assumptions regarding the propellant, operation times, and environment temperatures will be explained.



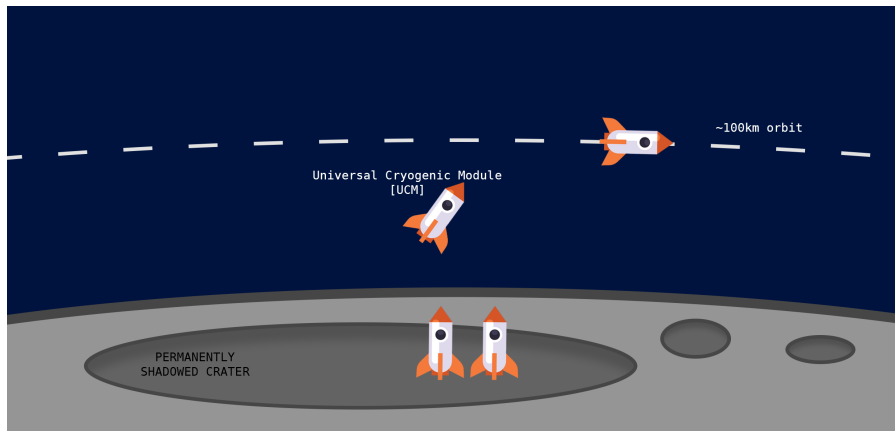
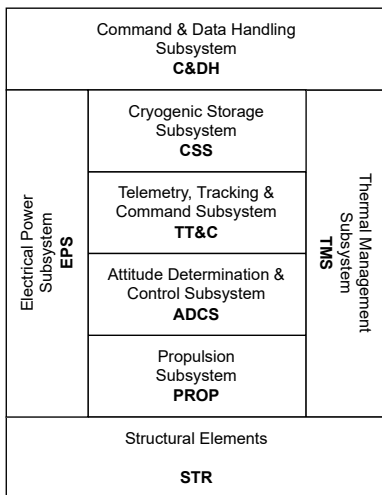


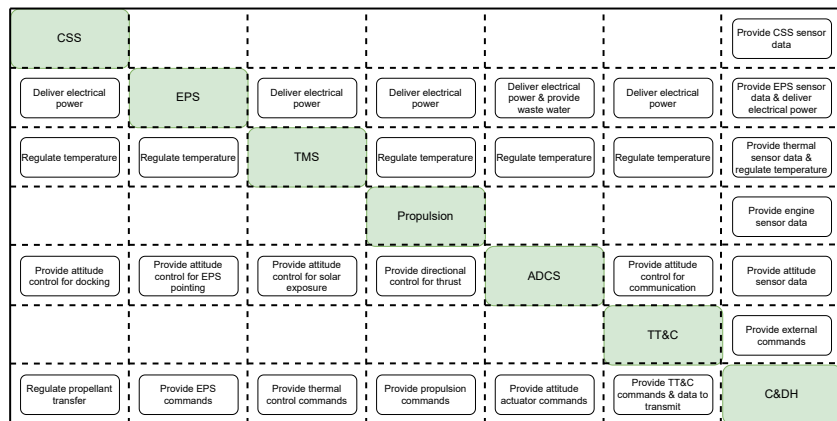
Figure 4.1: UCM mission concept.

The UCM will have to fulfill all stakeholder requirements which translate into functions. These functions translate into the subsystem overview of the UCM shown in Figure 4.2a. The cryogenic storage subsystem (CSS) will fulfill the function of storing and cooling the payload propellant. The propulsion subsystem (PROP) fulfills the function of transporting the UCM back and forth between the Lunar surface and low Lunar orbit. The attitude determination and control subsystem (ADCS) fulfills the function of having precise maneuvering capability. The telemetry, tracking and command subsystem (TT&C) fulfills the function of the UCM being subject to remote control and monitoring from Earth.

Finally, there are four over-arching subsystems that are important to the aforementioned subsystems and one another. The command and data handling subsystem (C&DH) controls all other subsystem and handles all internal data flows. The thermal management subsystem (TMS) manages and controls the temperatures of all other subsystems and the UCM's internal heat flows. The electrical power subsystem (EPS) provides power to all other subsystems when necessary. The structural elements (STR) encompass the landing gear and structural elements that physically hold the subsystems together that form the UCM.



(a) Overview of subsystems in each UCM



(b) N2 chart of the UCM

Figure 4.2: Subsystem overview

Figure 4.2b shows an N2 chart of the UCM which highlights important interactions between the subsystems of the UCM. All the subsystems are placed on the diagonal axis. Each function box describes a function to be performed by a corresponding subsystem on the horizontal axis for a subsystem on the corresponding vertical axis. Considering that the structural elements are not strictly a subsystem it has not been included in this N2 chart. From this diagram it is clear that the EPS, TMS, and C&DH subsystems are overarching subsystems as they interact with all other subsystems. A special case to be noted is that the EPS does not only provide power to the ADCS but also water for monopropellant production, this will be elaborated on further in Chapter 8. How the UCM is going to be sized, taking into account the aforementioned and shown interactions will be discussed next in Section 4.2.

## 4.2. Sizing Process

Figure 4.3 shows the process that has to be performed in order to size the universal cryogenic module for a given input. This input as can be seen consists of the specified allowed boil-off of both the CSS storage tanks. Additionally, the input consists of the amount of insulation layers used on both of the CSS storage tanks. The sizing process of the UCM consists of an initial static sizing process and an iterative sizing process. The static process is where subsystems that are considered to be independent of the other subsystems are sized. In the static process, the CSS, TT&C, and C&DH can be sized. The design principles used to size these subsystems will be elaborated on in Chapter 5 (CSS), Chapter 9 (TT&C), and Chapter 10 (C&DH).

In the iterative process, subsystems that are influenced by one another will be sized. Inside this process there are two tracking objects that continuously keep track of the relevant subsystem masses and the relevant subsystem power requirements. The EPS and TMS require as input the total power consumed by the entire system. These subsystems are sized first and then return their own mass and own power requirement to the relevant tracking objects. The STR requires the total system mass as input and returns its own new mass to the mass tracker object. Similarly, PROP requires the total system mass as input and when run, returns its own mass and power requirements to the relevant tracker objects. Finally, the ADCS is also part of this process as depending on the total mass of the system different amounts of propellant will be required to maneuver the UCM. The sizing processes belonging to the iterative process are described in Chapter 6 (EPS), Chapter 7 (PROP), Chapter 8 (ADCS), Chapter 11 (TMS), and Chapter 12 (STR).

This iterative process is repeated for these five subsystems until the total mass of the system starts to converge. So after the five subsystems are sized, a check is performed to see if the total mass compared to the previous total mass has changed significantly or not. If it has changed significantly, the process is repeated. If it has not changed by more than 1% the process is not repeated and the design process for this specific design has concluded. The outputs of the generator include: relevant masses, relevant powers, and extra information that is stored per subsystem that can be used for the final design.

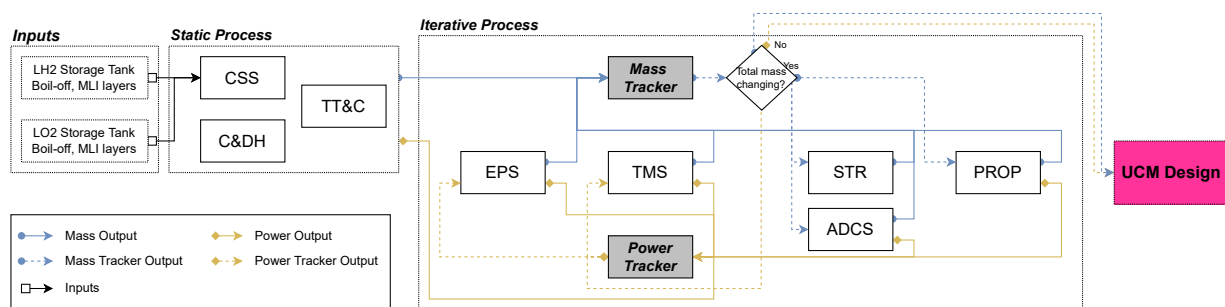


Figure 4.3: Block diagram of the UCM generator architecture.

In order to perform the calculations that will be required to size the universal cryogenic module certain assumptions regarding the propellant, operation times, and environment temperatures have to be made. With regard to the propellant consisting of liquid hydrogen ( $LH_2$ ) and liquid oxygen ( $LO_2$ ) several assumptions with regard to the oxidant to fuel ratio and operating properties were made. For all storage tanks involving cryogenic liquids will be assumed to contain saturated cryogenic liquids with properties adhering to the properties shown in Table 4.2. Constant operating pressures, densities, and temperatures will be assumed.

Table 4.2:  $H_2$  and  $O_2$  Cryogenic Liquid Properties

Liquid	Operating Temperature [K]	Operating Pressure [MPa]	Operating Density [ $\frac{kg}{m^3}$ ]	Latent Heat of Evaporation [ $\frac{kJ}{kg}$ ]
$H_2$	30	1.0	56	447
$O_2$	80	0.1	1191	213

For several subsystems, it is important to have operational durations defined. For example, for the EPS, depending on the how long the UCM is in the dark it will be required to have an energy storage capacity of a size dependent on the time in the dark where no sunlight is available. Following from this, eleven operation modes, corresponding operation durations, and corresponding temperatures that result are displayed in Table 4.3. These values will be used throughout the entire sizing process of the UCM. The time spent in between mission cycles, the idle time ("mode 0") was estimated based on the requirement that the COLD mission has to be able to launch 25 tonnes of propellant every 10 days. This requirement was negotiated with the stakeholders. The

minimum duration of "mode 0" in a mission with four UCMs is 40 days. As the minimum time will be the critical case as explained in Section 8.3.5, this is the value that will be used for the duration of this idle mode.

**Table 4.3:** The phase description, eclipse condition, time, and effective environment temperature corresponding to each mode.

Mode	Phase [-]	Eclipse [-]	Time [h]	Temperature [K]
Mode 0	Idle on Lunar surface	Yes	960.000	48.31
Mode 1	Launch	Yes	0.011	48.31
Mode 2	Ascent	No	0.393	384.95
Mode 3	Orbit	No	11.886	384.95
Mode 4	Orbit	Yes	7.196	96.91
Mode 5	Rendezvous	No	0.000	384.95
Mode 6	Rendezvous	Yes	0.100	96.91
Mode 7	Refuel	No	2.400	384.95
Mode 8	Refuel	Yes	1.600	96.91
Mode 9	Descent	No	0.380	384.95
Mode 10	Landing	Yes	0.033	48.31

As one of the driving stakeholder requirements is concerned with the boil-off of propellant, it is crucial to limit the flight time of the UCM. This is due to the fact that it heats up in orbit is substantially more than in a Lunar crater, especially when exposed to sunlight. In the mid-term report, the duration of ascent, descent and propellant transfer was estimated resulting in a mission cycle of 24 hours when excluding "mode 0" [5].

Using this, the duration of each mode in which the spacecraft will operate was calculated. First, the the total duration of each phase was determined. Using the calculations described in Section 7.4 the time for the launch and ascent phase was determined to total approximately 24 minutes. Using Section 8.3.2, the optimal total rendezvous time of six minutes was determined providing the total duration of the rendezvous phase. The total refuelling phase duration was estimated to be four hours as explained in Section 5.6. Again, using the calculations described in Section 7.4 the descent and landing phase durations were calculated to be approximately 23 and 2 minutes respectively. Using these phase times the orbit phase time could be calculated based on the total 24 hour mission cycle time which lead to approximately 19 hours of orbit time. An overview of these times can be seen in Figure 4.4.

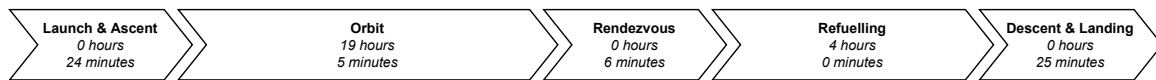


**Figure 4.4:** The UCM 24-hour mission cycle.

The following step was to determine how long the UCM would be in eclipse for each phase so that each mode time could be finalised. For for the launch phase the UCM will be in eclipse as the sunlight will not reach the spacecraft as the crater from which it launches blocks the light. For the ascent phase it was assumed that the spacecraft will be in sunlight as it has escaped the crater. Similarly, for the descent phase it was assumed that the spacecraft would be in sunlight and for the landing phase the spacecraft would once again, be in eclipse. In order to determine, the duration of "mode 3" through "mode 8" the sun and eclipse properties of the orbit would have to be determined.

$$\alpha = \arccos\left(\frac{R_{\text{moon}}}{R_{\text{moon}} + h_{\text{orbit}}}\right) \quad (4.1)$$

$$\theta_{\text{eclipse}} = 2 \cdot \beta = 2 \cdot (90 - \alpha) \quad (4.2)$$

$$f_{\text{eclipse}} = \frac{\theta_{\text{eclipse}}}{360} \quad (4.3)$$

$$f_{\text{sun}} = 1 - f_{\text{eclipse}} \quad (4.4)$$

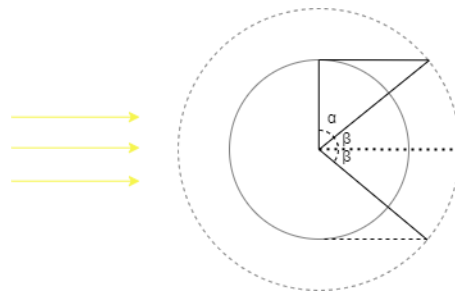


**Figure 4.5:** Relevant angles for shade calculations.

Using Equation 4.1 and Equation 4.2, the angle of the orbit for which the UCM is in eclipse per orbit cycle can be calculated according to Figure 4.5. From these values the fraction of time the UCM is in eclipse and sun can be calculated per orbit using Equation 4.3 and Equation 4.4 respectively. Knowing the radius of the Moon to

be 1737 km and the orbit to be 100 km a total orbit time of 1.963 hour. Using the calculated fractions, this leads to a time in eclipse of 0.774 hour and a time in sun of 1.189 hour per orbit. Propagating these times starting at "mode 3" through "mode 8" using the corresponding phase durations leads to the mode times displayed in Table 4.3.

In addition to knowing the durations of each mode, the effective environment temperature of the UCM had to be determined as well. To calculate the effective temperatures of the modes Equation 4.5 and Equation 4.6 were used [36].

$$T_{orbit} = \left[ \frac{A_C G_s \alpha + A F_{orbit} \epsilon + A F G_s \alpha a K_a}{A \sigma \epsilon} \right]^{\frac{1}{4}} \quad (4.5)$$

$$T_{crater} = \left[ \frac{A F_{crater} \epsilon}{A \sigma \epsilon} \right]^{\frac{1}{4}} \quad (4.6)$$

Where  $A$  is the effective surface area of the spacecraft,  $A_C$  is the cross-sectional surface area of the spacecraft,  $G_s$  the solar flux,  $F$  the view factor,  $\alpha$  the absorptivity of the spacecraft,  $\epsilon$  the emissivity of the spacecraft,  $\sigma$  the Stefan Boltzmann's constant,  $a$  the albedo of the Lunar surface,  $q_{orbit}$  the infrared radiation from the Lunar surface in orbit,  $q_{crater}$  the infrared radiation from the Lunar surface in the crater and  $K_a$  the albedo reflection factor [36]. The crater temperature used is the average of the Shackleton crater, as seen in Figure 4.6 [52].

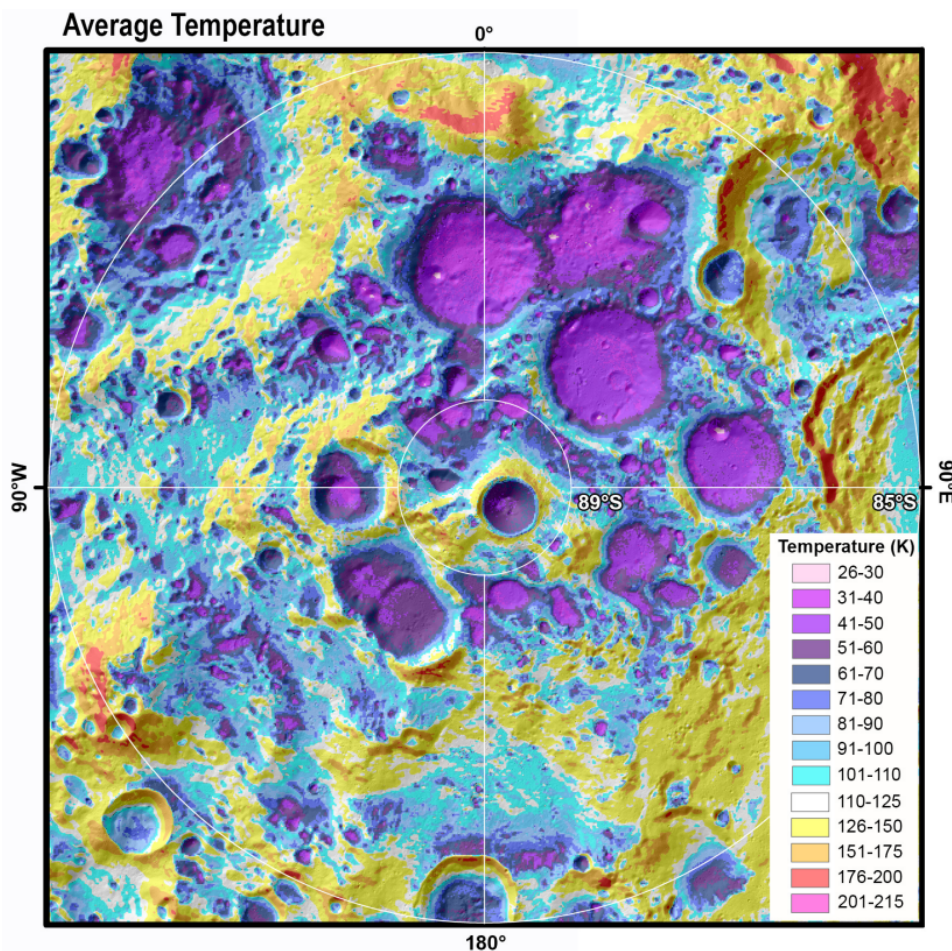


**Figure 4.6:** Average temperature in the crater. The mission will land in the crater closest to the south pole; Shackleton crater.

For the surface area of the spacecraft it was assumed that the spacecraft is a cylinder with a cone on top, with the underside of the cylinder being unavailable due to engines. The values for the size of the cylinder and cone were estimated from values in the midterm report [5]. In Table 4.4, Equation 4.7 and Equation 4.8 all of the values and formulas used can be found. For every mode the specific values of the spacecraft and environment were filled in, leading to the values found in Table 4.3.

**Table 4.4:** Constants related to temperature calculations.

Constant	Value	Unit
$r_{cylinder}$	3.5	m
$h_{cylinder}$	8	m
$r_{cone}$	3.5	m
$h_{cone}$	8	m
$G_s$ [43]	1420	$\frac{W}{m^2}$
$F$ [81]	0.99	—
$\alpha$ [35]	0.06	—
$\epsilon$ [35]	0.88	—
$\sigma$	$5.67 \cdot 10^{-8}$	$\frac{W}{m^2k^4}$
$a$ [43]	0.13	—
$q_{orbit}$ [81]	430	$\frac{W}{m^2}$
$q_{crater}$ [43]	5	$\frac{W}{m^2}$
$K_a$ [81]	0.8	$\frac{W}{m^2}$

$$A = 2r_{cylinder}\pi h_{cylinder} + h_{cone}r_{cone}\pi \quad (4.7)$$

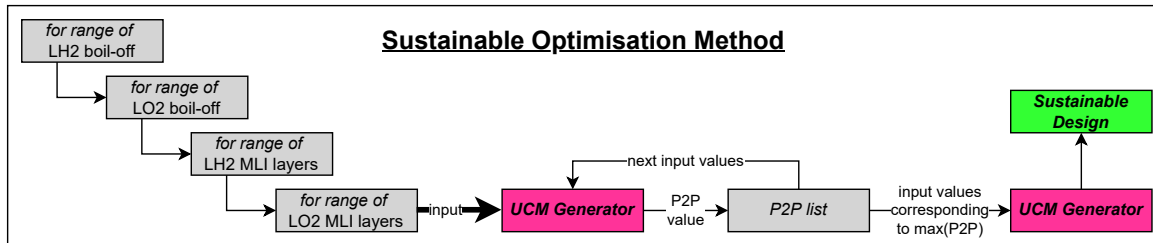
$$A_C = 2r_{cylinder}h_{cylinder} + h_{cone}r_{cone} \quad (4.8)$$

### 4.3. Sustainable Optimisation Method

As mentioned in Section 4.1, the boil-off amount for the propellant and the number of MLI layers are inputs used to size the UCM. In order to decide which combination of these inputs leads to the most desirable design, a criteria to be optimised for has to be chosen. As it is crucial in space projects to minimise the waste of resources a sustainable design criteria was chosen to optimise the UCM design.

$$P2P = \frac{m_{prop,sold}}{m_{prop,purchased}} \quad (4.9)$$

This criteria is the propellant sold to propellant bought ratio which was dubbed the P2P ratio as shown in Equation 4.9. By maximising this ratio, the least possible propellant is wasted whilst meeting the key stakeholder requirements. Figure 4.7 shows how the iterative process to design for the optimal P2P ratio works. For each combination of boil-offs and MLI layers the UCM generator designs a UCM as described in Section 4.2 and computes the P2P ratio. Then the input corresponding to the maximum P2P ratio is run through the UCM generator again resulting in the final design. The results of this iteration will be discussed in Chapter 13.

**Figure 4.7:** Block diagram for the sustainable design optimisation method.

Another note to make, is that both the UCM sizing code and the sustainable optimisation method have been implemented through computer programming. The programming language used is Python. Python was the chosen language as it is high-level (easy to learn) and object-oriented. The object oriented aspect was beneficial as classes allow for easier data bookkeeping and formatting. GitHub was used to facilitate the collaboration amongst team members whilst creating the code to implement the aforementioned sizing and optimisation methods.

# 5 Cryogenic Storage System

The cryogenic storage system has three key functions: store cryogenic liquid hydrogen ( $LH_2$ ) and oxygen ( $LO_2$ ), limit inward and outward heat flow into stored cryogenic liquids, and transfer the stored cryogenic liquids outward. *REQ-TC-UCM-CSS-01* states: "The  $LH_2$  and  $LO_2$  shall be stored separately." From this requirement it follows that the cryogenic storage system shall have two tanks. For each tanks the key functions result in five key elements as shown in Figure 5.1. The structural layer will fulfill the storage function. The insulation layer, cryocooler, and heater will fulfill the function of limiting the net inward and outward heat flows. The transfer mechanism will fulfill the cryogenic transfer function.

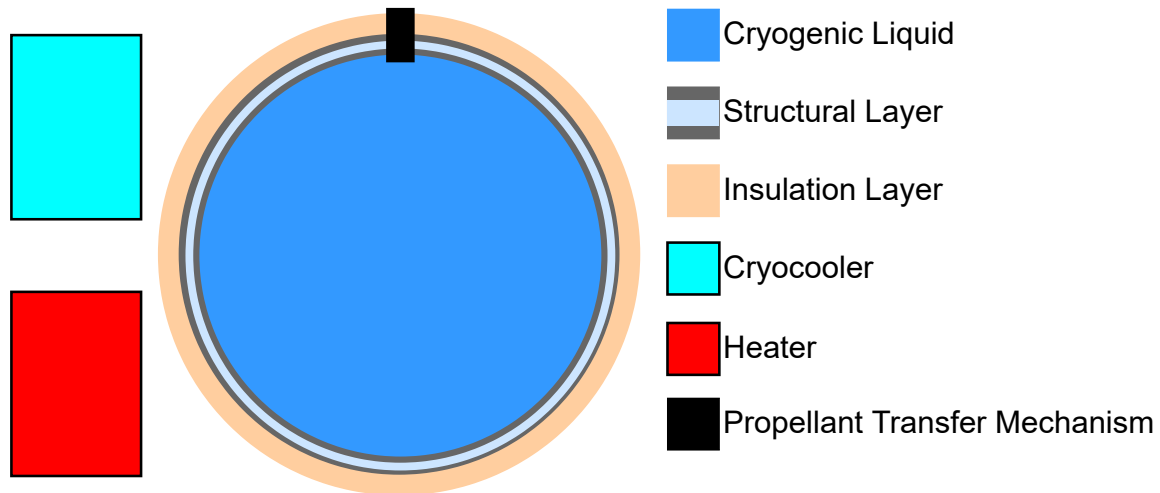


Figure 5.1: Overview of elements of the cryogenic storage system.

This chapter begins by summarizing the previously performed trade-off for and the imposed requirements on the cryogenic storage system in Section 5.1. Then the composite that will be used will be selected and the corresponding structural layer will be sized in Section 5.2 respectively. This will be followed by Section 5.3 describing the insulation choice and sizing method. Furthermore, a renewed heat flow calculation method and the propellant transfer method will be described in Section 5.4 and Section 5.6 respectively. The method of sizing the cryocoolers will be discussed in Section 5.5. Finally, the aforementioned methods will culminate into a large cryogenic storage sizing method in Section 5.7 which can be used in the sustainable optimisation algorithm described in Section 4.3.

## 5.1. Trade-off Summary & Requirements

In the mid-term report a trade-off was performed for various design choices concerning the cryogenic storage system. [5] The shape of each of the storage tanks was chosen to be spherical. Additionally, the trade-off resulted in each tank employing a combination of active cooling in the form of cryocoolers and insulation in the form of multi-layer insulation (MLI). One design choice that had not been made at the end of the mid-term report was the material choice for the structural layer of each tank.

In the mid-term report it was found that the mass of the representative composite design options was about 85% lower than the mass of the representative metal design. This was not the mass reduction predicted [5]. In this report, the structural layer sizing code was fixed which led to a 40% reduction in structural layer mass. This reduction was considered more realistic and in accordance with the sources found. Therefore, the design choice which considered the material choice could be made. Composites will be used for the structural layer of each tank in the cryogenic storage system. The renewed version of the composite structural layer sizing are discussed next in Section 5.2.

Table 5.1 shows the requirements for the CSS that were derived from the stakeholder requirements discussed in Table 4.1. These requirements cover both the storage tanks and the propellant transfer method that will be employed. The requirements touch all elements of the CSS that were described earlier. For example, *REQ-TC-UCM-CSS-27* through *REQ-TC-UCM-CSS-29* cover the failure modes of the storage tanks and are

applicable to the structural layer of each tank. In this fashion all requirements cover a specific element of each tank.

**Table 5.1:** The requirements imposed on the CSS

Requirement ID	Requirement
REQ-TC-UCM-CSS-1	The $LH_2$ and $LO_2$ shall be stored in separate storage tanks.
REQ-TC-UCM-CSS-2	The CSS shall have two spherical storage tanks.
REQ-TC-UCM-CSS-3	The CSS shall be able to store 25 tonnes of propellant at an oxidant to fuel ratio of 5.5.
REQ-TC-UCM-CSS-4	Each storage tank shall use cryocoolers for active cooling.
REQ-TC-UCM-CSS-5	Each storage tank shall use MLI for its insulation.
REQ-TC-UCM-CSS-6	Each storage tank shall be able to sustain at least 25 fill cycles.
REQ-TC-UCM-CSS-7	The $LH_2$ storage tank shall be fillable at a rate of at least 600 kg/s.
REQ-TC-UCM-CSS-8	The $LH_2$ storage tank shall be able to unload its contents at a rate of at least 600 kg/s.
REQ-TC-UCM-CSS-9	The $LO_2$ storage tank shall be fillable at a rate of at least 3500 kg/s.
REQ-TC-UCM-CSS-10	The $LO_2$ storage tank shall be able to unload its contents at a rate of at least 3500 kg/s.
REQ-TC-UCM-CSS-11	The $LH_2$ flow transfer rate shall be measureable to $\pm$ TBD kg/s.
REQ-TC-UCM-CSS-12	The $LO_2$ flow transfer rate shall be measureable to $\pm$ TBD kg/s.
REQ-TC-UCM-CSS-13	The $LH_2$ flow transfer rate shall be controllable within a range of TBD kg/s to TBD kg/s.
REQ-TC-UCM-CSS-14	The $LO_2$ flow transfer rate shall be controllable within a range of TBD kg/s to TBD kg/s.
REQ-TC-UCM-CSS-15	The $LH_2$ storage tank shall have a maximum boil-off rate of 0 g/s on the Lunar surface.
REQ-TC-UCM-CSS-16	The $LH_2$ storage tank shall have a maximum boil-off rate of 0.149 g/s during transfer.
REQ-TC-UCM-CSS-17	The $LH_2$ storage tank shall have a maximum boil-off rate of 0.149 g/s in orbit.
REQ-TC-UCM-CSS-18	The $LO_2$ storage tank shall have a maximum boil-off rate of 0 g/s on the Lunar surface.
REQ-TC-UCM-CSS-19	The $LO_2$ storage tank shall have a maximum boil-off rate of 0.816 g/s during transfer.
REQ-TC-UCM-CSS-20	The $LO_2$ storage tank shall have a maximum boil-off rate of 0.816 g/s in orbit.
REQ-TC-UCM-CSS-21	The $LH_2$ storage tank shall be able to sustain a pressure of 1 MPa.
REQ-TC-UCM-CSS-22	The $LO_2$ storage tank shall be able to sustain a pressure of 0.1 MPa.
REQ-TC-UCM-CSS-23	The CSS shall be able to measure the pressure in each storage tank to an accuracy of $\pm$ TBD Pascal.
REQ-TC-UCM-CSS-24	The $LH_2$ storage tank shall be operable between content temperatures of 20 and 40 Kelvin.
REQ-TC-UCM-CSS-25	The $LO_2$ storage tank shall be operable between content temperatures of 60 and 90 Kelvin.
REQ-TC-UCM-CSS-26	The CSS shall be operable between environment temperatures of 20 and 400 Kelvin.
REQ-TC-UCM-CSS-27	Each storage tank shall be able to vent gases resulting from boil-off.
REQ-TC-UCM-CSS-28	Each storage tank shall satisfy the leak-before burst condition.
REQ-TC-UCM-CSS-29	Each storage tank shall satisfy the critical buckling condition.

## 5.2. Composite Structural Layer

This section will outline the structural layer which makes up the payload tanks. Starting in Section 5.2.1, the concept of the structure is described. Following that is Section 5.2.2 which explains the equations used to size the structural layer of the tanks. Finally Section 5.2.3 presents the materials selected to size the tanks.

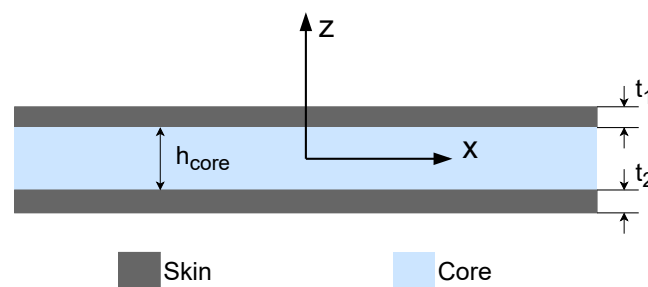


**Figure 5.2:** Overview of the structural layer configuration.

### 5.2.1. Concept

The composite structural layer of each storage tank are made up of three distinct layers: two skin layers and one core layer. A schematic of this can be seen in Figure 5.2. The composite skin layers will be created from a layup which attempts to mimic isotropic mechanical properties. The orientation of the fibres in the layup have been chosen to be  $[0^\circ, +45^\circ, +90^\circ, -45^\circ]$  with respect to the positive direction as shown in Figure 5.3. Considering that the storage tanks will be spherical, the stresses experienced by the structural layer will be uniform. This means that no optimisation using layups can achieve better physical properties in specific directions.

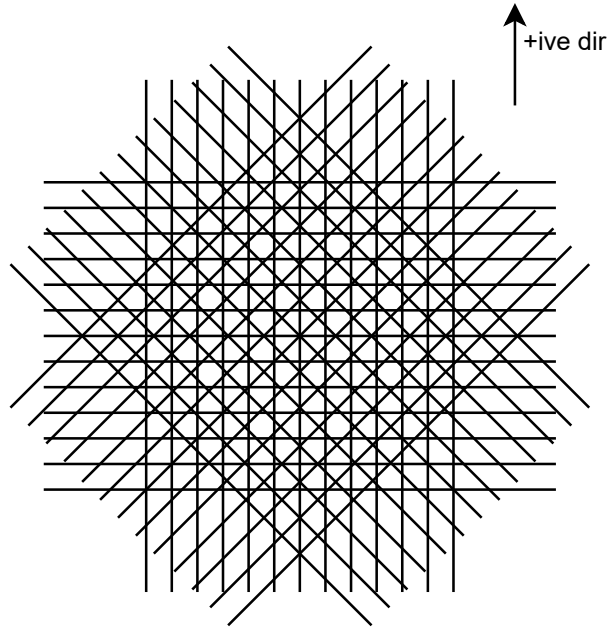


Figure 5.3: Orientation of fibres in layup.

The core layer will provide stiffness to the tank, multiple material options for this core were presented in the mid-term report [5]. The authors have now decided to use an aluminium honeycomb structure using aerogel as an insulative material to fill the voids. Multiple cryogenic tanks documented in literature use this design concept [25]. Properties of this core such as the high shear and compressive strengths compared to other core materials such as foam, significantly reduce the weight of the composite structural layer. The chosen aluminium honeycomb structure has a compressive strength of  $9.31\text{MPa}$  while a foam material (such as carbon-fused aerogel) only has a compressive strength of  $0.763\text{MPa}$ . A drawback of using aluminium honeycombs as the core material is their relatively high thermal conductivity of about  $0.05\text{W/mK}$  compared to the thermal conductivity of  $0.02\text{W/mK}$  for carbon-fused aerogel. However, the tank design for the cryogenic storage system does not rely on the core material as insulation. The primary element of each tank responsible for providing insulation is the insulation layer. The main job of the core material is to ensure that the structure of the tank is as light as possible while meeting the stiffness requirements.

### 5.2.2. Sizing Method

In order to size the structural layer, three variables need to be defined;  $t_1$ ,  $t_2$ ,  $h_{\text{core}}$  (see Figure 5.2). It is assumed that the hoop stress created by the internal pressure is carried by the composite skin layers only (see Figure 5.4). Furthermore compatibility equations can be derived due to the geometric relationship of the two skin layers.

$$t_1\sigma_1 + t_2\sigma_2 = pR \quad (5.1)$$

$$d\theta = \frac{dl_1}{R_1} \quad (5.2) \quad d\theta = \frac{dl_2}{R_2} \quad (5.3) \quad dl_1 = 2\frac{\sigma_1}{E_{\text{comp}}}\pi R_1 \quad (5.4) \quad dl_2 = 2\frac{\sigma_2}{E_{\text{comp}}}\pi R_2 \quad (5.5)$$

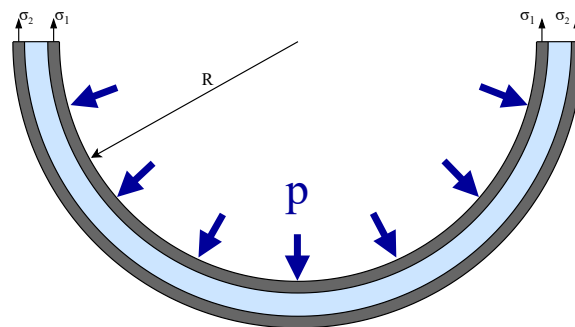


Figure 5.4: Stress experienced by tank skin layers.



Equations 5.1 through 5.5 contain five unknowns:

- $\sigma_1, \sigma_2$  stress in the inner and outer skin layers respectively [Pa].
- $dl_1, dl_2$  the circumference increase of a cross-section of the spherical tank due to the pressure increase of the inner and outer skin layer respectively [m].
- $d\theta$  the angle which is spanned by the arcs  $dl_1$  and  $dl_2$  [rad].

These quantities are used as inputs:

- $t_1$  and  $t_2$ , the thickness of the inner and outer skin layer respectively [m].
- $R$ , the radius of the tank up to the inner skin layer [m].
- $R_1$ , the radius of the tank up to the centre of the inner skin layer ( $R_1 = R + t_1/2$ ) [m].
- $R_2$ , the radius of the tank up to the centre of the inner skin layer ( $R_2 = R + t_1 + h_{\text{core}} + t_2/2$ ) where  $h_{\text{core}}$  is the thickness of the core layer (see Figure 5.2) [m].
- $E_{\text{comp}}$ , the Young's modulus of the composite skin layers, calculated using Equation 5.9 [Pa]

Equations 5.1 through 5.5 form a system of equations which can be solved by creating a matrix equation. This system of equations is solved for various combinations of  $t_1$  and  $t_2$  and it is checked whether the resulting  $\sigma_1$  and  $\sigma_2$  are below the allowable stress,  $\sigma_{\text{allow}}$  of the composite. In addition, it is necessary to check whether the core is not crushed by the outer composite skin. The compressive stress experienced by the core ( $\sigma_3$ ) is calculated using Equation 5.6. In this equation,  $R_3$  is the radius of the tank up to the end of the core layer ( $R_3 = R + t_1 + h_{\text{core}}$ ).

$$\sigma_3 = \frac{\sigma_2 t_2}{R_3} \quad (5.6)$$

Furthermore, in order to determine the minimum thickness of the core, wrinkling of the sandwich structure was investigated. As discussed in [34] there are four modes of wrinkling under compression. Symmetric and anti-symmetric with either full or partial core wrinkling. The failure mode depends on the geometry and the material properties of the sandwich structure. It was found that the desired failure mode with highest critical stresses in the case of our design is anti-symmetric, partial core wrinkling. The compressive force for failure in this mode is given by Equation 5.7 [34].

$$N_{xwr} = 0.51 t_f (E_{\text{comp}} E_{\text{core}} G_{xz})^{1/3} + \frac{G_{xz} h_c}{3} \quad (5.7)$$

Where:

- $N_{xwr}$ , is the compressive load [N/m].
- $t_f$ , is the average thickness of the faces [m].
- $E_{\text{core}}$ , is the Young's modulus in the direction of the thickness [Pa].
- $G_{xz}$ , is the shear modulus in the  $xz$  plane [Pa]

Sandwich wrinkling shall occur in this mode when the core thickness is sufficient and Equation 5.8 is satisfied [34]. Thus, in order to ensure no failure by wrinkling occurs in the tank, the core thickness was chosen such that Equation 5.8 is satisfied. From this it follows that the critical compressive load shall be above the maximum expected compressive load.

$$h_{\text{core}} \geq 3 t_f \left( \frac{E_{\text{comp}} E_{\text{core}}}{G_{xz}^2} \right)^{1/3} \quad (5.8)$$

### 5.2.3. Material Selection

*This section has been completed with the guidance of Prof. C.A. (Clemens) Dransfeld.*

In order to size the tank structure, the materials must be selected. Multiple options were considered and the winning material was selected based on an efficiency factor (see Table 5.2). The composite for the skin layers was selected based on the highest ultimate tensile strength to density ratio as this would lead to the thinnest skin layer and the lightest tank construction (see Equations 5.1 through 5.5). The honeycomb material was sized using data obtained from HexWeb's catalogue<sup>1</sup> where the "5052 Alloy Hexagonal Aluminum Honeycomb"

<sup>1</sup>[https://www.pccomposites.com/wp-content/uploads/2015/07/PCHC4-4TY4\\_TDS.pdf](https://www.pccomposites.com/wp-content/uploads/2015/07/PCHC4-4TY4_TDS.pdf)

was selected. The specific honeycomb structure was selected based on the lowest value for  $\frac{E_{\text{core}}}{G_{xz}^2} \rho_{\text{core}}$  since this results in the lowest thickness for the core (see Equation 5.8) and thus minimizes the mass of the tank. The chosen core material has the following geometrical and material properties:

- $d_c$  - 3.175mm,  $d_c$  represents the cell size as illustrated in Figure 5.6.
- $t_c$  - 0.0762mm,  $t_c$  represents the thickness of the cell wall as illustrated in Figure 5.6.
- $E_{\text{core}}$  - 6.21MPa,  $E_{\text{core}}$  is used in various equations in Section 5.2.2 to size the core material.
- $G_{xz}$  - 1.45MPa,  $G_{xz}$  is used in various equations in Section 5.2.2 to size the core material.
- $\rho_{\text{core}}$  - 123kg/m<sup>3</sup>,  $\rho_{\text{core}}$  is used in order to determine the mass of the tanks.

As mentioned in Section 5.2.1 a layup with orientation [0°, +45°, +90°, -45°] will be used. Effective material properties have been determined. This was done by using the Krenchel efficiency factor,  $\eta$ . For the stated layup,  $\eta = 0.375$  according to D. Richardson<sup>2</sup>. The following equations find the effective material properties:

$$E_{\text{comp}} = E_{\text{prepreg}}\eta \quad (5.9) \quad \sigma_{\text{allow}} = \sigma_{\text{ultimate}}\eta \quad (5.10)$$

Where  $\sigma_{\text{ultimate}}$  is the ultimate stress of the fibres.

By choosing a composite sandwich structure for the tanks, it is important to be aware of a number of aspects. Composites are generally not impermeable to cryogenic liquids and thus often require a liner [45]. For the proposed mission a liner will certainly be necessary due to the long mission life and high reliability requirement, failures such as the one experienced by the X-33 demonstrator project [25] must be avoided. A liner minimizes the contact of the cryogenic liquid with the composite structure, not only does this mean the boil-off losses will be minimized, but also limit the effect of hydrogen embrittlement as discussed in [45]. Hydrogen embrittlement causes the material to degrade, reducing the ductility and increasing the brittleness. This may lead to tank failure when a small deformation is imposed on the tank structure.

**Table 5.2:** Table showing composite options considered for tank skin layers

Carbon pre-preg	$\rho_{\text{comp}}$ [kg/m <sup>3</sup> ]	$E_{\text{comp}}$ [GPa]	$\sigma_{\text{ultimate}}$ [MPa]	efficiency factor
IM10 12k <sup>3</sup>	1,790	190	3,310	1.85
IM7/8552 <sup>4</sup>	1,570	161	2,540	1.62
<b>CYCOM® 5320-1<sup>5</sup></b>	<b>1,310</b>	<b>156</b>	<b>2,700</b>	<b>2.06</b>
HexTow® IM7 (HS-CP-5000) <sup>6</sup>	1,780	168	2,760	1.55
IM600 <sup>7</sup>	1,520	137	3,000	1.97
T800H <sup>8</sup>	1,810	170	2,650	1.46

### 5.3. Insulation Layer

The insulation layer will ensure, in combination with the cryocooler, that the contents of the tanks do not heat up at a rate that makes it impossible to maintain the desired boil-off level. MLI will be used as the insulation layer since it "provides unmatched insulating performance within a given thickness; no other material comes close"<sup>9</sup>. MLI insulation consists of multiple foils generally made of mylar or kapton. These foils are coated with a thin film of highly reflective metal. The foils are spaced by low density spacer materials which also have a very low thermal conductivity. The spacers impede the foils from touching which would severely diminish the insulative properties of the MLI. MLI can maintain a temperature gradient of a few hundred kelvin while generally only requiring a few millimeters of thickness [73].

The MLI layers were sized using commercially available products. Aluminium foil with a fiberglass spacer produced by Frako Term Sp. z o.o.<sup>10</sup> Variant ZLK / ZL was chosen which has the following properties:

- $N$  - 25 layers/cm, this value is used in Equation 5.11 and is a driving term since it is raised to the power of 2.56.

<sup>2</sup><https://sedyono.files.wordpress.com/2016/01/property-prediction.pdf>

<sup>3</sup><https://www.hexcel.com/Products/Resources/1664/hextow-laminate-properties-in-hexply-8552>

<sup>4</sup>[https://energy.ornl.gov/CFCrush/materials/uou/8552\\_eu.pdf](https://energy.ornl.gov/CFCrush/materials/uou/8552_eu.pdf)

<sup>5</sup><https://www.matweb.com/search/datasheet.aspx?matguid=72f0c103cb0141b3b1d2ce210cb811ca>

<sup>6</sup><https://www.matweb.com/search/datasheet.aspx?matguid=0a2c4758da1a4e45a7b0750924cf3ce2&n=1>

<sup>7</sup>[https://pureadmin.qub.ac.uk/ws/portalfiles/portal/241304940/IM600\\_133\\_Material\\_Data.pdf](https://pureadmin.qub.ac.uk/ws/portalfiles/portal/241304940/IM600_133_Material_Data.pdf)

<sup>8</sup><https://www.fibermaxcomposites.com/shop/datasheets/CarbonT800MDS.pdf>

<sup>9</sup><https://www.mtm-inc.com/multi-layer-insulation.html>

<sup>10</sup><https://frakoterm.com/cryogenics/multi-layer-insulation-ml/>

- $\rho_{\text{MLI}} - 0.032 \text{ kg/m}^2$  layer, this value is used to find the mass of the insulation layer in the main sizing function presented in Figure 5.11.
- Minimum operating temperature  $4\text{K}$ , and thus lies comfortably within the operating temperatures of the tanks.

## 5.4. Heat Flow Calculation Method

In order to determine the heat flow into the tank, the insulation layer as well as the structural layer was investigated. In order to model the heat flow through the MLI layers the Lockheed equation is used: [37]

$$q_{\text{MLI}} = \frac{C_c N^{2.56} T_m}{n} (T_3 - T_2) + \frac{C_r \epsilon}{n} (T_3^{4.67} - T_2^{4.67}) \quad (5.11)$$

$$T_m = \frac{T_2 + T_3}{2} \quad (5.12)$$

$$\epsilon = 6.8 \cdot 10^{-4} \cdot T_m^{0.67} \quad (5.13)$$

- $q_{\text{MLI}}$  - total heat flux transmitted through the MLI [ $\text{mW/m}^2$ ]
- $C_c$  - conduction constant ( $8.95 \cdot 10^{-5}$ )
- $C_r$  - radiation constant ( $5.39 \cdot 10^{-7}$ )
- $\epsilon$  - MLI shield-layer emissivity
- $N$  - MLI layer density [layers/cm]
- $n$  - number of MLI layers
- $T_2$  - Temperature at MLI interface with structural layer (see Figure 5.5) [K]
- $T_3$  - Temperature at MLI interface with environment (see Figure 5.5) [K]

In order to calculate the heat flow through the structural layer, only the core is considered. The conductivity of the core ( $k_{\text{core}}$ ) and the heat flow through it ( $q_{\text{core}}$ ) is determined using the following equations:

$$k_{\text{core}} = \frac{k_{\text{alu}} A_{\text{alu}} + k_{\text{gel}} A_{\text{gel}}}{A_{\text{gel}} + A_{\text{alu}}} \quad (5.14)$$

$$q_{\text{core}} = \frac{k_{\text{core}}}{h_{\text{core}}} (T_2 - T_1) \quad (5.15)$$

- $k_{\text{alu}}$  - conductivity of aluminium [ $\text{W/mK}$ ]
- $k_{\text{gel}}$  - conductivity of aerogel [ $\text{W/mK}$ ]
- $A_{\text{alu}}$  - surface area of aluminium hone-comb structure when looking at a cross-section (see Figure 5.6) [ $\text{m}^2$ ]
- $A_{\text{gel}}$  - surface area of aerogel when looking at a cross-section (see Figure 5.6) [ $\text{m}^2$ ]

Looking at Equation 5.11 and Equation 5.14, it can be observed that  $T_2$  is the only unknown parameter. This value can be determined using the fact that  $q_{\text{MLI}}$  and  $q_{\text{core}}$  must be equal to each other once equilibrium has been reached, i.e. the temperature of the layers remains constant. In order to obtain  $T_2$ , a numerical method has been used to find the root of the following expression  $q_{\text{MLI}}(T_2) - q_{\text{core}}(T_2) = 0$ .

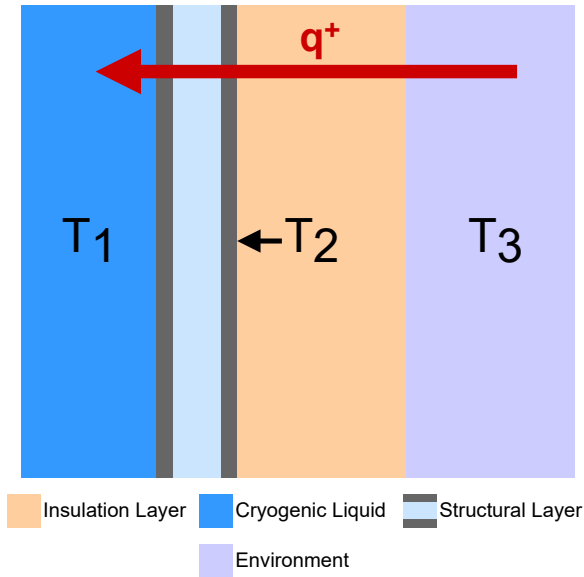


**Figure 5.5:** Temperature definitions for heat flow calculations and positive direction for heat flow ( $q$ ).

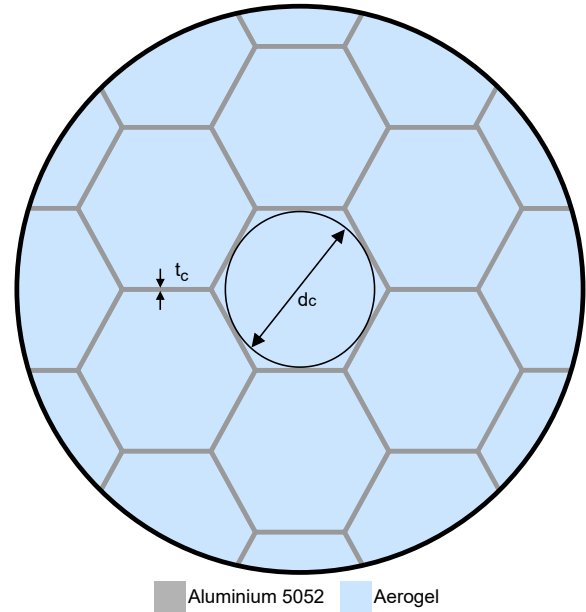


**Figure 5.6:** Schematic of a cross-section of core material with definition of important geometrical quantities.

## 5.5. Cryocoolers

The payload storage tanks will be cooled by cryocoolers, it is thus required to estimate the mass and power consumption of this subsystem. This section describes the sizing methods used to size the cryocooling aspect of the CSS. This sizing will be done based on the required cryocooling heat,  $q_{cryo}$  as well as the temperature of the cold stage  $T_c$  and reject temperature  $T_h$ .

In the case of liquid oxygen, a cryocooler operates by removing a certain amount of heat  $q_{cryo}$  from a cold reservoir at a temperature  $T_c$ . While doing so, the cryocooler will use a certain input power  $P_{in}$  and transfer the heat to a hot reservoir at temperature  $T_h$ . In the case of liquid hydrogen, the storage temperatures are significantly lower. In the range of 6-40 Kelvin. For this, multistage cryocoolers are needed in contrast to liquid oxygen which only require a single stage. Multistage cryocoolers work by arranging single stage cryocoolers in series. Generally placing two cryocoolers in series is sufficient to achieve the temperatures required to store liquid hydrogen. The first stage operates between the temperatures  $T_c$  and  $T_m$  the second stage operates between the temperatures  $T_m$  and  $T_h$  where  $T_m$  is an intermediate temperature between  $T_c$  and  $T_h$ . This reduces the temperature gradient each cryocooler has to achieve [39].

### 5.5.1. Power Sizing Method

The first cryocooler parameter that may be determined is the necessary input power. For both single and multistage cryocooler the total input power is defined as seen in Equation 5.16 where  $\epsilon$  is the Carnot efficiency and  $\eta$  is the efficiency of the cryocooler as fraction of the Carnot efficiency [39]. The Carnot efficiency is also given by Equation 5.17 [10].

$$P_{in} = \frac{q_{cryo}}{\eta\epsilon} \tag{5.16}$$

$$\epsilon = \frac{T_c}{T_H - T_c} \tag{5.17}$$

In order to determine  $\eta$  a separate method is employed for both single and multi stage cryocoolers. For single stage Equation 5.18 from [39] is used.

$$\log_{10}(\eta) = -0.92237 + 0.07763 \log_{10}(1 + q_{cryo}) \tag{5.18}$$

In the case of a multistage cryocooler, Strobridge's correlation from Figure 5.7 will be used. This is the lowest estimation for efficiency compared to others regressions and thus will serve as a conservative estimate. The multistage cryocooler will need to provide a cooling power with an order of magnitude of  $10^2 W$ . Using Figure 5.7  $\eta = 0.1$ .

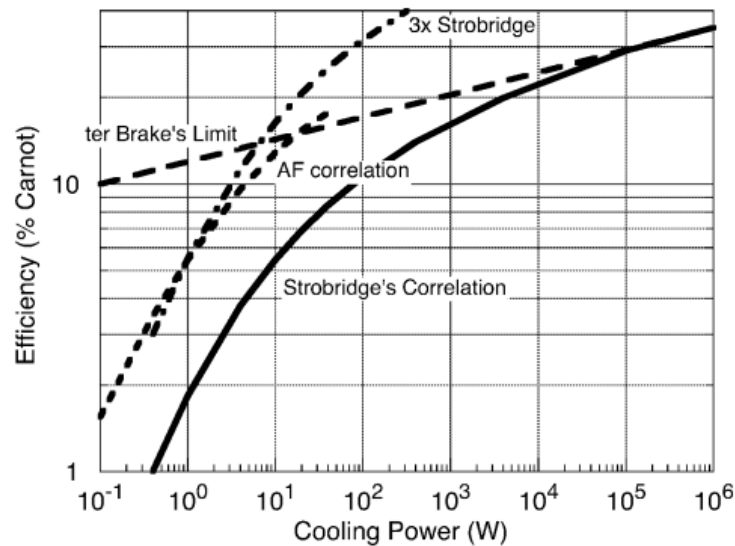


Figure 5.7: Cryocooler efficiency correlations from the data of Strobridge, ter Brake and AFRL [39]

### 5.5.2. Mass Sizing Method

Having estimated the necessary input power for the cryocooler, the next step is to determine an expected mass. This is necessary as the addition of a cryocooling system is an alternative to a purely passively cooled cryogenic tank. System mass can act as a driving criteria for trade-off between alternate configurations as it heavily influences other subsystems such as propulsion. The equations used for mass sizing of single and multi stage cryocoolers respectively are Equation 5.19 and Equation 5.20 as given by [39].

$$m = 0.0711P_{in}^{0.905} \quad (5.19)$$

$$m = 0.1422 * P_{in}^{0.905} \quad (5.20)$$

## 5.6. Propellant Transfer Mechanism

The final step of sizing cryogenic tanks is defining the transfer method of the cryogenic fluid out of the tank itself. Various issues in micro-gravity propellant transfer must be overcome, such as requiring propellant settling in order to avoid gas bubble formation at the location of the pump inlet. In the past, this has been achieved by accelerating at low speeds, facilitating propellant settling at the bottom of tanks, enabling pumping [41].

In order to achieve this acceleration, two methods were considered and compared: linear acceleration and centripetal acceleration. It was assumed that the customer S/C will have a maximum mass of 125 tonnes and the propellant transfer time is four hours to minimise the mission duration. Using these assumptions, the amounts of propellant needed for the spin and burn time were compared. Extrapolating based on the flight-tested relationship in Kutter et al, an acceleration of  $0.00416 \frac{m}{s^2}$  will be required to pump  $1.736 \frac{kg}{s}$ , allowing all 25 tonnes to be pumped over the duration of 4 hours [41].

In the linear case, the low acceleration shall be obtained by actuating the ADCS thrusters for the duration of the burn. In the centripetal case the acceleration shall be obtained by introducing an angular velocity,  $\omega$  into the system using these actuators given by Equation 5.21. These two different acceleration cases are best illustrated by Figure 5.8, where the red refers to the pump location, the yellow to a bearing, and the dark blue to the docking port. In the centripetal acceleration, the propellant collects along the sides of the tank, whilst for the linear acceleration the propellant collects on the bottom. It should be noted that a pump on either side is not required. However, this could be beneficial for the mass moment of inertia.

Based on these concepts, the required burn time and propellant required for the burn will be compared. How these values are calculated can be read in Chapter 8, whilst the values themselves can be found below in Table 5.3. Due to the sole need for an initial burn in the rotational case, a large propellant savings occurs when compared to the linear acceleration, which requires a constant burn throughout the duration of the refuelling. Furthermore, this burn would exceed the maximum RCS burn time of 120 seconds, whilst generating a total  $\Delta V$  of  $60 \frac{m}{s}$  throughout the duration of the burn, which would be detrimental for orbital maintenance. It is for these reasons, that the centripetal acceleration has been selected for propellant transfer method.

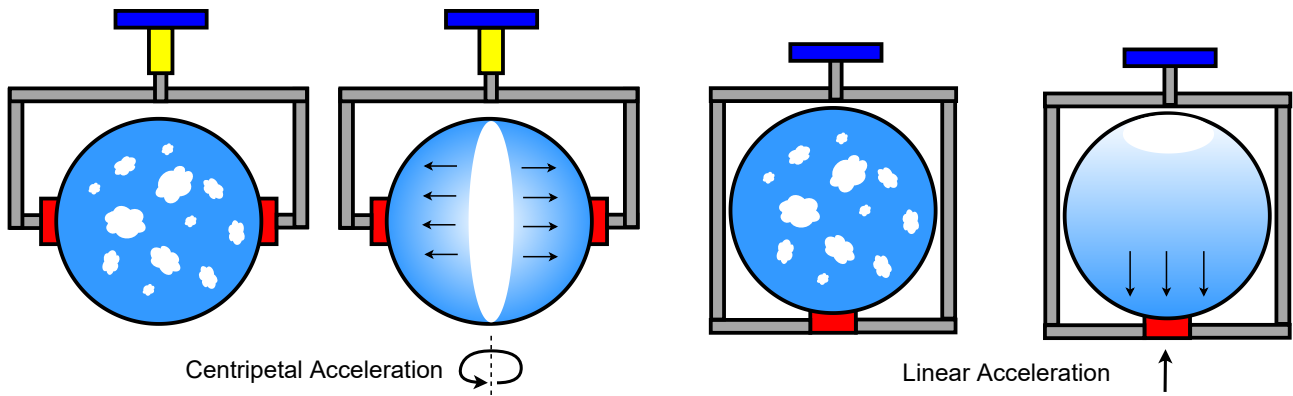


Figure 5.8: Propellant Behaviour for Different Transfer Mechanisms

Table 5.3: Burn Time and Propellant Required Per Fuel Transfer Mode

$$\omega = \sqrt{r_{\text{tank}} \cdot a_{\text{desired}}} = 0.3898\text{RPM} \quad (5.21)$$

	Linear Acceleration	Rotating Spacecraft
Burn Time (s)	14400	5.91
Propellant Required (kg)	8076	6.63

Various further considerations for design must be made in order to incorporate this centripetal acceleration, most notably pump selection and bearing design. Centrifugal pumps shall be used due to the low gravity conditions, in a similar manner to the pumps used in the RLV X-33 [74]. The SICERA® KZ-8L has been selected due to its ability to operate in cryogenic conditions, in combination with its low mass of 32kg, requiring 1.5kW per pump [65]. However, as a result of using the centrifugal pump, an interesting behaviour occurs that has to be accounted for, namely the precession force caused by the gyroscopic effect of the rotating motors. This is caused by the spinning of these pumps away from the center of gravity. This would create a torque on the spacecraft, causing an angular acceleration in a certain direction, in combination with a resulting force perpendicular to the axis of rotation, better explained by means of Figure 5.9b. In order to counteract this, two pumps must be installed with opposite directions of rotation. This will lead to their respective gyroscopic effects cancelling out one another. This is visualised in Figure 6.3. A total of 4 pumps will thus be used, with two sets of counter-rotating pumps, possessing a mass of 128kg and 6kW power required.

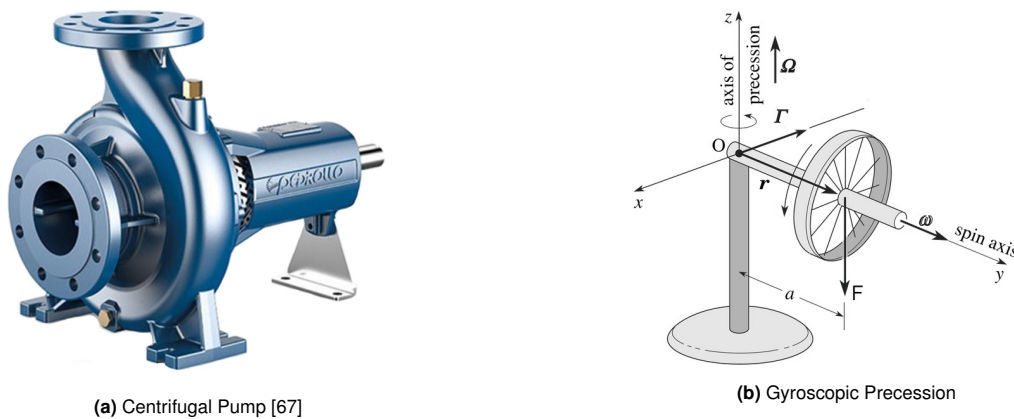


Figure 5.9: Centrifugal pump (left) and gyroscopic precession (right)

Bearings within the pump/feed system will need to be used in order to facilitate the rotation of the spacecraft. The location of these bearings must be along the line of rotation, and as such is it most convenient to be incorporated near the docking mechanism, which will not rotate along with the spacecraft, visible below as the yellow area in Figure 6.3. For these, bearings design for use in cryogenic conditions and pumps shall be used, similar to the SKF-VC4444 bearings suitable for use for liquid hydrogen [67]. Cryogenic bearing have a wide usability range, most commonly used in pumps and for cooling of drill bits and other large-scale industrial applications [67] [15]. These bearings are able to sustain rotation speeds well above the required 0.3898 RPM, whilst not being susceptible to vibrations. These bearings require no lubrication other than the cryogenic liquid for heat dissipation, utilizing Tungsten Disulfide as a dry lubrication within the bearings, whilst being designed for space use and as such as suitable for this application [15] [20]. Heat treatment processes ensures uniform

and consistent material contraction throughout the temperature gradient, preventing eventual stresses or cracks being introduced into the pump and piping system [15].

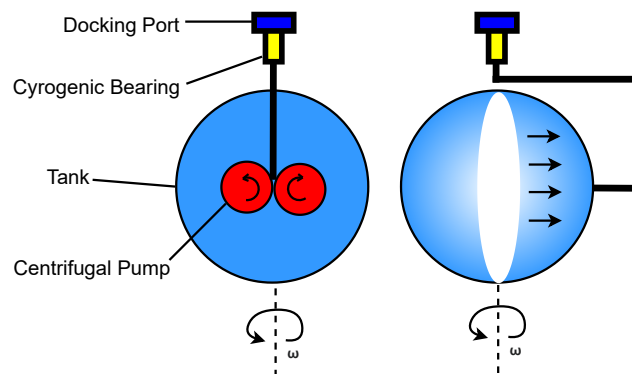


Figure 5.10: Two Counter-Rotating Centripetal Pumps

Furthermore, it should be noted that the heat and friction generated through the pumping system introduces an unavoidable required boil-off into the system. This occurs as a result of the heat generated from the (rotational) motion in (centrifugal) pumps, and is unavoidable as cryocooling within the pumps themselves is unfeasible. This boil off is equal to 1.2% for the hydrogen pumps, and 0.8% for the oxygen pumps, whilst further in the pipe system a boil off of 0.6% will occur and is not avoidable [74]. In order to still deliver the desired propellant, an extra 1.83% hydrogen must be brought with, in combination with 1.41% extra oxygen [74].

## 5.7. Complete Sizing Method

The sizing methods described in Sections 5.2.2, 5.4 and 5.5 were combined in a python script in order to arrive at a converged design. Figure 5.11 shows a schematic of the inputs, outputs and main functions of the script. There are a number of constant inputs:

- **content pressure** - The pressure at which the cryogenic liquid is to be stored 10 and 1 *bar* for liquid hydrogen and liquid oxygen respectively.
- **content volume** - The volume needed to store the required mass of cryogenic liquid 77 and 20  $m^3$  for liquid hydrogen and liquid oxygen respectively.
- **content temperature** - The temperature at which the cryogenic is to be stored 30 and 80 *K* for liquid hydrogen and liquid oxygen respectively.
- **environment temperature** - The temperature the outside of the tank experiences. The spacecraft will experience a range of temperatures, for this multiple modes were defined by the authors. These modes are presented and described in Chapter 11.
- **content latent heat of evaporation** - The latent heat of evaporation of the respective cryogenic liquid. This is needed in order to determine the amount of boil-off for a given heat leak into the tank. 447 and 213 *kJ/kg* for liquid hydrogen and liquid oxygen respectively.

Furthermore there are two inputs that the user varies:

- **number of MLI layers** - The MLI layers used. These will be varied in order to find an optimal design based on the P2P ratio as explained in Section 4.3.
- **boil-off rate** - The allowed boil-off percentage per month. This value will also be varied in order to find an optimal design based on the P2P ratio.

The structural layer sizing function works by iterating over various values for  $t_1$  and  $t_2$ . The required core thickness is then calculated using Equation 5.8 where  $t_f = \frac{t_1 + t_2}{2}$ . Following this, it is made sure that the combination of  $t_1$ ,  $t_2$  and  $h_{core}$  meet the allowable stress requirements, if this is not the case the design is disregarded. After all feasible design options have been collected, the one with the lowest mass is chosen in order to continue the sizing process.

The insulation layer sizing function uses the user input of the number of MLI layers and the outer radius of the tank (from the structural layer sizing function) and calculates the mass of the insulation and the outer surface area of the tank.

Following this, the heat flow calculation method uses the content and environmental temperatures, the core thickness and the number of MLI layers in equations 5.11 and 5.15. Then, using the outer surface area of the tank the inward / outward heat flow is calculated.

The next function is the heat requirement calculator. This function uses the latent heat of evaporation of the cryogenic fluid and the specified boil-off rate to calculate an allowable boil-off mass. From this an allowable (inward) heat flow is calculated and compared to the inward heat flow from the previous block. If the inward heat flow is larger than the allowable heat flow, a cooling requirement is sent to the next block. If the inward heat flow is lower than the allowable heat flow no cooling is required and the following block is not executed. If the environmental temperature is lower than the temperature of the cryogenic liquid, there will be an outward heat flow and a heater is required.

The following two blocks depend on the input from the previous block. If cooling is required as determined by the heat requirement calculator, the cryocooler is sized using equations 5.16, 5.19 and 5.20. If heating is required, the method described in Section 11.3.6 will be used.

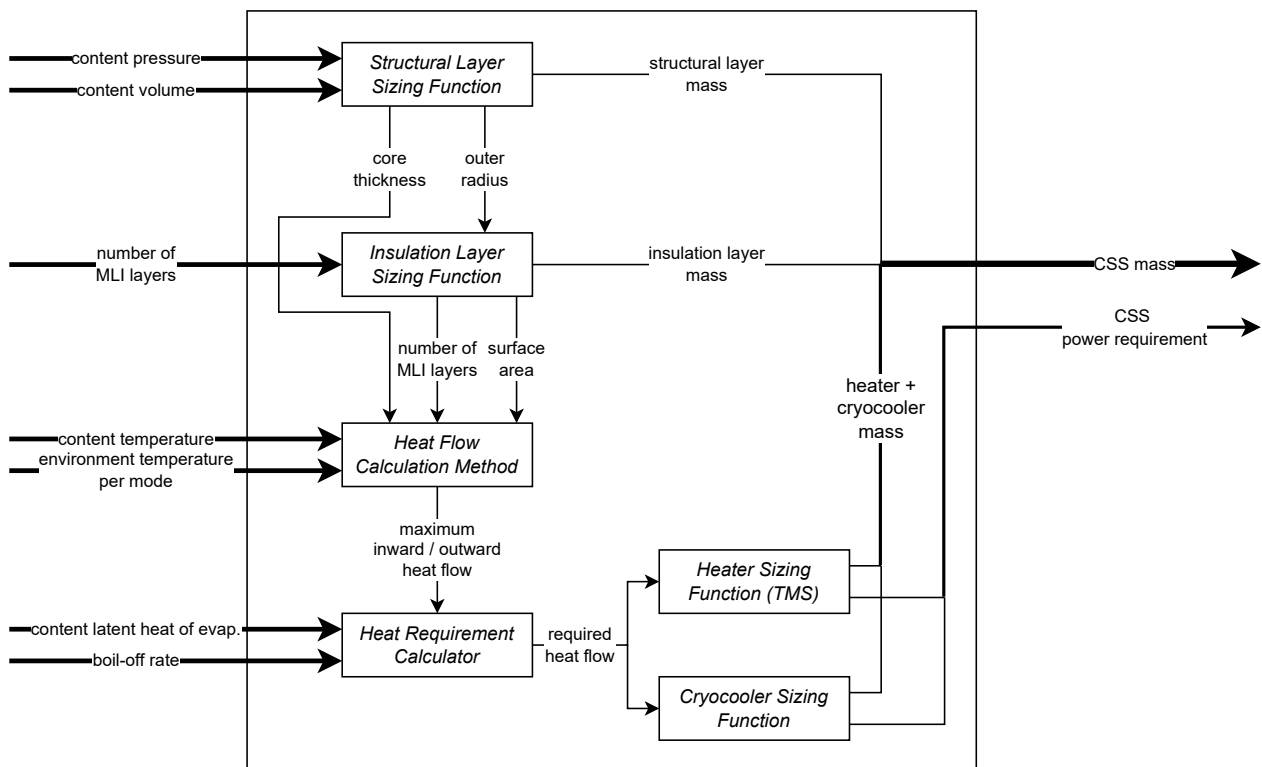


Figure 5.11: Block diagram for the sizing code of the cryogenic storage system.



# 6 Electrical Power System

The electrical power system (EPS) is responsible for providing power to all other subsystems of the UCM. The EPS will consist of three key elements: power generation, power storage, and power distribution. This chapter will first summarise the trade-offs performed and cover the requirements imposed on it in Section 6.1. Then the power consumption profiles will be discussed in Section 6.2, before an overview of the finalised power profiles is provided in Section 6.3. This will be followed by the sizing of the solar panels and fuel cells in Section 6.4 and Section 6.5 respectively. Then a system overview in Section 6.6. Finally, a budget analysis will be performed for this system in Section 6.7, evaluating the cost-effectiveness of the system and possible alternatives.

## 6.1. Requirements & Trade-off Summary

Table 6.1 shows an overview of the requirements on the EPS that followed from the stakeholder requirements (Chapter 4) and the aforementioned trade-off. The requirements cover efficiency, reliability, power, and energy related values. Prior trade-off resulted in a concept selection wherein fuel cells are used in eclipse, whilst idling and in the crater, and solar cells in sunlight. This concept allowed for the best compromise as a result of the trade-off between weight, sustainability, and reliability.

**Table 6.1:** EPS requirements

ID	Requirement
<i>REQ-TC-UCM-EPS-1</i>	The solar panels shall provide 3524 W at EOL%
<i>REQ-TC-UCM-EPS-2</i>	The solar panels shall have a degradation of no more than 3% per year
<i>REQ-TC-UCM-EPS-3</i>	The EPS shall provide 3524 W via solar panels when in sunlight
<i>REQ-TC-UCM-EPS-4</i>	The EPS shall provide 9343 W via fuel cells during idle and eclipse
<i>REQ-TC-UCM-EPS-5</i>	The dry mass of the fuel cells shall be no more than 5 kg
<i>REQ-TC-UCM-EPS-6</i>	The fuel cells shall have an efficiency of 50%
<i>REQ-TC-UCM-EPS-7</i>	The power distribution unit shall have an efficiency of 80%
<i>REQ-TC-UCM-EPS-8</i>	The UCM's shall be self-sufficient for power generation needs

## 6.2. Power Consumption Profiles

The operational modes that were described in Section 4.2 (Table 4.3) are important to the sizing process of the EPS. Whether the UCM is in the sun or not will dictate whether the fuel cell or solar panel will be used. When the UCM is in sunlight, solar panels will be used, whilst in eclipse the fuel cell shall be used. The exceptions being the ascent, descent, and refuelling modes where the fuel cell will be used for reliability reasons. When in eclipse, and whilst idling in the crater the fuel cells will be used. An overview showing the aforementioned modes can be found in Table 6.2.

**Table 6.2:** Operational Modes of the EPS

Mode #	Description	Eclipse	Operational System	Time (h)
<i>Mode 0</i>	Idling in Crater	Yes	Fuel Cell	>960.00
<i>Mode 1</i>	Launch	Yes	Fuel Cell	0.10
<i>Mode 2</i>	Ascent	No	Fuel Cell	0.39
<i>Mode 3</i>	Orbit-Sun	No	Solar Panel	11.89
<i>Mode 4</i>	Orbit-Eclipse	Yes	Fuel Cell	7.19
<i>Mode 5</i>	Rendezvous-Sun	No	Solar Panel	0.10
<i>Mode 6</i>	Rendezvous-Eclipse	Yes	Fuel Cell	0.10
<i>Mode 7</i>	Refuel-Sun	No	Fuel Cell	2.40
<i>Mode 8</i>	Refuel-Eclipse	Yes	Fuel Cell	1.60
<i>Mode 9</i>	Descent	No	Fuel Cell	0.38
<i>Mode 10</i>	Landing	Yes	Fuel Cell	0.30

For the solar panel sizing, the peak power for each of its active modes will be most important. However, for the fuel cells, not only the peak power will be important but also the duration of each mode. This is because the

fuel cells will need to bring a specific amount of propellant depending on both the peak power and the duration of the corresponding mode. These durations can also be found in Table 6.2. Throughout the sizing method sections in this chapter, these power profiles will prove essential.

### 6.3. EPS System Profiles

An overview of the EPS power generation profiles for different modes is presented below in Table 6.3, based on the power requirements collected in Chapters Chapter 13. Based on analysis of these power modes, it can be determined that Mode 7 is critical for fuel cell use, requiring a power of 9343 W, whilst Mode 5 is critical for solar cell use, requiring a power of 3524 W, and as a result these components must be sized accordingly.

**Table 6.3:** Power Required Per Usage Mode in Watts.

Subsystem/Mode	0	1	2	3	4	5	6	7	8	9	10
ADCS	3122	286	286	264	264	299	299	250	250	286	286
CDH	60	180	60	60	60	180	180	60	60	60	180
CSS	0	0	2391	2391	0	2391	0	2391	0	2391	0
EPS	206	49	216	220	60	231	55	219	51	216	57
PUMP	0	0	0	0	0	0	0	6000	6000	0	0
TMS	123	123	123	123	123	123	123	123	123	123	123
TTC	75	225	225	300	300	300	300	300	300	225	225
<b>TOTAL</b>	<b>3586</b>	<b>863</b>	<b>3301</b>	<b>3358</b>	<b>807</b>	<b>3524</b>	<b>957</b>	<b>9343</b>	<b>6784</b>	<b>3301</b>	<b>871</b>

This can better be visualised by means of Figure 6.1, wherein the power consumption throughout the entire mission duration can be seen. This further allows the critical cases for the fuel cell and solar panels to be visualized, being the peaks at power point 7 and point 5 respectively. It should be noted that for Mode 0 the non-generative power requirement is assumed, as peroxide production will not occur near (within an hour) to the take-off and landing.

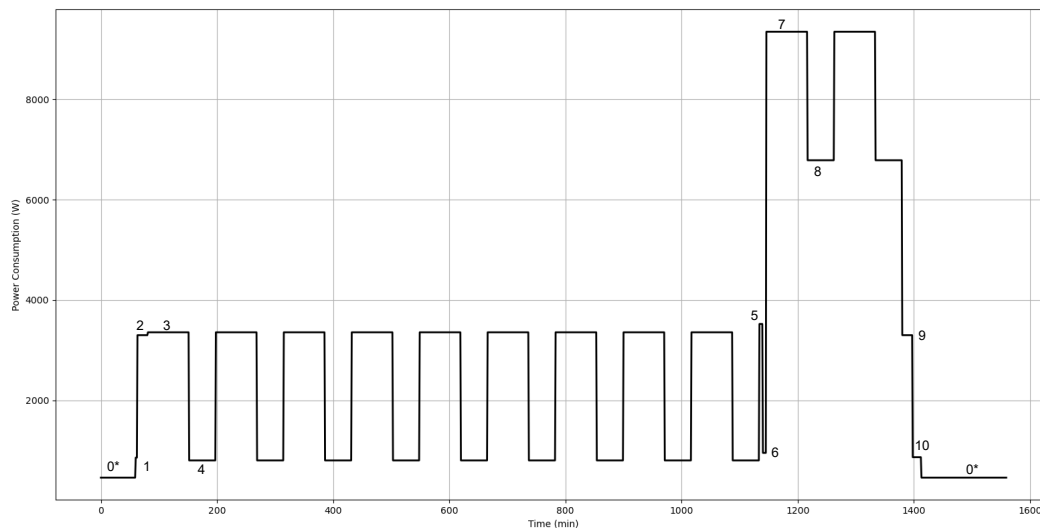


**Figure 6.1:** EPS Power Consumption During a Refuel Mission

### 6.4. Solar Panel Selection, Configuration, & Sizing

There exist big differences between different types of solar panels. Some optimise weight per wattage produced, meanwhile, some optimise for weight per square meter. Selecting the right solar panel for this mission is therefore critical. As preliminary estimations of the spacecraft size, derived from the size of the payload and propulsion tanks and wattage per meter of a space grade solar panel [5], show that the surface area of the spacecraft will not be a limiting factor for the solar panels. As deployment mechanism of solar panels tend to be the main mode of failure [86], body mounted solar panels are preferred. Factoring in the fact that there is a large amount of available surface area on the spacecraft, body mounted solar panels are the best configuration option, in combination with the low TRL of high cycle redeployable solar panels.

Considering that surface area will not be the constraining factor, the solar panels should be optimised for wattage per weight;  $\frac{W}{kg}$ . The solar panel type with the highest value of  $\frac{W}{kg}$  was found to be of the triple junction Gallium Indium Phosphide/ Gallium Arsenide/ Gallium Indium Arsenide (GaInP/GaAs/GaInAs) type, designed by Microlink Devices Inc. This solar panel demonstrated that it could produce  $3.8 \frac{kW}{kg}$  [13]. In Table 6.4 a data sheet is given for the chosen solar panel.

**Table 6.4:** Data sheet for Microlink Devices' GaInP/GaAs/GaInAs solar cell[13].

Characteristic	Value	Unit
Solar cell area	20	cm <sup>2</sup>
Short current density ( $J_{sc}$ )	15.93	$\frac{mA}{cm^2}$
Open circuit voltage ( $V_{oc}$ )	3.0	V
Watt per solar cell	0.9558	W
Fill factor	86.89	%
Watt per square meter	415.8	$\frac{W}{m^2}$
Efficiency at AM0 1-Sun	30.4	%
Specific power solar cell	3.8	$\frac{kW}{kg}$
Specific power solar panel	1.7	$\frac{kW}{kg}$
Cost	2000	$\frac{\$}{W}$

Using this data, the mass and size of the solar panels can be estimated. It should be noted that the solar cells themselves are assumed to be fixed, and as such rigidly mounted onto the surface of the structure. This allows weight savings on the structural size, having thin cells without heavy deployment mechanisms, determined through the following equations.

$$M_{Panels} = \rho_{area} \cdot A_{Panels} \tag{6.1}$$

$$A_{Panels} = \frac{P_{Req}}{S \cdot \eta_{EOL}} \tag{6.2}$$

### 6.5. Fuel Cell Sizing

One of the most important factor to consider when sizing for a hydrogen fuel cell system is the required size of the system, as larger membrane areas allow a larger amount of power to be generated, with current peak fuel cell performance able to produce  $370 \frac{mW}{cm^2}$  [54]. Based on this peak power density per area, a selection of efficiency and weight of the fuel cell system must be made. An overview of these options can be found below in Table 6.5 [4]. Sizing for optimum weight/fuel cell efficiency, a stack efficiency of 50% has been selected, producing a fuel cell of weight  $10 \frac{kg}{m^2}$ . Fuel cells of this efficiency also typically have a much higher TRL and lifetime, providing a more reliable system for long-term use [4]. This area density, in combination with the aforementioned power density per area allows the fuel cell to be sized, highlighted below in Equation 6.3. This peak efficiency produces power at 0.7 V, and thus must be transformed to higher or lower voltages for individual sub-components [54].

**Table 6.5:** Fuel Cell Efficiency and System Weight [4]

$$M_{Fuel Cell} = \frac{\text{Weight Density}}{\text{Power Density}} \cdot \text{Power} = \frac{\frac{kg}{m^2}}{\frac{W}{m^2}} \cdot W \tag{6.3}$$

Efficiency (%)	Fuel Cell Weight ( $\frac{kg}{m^2}$ )
0.3	5
<b>0.5</b>	<b>10</b>
0.6	25

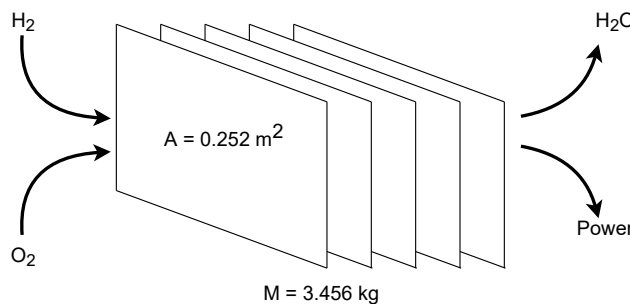


**Figure 6.2:** Fuel Cell Sizing

Based on this usage, the fuel required for the fuel cell can be estimated for the different usage modes, using the formulas below, where  $m$  corresponds to the molar mass.

$$M_{\text{Oxygen}} = \frac{m_{\text{oxygen}}}{2 \cdot m_{\text{hydrogen}}} \cdot M_{\text{Hydrogen}} \quad (6.4)$$

$$M_{\text{Hydrogen}} = \frac{P_{\text{Req}} \cdot t_{\text{missionHours}} \cdot f_{\text{eclipse}}}{\text{Specific Energy Liquid Hydrogen} \cdot \eta_{\text{Fuel cell}}} \quad (6.5)$$

## 6.6. System Overview

An overview of the associated system results are summarized below in Table 6.6. It should be noted that for redundancy, additional solar panels area shall be included across the surface of the spacecraft, facilitating power generation without precise attitude positioning with respect to the sun, in combination with an additional fuel cell for redundancy. An overview of the origin of these values can be found in Chapter 13. Cost results are further elaborated upon in Section 6.7.

**Table 6.6:** EPS System Results

Peak Solar Panel Power (W)	3523.52
Peak Fuel Cell Power [W]	9342.69
Solar Panel Mass [kg]	2.07
Solar Panel Size [m <sup>2</sup> ]	11.97
Fuel Cell Mass [kg]	3.46
Overall 10Y System Cost [\$]	146,286,155

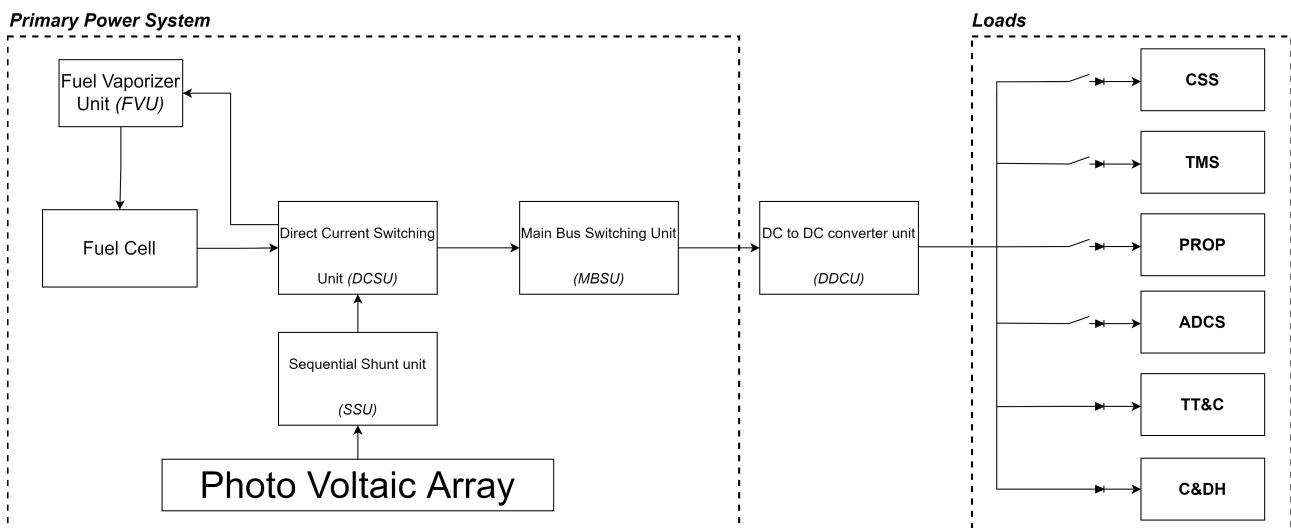


**Figure 6.3:** Electrical block diagram of UCM.

## 6.7. EPS Budget Analysis

Evaluation of the selected EPS system compared to other alternatives is fundamental in the decision for which EPS system will be implemented. 6 operational configurations were considered, 4 of which provided self-sufficient power generation, whilst 2 of which involved directly purchasing power from the Artemis program. The self-sufficient power generation options considered were that of purchasing fuel regularly from the Artemis program, or having an additional lander placed in the sunlight of the crater, which will then transfer power to the UCM modules. All surface to surface power transmission methods incur the use of an additional lander, and this must generate sufficient power for all of the 4 stationed UCM modules, and is assumed to be a light-weight retrofitted version of the UCM, with a reduced price of 300\$ M. Solar panels shall be used for power generation on this crater edge during sunlight, and during the 65 hour Lunar nights, the UCM shall then switch to using the hydrogen fuel cell. The power transfer methods considered were copper wire transmission, radio frequency transmission, and laser transmission. The distance in question will be from the edge of the crater rim where sunlight is present, to the basin of the crater, where the water ice is present, and as such the UCMs shall be stationed for refuelling, visible below in Figure 6.4. This distance can be approximated as 11.30 km, however for comparison with Kerslake et al, a distance of 10 km shall be approximated [38].

Of the 3 surface to surface power transmission methods, copper wire transmission has the highest efficiency and TRL of 9, however requires the use of an additional rover for laying of the wire. A rover capable of this feat

selected for reference is the NASA Viper Rover, incurring an additional cost of 433.5\$M, however this cost will likely be higher due to the cost of retrofitting for the additional spool laying mechanism and to be able to hold the high-mass (8223 kg) spool [49]. Whilst the amount of expensive instrumentation on the rover can be limited, the redesigning of the rover to be able to handle the payload will likely incur higher costs than the instrumentation itself. The radio-frequency transmission system incurs the use of state of the art magnetrons, and requires deployable transmission and receiving dishes for packaging in launch. Frequency optimisation encourages the use of a 5.8 GHz transmitter, however the efficiency of this system quickly drops off with distance, proportional to the inverse square law [38]. Laser transmission facilitates power beaming by use of laser, having similar efficiencies irrespective of distance to the source, with laser temperature optimisation encourages the use of a 293 K laser. Laser transmission however produces a large heat flux on the spacecraft itself, equal to 5 times the solar heat flux, requiring the incorporation of significant heat shielding on the UCM [38]. An overview of the associated efficiencies of each system, optimised for a 10 km range Lunar surface-to-surface power transmission in accordance with Kerslake et al, can be found below in Figure 6.4.

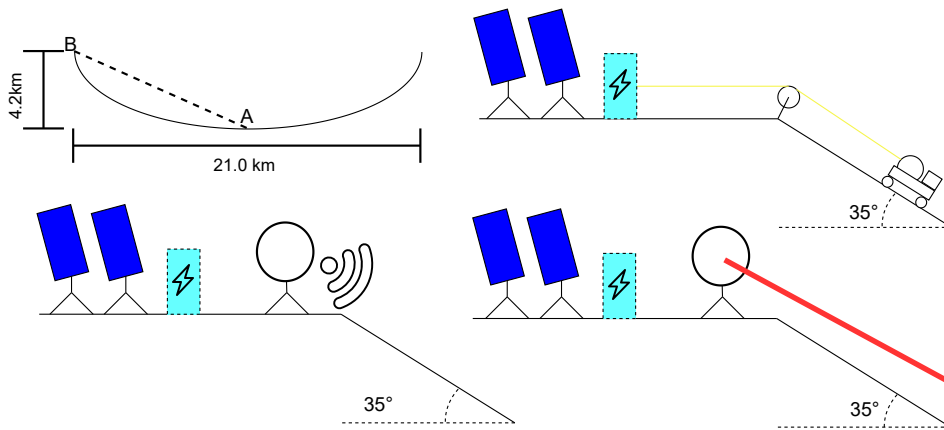


Figure 6.4: Surface To Surface Power Generation Methods

For this analysis, a idle power requirement of 4 kW was assumed, in combination with an required  $H_2O_2$  mass of 1050 kg, providing a safety margin on the aforementioned idle power required of 3586 W. An important factor for consideration is the associated cost for the Artemis program of producing propellant and water, summarized below in Table 6.7 [14]. Using the total mission power spent on each part of the manufacturing process, and overall fuel cost per kg, a proportional relationship can be assumed to determine the associated cost per kilogram of water. This cost can be assumed to be the price both at which water shall be purchased at, and sold back to Artemis, as they would no longer have to expend the additional energy on water extraction. This in term implies fuel can be purchased for  $500 - 142.86 = 357.14 \frac{USD}{kg}$ , if the water produced is directly sold back to Artemis. It should be noted that there will likely be additional costs incurred on Artemis' side from storing water in the Lunar crater, in combination with the extra power required for this storage, however the feasibility of this investigation will be limited to the production costs.

Table 6.7: Artemis Program Cost Distribution

Manufacturing Process	Power Required [W]	Percent Total Power	Cost Per [kg]
Mining	800	0.286	142.86
Electrolysis	1235	0.441	220.54
Residual Systems	765	0.273	136.61
Total	2800	1	500

A cost analysis must be made for both reoccurring material costs, in combination with upfront hardware costs. For the reoccurring material (fuel) costs, two cost periods shall be considered, namely that in which  $H_2O_2$  is being generated, and that in which it is not being generated. For the  $H_2O_2$  generation period, the power requirement is 4 kW, and an excess water amount of 2.59 kg per day shall be generated, which can then in turn be sold back to the Artemis mission. During the non  $H_2O_2$  generation period, the period requirement is assumed to be 500 W, with all excess water produced being sold back to Artemis, reducing the propellant cost to the aforementioned  $357.14 \frac{USD}{kg}$ . An overview of the costs that will be incurred throughout the mission is summarized

below in Table 6.8, where the factor of operation (FO) refers to how often this cost will occur, with each launcher idling, and 10 launches per year. A similar cost is incurred for the surface to surface transfer systems, however only during the long Lunar eclipse periods, accounting for 17.9% of surface time, also presented below in Table 6.8. In this scenario, local power generation will be occur via means of hydrogen fuel cell in the UCM, requiring fuel.

**Table 6.8:** Recurring Costs of Fuelcell-based EPS System

	Mass [kg]	Cost (\$)	FO	Cost 1Y (\$)	Cost 10Y (\$)
<b>Fuel-Cell Based Systems</b>					
Purchased $H_2 + O_2$ (Generation)	1,827	913,628	10	9,136,282	91,362,829
Sold $H_2O$ (Generation)	103	-14,823	10	-148,230	-1,482,300
Purchased $H_2 + O_2$ (Idle)	1,777	634,966	4	2,539,864	25,398,649
				<b>11,527,917</b>	<b>115,279,178</b>
<b>Surface To Surface Systems</b>					
Purchased $H_2 + O_2$ (Night)	318	113,658	4	454,635	4,546,358
Purchased $H_2O$ (Generation)	1,225	175,000	10	1,750,000	17,500,000
				<b>2,204,635</b>	<b>22,046,358</b>

In combination with these costs, the initial system hardware costs and weights must additionally be considered. In accordance with Kerslake et al, these costs and weights are presented below in Table 6.9. It should be noted that the efficiencies of the system result in different required origin power generation requirements, with most notably the low efficiency of the radio-frequency system creating incredibly high lander power demands. Furthermore, the power required at origin refers to the power needed to be generated at the lander, however for the fuel cell system it refers to how much power the Artemis mission will expend to create the fuel. Furthermore, the solar panel size refers to the solar panel size on the lander itself for the surface to surface power transfer mechanisms, but for the panel size on the UCM itself for the fuel cell system.

**Table 6.9:** Initial System Costs and Total EPS System Costs

	Fuel Cell	Copper Wire	Radio Frequency	Laser
Efficiency w.r.t. Origin Power (%)	40.00	71.90	0.10	19.60
Power Gen Req @ Origin (W)	40,000	22,253	16,000,000	81,633
Power Transfer System Mass (kg)	0	8223	87872	1677
EPS Mass (kg)	14.94	16.59	4,221.26	32.21
EPS Panel Size* ( $m^2$ )	54.37	75.62	54369.82	277.40
EPS Lander Cost (\$)	0	44,506,259	32,000,000,000	163,265,306
EPS 4x UCM Cost (\$)	31,006,976	31,006,976	31,006,976	31,006,976
Material Reoccurring Costs 10Y (\$)	115,279,179	22,046,358	22,046,358	22,046,358
<b>Fixed Costs (\$)</b>	<b>146,286,155</b>	<b>97,559,593</b>	<b>32,053,053,334</b>	<b>216,318,640</b>
Lander Cost (\$)	0	300,000,000	300,000,000	300,000,000
Rover Cost (\$)	0	445,000,000	0	0
<b>Total Costs (\$)</b>	<b>146,286,155</b>	<b>842,559,593</b>	<b>32,353,053,334</b>	<b>516,318,640</b>

From analysis of this table, it is evident that the purchasing fuel option is the most cost effective configuration. This is largely driven by the high costs of landing another spacecraft solely for power generation, and the rover costs from cable-laying. It should be however noted that these values are highly speculative, and are subject to changes based on lander and rover design, further requiring additional operational costs. It can however be concluded that this will be the cheapest option in all scenarios, as it is unfeasible to provide a Lunar lander and rover for under \$48,726,562, under which would be the price points for which the surface to surface power transfer options are cheaper.

### 6.7.1. Sensitivity Analysis

In order to analyse the legitimacy of the budget analysis, a sensitivity analysis must be performed. This budget is most sensitive to propellant price and power required of the system, and as such, a sensitivity analysis will be performed for these variables. The price of propellant shall be analyzed from  $500 - 3750 \frac{\$}{kg}$ , as this is the feasible purchase range from Artemis [14]. Power ranges on the other hand shall be analyzed in the range of  $0 - 10$  kW, however it should be noted that these values refer to the peak power requirements on the Lunar surface, whilst  $H_2O_2$  is being generated, as this is the most relevant mode for cost analysis. The same method used in Section 6.7 shall be used for this. The results of this can be found below in Figure 6.5 and Figure 6.6. It should be noted that the EPS system cost is highly dependant on the deployment rover costs, and as such the costs of

the system with and without these support components has been analysed. Furthermore, the radio-frequency option has been disregarded for the sensitivity analysis due to the incredibly high system cost as a result of the transmission losses experienced.

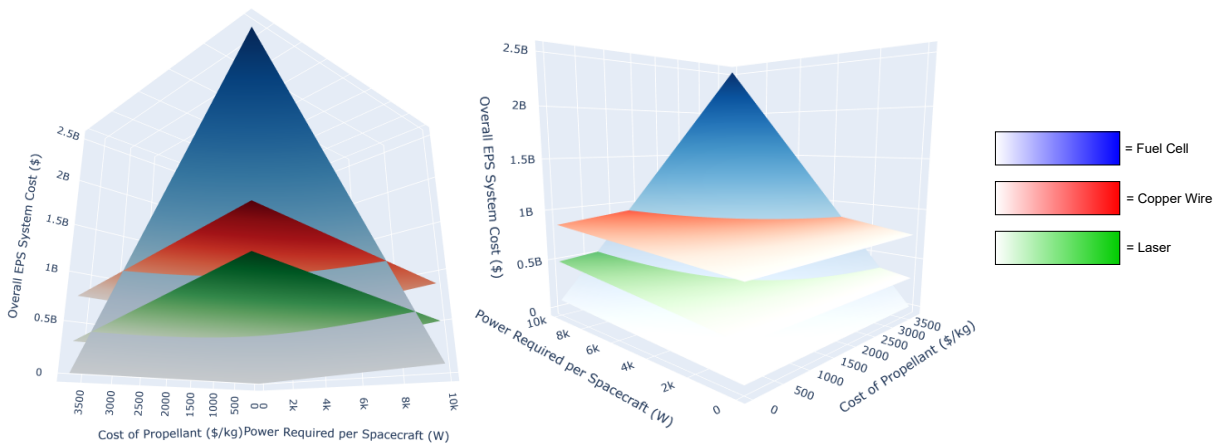
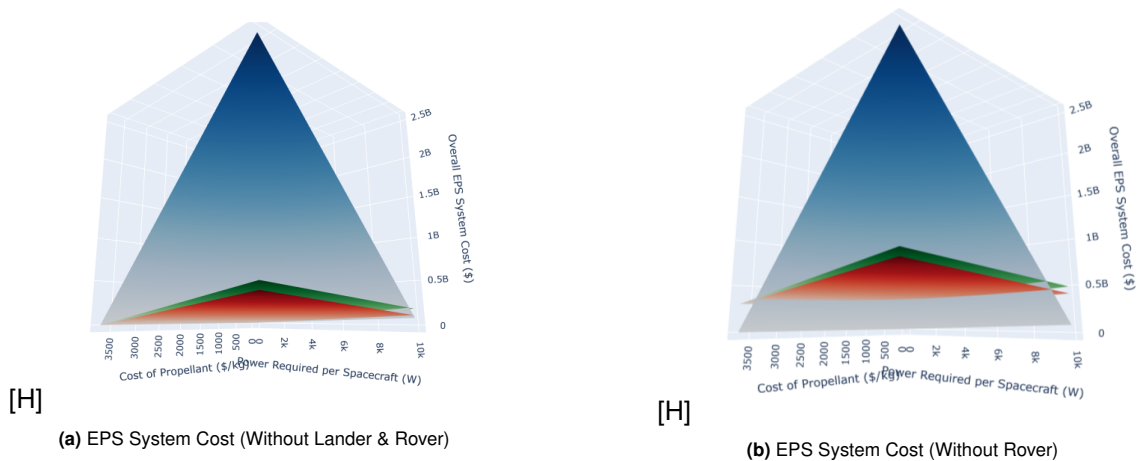


Figure 6.5: EPS System Cost (With Support Components)

Upon analysis of these sensitivity results, it can be determined that the fuel cell system is highly sensitive to both propellant costs and the system power required, with it being the most cost-effective system in relatively lower power and cost ranges, with the laser system being the most cost-effective system in the higher power required and cost regions. This is not to the same extent true for the copper wire and laser based systems, having a relatively stable prices as a result being less dependent on power required and cost of propellant. Furthermore, this analysis verifies the selection of the fuel cell based system for our specified idle power range, namely at the power required of 4 kW and price point of 500\$. Figure 6.6 on the other hand assists in determining the root cause of this, as the system costs without the lander and rover and without the rover are displayed respectively.



[H]  
(a) EPS System Cost (Without Lander & Rover)

[H]  
(b) EPS System Cost (Without Rover)

Figure 6.6: EPS System Costs without Various Support Components

From this, it can be determined that the large majority of the costs incurred for surface to surface systems originate from these lander and rover costs. The rover costs are the largest expenditure for the copper wire based system, and as a result, without these costs, it outperforms both the laser and fuel cell based systems in the majority of higher power and price ranges. This could potentially be achieved by using one of Artemis' rovers for spool deployment, or by re-using a maintenance rover should this rover be required. Without these rover costs, the copper wire system can outperform the fuel cell system by factor 5 in the higher power and cost ranges, however it can be determined that for the specific mission scenario in question, the fuel cell system does indeed offer the most cost-effective solution. This is better visualized via means of Figure 6.7, providing a bottom-view of Figure 6.6b. In this figure, it becomes apparent which option provides the most cost effective solution for all power and price levels, with the 4 kW power consumption and 500\$ price point falling in the range of the fuel cell scenario.

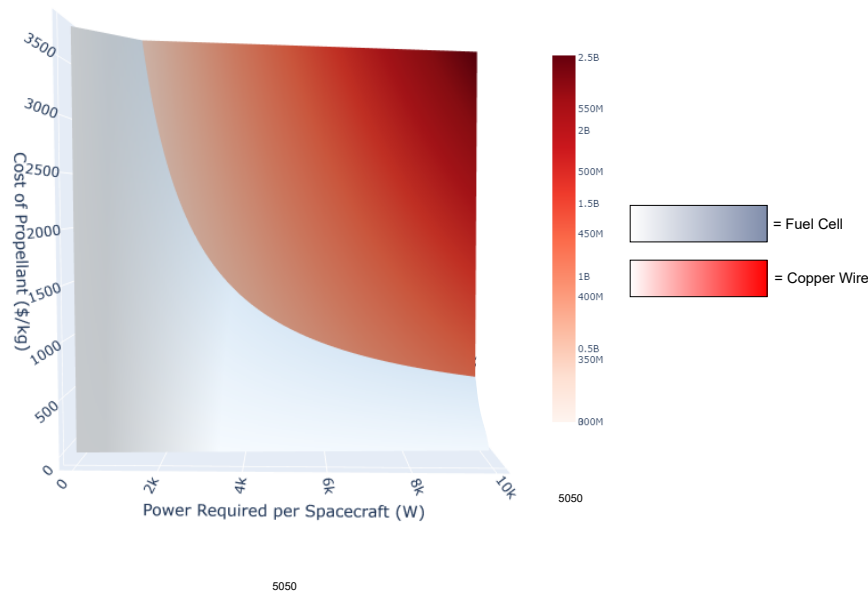


Figure 6.7: 2D Cost View of Support Without Rover

### 6.7.2. Direct Purchasing of Power from Artemis

Although a violation of REQ-TC-UCM-EPS-8, the possibility of purchasing power directly from the Artemis mission should be considered for the possible cost savings it can provide. Two scenarios were considered in which Artemis provides power, either by means of solar panels or by means of a nuclear reactor. As was mentioned in Table 6.7, an estimated 2.8 MW of power will be generated for all Artemis power needs, being delivered at an estimated EPS system cost of 600\$M for a set of 3 nuclear reactors capable of generating 2.8 MW of power [14]. This results in an estimated cost of  $214.29 \frac{\$}{kg}$ , assuming proportional scalability of the system. Assuming solar panel expansion costs to be the direct expansion costs of the NASA solar farm, should they use solar cells instead of a nuclear reactor, the cost of expanding the farm will be  $2000 \frac{\$}{kg}$ , as was mentioned in Table 6.4. In both scenarios, water will have to be directly purchased for  $H_2O_2$  production, and as such will incur the water costs of  $142 \frac{\$}{kg}$ , as was mentioned in Table 6.7. An overview of these associated costs are visible below in Table 6.10, where the power generation type refers to type of power generation used on the Artemis mission.

Table 6.10: Direct Purchasing Costs of EPS from Artemis

	Solar Panels	Nuclear Powered
Price (\$/W)	2,000.00	214.29
EPS Cost (\$)	32,000,000	3,428,571
Water Costs (\$)	17,500,000	17,500,000
Total EPS Cost (\$)	<b>49,500,000</b>	<b>20,928,571</b>

From this, it can be determined that direct purchasing of power from Artemis can provide substantial cost savings when compared to independent power generation systems, providing a potential savings of 96,786,155\$ should Artemis use solar panels for power generation, or 125,357,583\$ should Artemis use nuclear reactors for power generation. This option should thus be further investigated in accordance with stakeholders for the cost savings it can provide.



# 7 Propulsion System

The propulsion system is an essential subsystem of the UCM. Its key function is to translate the entire UCM from the Lunar surface to orbit and back, a certain amount of times. This function translates into several key elements that the PROP will be composed of. These elements are: engines, propellant storage tanks, and plumbing. From the aforementioned, requirements follow which will be discussed in Section 7.1 along with a trade-off summary. Following this the engines will be selected in Section 7.2. Moving the UCM from surface to orbit creates  $\Delta V$  requirements on the system which will be described in Section 7.3, and the operations profile will be presented in Section 7.4. Following the operations profile, all elements related to engine ignition and plumbing are described in Section 7.5 and Section 7.6.

## 7.1. Requirements & Trade-off Summary

The list of main requirements for the propulsion system is found in Table 7.1 below. Requirements have been revisited, as some requirements were redundant or not verifiable, explaining why some requirement ID's are missing. The following subsections give a brief overview of the results of the extensive trade-offs performed in

Requirement ID	Requirement
REQ-TC-UCM-PROP-3	The propulsion system shall have a specific impulse of at least 440 s
REQ-TC-UCM-PROP-4	The main propulsion system shall use $LH_2$ as fuel
REQ-TC-UCM-PROP-5	The main propulsion system shall use $LO_2$ as oxidizer
REQ-TC-UCM-PROP-6	Each engine has to perform at least 50 ignitions.
REQ-TC-UCM-PROP-7	The reaction control system shall use $H_2O_2$ as monopropellant
REQ-TC-UCM-PROP-9	The RL-10 CECE engine shall provide a maximum thrust of 66.7 kN
REQ-TC-UCM-PROP-10	The Vinci engine shall provide a maximum thrust of 180 kN
REQ-TC-UCM-PROP-12	The main propulsion system shall allow for at least 120s of hovering before touchdown.
REQ-TC-UCM-PROP-13	The exhaust flow of the propulsion system shall not damage other elements.
REQ-TC-UCM-PROP-15	The ignition system shall be non-toxic.
REQ-TC-UCM-PROP-16	The ignition system shall use $GH_2$ & $GO_2$
REQ-TC-UCM-PROP-17	The main propulsion system shall be able to provide a $\Delta V$ of 1936 m/s for the Lunar ascent phase.
REQ-TC-UCM-PROP-19	The main propulsion system shall be able to provide a $\Delta V$ of 1961 m/s for the initial Lunar descent burn.
REQ-TC-UCM-PROP-20	The main propulsion system shall be able to provide a $\Delta V$ of 195 m/s for the descent hovering before touchdown.
REQ-TC-UCM-PROP-21	The propulsive system shall ensure that the vertical speed at touchdown does not exceed 2 m/s

Table 7.1: Table of Propulsive system (revisited) requirements

the midterm report [5]. More detail regarding each single trade-off can be found in the midterm report.

### 7.1.1. Propellant Trade-off

For the propellant type, certain cryogenic, semi-cryogenic and storable propellants were considered. This includes  $LH_2/LO_2$ ,  $LCH_4/LO_2$ , RP-1/ $LO_2$ , and the combination of Hydrazine and Nitric Acid. This trade-off showed that hydrolox is the clear winner in propellant selection. Its highest ISP, lowest cost, and availability on the Lunar moon thanks to NASA's Artemis mission [50] made it the only viable option.

### 7.1.2. Ignition System Trade-off

The next trade-off performed was done to identify which type of ignition system suits the mission profile the best. The considered ignition systems were the following: plasma igniters, laser ignition, coil-on-plug torch ignition, hypergolic chemicals, and pyrotechnics. This trade-off also had a clear winner, in this case, the coil-on-plug torch ignition. Other options also had high cycle count, high sustainability, but the technological readiness and negligible power requirements of the coil-on-plug torch ignition system made it the first choice. Furthermore, it uses GOX and GH2, which can be created from the propellants allocated for propulsion.

### 7.1.3. Engine Cycles Trade-off

The last trade-off performed resulted in the preferred cycle for the engines. Five cycles were considered: staged combustion, closed & bleed expander cycles, gas generators, and pressure-fed engines. Due to the simplicity, low cost, and high efficiency, expander cycles were favored during the engine selection. Closed cycles were ranked above bleed expanders as they do not vent any gas into the Lunar atmosphere, to avoid contamination and also because the vented materials could potentially be re-used.

## 7.2. Engine Selection & Tank Design

### Engine selection

From the results of the trade-offs and with the use of preliminary  $\Delta V$  calculations and mass budgets, the engine selection and configuration can be performed. To do this, an engine catalogue was created from the available public data, as no existing and reliable engine catalogue was found. Said catalogue can be found in the midterm report [5]. Two different engines were chosen, the Vinci engine of ESA manufactured by ArianeGroup and the CECE variant of the RL-10 engine of NASA manufactured by Aerojet Rocketdyne. Both are hydrolox expander cycle engines that can be gimbaled, but have different thrust levels. The Vinci has an impressive maximum thrust of 180 kN [77], making it an ideal option for the ascent phase. On the other hand, the CECE can provide up to 66.7 kN, but with great throttleability, going down to around 7% of its maximum thrust [27]. This makes it ideal for descent and hovering, as it offers a great range of control for the thrust of the UCM. Additionally, the CECE is selected for descent exclusively to fit in the cycle life of 50 per engine. Because of thrust symmetry, and very high initial mass at lift-off as the UCM carries 25 tonnes of payload, the configuration was chosen to be dual Vinci engines with one CECE engine between both. Figure 7.1 below shows a schematization of said configuration:

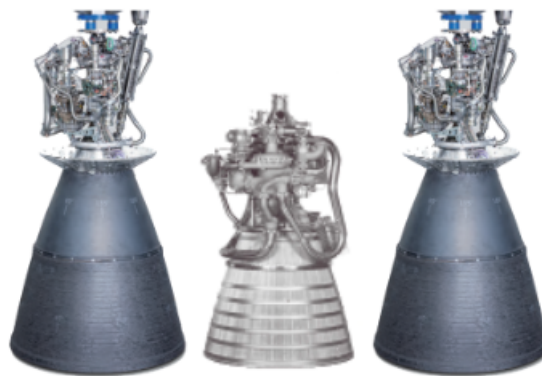


Figure 7.1: Engine configuration

### Propellant tank design

Further, the complimenting set of  $LH_2$  and  $LO_2$  tanks had to be designed for storage of the propellant. These tanks will be found at the bottom of the craft to reduce piping necessary and there shall be multiple tanks in order to fit into the desired fairing dimensions. In the end, four spherical tanks for  $LH_2$  and two spherical tanks for  $LO_2$  were designed. To size the propellant tanks, the methods described in Chapter 5 were used. It should be noted however, as these tanks are not used for prolonged storage on the Lunar surface and in order to reduce complexity of the system, only MLI insulation is used for thermal control.

## 7.3. $\Delta V$ Budget & Thrust Level

In order to choose viable engine configurations, what the system has to be able to perform needs to be identified. The  $\Delta V$  budget is the metric used to assess the requirement on performance which dictates the options for the design of the propulsive system. Before discussing the budgets of each segment in more detail, the main assumptions taken are listed in table Table 7.2 below. Most of the assumptions are taken from the Midterm report [5], but there have been changes as seen by the assumption ID's. The calculation method and formulas used for the  $\Delta V$  budgets remain the same as in the previous report, making use of the Tsiolkovsky ideal rocket equation including gravity losses, and B. Zandbergen's method for calculating the required  $\Delta V$  to go from surface to orbit on any celestial body [89]. More detail about these calculations can be found in the midterm report [5]. Since then, the only changes for the  $\Delta V$  budgets stem from different initial thrust-to-weight ratios due

ID	Assumption
ASSU-PROP-DELTAV-01	The increase in velocity results from an instantaneous impulse.
ASSU-PROP-DELTAV-04	The contribution of the moon's rotation about its own axis on the UCM's speed is neglected as the launches will happen at the moon's polar region.
ASSU-PROP-TRAJ-ASC-01	The ascent trajectory is a direct ascent with a single burn.
ASSU-PROP-GIMB-01	All engines have low but existing gimbaling capabilities [6][61].

**Table 7.2:** Assumptions for the propulsion system.

to the change in dry mass of the UCM. The new  $\Psi_0$  ratios are given by:

$$\Psi_{0_{ascent}} = \frac{T_{ascent}}{m_{ascent_0} \cdot g_{moon}} = \frac{360000}{54797 \cdot 1.625} = 4.043 \quad (7.1)$$

$$\Psi_{0_{descent}} = \frac{T_{descent_0}}{m_{descent_0} \cdot g_{moon}} = \frac{66700}{10572 \cdot 1.625} = 3.88 \quad (7.2)$$

The maximum load on the spacecraft will happen right before the end of the ascent burn, when the thrust is still nominal and where the mass of the spacecraft is lower as almost all the propellant has been burned down. To find this value, it is assumed that all the propellant is burned. However, due to the taken margins and, as mentioned to the group by Dr. Atli-Veltin, the fact that cryogenic tanks should never be fully emptied, to keep them cold until the next filling, all the propellant will in reality most likely never be burned. The maximum acceleration experienced by the spacecraft is then:

$$a_{max} = \frac{T_{ascent} - (m_{ascent_0} - m_{prop_{ascent}}) \cdot g_{moon}}{m_{ascent_0} - m_{prop_{ascent}}} = 8.50[m/s^2] \quad (7.3)$$

This roughly equals  $5.23 g_{moon}$  and the stressed caused by this acceleration will not turn out to be problematic for the structures of the spacecraft. During the ascent and descent, the thrust is kept at maximum nominal thrust of the engines as doing otherwise would increase the gravity losses, increasing the amount of propellant needed, reducing the P2P ratio of the operations. This also simplifies the burn time calculations, as the mass flow is constant and the burn time can simply be calculated by the following equation:

$$t_b = \frac{M_{prop}}{\dot{m}} \quad (7.4)$$

During the hover period, the thrust level is required not to be constant, so as to account for the loss of propellant. From a simple free-body-diagram and sum of forces, the thrust can be found to be given by:

$$T_{hover} = g_{moon} \cdot \left[ (m_{dry} + m_{prop_{hovering}}) - \left( \frac{m_{prop_{hovering}}}{t_{hover}} \right) \cdot t \right] \quad (7.5)$$

Two minutes of hovering have been deemed enough for the spacecraft to land properly. This is more time than what previous Lunar missions had allocated for hovering maneuvers. The thrust level during hovering can be seen in figure Figure 7.2 below:

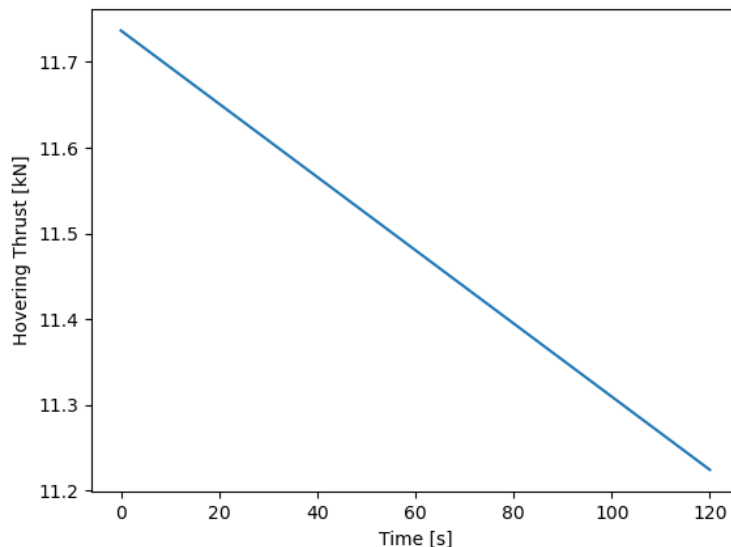


**Figure 7.2:** Thrust level during hovering

The thrust during hover varies from around 11.7 kN to 11.2 kN. This is a change from 17.5% to 16.7% of the maximal thrust, which is in theory doable by the CECE engine [27]. Once the spacecraft is done hovering, the CECE will be throttled down to slow down the descent for a smooth touchdown and to comply with *REQ-TC-UCM-PROP-21*.

## 7.4. Operations Profile

The mission is divided in individual operational cycles, in which each time a customer is refueled. A cycle is thus defined as a single UCM going to orbit, performing the refueling sequences, landing and refueling its own cargo and propulsion system. From requirement *REQ-SH-12* of Table 4.1, the number of operations per UCM can be determined, leading to a minimum of 25 operations per each UCM's lifetime. Per engine, this means:

- **Vinci:** Each Vinci engine will have to perform 25 cycles that include one ascent burn and one circularization burn. Thus, the Vinci engine has to allow for at least 50 ignition cycles.
- **RL-10-CECE:** The RL-10-CECE engine will have to perform 25 cycles that include one descent burn and the hovering and touchdown burn. Thus, the RL-10-CECE engine also has to allow for at least 50 ignition cycles.

A schematization of each phase of the operations with its corresponding required  $\Delta V$  is shown in Figure 7.3 below: Note that there is an important change since the Midterm report [5]: the docking and rendezvous is now

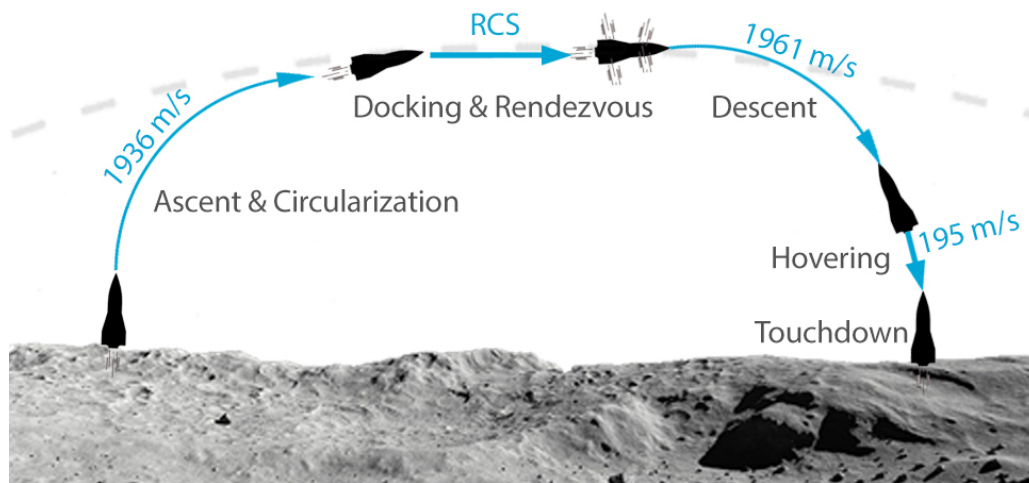


**Figure 7.3:** Operation cycle and corresponding segment  $\Delta V$  values

taken in charge by the RCS system as discussed in Chapter 8 instead of the propulsion system. This change is done because of reignition issues, and for more precision due to low thrust gimbaling capabilities in the main propulsive system.

From these assumptions, a code calculating the required propellant mass, burn time and coasting time was written. Note that the ascent and circularization burns are taken as a single burn in the  $\Delta V$  calculations as given by B. Zandbergen's [89] guide, and are not a Hohmann transfer. A Lunar direct ascent is slightly less efficient than a Hohmann transfer, but there is a reason to consider a direct ascent instead of a Hohmann transfer. This reason is linked to the reignition capabilities of the engines. If the UCM were to do a Hohmann transfer to LLO, it would have to have a minimum of two burns, with probably a third burn for finishing circularization or circularization correction. This would lead to a probable minimum of 75 burns per Vinci engine per lifetime, which above the usual life cycle of an engine due to turbopump degradation, as explained to the team by Dr. Dinesh. Also, this would decrease the reliability of the spacecraft as there are more chances of failure for the ignition system, negatively affecting the mission. With this in mind, the thrust & time budgets of an operational phase are computed and compiled in the table below:

Ascent	Value	Descent	Value	Hovering	Value
Burn time [s]	496.9	Burn time [s]	134.2	Hovering time [s]	120
Coast time [s]	1191.6	Coast time [s]	1207.1	Thrust [kN]	10.96 - 10.48
Thrust [kN]	360	Thrust [kN]	66.7	Used Propellant [kg]	315
Used Propellant [tons]	19.63	Used Propellant [tons]	4.10		

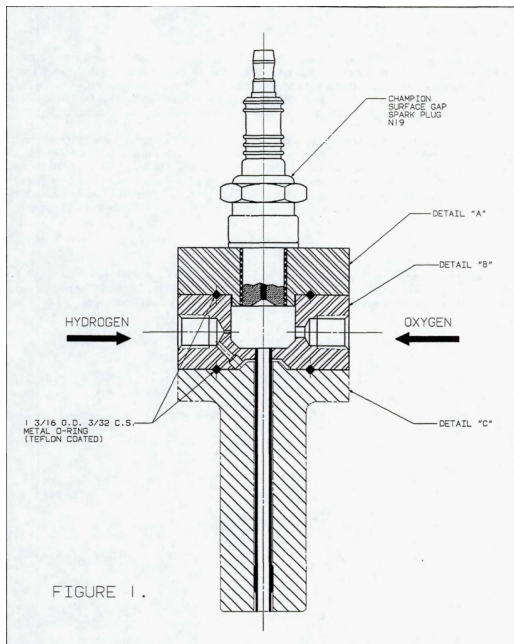
Table 7.3: Thrust, Propellant use and Time duration of each phase of a cycle.

## 7.5. Engine Ignition

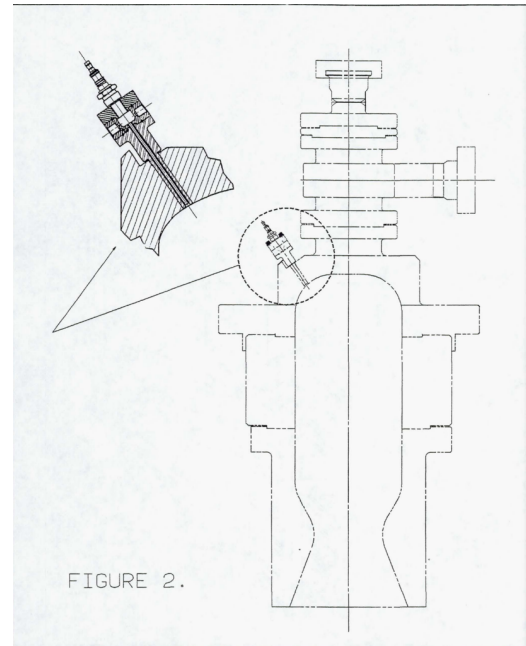
The spacecraft requires a high cycle ability due to the prescribed 10 year mission lifetime. From this it follows naturally that the engine ignition needs to be highly repeatable. In order to confirm the high cycle ability of the propulsion system it is important to understand the working principles and sequences of engine ignition. It is known that for this propulsion system's ignition system gaseous hydrogen ( $GH_2$ ) and oxygen ( $GO_2$ ). This section will first cover the selected method of ignition in Section 7.1.2 with further, sizing of the tanks for the  $GH_2$  and  $GO_2$  in Section 7.5.2. This will be followed by the presentation of the ignition sequencing in Section 7.5.3.

### 7.5.1. $GO_2$ and $GH_2$ spark plug ignitor

To begin with, the engine ignition requires an initial input of energy to commence the reaction between the propellants in the combustion chamber of the engine. This is to be delivered by a retro-fitted  $GO_2$  and  $GH_2$  spark plug ignited torch. This torch has been selected in the previous midterm report [5], it can be seen in Figure 7.4a and in Figure 7.4b.



(a) Detailed view of spark plug torch ignitor [58]



(b) Torch placement respectively to the engine [58]

### 7.5.2. $GO_2$ and $GH_2$ Sizing

In order to size the tanks, the amount of  $GO_2$  and  $GH_2$  required for ignition needs to be obtained. Throughout a single mission cycle, there will be a total of  $n$  ignitions required. This can be derived from the mission profile: two Vinci engine ignitions for ascent, two Vinci engines to be ignited for orbit circularisation (this is a precautionary measure in case of a failed initial burn), one RL-10 ignition for de-orbit, and one RL-10 ignition for hover. Thus, the number of ignitions required per mission cycle,  $n = 6$ . Equation 7.6 and Equation 7.7 present the calculations of the required masses for  $GO_2$  and  $GH_2$  respectively. The variables,  $m_{GO_2}$  &  $m_{GH_2}$  represent the mass of  $GO_2$  and  $GH_2$  respectively.  $t_{GO_2}$  and  $t_{GH_2}$  are the times that the respective gas flows for.  $\dot{m}_{GH_2_{out}}$  and  $\dot{m}_{GH_2_{in}}$  refer to the hydrogen mass flow inside and outside of the torch, these are differentiated since the outside flow provides cooling.

$$m_{GO_2} = \dot{m}_{GO_2} \cdot t_{GO_2} \cdot n \quad (7.6)$$

$$m_{GH_2} = (\dot{m}_{GH_2_{out}} + \dot{m}_{GH_2_{in}}) \cdot t_{GH_2} \cdot n \quad (7.7)$$

Additionally, as mentioned in the paper written by G. Repas [58], the experimental torch was operated at ambient temperature, thus it was decided to also operate the torch at the average earth temperature of 288 K or 15 C°.

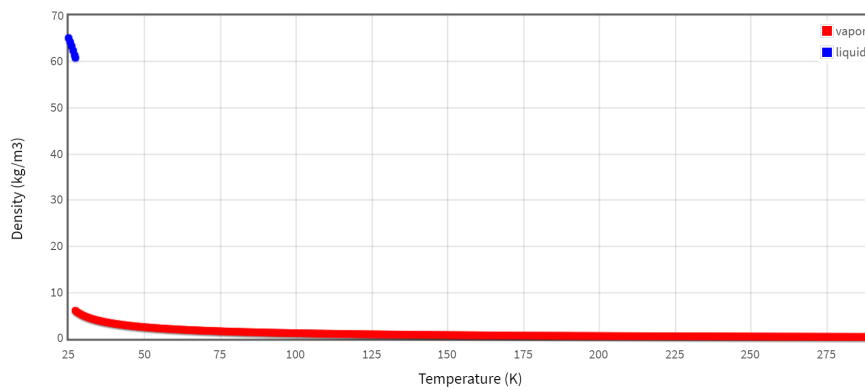


Figure 7.5: GH2 isobaric property graph

This implies that all elements of the system for ignition should be heated to 288 K, however, knowing that the mass of all elements is negligible, therefore making the power required negligible. The  $GO_2$  and  $GH_2$  are to be stored at a lower pressures than the liquid propellant for the main engines. This is to have a pressure differential between the main engine propellant tanks and gaseous propellant tanks. Thus, the  $GO_2$  and  $GH_2$  will be stored at pressures of 0.3 bar and 5 bar respectively. This was chosen after by trying to minimise the volume of the gaseous tanks, with also retaining at least a pressure ratio of 2 between the propellant tank and the gaseous tank, for easy insertion of propellant to the gaseous tanks. However, this should be optimised even further in future design phases. Most important of all, it was to obtain condition under which the liquid would vaporise spontaneously. This was obtained by initially taking half of the input pressure and then by observing Figure 7.5<sup>1</sup> & Figure 7.6<sup>2</sup> from which it could be seen whether the pressure had to be tweaked further. This was done assuming an isobaric process, since the liquid would enter the system and it would not be an isochoric process, however it was assumed that the tank pressure could be retained with a regulator at the specified pressure. Finally, by using the ideal gas laws, the densities and volumes for each gas could be obtained. These were calculated to be 0.0509 m<sup>3</sup> and 1.8328 m<sup>3</sup> for  $GO_2$  and  $GH_2$  respectively.

	Mass Flow [kg/s]	Flow Duration [s]	Mass [kg]	Volume [m <sup>3</sup> ]	Pressure [MPa]	Density [kg/m <sup>3</sup> ]
<b>GOX</b>	0.002266	1.00	0.002266	0.0057	0.5	0.4009
<b>GH2</b>	0.113398	0.75	0.085049	0.2036	0.03	0.4176

	No. Ignitions		Safety margin		Tank Diameter [m]
	6		1.5		
	No Margin		With Margin		
	Volume [m <sup>3</sup> ]	Mass [kg]	Volume [m <sup>3</sup> ]	Mass [kg]	
<b>GOX</b>	0.034	0.014	0.0509	0.0204	0.2298
<b>GH2</b>	1.222	0.510	1.8328	0.7654	0.7592

### 7.5.3. Ignition Sequence

The ignition sequences will be split into two categories: those that occur on the ground and those that occur in space. The main difference between the two categories is whether the craft has a weight or is weightless. On the Lunar surface, Lunar gravitational field aids in separating entrapped (settling) bubbles and provides additional fuel and oxidiser pressure. In space or in orbit, the s/c does not experience a net weight, so the aforementioned effects do not occur. However, relative to the vacuum all tanks are pressurised which will aid in expelling propellant for ignition. The ignition sequences for both on the Lunar surface and in orbit are shown below:

#### 1. Lunar surface

- (a) The on site sequence begins with the vaporisation of  $LO_2$  &  $LH_2$ . Where 0.014 kg of  $LO_2$  and 0.510 kg of  $LH_2$  are deposited from the propellant tank, to the gaseous tank, where then it is vaporised and

<sup>1</sup>[https://webbook.nist.gov/cgi/fluid.cgi?P=5&TLow=25&THigh=290&TInc=0.5&Applet=on&Digits=5&ID=C1333740&Action=Load&Type=IsoBar&TUnit=K&PUnit=bar&DUnit=kg%2Fm3&HUnit=kJ%2Fkg&WUnit=m%2Fs&VisUnit=uPa\\*s&STUnit=N%2Fm&RefState=DEF](https://webbook.nist.gov/cgi/fluid.cgi?P=5&TLow=25&THigh=290&TInc=0.5&Applet=on&Digits=5&ID=C1333740&Action=Load&Type=IsoBar&TUnit=K&PUnit=bar&DUnit=kg%2Fm3&HUnit=kJ%2Fkg&WUnit=m%2Fs&VisUnit=uPa*s&STUnit=N%2Fm&RefState=DEF)

<sup>2</sup>[https://webbook.nist.gov/cgi/fluid.cgi?P=0.30&TLow=70&THigh=288&TInc=0.5&Applet=on&Digits=5&ID=C7782447&Action=Load&Type=IsoBar&TUnit=K&PUnit=bar&DUnit=kg%2Fm3&HUnit=kJ%2Fkg&WUnit=m%2Fs&VisUnit=uPa\\*s&STUnit=N%2Fm&RefState=DEF](https://webbook.nist.gov/cgi/fluid.cgi?P=0.30&TLow=70&THigh=288&TInc=0.5&Applet=on&Digits=5&ID=C7782447&Action=Load&Type=IsoBar&TUnit=K&PUnit=bar&DUnit=kg%2Fm3&HUnit=kJ%2Fkg&WUnit=m%2Fs&VisUnit=uPa*s&STUnit=N%2Fm&RefState=DEF)

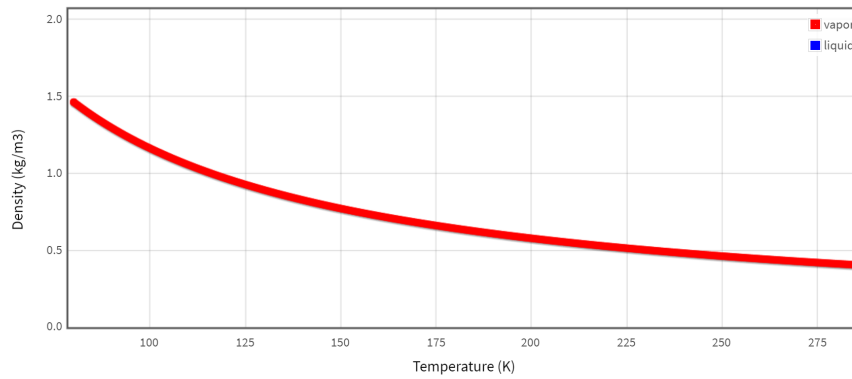


Figure 7.6: GOX isobaric property graph

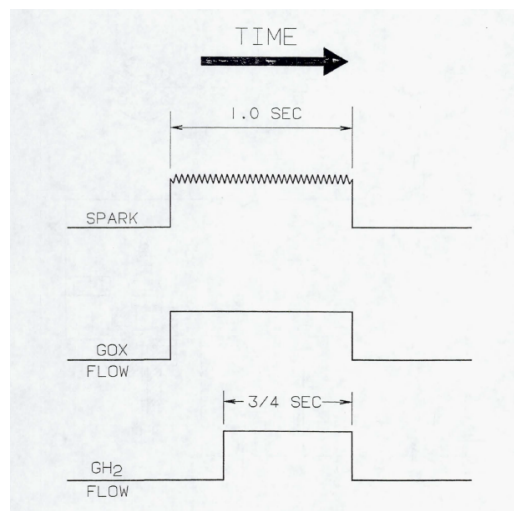


Figure 7.7: Torch ignition sequence w.r.t. time [58]

stored at the gaseous state. It is to be stored at a pressure lower than that of the main tank, as to prevent the necessity to pump the propellant.

- (b) Further, all lines leading to the external environment are to be purged. This prevents the accumulation of voids in the lines and primes the lines for usage.
- (c) Next, the torch is to be ignited. The torch ignition sequence takes around 1s. A time detailed illustration of the process can be seen in Figure 7.7. It begins with a flow of hydrogen, which flows outside (this is for cooling reasons) of the torch as well as through the inside. Next the gaseous oxygen flow is activated, and the torch is ignited.
- (d) Next the injectors are activated and the combustion commences at a low thrust level. Then, gradually the thrust is increased to the maximum thrust, this is done to introduce the loads gradually.

## 2. In space

- (a) A timed pulse of 20s of thrust is given by the RCS to settle the fluids for ignition. This pulse is calculated using the time needed for a droplet of liquid to travel from the top of the largest propulsion tank to the bottom using Equation 7.8. The variables are  $t_{settle}$  - time to settle,  $d$  diameter,  $M$  dry mass,  $T_{RCS}$  thrust of the RCS.

$$t_{settle} = \sqrt{\frac{2dM}{T_{RCS}}} \quad (7.8)$$

- (b) Then, the lines are purged.
- (c) The ignition torch is ignited
- (d) Selected engine(s) are ignited at low thrust. Thrust is throttled to require levels for the mission phase.

## 7.6. Plumbing

The main propulsive system (MPS) requires a plumbing system to operate predictably and reliably. A plumbing system provides pathways and connections between gaseous/liquid containers and various apparatus. Therefore, a plumbing diagram was drawn up to define the various connections, fuel pathways and such. This diagram can be seen in Figure 7.8.

### 7.6.1. Engine Feed Systems

The engines of the propulsion system will require high-rate flow of large volumes of cryogenic propellant. Therefore, the plumbing with regard to the main engines will be crucial. The journey of both the oxidiser and the fuel begins at their respective propellant tanks. Before initiating the flow process of the propellant, both the oxidiser and fuel should be settled (no entrapped bubbles in the liquid, gasses and liquids separated). On the Lunar surface the gravity will aid in settling the propellants. In space (orbit) the ADCS (RCS) will aid in settling the propellants whilst in microgravity as explained in Section 7.5. Once settled the propellants, the flow process will be initiated by means of opening the tank valves so that the propellant can enter the main lines. Additionally, all the valves leading to vacuum (the engines) will be opened. This is done by purging the lines until all volumes in the feed system have been sufficiently filled with propellant. Additionally, during this priming/purging process the fuel has to pass through the pump, then pass through the nozzle cooling lines and then the turbine. The pressure within the propulsion propellant tanks is beneficial to helping this process along. After ignition, the pumps will pump the propellant to the engines, and the thrust generated, will continue to keep the liquid propellant settled.

### 7.6.2. Ignition Feed System

In order to operate the ignitor torches, a feed system connecting the GOX and GH<sub>2</sub> tanks has to be used. The lines used in this feed system will be designed for non-cryogenic and gaseous applications. They will operate at lower pressures and higher temperatures. One of the main differences of the ignition feed system in comparison to the engine feed systems is that a much lower amount of propellant has to be transported through the lines. The feed process of the ignition feed system is initiated by feeding liquid hydrogen and oxygen through a series of valves into a heating element so that they vaporise and become GOX and GH<sub>2</sub>. These gasses will be used to fill the GOX and GH<sub>2</sub> tanks at the beginning of each mission cycle. This will be done on the Lunar surface so that gravity can aid in filling these tanks. Then, for each of the six ignitions the gasses are funneled into the torches enabling engine ignition.

### 7.6.3. Emergency Propellant Feed

In case of a declined or aborted mission cycle, an emergency propellant feed system has to be created. This emergency feed system is able to use the CSS propellant to feed the main propulsion engines. An emergency propellant feed that is operated in case of a declined or aborted resupply mission is accounted for. In this situation, the ADCS (RCS) can be used to settle the CSS propellant and initiate the flow process into the main engine propellant tanks. In this case the payload is used to refuel the propulsive system. The way the RCS can influence the propellant transfer is described in Section 5.6.

### 7.6.4. Secondary Feed Lines

Other than the main systems plumbing for some of the auxiliary systems must be accounted for. One of these is the feed for the hydrogen fuel cell. With The hydrogen fuel cell system requires an input of  $LO_2$  and  $LH_2$ . This will also be supplied from the propulsive tank. With valves to modulate the flow required for the fuel cell. This operation is to take place with the help gravity. Further, venting was included to provide ways of relief in case of over-pressurisation, or other emergency situations.



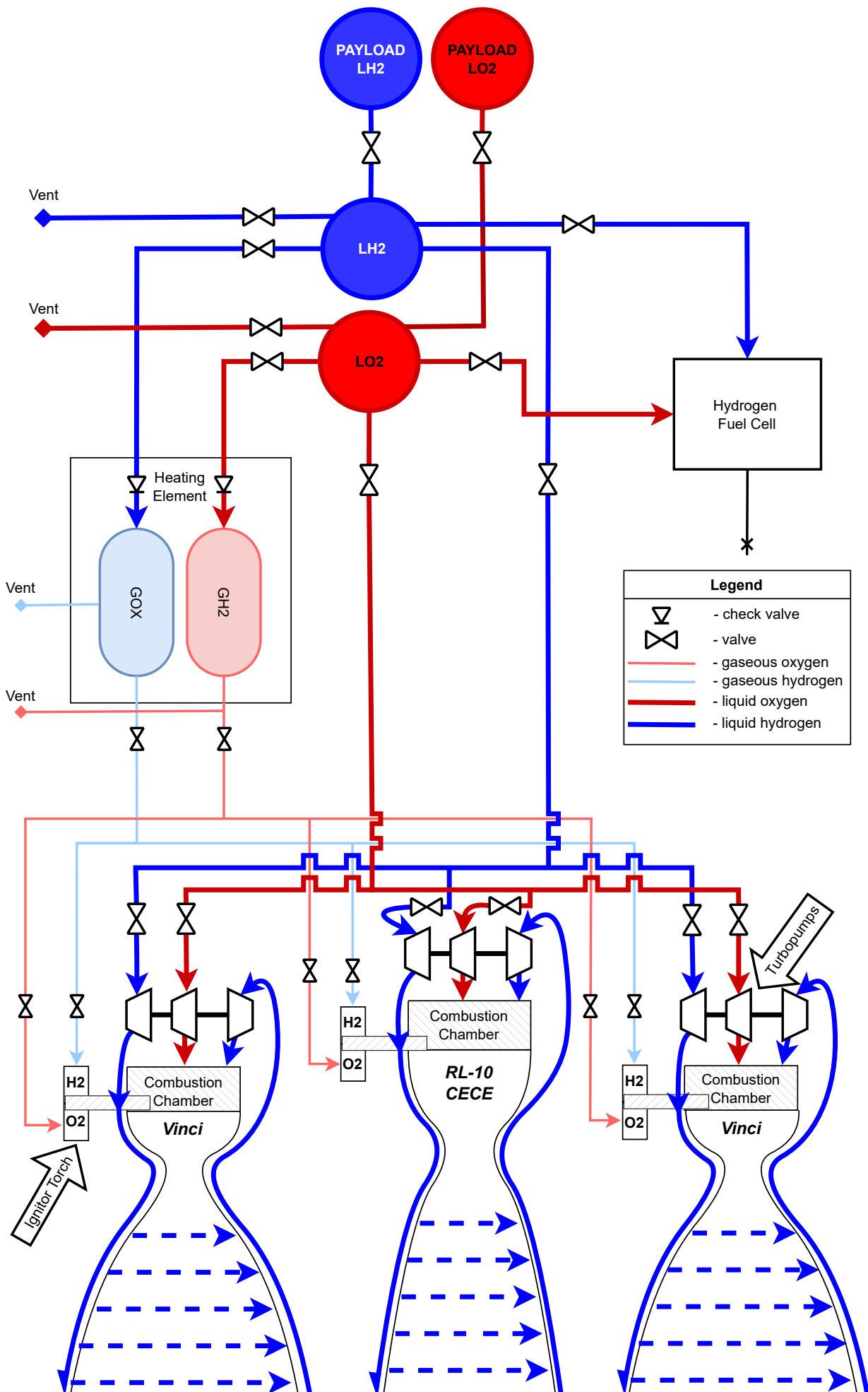


Figure 7.8: Main propulsive system plumbing diagram

# 8 Attitude Determination & Control System

The attitude determination and control system (ADCS) is the subsystem in the UCM that will be responsible for the determination of the orientation of the vehicle and correcting this attitude if desired. Such corrections are performed by the reaction control system, an element of the ADCS which is able to slew the vehicle in a certain manner. Additionally, the reaction control system will perform one of the critical parts of the mission: rendezvous and docking with the customer spacecraft. First, in Section 8.1, the requirements for this subsystems are revisited and an overview of the available options is given. Next, the attitude determination system is described in Section 8.2. Afterwards, in Section 8.3, a description is given of the reaction control system. The authors of this chapter would like to express their gratitude to Dr. B.V.S Jyoti, Dr. D. Mengu, Dr. A. Cervone and Ir. J. Bouwmeester for sharing their knowledge in this field and assisting in the solving of problems.

## 8.1. Requirements & Trade-off Summary

For attitude determination, the main requirement was dedicated to the pointing accuracy of the vehicle. It was found for low impact docking that the angular misalignment between the two satellites should be no more than  $\pm 0.2^\circ$  for all three body axes at a maximum relative rotational speed of  $\pm 0.05^\circ/\text{s}$ . In such a way, axial and lateral loads of no more than 220 N and bending and torsional moments of 200 Nm are imposed on the docking mechanism [24]. Furthermore, it was determined that such a pointing accuracy shall be achievable in 99.7% of the times ( $3\sigma$ ).

For the actuators for the reaction control system, initially a maximum slew rate of  $15^\circ/\text{min}$  was determined for sizing. However, from Section 5.6, it was determined that a much faster slew rate has to be achieved for the vehicle in order to transfer the propellant to the customer, namely  $140^\circ/\text{min}$ . The reaction control system will also play an important role during rendezvous and docking of the two spacecraft, which will put requirements on the RCS in terms of  $\Delta V$ . Finally, the RCS should be able to counter disturbance torques that act on the UCM, which will require propellant as well. The modelling of both rendezvous and disturbances will be further explored in Section 8.3. All the requirements for the ADCS are summarized in Table 8.1.

**Table 8.1:** The requirements imposed on the ADCS

Requirement ID	Requirement
REQ-TC-UCM-ADCS-1	the UCM shall have a pointing accuracy of $\pm 0.2^\circ$ around all three body axes 99.7% of times ( $3\sigma$ )
REQ-TC-UCM-ADCS-2	the UCM shall be able to determine its rotational rate with an accuracy of $\pm 0.05^\circ/\text{s}$ around all three body axes 99.7% of times ( $3\sigma$ )
REQ-TC-UCM-ADCS-3	the UCM shall have a maximum slew rate of $140^\circ/\text{min}$
REQ-TC-UCM-ADCS-4	The UCM shall achieve the maximum slew rate in less than 120 s
REQ-TC-UCM-ADCS-5	The UCM shall be in Low Lunar Orbit at 100 km
REQ-TC-UCM-ADCS-6	The UCM shall have an orbital inclination of $90^\circ$
REQ-TC-UCM-ADCS-7	The UCM shall have an orbital eccentricity of 0
REQ-TC-UCM-ADCS-8	The RCS shall provide 45.43 m/s of $\Delta V$ for rendezvous and docking
REQ-TC-UCM-ADCS-9	The RCS shall provide 2.5 m/s of $\Delta V$ for attitude maintenance

The trade-off for the attitude determination system and for the reaction control system was performed in the midterm report [5]. For attitude, it considered sun sensors, star sensors, Earth sensors and gyroscopes and found a combination of sun- and star sensors to be the best performing combination. Additionally, thrusters were chosen as actuators, since reaction- or momentum wheels would have to be desaturated every time when the UCM descends to the Lunar surface, leading to inefficiencies in the usage of propellant. Furthermore, control momentum gyro's could not provide control torques of sufficient magnitude to slew the vehicle. Further sizing of the attitude determination and control system is done in Section 8.2 and Section 8.3.

## 8.2. Attitude Determination

Determination of the attitude of the vehicle is crucial in order to dock successfully to the customer satellite. In such a way, the docking mechanisms of the two vehicles are aligned within an acceptable margin such that a connection can be made. Otherwise, additional fuel would need to be spent to make the two spacecraft line

up, which is undesirable. Additionally, as there are no pointing requirements from the payload, this mission phase was considered to be the most stringent case for attitude determination. In the midterm report, it was determined that for absolute attitude determination, the combination of a sun sensor and a star sensor would have the best performance according to the criteria [5]. This is due to the fact that for full three axis attitude knowledge, at least two external non-parallel vector measurements need to be taken [81]. A sun sensor can determine one of these two vectors, whereas a star sensor is able to measure more than one vector, depending on the number of identified stars, since each tracked star acts as a reference vector [81]. However, a study of on-orbit spacecraft failures shows that failure is related to the ADCS in 32 % of the cases [72]. Therefore, it was decided that an additional set of sensors is necessary for redundancy. The mass and power consumption were already determined to be 1.05 kg and 1.5 W for the sun sensor and 3.5 kg and 12.5 W for the star sensor [5].

Since the launcher will be spinning at  $140^\circ/\text{min}$  during the propellant transfer, absolute attitude determination is not possible, because most star trackers lose their focus at slew rates larger than  $18^\circ/\text{min}^1$ . Therefore, a relative attitude determination method is required, independent of the information provided by the star- and sun trackers. Previously, the implementation of a gyroscope was discarded. However, as it is the only device in the trade-off table that can determine relative attitude, a gyroscope will be required to measure the angular rates of the vehicle [5]. Therefore, for full three axis determination, three gyroscopes would be necessary, with the note that a fourth gyroscope should be added again for redundancy [72]. It is however also possible to put all four gyroscopes off axis to increase the redundancy of the device. Such a configuration is called an Inertial Reference Unit (IRU) [84]. With the addition of accelerometers, such a unit is called an Inertial Measurement Unit (IMU), which can provide data on traversed distance and the velocity of the vehicle [84], which is necessary to know such that the relative velocity of the two vehicles can be monitored during rendezvous and docking. Thus, an inertial measurement unit will be implemented as a part of the ADCS. For the further system design, the main focus was to find the mass and power consumption of the IMU. These were found to be 20 kg and 50 W, respectively [81].

During docking, it is necessary to monitor the distance between the two vehicles and their relative velocity and orientation. These functions are commonly performed by a visual sensor for autonomous docking applications. In this case, a general sensor that satisfied the stated pointing accuracy requirement was found, making use a 3D imaging technique, called Laser Imaging Detection and Ranging (LIDAR). It was found that such a sensor would typically have a mass of 14 kg and a power consumption of 35 W [84].

Finally, although the IMU can provide measurements about orbital position based on the double integration of the acceleration rates, an altimeter is required for the final part of the descend phase, namely hovering. It is beneficial to have a separate altimeter to monitor altitude, because integrating the acceleration twice will cause errors in position to propagate in a cubic fashion [66]. This is of course undesirable, which is why an altimeter must be added as well. Therefore, a generic altimeter was found that can determine altitude with an accuracy of 1 m at an altitude of 50 m and 10 m at an altitude of 50 km. The device has a mass of 3.6 kg and 22 W of power consumption [84].

Now that all sensors have been found, an overview can be made of what sensors will be active during what phase of the mission. In such a way, the total power consumption can be determined. This overview is given in Table 8.2, where an X indicates that that specific is sensor is active during that mission phase. It can be seen that the combination of sun and star sensor is active during all parts of the mission, except when docked as the sensors then lose their resolution and cannot determine the altitude of the vehicle. Furthermore, during docking, all sensors are used, which requires the most power, namely 99 W. Additionally, the total mass of the attitude determination system was found to be 46.7 kg.

**Table 8.2:** Overview of working attitude and altitude sensors during different mission phases

Sensor\Mission Phase	Ascent	Rendezvous	Docking	Docked	Descent
<i>Sun Sensor</i>	X	X	X		X
<i>Star Sensor</i>	X	X	X		X
<i>Inertial Measurement Unit</i>	X	X	X	X	X
<i>Docking Sensor</i>			X		
<i>Altimeter</i>	X				X
<i>Redundant Sun Sensor</i>					
<i>Redundant Star Sensor</i>					
<b>Power Consumption [W]</b>	86	64	99	50	86

<sup>1</sup>URL:<https://fermi.gsfc.nasa.gov/science/resources/swg/may00/SRitz.pdf>

Furthermore, an overview of the architecture of the attitude determination system is given in Figure 8.1. The sensors determine the orientation of the vehicle for all three body axis. An additional attitude measurement follows from integrating the angular rates of the vehicle, which allows for comparison of the data and the final determination of the orientation. This determined attitude is then compared against the desired reference attitude and if an offset exists, the reaction control system will have to slew the vehicle into the desired direction. Furthermore, the accelerometers can give information about the velocity and position of the launcher through integration. Finally, for docking, the docking sensor keeps track of the relative distance and orientation between the vehicles. From the defined docking procedures, it can then be determined whether the reaction control system should provide additional performance in terms of velocity or orientation.

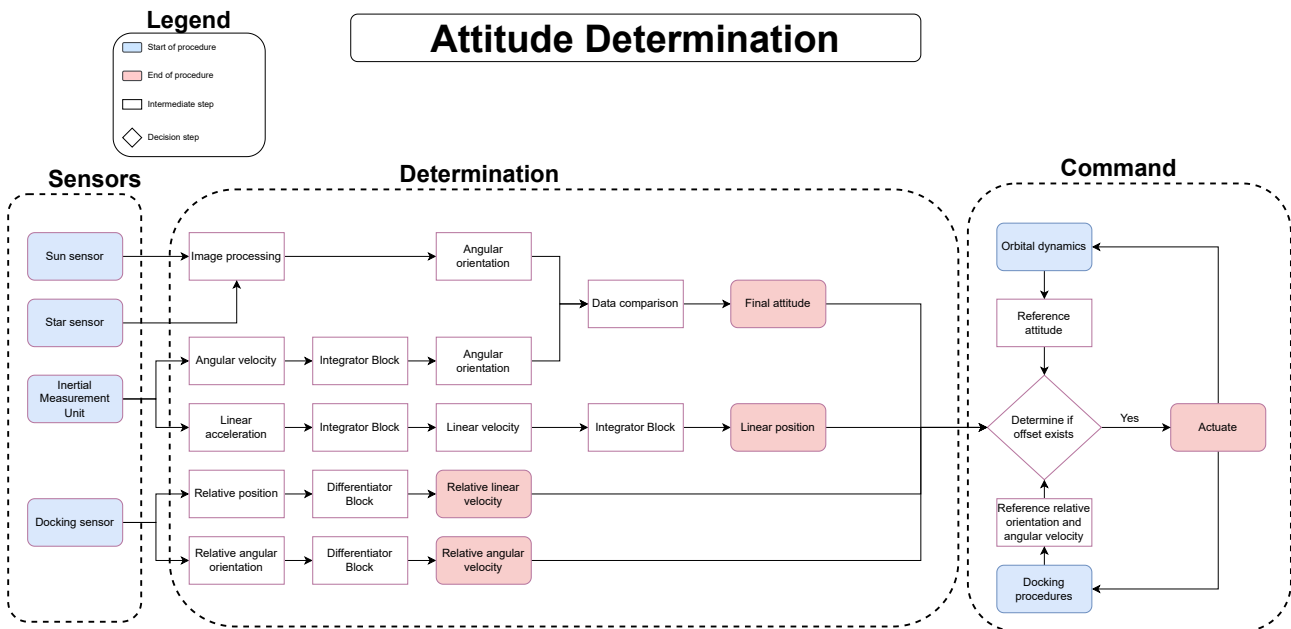


Figure 8.1: Attitude Determination System Architecture

## 8.3. Reaction Control System

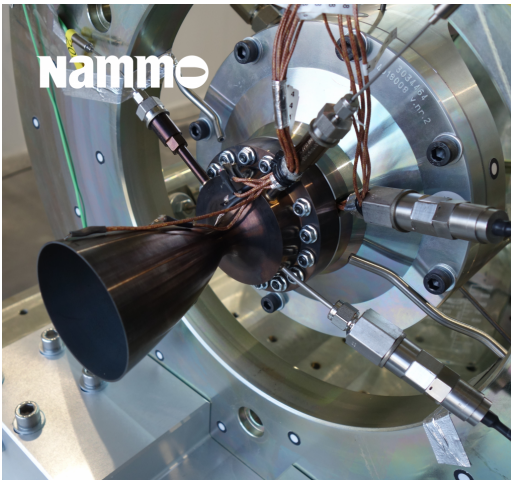
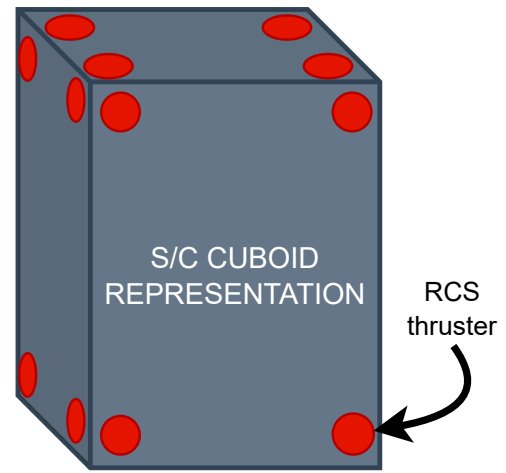
It is key that the spacecraft is capable of manipulating its position and orientation in space and time. To accomplish this, a hydrogen peroxide monopropellant reaction control system shall be used and discussed in this section. Firstly, the specific thruster selection along with the layout is discussed in Section 8.3.1. In Section 8.3.2, Section 8.3.3 and Section 8.3.4 the budgets for rendezvous and docking, propellant transfer and attitude maintenance are discussed, respectively. Furthermore, the monopropellant production is presented in Section 8.3.5 and the storage in Section 8.3.6.

### 8.3.1. Thruster Selection & Clusters

One of the most critical RCS sizing parameters is the thrust capability, alongside with the specific impulse and the burn time of the thruster. Therefore selecting a thruster is key to the success of the mission. From the previous midterm report [5], it was decided to use a monopropellant thruster system that runs on  $H_2O_2$ . With this in mind, and having contacted Dr. A. Cervone, a thrust range of 100 – 500N per thruster was recommended. Additionally, the Automated Transfer Vehicle developed by ESA, a vehicle with a maximum mass of 20 750 kg<sup>2</sup>, quoted RCS thrust figures of 220 N per thruster [84]. With this in mind, the Nammo 220 N H<sub>2</sub>O<sub>2</sub> monopropellant thruster<sup>3</sup> (used on the Vega-C upper stage) was selected. It can be seen in Figure 8.2a:

<sup>2</sup>[http://waterrocket.explorer.free.fr/pdf/jules%20verne%20ATVfs003\\_12\\_atv.pdf](http://waterrocket.explorer.free.fr/pdf/jules%20verne%20ATVfs003_12_atv.pdf)

<sup>3</sup><https://www.nammo.com/product/220n-h2o2-thruster/>

(a) 220 N  $H_2O_2$  Nammo thruster<sup>3</sup>

(b) Cuboid representation of RCS system

Further, the number of thrusters and their placement was to be obtained. At this point the spacecraft was treated as an cuboid. This simplification is fair to obtain the number of thrusters for translation and rotation along all 3 axis of the s/c. The main design philosophy here was to provide coupled moments for rotation and equal thrust for acceleration and deceleration in a single axis. As seen in Figure 8.2b, this resulted 4 thrusters per face, with each thruster placed at the corners, belonging to a cluster of 3 thrusters. Additionally, 4 thrusters are assumed to operate at any one moment. This comes in at a total of 24 thrusters, weighing in at 35.52 kg and a power requirement of 200 W (50 watts per thruster)<sup>3</sup>.

### 8.3.2. $H_2O_2$ Budget for Rendezvous and Docking

The rendezvous and docking phase of the mission is critical to mission success. If the UCM is not able to dock to the customer satellite for propellant transfer, mission failure will occur. This phase imposes on a  $\Delta V$  capability requirement on the RCS. This requirement in turn leads to a certain amount of required  $H_2O_2$  per mission. First the required  $\Delta V$  has to be estimated and then the required hydrogen peroxide can be determined.

This estimation was made with help of the Clohessy-Wiltshire equations, a set of linearised differential equations that describes the relative motion of a chase vehicle that is in close proximity to a target vehicle for circular orbits, as given in Equation 8.1 to Equation 8.3. In the Clohessy-Wiltshire equations, a coordinate system is placed in the target vehicle, where the x-direction points along the radial direction, y along the flight direction and the z-direction is out of the plane to complete a right handed coordinate system [83]. Furthermore,  $n$  indicates the mean motion of the target vehicle in its orbit that is at an altitude  $r$  from the surface, as given by Equation 8.4.

$$\ddot{x} - 2n\dot{y} - 3n^2x = 0 \quad (8.1) \quad \ddot{y} + 2n\dot{x} = 0 \quad (8.2)$$

$$\ddot{z} + n^2z = 0 \quad (8.3) \quad n = \sqrt{\frac{\mu_{planet}}{(R_{planet} + r)^3}} \quad (8.4)$$

It should be noted that the in-plane equations (Equation 8.1 and Equation 8.2) are decoupled from the out-of-plane equation (Equation 8.3). Furthermore, with the assumptions that the two vehicles are in the same orbital plane, Equation 8.3 can be dropped in total.

A common way to rendezvous with a target vehicle is by performing two impulsive maneuvers, where the first impulsive maneuver provides sufficient  $\Delta V$  to catch up with the target vehicle and where the second maneuver is required to slow the chase vehicle down at the target. Say the chase vehicle should rendezvous with the target at a certain time  $t$  and has initial position components relative to the target before the first maneuver  $x_0^-, y_0^-$ . Then, the velocity components of the chase vehicle right after the first burn can be calculated using Equation 8.5 and Equation 8.6 [83].

$$\dot{x}_0^+ = \frac{x_0^- n(4 \sin nt - 3nt \cos nt) - 2y_0^- n(1 - \cos nt)}{3nt \sin nt - 8(1 - \cos nt)} \quad (8.5)$$

$$\dot{y}_0^+ = \frac{x_0^- n(6 \sin nt - 14nt(1 - \cos nt) + 2y_0^+ n \sin nt)}{3nt \sin nt - 8(1 - \cos nt)} \quad (8.6)$$

The required change in velocity for the first burn is then given by Equation 8.7, where  $x_0^-$  and  $y_0^-$  are the velocity

components of the chase vehicle relative to the target before the burn, which can be determined from orbital characteristics. Afterwards, the second burn can be initiated to stop the chase vehicle at the specified time  $t$  to stop the chaser at the target. The required change in velocity can be computed using Equation 8.8, with  $\dot{x}(t)$  and  $\dot{y}(t)$  being the velocity components of the target at time  $t$  [83].

$$\Delta V_1 = \sqrt{(\dot{x}_0^+ - \dot{x}_0^-)^2 + (\dot{y}_0^+ - \dot{y}_0^-)^2} \quad (8.7)$$

$$\Delta V_2 = \sqrt{\dot{x}^2(t) + \dot{y}^2(t)} \quad (8.8)$$

In such a way, by combining the velocity changes of the two maneuvers, a total  $\Delta V$  for the rendezvous and docking phase can be found for different altitudes and rendezvous times. This altitude is the distance the chaser starts behind and below the target. The  $\Delta V$  budget can then be translated into a certain amount of propellant that is needed by the RCS, as given in Figure 8.3.

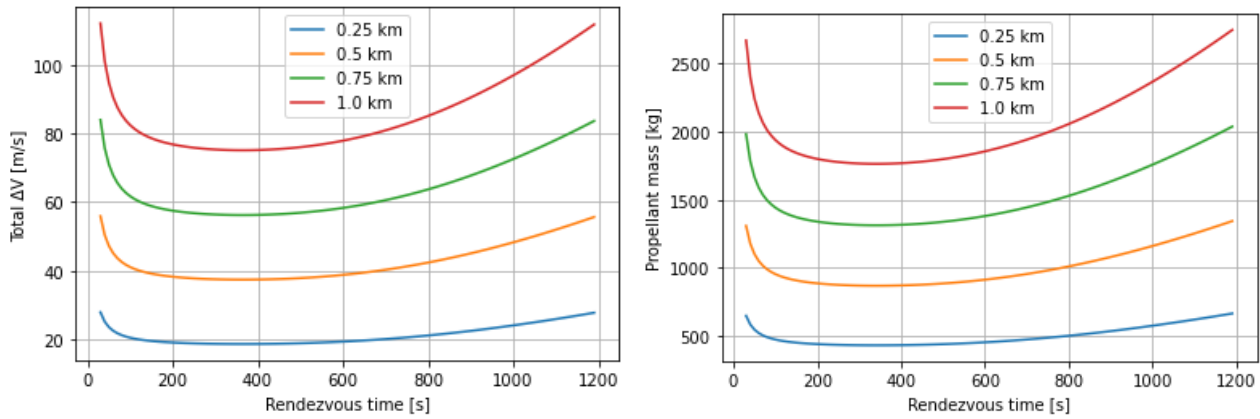


Figure 8.3:  $\Delta V$  and propellant mass required for rendezvous and docking for different altitudes and rendezvous times

It can be seen that if the launcher starts 0.5 km behind and below the customer satellite, a total  $\Delta V$  of 37.93 m/s would be needed, which translates into the RCS needing a propellant mass of 868 kg at an optimal rendezvous time of 6 minutes. Furthermore, when the propellant transfer is finished, the RCS should coast the empty launcher away from the customer before the main propulsion system can start. Using the same procedure, if an initial separation of 0.1 km is desired, a total  $\Delta V$  of 7.5 m/s would be needed to be delivered, resulting in a propellant mass of 56.4 kg. Additionally, the rendezvous phase of the mission has been plotted in Figure 8.4, where the UCM starts 0.5 km below and behind the customer, after which a burn by the RCS is performed to meet the customer spacecraft in its orbit in the previously indicated 6 minutes. After these six minutes, when the UCM has met the customer spacecraft, the second burn is performed to slow down.

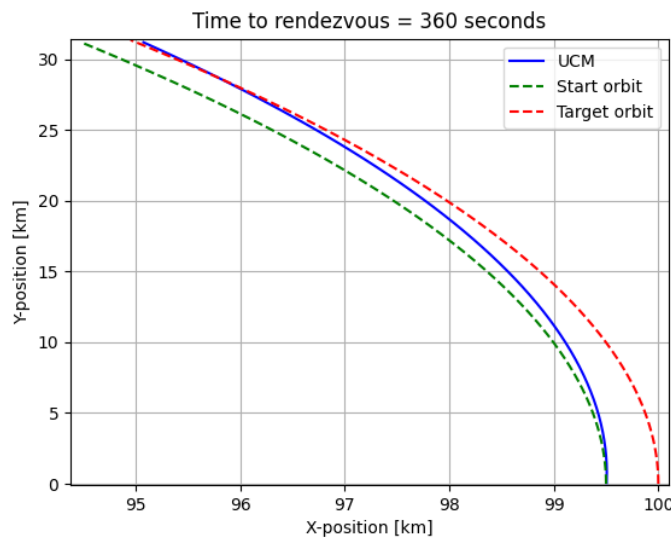


Figure 8.4: Rendezvous of the UCM and the customer spacecraft

### 8.3.3. $H_2O_2$ Budget for Propellant Transfer

After successful docking, the transfer of propellant from the UCM to the customer spacecraft can commence. In Section 5.6, it was determined to make use of centripetal acceleration for the propellant transfer. Therefore, a rotation of  $140^\circ$  is desired and should be delivered by the RCS thrusters. In order to find out how much propellant should be taken onboard for this maneuver, an estimation of the propellant burned by the thrusters during this maneuver was made. The rotational motion of a rigid body with three rotational degrees of freedom is given by Euler's rotational equations, as given in Equation 8.9 [84].

$$\mathbf{J}\dot{\boldsymbol{\omega}} + \boldsymbol{\omega} \times \mathbf{J}\boldsymbol{\omega} = \mathbf{M} \quad (8.9)$$

Equation 8.9 can be rewritten into a set of nonlinear coupled ordinary differential equations for each one of the three body axis. For example, for a moment in the x-direction, Equation 8.9 can be rewritten into Equation 8.10, with  $J$  being the mass moment of inertia around a certain axis and  $\omega$  the angular velocity. If the assumptions is made that the vehicle is stationary around all three axes, as all rotational rates should have been reduced to zero for docking, then Equation 8.10 simplifies to Equation 8.11 [84].

$$J_x \dot{\omega}_x - (J_y - J_z)\omega_y \omega_z = M_x \quad (8.10) \quad J_x \dot{\omega}_x = M_x \quad (8.11)$$

In such a way, by providing a constant moment around a certain axis, a constant angular acceleration around that axis is achieved. If this angular acceleration is applied for the required time  $t$ , the desired angular velocity can be achieved. The moments of inertia of the UCM were obtained from the CAD model, which is further described in Section 12.3.3. For the axis of rotation for the propellant transfer, the mass moment of inertia  $I_{yy}$  was found to be  $261\,772 \text{ kgm}^2$ .

Consequently, by taking the product of thrust times moment arm, each thruster can apply a moment of  $440 \text{ Nm}$  around the body axis of rotation. With four thrusters being active around one axis, a total moment of  $1760 \text{ Nm}$  can be achieved. Therefore, the desired rotational can be achieved in  $5.9 \text{ s}$ . The used propellant during this burn can be computed from Equation 8.12 [81], where  $n$  is the number of active thrusters.

$$m_{fuel} = \frac{n F_{thrust} t_{burn}}{g_0 I_{sp}} \quad (8.12)$$

Consequently, a propellant mass of  $6.63 \text{ kg}$  would be needed to accelerate the launcher to the desired rotational speed and decelerate it back to stationary afterwards.

### 8.3.4. $H_2O_2$ Budget for Attitude Maintenance

During flight, four major disturbance torques can be identified to be acting on the spacecraft, namely torques due to solar radiation pressure, atmospheric drag, magnetic fields and gravity gradient. However, only solar radiation pressure and gravity gradient need to be considered, as there is neither an atmosphere nor a magnetic field present on the Moon. In order to see if the remaining disturbance torques are of significant influence, their maximum torque was estimated using Equation 8.13 and Equation 8.14 [81]. Therefore, most values in Table 8.3 are upper limits. In such a way, if the disturbance torque is not of a large magnitude, it can be estimated that the disturbance torque will not exceed this value during operation of the UCM.

$$T_s = \frac{\Phi}{c} A_s (1 + q) (c p_s - c m) \cos \phi \quad (8.13) \quad T_g = \frac{3\mu}{2R^3} |I_{xx} - I_{zz}| \sin 2\theta \quad (8.14)$$

**Table 8.3:** Design variables and values used to estimate disturbance torques acting on the UCM [81]

Solar Radiation Pressure				Gravity Gradient			
Variable	Value	Unit	Description	Variable	Value	Unit	Description
$A_s$	88	$m^2$	Sunlit surface area	$I_{xx} - I_{zz}$	129787	$kgm^2$	Difference in MMOI
$q$	1	-	Unitless reflectance factor	$\theta$	$\frac{5}{180}\pi$	rad	Difference between local vertical and principal axis
$c p_s - c m$	1	m	Difference in center of pressure and mass				
$\phi$	0	rad	Angle of incidence				

Consequently, it was possible to estimate the angular drift that would be caused during the refuelling period of four hours, as indicated in Table 8.4. Based on the drift, a decision could be made whether the RCS should be able to counteract the disturbance torque or whether it was deemed insignificant.

**Table 8.4:** Disturbance torques and the caused angular drift during refuelling

Disturbance Torque	Torque Magnitude [Nm]	Angular Drift [°]	Deemed Significant?
<i>Solar Radiation Pressure</i>	0.0008	0.0015	No
<i>Gravity Gradient</i>	0.0266	0.083	No

Since both disturbance torque only cause angular drifts that are less than half of the pointing accuracy of the UCM in the worst case scenario, they were deemed of insignificant influence for the RCS to counteract them during the refuelling period. Further attitude maintenance was assumed to be small in terms of  $\Delta V$  and therefore a  $\Delta V$  of 2.5 m/s was estimated for other attitude maneuvers at maximum weight [81]. Such maneuvers include for example hovering after descend and other small corrections. This leads to a propellant mass of 101 kg. In such a way, each of the twenty four thrusters can fire for a total of three minutes to perform these additional corrections during flight. To conclude, Table 8.5 gives an overview of all the maneuvers performed by the RCS and its corresponding  $H_2O_2$  usage.

**Table 8.5:** Overview of total  $H_2O_2$  required by the RCS

Maneuver	Propellant Usage [kg]
<i>Docking and rendezvous</i>	868
<i>Propellant transfer</i>	6.6
<i>Undocking</i>	56.4
<i>Attitude maintenance</i>	101
<b>Total</b>	<b>1032</b>

### 8.3.5. $H_2O_2$ Monopropellant Production

As previously indicated, the monopropellant that was chosen for the RCS is hydrogen peroxide ( $H_2O_2$ ). Since it is unfeasible to bring enough monopropellant for the ten year mission duration, it should be produced in-situ during operations. Producing the hydrogen peroxide on the Lunar surface separate from the UCM is not an option as it is an power intensive process and no readily available energy exists in the permanently shaded Lunar crater. The hydrogen peroxide will be produced from water. The water from which the hydrogen peroxide will be produced originates from the fuel cell. The fuel cell makes electrical energy by combining hydrogen and oxygen; the byproduct of this is water as described in Section 6.5. Instead of venting this water into space, it will be recycled and reused to make the monopropellant the RCS needs. As every resource on the moon is precious, the recycling of the water will improve the sustainability and overall feasibility of the mission.

Unfortunately, the amount of water produced by the fuel cell is not equal to the amount of water needed to make the hydrogen peroxide. There will be an excess of water generated by the fuel cells, equal to 2.59 kg per day. As a result this excess water will be sold back to NASA for 142.86\$ per kg, as was mentioned in Table 6.7.

The machine that will produce the hydrogen peroxide from the water will be SolveGE's Hydrogen Peroxide Printer <sup>4</sup>. Information about the printer was found with the help of the CEO of SolveGE; Dr. B.V.S Jyoti. From pure water, the printer can create a mixture of 10% hydrogen peroxide, 81% water and 9% waste. The power required to create 1 kg of hydrogen peroxide is equal to 3 kWh. Once the mixture with 10% hydrogen peroxide is made and the waste is filtered out, it can be concentrated via passive concentration. This process uses no additional energy and can create hydrogen peroxide concentrations upwards of 85%. The highly concentrated hydrogen peroxide will then be stored and ready for use by the RCS. The leftover water is then recycled and stored so that it can be used again in a future cycle. In Figure 8.5 the hydrogen peroxide cycle can be seen.

<sup>4</sup>URL:<https://solvege.com/services/>



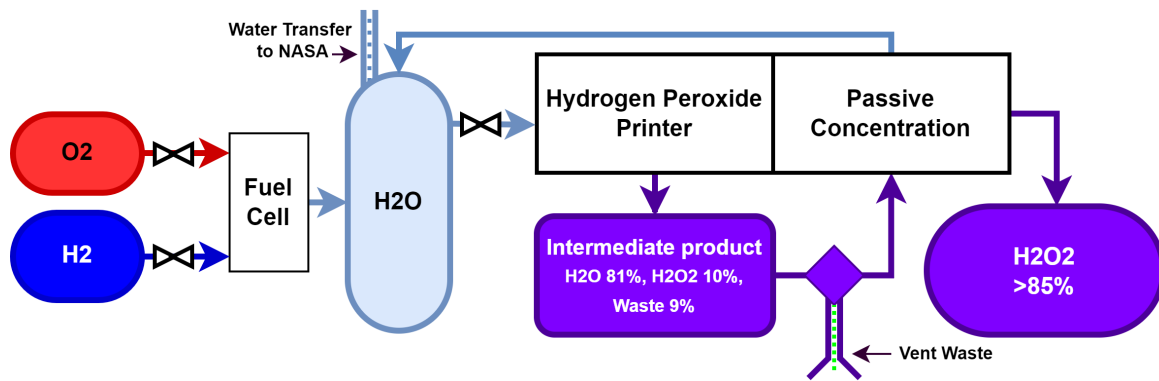


Figure 8.5: Overview of the Hydrogen Peroxide Cycle.

For the RCS 1032 kg of hydrogen peroxide is needed per launch. As a launcher will fly once every forty days, 25.8 kg should be produced daily by the hydrogen peroxide printer. As only 10% of the water from the fuel cell is transformed into hydrogen peroxide, a reservoir of water will exist to be able to produce the required amount of monopropellant. To create the 25.8 kg of hydrogen peroxide daily, a reservoir of 258 kg of water is needed. The hydrogen peroxide printer was specified to be modular and 1 kg of machine is able to produce 1 kg per day. Thus, the printer will weigh roughly 26 kg to be able to produce the required hydrogen peroxide.

The production of the hydrogen peroxide will only occur when the UCM is idling on the Lunar surface in between mission cycles. The previously mentioned water reservoir will be sold and emptied before the next launch of the UCM. This is done to reduce the amount of propellant needed for the UCM to get into LLO, as the weight of the propellant to get the water into orbit is larger than the weight of the water itself. Once the launcher lands again the reservoir will of course be empty.

### 8.3.6. Monopropellant Storage & Plumbing

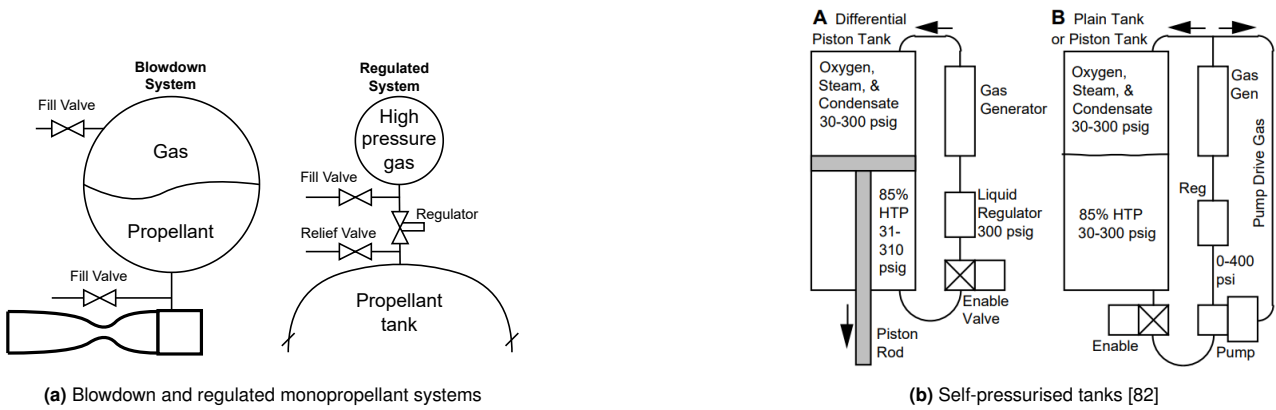
As the monopropellant is manufactured and used, it is necessary to store it. However, storage and plumbing of hydrogen peroxide comes with its own challenges. The first of is the pressurization of the fluid for usage. Methods for pressurisation can be summarised as:

- **Regulated** - the regulated system is to use a highly pressurised gas in a separate tank, which is then used to regulate the pressures of the monopropellant tank. The advantages in relation to the blowdown system are that the ISP and thrust are constant and that the controller logic is simpler. However, this system has to carry the additional weight of the regulator and the regulator may fail. The relevant illustration can be seen in Figure 8.6a [63].
- **Blowdown** - the blowdown system is characterised by the fact that the pressurised gas and the propellant share the same tank. This design is simpler than the regulated system, due to a lack of moving parts. However, this results in a drop in specific impulse with drops in feed pressure. This design is also larger in volume than its regulated counterpart, since it is held at a lower pressure. The illustrated method can be seen in Figure 8.6a [63].
- **Self Pressurised** - Finally, the self pressurised method is characterised by the propellant being used to generate the gas required to pressurise the system. This system can be seen in Figure 8.6b, and a similar piston driven tank is to be used in this application as well. In this system, the monopropellant is sent on a one way path to the catalyst where it reacts emitting steam and other gasses, which are then directed back into the tank to pressurise the system. However the hot gasses and the propellant must be separated to prevent the degradation of  $H_2O_2$ , and thus a piston is to be used [82].

Finally, to select one of the technologies one vital factor was sustainability. Historically, most monopropellant systems have used inert gasses to prevent the pressurant gas reacting with the propellant. This is non sustainable and thus any pressurants that need to be shipped are to be avoided. Further, blowdown and regulated systems require an inert gas, therefore unacceptable. Ruling the self pressurised method as the winning choice.

However, the storage of  $H_2O_2$  poses challenges of its own which must be accounted for. These issues became apparent after a consultation with the experts of SolvGE. Firstly, the tank must be lined with a non reactive material like teflon or pure aluminium, to prevent degradation of the  $H_2O_2$ . Further, as already mentioned, the hot pressurant gas must be isolated from the propellant to prevent degradation or even explosion. Moreover, high purity hydrogen peroxide must be stored above  $0\text{ }^\circ\text{C}$ , as to not freeze. Additionally, bearing in mind that the

pressurisation is accomplished by the use of a piston as seen in Figure 8.6b, the tank thus would also have to be cylindrical with spherical end caps.



To sum up previous points, a preliminary plumbing system diagram was drawn up. It can be observed in Figure 8.7. It can be seen that the feed towards the pressurised catalyst has two valves, this is done to increase redundancy, since if these valves are to fail, an explosion would be imminent.

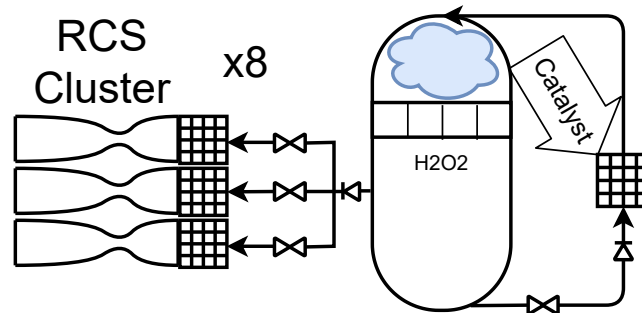


Figure 8.7: RCS plumbing diagram

Additionally, the hydrogen peroxide tank was sized based on the amount of  $H_2O_2$  it is required to store. From Table 8.5, it can be seen that the tank should be able to store 1032 kg of propellant. This leads to a required tank volume of  $0.71 \text{ m}^3$ <sup>5</sup>. As the tank will be of cylindrical shape, various combinations of tank radius and length were iterated over to find all of the combinations that satisfied the volume criterion. Afterwards, the combination was chosen featuring a length that would fit inside the spacecraft, since it is placed horizontally inside the UCM. In such a way, an inner tank diameter of 60 cm and length of the cylindrical part of 1 m was found. In order to get an estimate of the mass of this tank, Equation 8.15 was used that is based on Composite Overwrapped Pressure Vessel (COPV) data [3]. Consequently, this would lead to a tank mass of 85.3 kg. These tank characteristics are summarized in Table 8.6.

$$M_{COPV} = 115.3 \cdot V_{COPV} [m^3] + 3 \tag{8.15}$$

Table 8.6:  $H_2O_2$  tank characteristics

Characteristic	Value	Unit
Hydrogen peroxide tank mass	85.3	[kg]
Hydrogen peroxide tank diameter	60	[cm]
Hydrogen peroxide tank cylinder length	1	[m]

<sup>5</sup><https://webbook.nist.gov/cgi/cbook.cgi?Name=hydrogen+peroxide&Units=SI#>

# 9 Telemetry, Tracking, & Command

The telemetry, tracking, and command system (TT&C) handles all external communication of the UCM. *REQ-SH-18* and *REQ-SH-19* state that the UCM and specifically the propellant transfer mechanism shall be remotely controllable from Earth. The TT&C system is therefore crucial in fulfilling this requirement, as without it, no data exchange with Earth could occur in near real-time. From these stakeholder requirements and initial investigation, a specific set of system requirements were created and are explained in Section 9.1. Following the requirements, the concept that forms the TT&C is described in Section 9.2. Finally, antennas will be selected and sized such that this subsystem can be used to size the UCM as described in Chapter 4.

## 9.1. Requirements

Table 9.1 shows the requirements that were created for the TT&C system. Requirements *REQ-TC-UCM-TTC-1*, *REQ-TC-UCM-TTC-2*, and *REQ-TC-UCM-TTC-3* cover the required data rates throughout the mission. *REQ-TC-UCM-TTC-4* and *REQ-TC-UCM-TTC-5* cover the precision and correctness of the communication data flow. These five requirements form the basis of this subsystem and were derived in the mid-term report [5].

**Table 9.1:** The requirements imposed on the TT&C system.

Requirement ID	Requirement
<i>REQ-TC-UCM-TTC-1</i>	A 15 Mbps communication data rate shall be possible during docking and landing
<i>REQ-TC-UCM-TTC-2</i>	A 5 Mbps communication data rate shall be possible during all phases of the mission
<i>REQ-TC-UCM-TTC-3</i>	A 20 kbps communication data rate shall be possible during emergency contact
<i>REQ-TC-UCM-TTC-4</i>	The TT&C shall have a bit error rate no higher than $10^{-9}$
<i>REQ-TC-UCM-TTC-5</i>	The TT&C shall have a link budget margin of at least 3 dB

## 9.2. Concept

The communication infrastructure of the COLD mission is a rather complicated web of links between different entities located at varying distances from each other. In terms of internal communications, the UCMs in different stages, that is in orbit, during ascent or descent, as well as landed on the Lunar surface need to communicate with each other. In order to assure continuous communication with ground control, relay satellites have to be used. As mentioned in the preliminary analysis report for the COLD [5], relay spacecraft such as NASA's Gateway, Lunar Pathfinder and in general future satellites of the ESA's Moonlight initiative will be used. These would necessitate external partnerships with governmental agencies, or perhaps commercial Lunar communication providers, the costs of which are taken into account in the form of operational costs in Chapter 16.

The ground centers with which the different COLD mission segments would communicate are modeled after the worldwide net of Near Earth Network's satellite dishes, of 10 meter diameter each. This is because this range of ground antennas is rather common and does not include expensive to use infrastructure such as the 35 meter dishes. This also allows for a constant stream of data to be achieved, due to the large ground station availability, required for fast response during emergencies. Remote control, while possible, would not however be advised due to the 2.4 second delay between the input and reaction, as the light takes 1.2 seconds to travel from Earth to the Moon. However the delay should be low enough to allow for reacting to problems during docking for example. Landing would however have to be done autonomously due to the larger velocities at play.

Different communication elements and link are depicted in Figure 9.1, which details how elements of the concept will communicate, and how they will do so. The communication flows are shown using double-sided arrows and are differentiated based frequency band and on communication type. The main communication type is for the nominal mission data rates described by *REQ-TC-UCM-TTC-1* and *REQ-TC-UCM-TTC-2*. The secondary communication type covers the emergency data rates and required antenna pointing data rates. This diagram shows that the relay is an essential element to the communication system as it facilitates smooth communication between the Earth and the UCM.

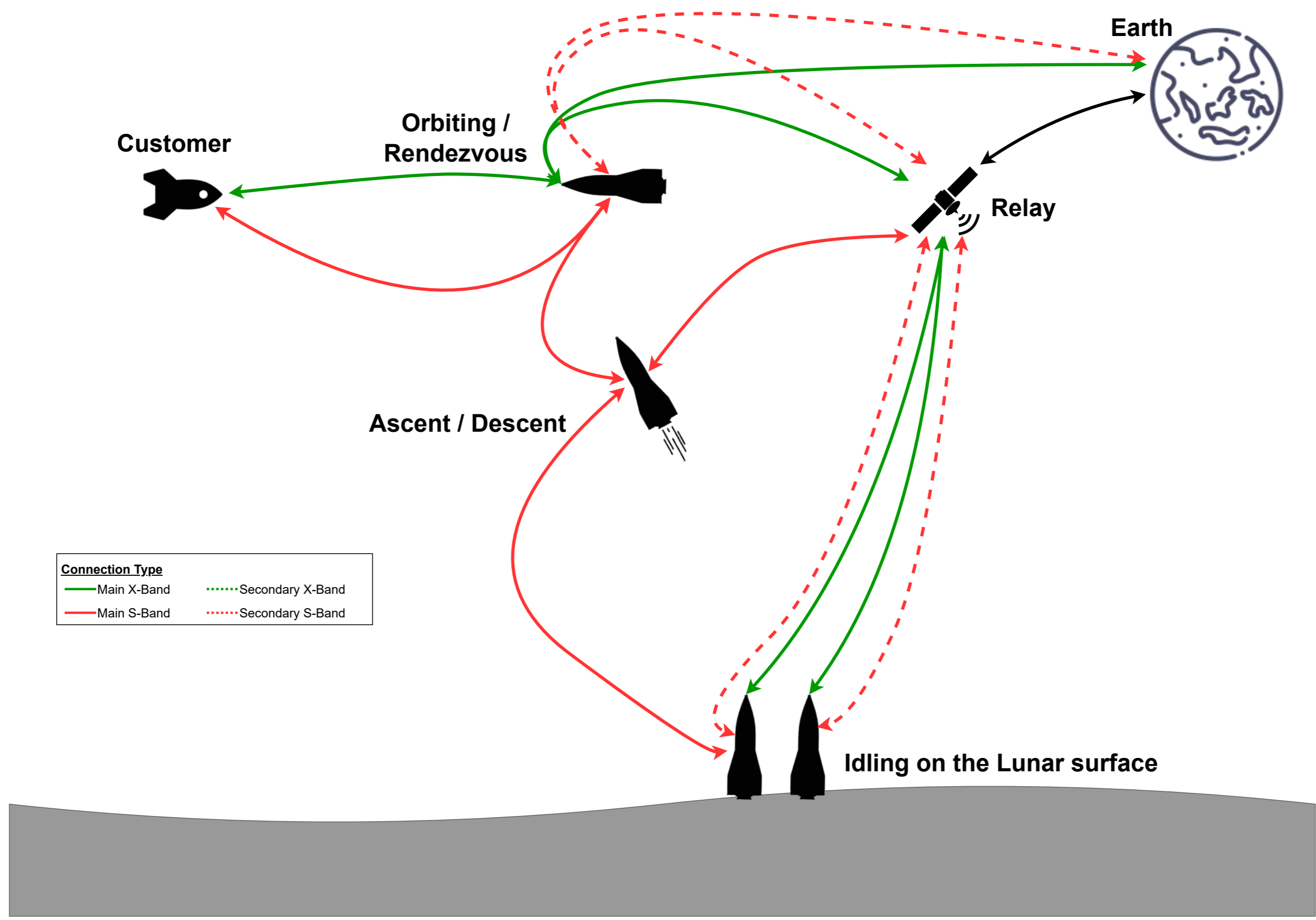


Figure 9.1: External communication flow diagram

## Link Budget

In order to size the TT&C system for the UCM it was necessary to perform multiple link budget calculations, for each of the connections presented in Figure 9.1. Once again, in a similar fashion as in the preliminary sizing report [5], this procedure is described in detail by Wertz [81]. The main equation used in these calculations is Equation 9.1. The different symbols appearing in it are explained in the tables with results of the link budget calculations: Table 9.2 and 9.3. The first table represents the critical link budget for the S-band antenna sizing, while the second one, the critical scenario for the X-band antenna. The link budget calculations for other connections are omitted, as they do not provide any additional information, yet were still necessary to determine, as to allow for finding of the critical connection.

$$\frac{E_b}{N_0} = \frac{P \cdot L_l \cdot G_t \cdot L_a \cdot G_r \cdot L_s \cdot L_{pr} \cdot L_r \cdot L_{mod}}{R \cdot k \cdot T_s} \quad (9.1)$$

**Table 9.2:** Link budget for the UCM in orbit and Earth connection (UCM to Earth is classified as downlink, the inverse as uplink). Here the communications are conducted via the medium gain antenna phased array on the S-band

Parameter	Variable	Downlink		Uplink	
		Value	Reference	Value	Reference
Transmitter power (LOM)	P	15 W			
Loss factor transmitter	$L_l$	0.8	[88]	65 dB	[62]
Transmitting antenna gain	$G_t$	20.9 dB			
Transmission path loss	$L_a$	-0.5 dB	[88]	-0.5 dB	[88]
Receiving antenna gain	$G_r$			18.2 dB	
Loss factor receiver	$L_r$	31 dB (EIRP)	[62]	0.8	[88]
System noise temperature	$T_s$			316.23 K	[9]
Space loss	$L_s$	-211.4 dB		-211 dB	
Antenna pointing loss	$L_{pr}$	-0.1 dB	8.1	-0.1 dB	8.1
Required data rate	R	1E07 bps		2E06 bps	
Modulation losses	$L_{mod}$	0 dB		-5 dB	[70]
Boltzmann constant	k	228.6 dB		228.6 dB	
SNR	$E_b/N_0$	9.3dB		5.6 dB	
Required SNR	$E_b/N_0$	2.6 dB	[88]	2.6 dB	[88]
<b>Margin</b>		<b>6.7 dB</b>		<b>3 dB</b>	

**Table 9.3:** Link budget for the UCM in orbit and Relay connection (UCM to Relay is classified as downlink, the inverse as uplink). Here the communications are conducted via the high gain antenna phased array on the X-band. The relay satellite taken as a reference in this budget calculation is the NASA's Gateway station.

Parameter	Variable	Downlink		Uplink	
		Value	Reference	Value	Reference
Transmitter power (LOM)	P	15 W		100 W	[9]
Loss factor transmitter	$L_l$	0.8	[88]	0.8	[88]
Transmitting antenna gain	$G_t$	34.4dB		35 dB	
Transmission path loss	$L_a$	0 dB	[88]	-0.5 dB	[88]
Receiving antenna gain	$G_r$	36.3 dB		33 dB	
Loss factor receiver	$L_r$	0.8	[88]	0.8	[88]
System noise temperature	$T_s$	316.23 K	[9]	316.23 K	[9]
Space loss	$L_s$	-208.3 dB		-206.9 dB	
Antenna pointing loss	$L_{pr}$	-0.1 dB	8.1	-0.1 dB	8.1
Required data rate	R	1E07 bps		2E06 bps	
Modulation losses	$L_{mod}$	0 dB		-5 dB	[70]
Boltzmann constant	k	228.6 dB		228.6 dB	
SNR	$E_b/N_0$	5.7 dB		17.5 dB	
Required SNR	$E_b/N_0$	2.6 dB	[88]	2.6 dB	[88]
<b>Margin</b>		<b>3.1 dB</b>		<b>11.9 dB</b>	

The link budgets presented in Table 9.2 and 9.3 were created using multiple assumptions, presented below. Additionally, for the LOM - relay satellite connection, the NASA's Gateway was chosen as a benchmark

for the relay, as it is expected that the station will possess large data transmission capabilities. As such it could incorporate the day to day data transfer of COLD's segments without losing too much of its capacity [Baldwin2021]. Its communication antenna was assumed to be 1 meter in diameter with a power of 100 W and system temperature of 316.23 K, while its orbit reaches 70000 km above Lunar poles [16] [9]. The assumptions in question are

- *ASSU-TTC-GEN-01*: Convolutional code types were used for every connection link, as this is the coding most commonly used for this type of mission as per [17]. The LDPC coding could also be used, in order to increase the signal to noise ratio budget, yet this was deemed unnecessary, as it would include additional system complexity, and the convolutional codes are sufficient.
- *ASSU-TTC-GEN-02*: The coding rate associated with the coding technique is 0.5, meaning that for every 1 bit of useful information, 2 bits of data have to be sent [17]
- *ASSU-TTC-GEN-03*: Pointing accuracy is at worst 0.2 degrees as prescribed in Table 8.1
- *ASSU-TTC-GEN-04*: System temperatures for all relay satellites not part of the COLD mission are assumed to be equal to 316.23 K as detailed in [9]
- *ASSU-TTC-GEN-05*: The required **bit error rate** (BER) is assumed to be **1E-9** as similar values are often used in NASA standards [9]
- *ASSU-TTC-GEN-06*: The modulation losses in the link budget represent the losses due to the use of a residual carrier signal in better position and velocity determination. This is very important, as precise knowledge of these parameters could mean the difference between a successful landing on the Lunar surface and a premature end of the mission due to a catastrophic failure.

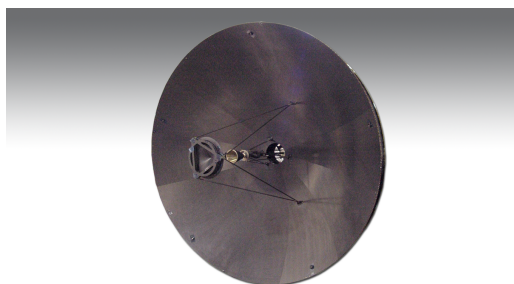
### 9.3. Antenna Selection

Based on the data rate requirements as well as the link budget findings, the final sizing of the antennas for the COLD concept was made. As mentioned in Section 9.2, three medium gain antennas are placed equidistantly around the spacecraft as to simulate an omni-directional antenna. These will be flat, phased array antennas, since these would be the easiest to place on the UCM. The NASA's Orion capsule also uses phased array antennas<sup>1</sup>, and as such similar devices will be used for UCM. Unfortunately, no detailed information regarding this type of antennas was publicly available, as manufacturers do not disclose this information because of industrial confidentiality.

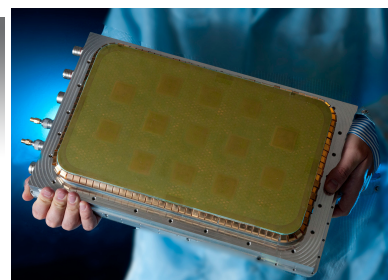
As for the main high gain antenna, a single typical parabolic antenna was chosen. This antenna would be located near the top of the spacecraft, and have an adjustable pointing as to not require the spacecraft to move in order to establish communication. As such, the medium gain antennas would acquire the correct positioning information from the target antenna, and then this information will be relayed to the high gain antenna, which would then point itself in the correct direction. Both the high and the medium gain final antenna parameters can be seen in Table 9.4. Both the phased array and parabolic antenna examples can be seen in Figure 9.2b and Figure 9.2a respectively.

**Table 9.4:** Selected antenna properties

Antenna	Frequency Band	Power Draw [W]	Area [ $m^2$ ]
<i>Phased Array</i>	S-Band	75	1.3
<i>Parabolic</i>	X-Band	75	2



(a) Picture of an example parabolic antenna



(b) Picture of an example phased array antenna, used on the Orion capsule spacecraft

**Figure 9.2:** The two antennae used on the UCM

<sup>1</sup><https://spaceflight101.com/spacecraft/orion/>

# 10 Command & Data Handling

The Command & Data Handling (C&DH) subsystem is the main controller of the UCM and is responsible for the data processing and control of all subsystems. As this system was not treated in previous reports, the design of the C&DH subsystem began with a detailed definition of its functionalities and requirements in Section 10.1. This is then followed by an architecture design that can be seen in Section 10.2. Finally, a basic power consumption estimation as explained in Section 10.3 was made in order to accurately size the EPS.

## 10.1. Functionality & Software

In this section, the necessary software procedures are defined as part of Section 10.1.1. Then, in Section 10.1.2 the requirements following from these software procedures are created to describe the necessary functionality of the C&DH subsystem.

### 10.1.1. Software procedures

As the key functionality of the C&DH subsystem is to provide commands to all other subsystems, the requirements for the subsystem can be constructed based on the functional flow and breakdown of the UCM launcher. Both the functional flow and the functional breakdown are presented and explained in detail in Chapter 14. However, for the purposes of initial design of the C&DH subsystem, they were used to construct a software diagram as can be seen in Figure 10.1. Due to the complexity of the mission, the software was divided in five primary blocks. One for processes that are independent of mission phase and four for processes depending on mission phase.

Starting with the surface mission phase, the software on board the UCM shall have two distinct procedures. The first procedure is necessary to control the propellant transfer and storage, as well as the procedure of disconnecting from the propellant production line. The second procedure is dedicated to power generation and distribution in the UCM. The software is required to monitor and process the power consumption data of all subsystems and allocate a fitting amount of  $LH_2$  &  $LO_2$  to the fuel cell. In addition, as  $H_2O$  is a byproduct of the fuel cell,  $H_2O_2$  production should also be managed by this component of the software.

In the ascent phase of the mission, the power generation and distribution software procedures are identical to the surface phase, bar the lack of  $H_2O_2$  production management. On the other hand, the rest of the software procedures are vastly different. Before beginning the ascent, the UCM computer should determine the necessary flight trajectory to achieve the desired orbit and wait for a take-off go-ahead. Once it is received, commands to the propulsion system and ADCS may be provided to ignite and burn the ascent thrusters and maintain a stable trajectory. When the spacecraft reaches the desired altitude, the propulsion system should be commanded once more to perform a circularisation burn.

Next, the operations in orbit are treated. During this time, the UCM must perform close approach and docking with customer spacecraft, as well as the propellant transfer procedure. The software on board must thus accommodate this. The computer will therefore start the orbit phase of the mission by determining the rendezvous time and position and monitor if the customer spacecraft is within close proximity. Once it is, the ADCS shall be commanded to perform the docking procedures. It is important to note, that in the case docking fails due to a critical warning, the UCM should abort docking and stand by for commands from the ground station in order to prevent damage to the UCM or the customer S/C. When the docking is successful, propellant transfer may be initialized and monitored. Finally, the onboard software should be capable of issuing necessary commands to detach from the customer S/C and begin the descent phase. Parallel to this software procedure, the power generation and distribution software should be run. While in orbit, similar to the ascent phase no  $H_2O_2$  production takes place. However, due to the changing environment it is possible to use the solar panels mounted on the UCM while it is not in eclipse. Therefore, the software shall be able to determine if the spacecraft is in eclipse and if the attitude of the spacecraft allows for optimal solar panel power production.

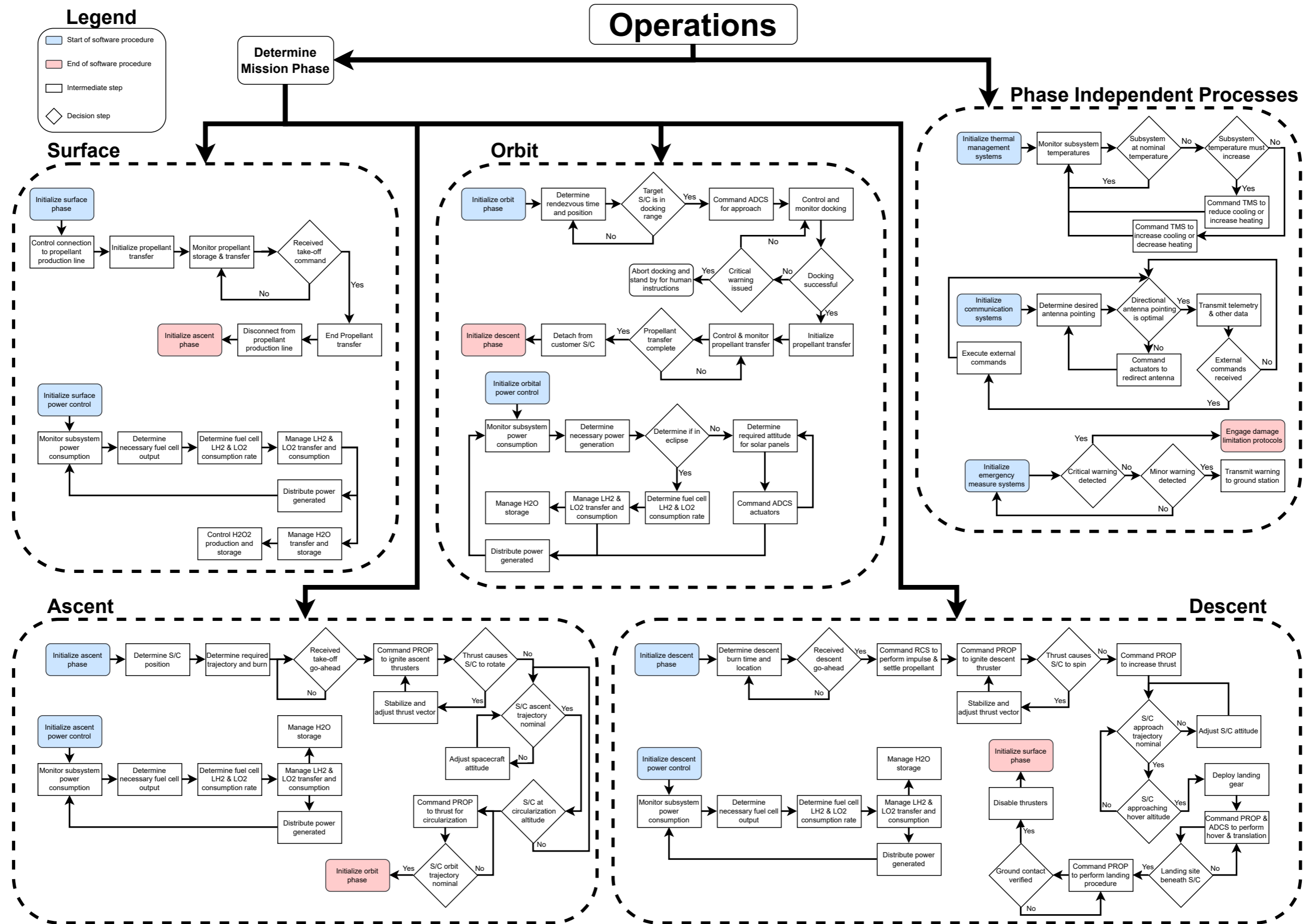


Figure 10.1: Software diagram for lifetime operations



The fourth mission phase dependent software block is dedicated to the descent of the UCM. The power generation and distribution software must perform the exact same functionalities during descent as during ascent. Thus, in order to reduce necessary onboard data storage, the software may be reused. The other functionalities however, are vastly different. The descent phase begins with the onboard software identifying the burn time and location necessary to arrive at the desired landing site. With confirmation from Earth to proceed with descent, the computer must command the ADCS and propulsion systems to settle the propellant tanks, stabilize the spacecraft and begin the descent burn. Similar as during ascent, the onboard computer must maintain a nominal trajectory and attitude. Once the UCM is sufficiently low, the landing gear should be deployed and ADCS and propulsion systems may be commanded to begin hover procedures. During this time, the software must determine the location of the landing site and position the UCM with sufficient accuracy. In the end, the propulsion system should be throttled down to allow for final descent, and all thrusters should be disabled once ground contact is verified.

Finally, mission phase independent processes should be covered. At this stage of the design three software procedures, all running in parallel at all times were defined. The first concerning with the thermal management of the spacecraft. As active thermal control is employed in the UCM, the software must be able to process temperature measurement data and command the TMS to heat or cool UCM components accordingly. The telecommunications subsystem is also designed to operate at all times. In order to ensure no mission failure occurs, the software onboard the UCM must determine and enforce optimal antenna pointing, provide all necessary data to transmit and be capable of executing any external commands received. The last of the software processes defined is the emergency measure treatment. If a warning from any subsystem or sensor is detected, the software shall be able to determine the severity of the warning and select an appropriate course of action. This is done to minimize potential damage to both the UCM and surrounding systems in case of failure.

### 10.1.2. Requirements

With the necessary software procedures defined in the previous subsection, a list of requirements on the C&DH subsystem can be generated. These requirements are to serve as guidelines to determine the architecture of the computer systems and can be seen in Table 10.1.

## 10.2. Configuration and Data Handling

The configuration of the hardware of the C & DH subsystem to fulfill its requirements is presented in Figure 10.2. Each subsystem of the spacecraft is shown with its relevant data handling hardware and data connections with the common data bus. The cryogenic storage system will require various sensors in order to monitor the condition of the payload. Based on these sensors the common data bus may send a command to the heater or cryocooler controller in order to maintain the required temperature and pressure. The electrical power system will require various sensors in order to monitor the output of the solar panels and fuel cells. Furthermore the EPS will include a power distribution control module which will manage a DC to DC converter in order to provide the correct voltage to other electrical components. The structures will include a strain sensor in the landing gear. This will be used to monitor the mass of the spacecraft when on the Lunar surface and serve as a way to calculate the mass of propellant received from NASA. Furthermore a landing gear controller will be included to actuate the deployment servo. The ADCS will include multiple sensors which will, in combination with an attitude determination module, determine the attitude of the spacecraft. Furthermore, a thruster controller will be included which will actuate the thrusters for maneuvers and attitude control. The TT&C subsystem will include an antenna pointing module to control the directional antennae. Moreover, various modules are included in order to be able to receive and transmit information. Finally, the TMS will include temperature sensors in various places around the spacecraft in order to monitor the temperature of important components. In addition, three control modules for the radiator, heater and coolers will be included which will manage the temperature of the spacecraft.

## 10.3. Power consumption estimation

In order to complete the sizing of the UCM, a mass and power consumption estimation was necessary. As the C&DH subsystem has the smallest contribution to total mass of the spacecraft [81], a very trivial estimate was used at this stage of design. It was assumed that the mass of the C&DH subsystem of the UCM will not exceed that of the Apollo guidance computer which weighs a total of 55 kg<sup>1</sup>.

---

<sup>1</sup><https://history.nasa.gov/computers/Ch2-5.html>

**Table 10.1:** Table of Command & Data Handling subsystem requirements

Requirement ID	Requirement
REQ-TC-UCM-CDH-1	The UCM shall be able to determine the optimal flight trajectory for ascent
REQ-TC-UCM-CDH-2	The UCM shall be able to determine the necessary flight trajectory for descent
REQ-TC-UCM-CDH-3	The UCM shall be able to determine necessary maneuvers to achieve desired flight trajectory
REQ-TC-UCM-CDH-4	The UCM shall be able to determine it's own position with an accuracy of TBD meters
REQ-TC-UCM-CDH-5	The UCM shall be able to determine it's own attitude with an accuracy of TBD degrees
REQ-TC-UCM-CDH-6	The UCM shall be able to determine the relative position of a customer S/C with an accuracy of TBD meters
REQ-TC-UCM-CDH-7	The UCM computer shall control the propulsion system engines
REQ-TC-UCM-CDH-8	The UCM computer shall control the RCS thrusters
REQ-TC-UCM-CDH-9	The UCM computer shall determine the necessary power consumption of all subsystems every TBD seconds
REQ-TC-UCM-CDH-10	The UCM computer shall distribute produced power among subsystems to meet power consumption needs
REQ-TC-UCM-CDH-11	The UCM shall be able to determine whether it is exposed to direct sunlight
REQ-TC-UCM-CDH-12	The UCM shall be able to determine the preferred attitude for solar panel operation with an accuracy of TBD degrees
REQ-TC-UCM-CDH-13	The UCM computer shall control the rate of $H_2O_2$ production
REQ-TC-UCM-CDH-14	The UCM computer shall monitor all subsystem temperatures with an accuracy of TBD Kelvin
REQ-TC-UCM-CDH-15	The UCM computer shall be able to control the active components of the TMS
REQ-TC-UCM-CDH-16	The UCM computer shall be able to determine the desired directional antenna pointing with an accuracy of TBD degrees
REQ-TC-UCM-CDH-17	The UCM shall be able to point the directional antenna with an accuracy of TBD degrees
REQ-TC-UCM-CDH-18	The UCM computer shall provide TT+C with telemetry to transmit
REQ-TC-UCM-CDH-19	The UCM computer shall be able to process external commands
REQ-TC-UCM-CDH-20	The UCM computer shall monitor all fluid storage on the UCM
REQ-TC-UCM-CDH-21	The UCM computer shall monitor all fluid flow in the UCM
REQ-TC-UCM-CDH-22	The UCM computer shall be able to actuate all fluid flow controllers
REQ-TC-UCM-CDH-23	The UCM computer shall be able to deploy landing gear
REQ-TC-UCM-CDH-24	The UCM computer shall be able to verify touchdown
REQ-TC-UCM-CDH-25	The UCM computer shall be able to select appropriate course of action when sensor warnings are detected
REQ-TC-UCM-CDH-26	The UCM computer shall be able to actuate the docking mechanism

A more important parameter contributing to the sizing of the other subsystems of the UCM is the power consumption. For planetary spacecraft the power consumption of an on-board processing unit can be estimated as 11% of the total power consumption [81]. However, as this empirical relationship was developed from missions without extremely high power consumption elements such as cryogenic pumps or  $H_2O_2$  production units and these components do not require much additional processing power, these terms of the total power consumption were excluded. The final power consumption of the C&DH is defined in Equation 10.1.

$$P_{C\&DH} = 0.11(P_{total} - P_{pump} - P_{H_2O_2}) \quad (10.1)$$

In Equation 10.1 several variables are used which are defined in the following list:

- $P_{C\&DH}$  is the power consumption of the C&DH subsystem.
- $P_{total}$  is the total power consumption of the UCM.
- $P_{pump}$  is the power consumption of the payload pump systems.
- $P_{H_2O_2}$  is the power consumption of the hydrogen peroxide printer.

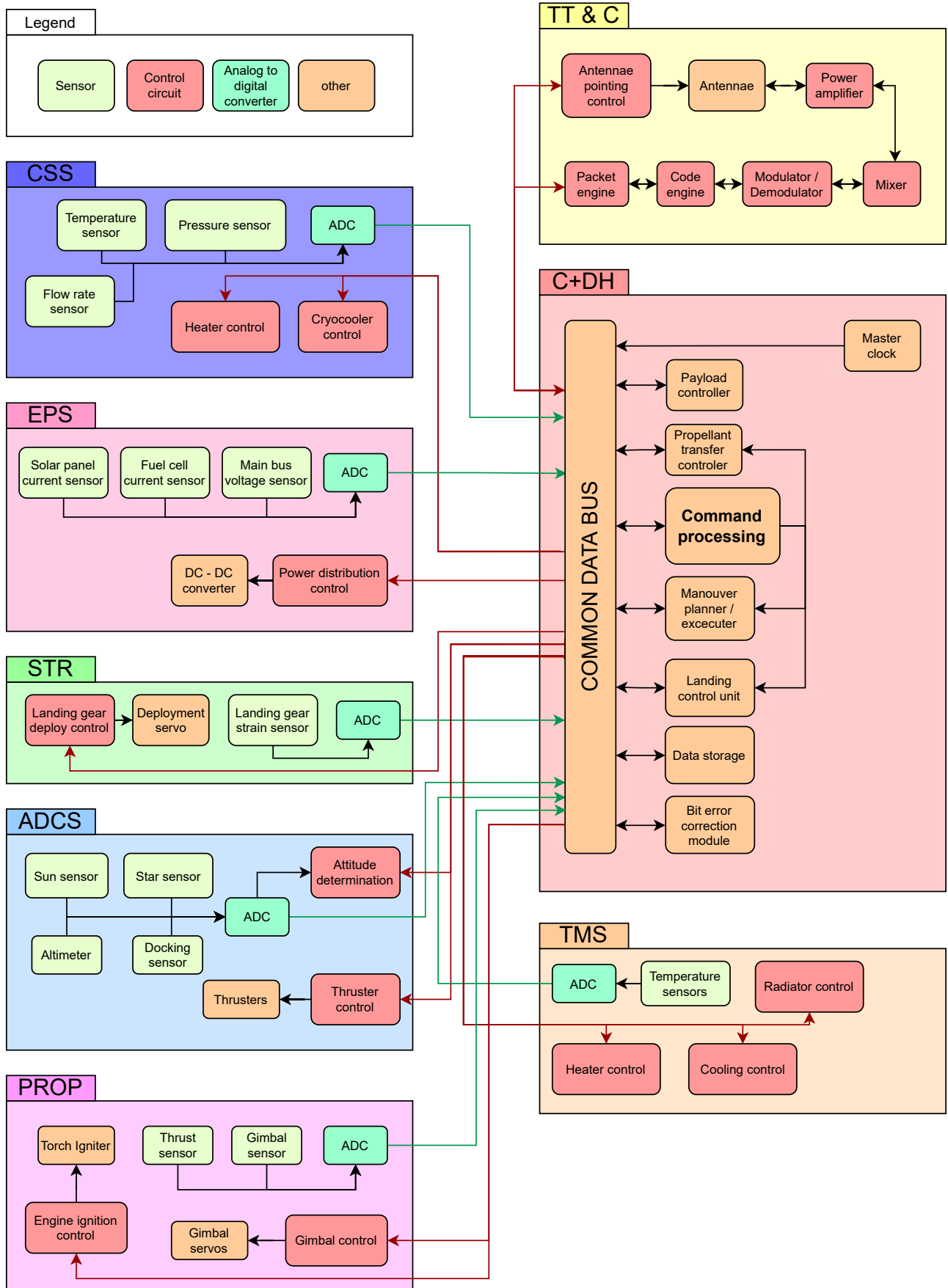


Figure 10.2: UCM data handling diagram

# 11 Thermal Management System

The thermal management system (TMS) is a crucial subsystem of the UCM responsible for managing all temperatures throughout the spacecraft. Several requirements were created for the TMS which are described in Section 11.1. Then, the different operating conditions the TMS will have to work with will be described in Section 11.2. Finally, the method of control will be described in Section 11.3.

## 11.1. Requirements

In this section the requirements for the thermal control system can be found in Table 11.1.

**Table 11.1:** The requirements imposed on the TMS.

Requirement ID	Requirement
REQ-TC-UCM-TMS-1	The thermal control system shall be able to dissipate 3329 W.
REQ-TC-UCM-TMS-2	The thermal control system shall have 41.9 m <sup>2</sup> of radiators.
REQ-TC-UCM-TMS-3	The thermal control system shall recycle 1355.45 W of waste heat in the crater.
REQ-TC-UCM-TMS-4	The mass of the radiators shall be 138.25 kg.
REQ-TC-UCM-TMS-5	The heat pipe system shall use ammonia as cooling fluid.
REQ-TC-UCM-TMS-6	The heat pipe system shall use variable conductance heat pipes.
REQ-TC-UCM-TMS-7	The non condensable gas used in the variable conductance heat pipes shall be hydrogen.
REQ-TC-UCM-TMS-8	The heat pipe system shall use an artery wick with four channels.
REQ-TC-UCM-TMS-9	The heat pipe system shall consist of 27 heat pipes.
REQ-TC-UCM-TMS-10	The spacecraft shall use barium sulphate with polyvinyl alcohol as coating.
REQ-TC-UCM-TMS-11	The Thermal Control System shall use kapton heaters.
REQ-TC-UCM-TMS-12	The Thermal Control System shall use 130.67 W to heat the payload oxygen and water tanks.

## 11.2. Mission Profiles

In spacecraft thermodynamics, Equation 11.1 holds for the heat equilibrium of a spacecraft. With  $Q_{out}$  the heat radiated by the spacecraft,  $Q_{rad}$  the heat received from the environmental radiation and  $Q_w$  the internal heat to be dissipated of the spacecraft.

$$Q_{out} = Q_{rad} + Q_w \quad (11.1)$$

To size the TMS, the critical operation mode for the TMS should be identified first. As shown in Equation 11.1, heat to be dissipated and radiation received from the Lunar environment will influence the TMS the most. As the to be dissipated heat closely relates to the amount of power the spacecraft uses, the most critical mode for this factor can be identified. The heat to be dissipated was calculated using Equation 11.2.

$$Q_w = \sum (P_{subsystem} \cdot (1 - \eta_{subsystem})) \quad (11.2)$$

In Equation 11.2,  $Q_w$  is the waste heat,  $P_{subsystem}$  is the power per subsystem and  $\eta_{subsystem}$  the efficiency per subsystem. For some subsystems the efficiency is zero, as all the electrical energy is converted into heat energy. For example, this is true for the C&DH subsystem.

The radiation from the environment can also be modelled. There are two main sources of radiation in the Lunar environment; Solar radiation and infrared radiation from the surface of the Moon [81]. In figure Figure 11.1 the radiation the spacecraft will receive while in LLO is modelled. This was done with data from the Lunar Reconnaissance Orbiter Mission Design [43]. Peak radiation is received when the ascending node,  $\Omega$ , is equal to 0 ° and the spacecraft is directly between the Moon and the Sun ( $\theta = 180$ ). This peak radiation is equal to 2868.87  $\frac{W}{m^2}$ . The following equations were used to calculate the total environmental radiation [43]:

$$Q_{rad} = Q_{solar} + Q_{IR} \quad (11.3)$$

$$Q_{IR} = (C1 - C2) \cdot \cos \theta \cos \Omega + C2 \quad (11.4)$$

$$C1 = Q_{Lunar\ max} = Q_{solar}(1 - F_{albedo}) \quad (11.5)$$

With  $Q_{solar}$  being the radiation from the sun ( $1420 \frac{W}{m^2}$ ),  $Q_{IR}$  the infrared radiation from the Lunar surface,  $C1$  the maximum infrared Lunar flux ( $1335 \frac{W}{m^2}$ ),  $C2$  the minimum infrared Lunar flux ( $5 \frac{W}{m^2}$ ),  $F_{albedo}$  the albedo of the Lunar surface (0.13),  $\theta$  the true anomaly and  $\Omega$  the ascending node of the polar orbit [43].

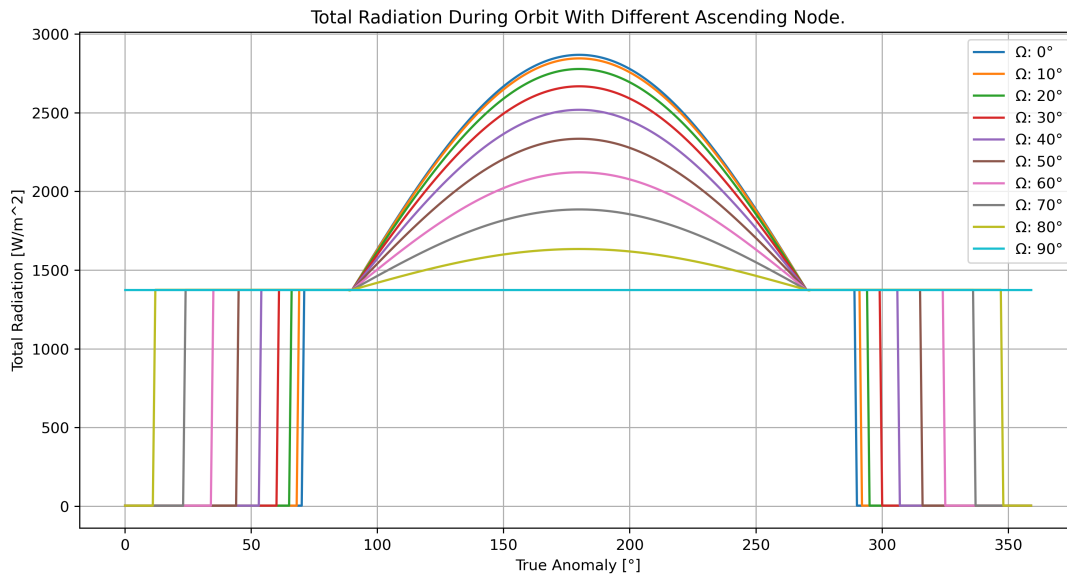


Figure 11.1

The TMS is part of the iterative design code that was coded in Python. This code first identified the most critical time for the TMS by calculating the radiator area for every mode. The most critical time for the TMS was identified to be when the spacecraft is refueling the customer in LLO in the sun (mode 7). This is because the pump uses a lot of power, and the radiation from the environment is at its peak. Thus, the TMS shall be designed and sized for this specific phase of the mission.

## 11.3. Thermal Control System

To be able to control temperature of the spacecraft the spacecraft will make use of thermal control devices. Designing this system is challenging, as both the waste heat and environmental radiation differ drastically per phase of the mission. Also, many components of the subsystem shall be kept at specific temperature ranges.

### 11.3.1. Variable Conductance Heat Pipes

Variable Conductance Heat Pipes (VCHP) will be used on the spacecraft for thermal control. To explain how VCHP work, first ordinary heat pipes should be explained. On one end of the heat pipe heat is applied, turning the cooling fluid into a vapour (the evaporator). The vapour then travels to the cooler end of the pipe via an adiabatic part of the pipe, where it condenses (the condenser). The fluid then travels back to the warmer side of the via a wick in the side of the pipe, where it can then again be vaporised. This way the heat pipe has very high thermal conductivity, up to  $100000 \frac{W}{m} \cdot K$  [53].

The limitation of heat pipes is that the condenser area can not be controlled; no specific temperature range can be kept for the condenser and the component that cools the condenser. This is where VCHP have a clear advantage, as they use a Non Condensable Gas (NCG) to control the condenser area. Looking at Figure 11.2 two power modes can be observed; One where there is a relatively high amount of waste heat and another where there is relatively less waste heat.

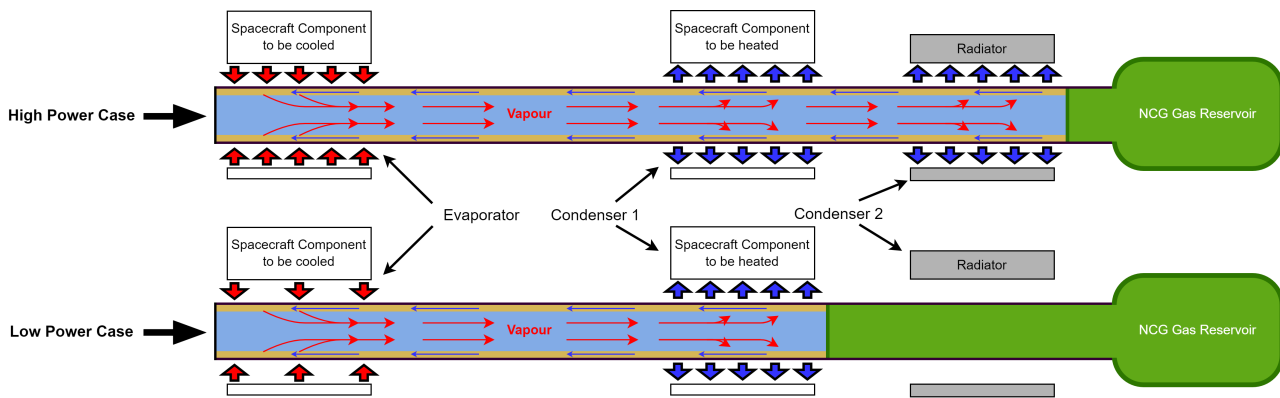


Figure 11.2

In the high power case all of the condensers are used. The front of the NCG can be moved, controlling the area where the heated vapour can condense. This way the to be heated component of the spacecraft can be kept at a specific temperature. This also improves the efficiency of the system; Instead of radiating waste heat into space, it is reused to heat certain spacecraft components. In the low power case only the first condenser is used. As less heat is added to the system, less condenser area is needed to heat the spacecraft component. The front of the NCG can be controlled by changing the temperature of the reservoir <sup>1</sup>. This is why VCHP are a form of active thermal control.

### 11.3.2. Variable Conductance Heat Pipes Design

To implement the heat pipes into the spacecraft architecture the heat output and size of the heat pipes should be determined. In this subsection the heat pipes will be sized and the heat output will be analysed.

To begin the sizing some preliminary assumptions should be made for the piping system. Ammonia shall be used as working fluid with a maximum temperature of 313.15 K. This is because the temperature operating range of ammonia (200 – 405 K [46]) is the best fit for the temperature operating range for the spacecraft and ammonia fluid systems have a TRL of 9. From preliminary spacecraft sizing in the midterm report [5], the length of the heat pipe, evaporator and condenser shall be 3 m, 0.36 m and 0.36 m, respectively, to be able to connect spacecrafts components to each other and to the radiators. This length can later be varied if needed.

The NCG used in the VCHP shall be hydrogen. This NCG has been successfully implemented in an ammonia heat pipe system before<sup>2</sup>. Also, as hydrogen has a very low freezing point (14 K <sup>3</sup>), the hydrogen gas will never freeze, even in the coldest mode inside the crater.

According to the wick selection process described Heat Pipes (Sixth Edition) [56], the optimal wick configuration for the heat pipes is a four channel artery wick system as shown in Figure 11.3. This is a wick where there are four tubes inside the vapor tube that transport the liquid back to the evaporator. The mesh shall be made out of titanium with mesh size 400 with corresponding capillary radius,  $r_c$ , of 0.0015 cm.

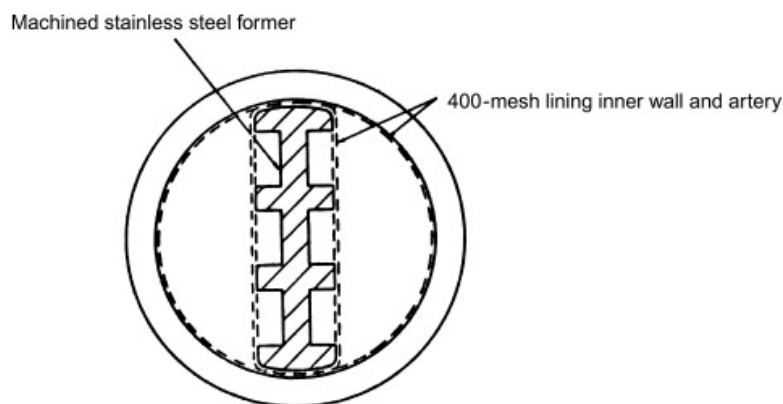


Figure 11.3: Artery wick design. This design uses six channels, while the chosen design uses four[56].

<sup>1</sup>URL:[https://tfaws.nasa.gov/TFAWS06/Proceedings/Thermal%20Control%20Technology/Papers/TFAWS06-1033\\_Paper\\_Matonak.pdf](https://tfaws.nasa.gov/TFAWS06/Proceedings/Thermal%20Control%20Technology/Papers/TFAWS06-1033_Paper_Matonak.pdf)

<sup>2</sup>URL:[https://www.jstor.org/stable/pdf/44735761.pdf?refreqid=excelsior%3Ac55cb2a95edf9bd437c3cd892d232932&ab\\_segments=&origin=&acceptTC=1](https://www.jstor.org/stable/pdf/44735761.pdf?refreqid=excelsior%3Ac55cb2a95edf9bd437c3cd892d232932&ab_segments=&origin=&acceptTC=1)

<sup>3</sup>URL:[https://www.engineeringtoolbox.com/hydrogen-d\\_1419.html](https://www.engineeringtoolbox.com/hydrogen-d_1419.html)

To determine the amount of heat the the heat pipes can transport Equation 11.6 should be solved for Q [56]. Before this is possible the individual variables should be known.

$$\Delta P_c = \Delta P_{lm} + \Delta P_{la} + \Delta P_g + \Delta P_{vl} \quad (11.6)$$

In Equation 11.7, Equation 11.10, Equation 11.9, Equation 11.8 and Equation 11.11 the variables will be determined [56].

$$\Delta P_c = \frac{2\sigma_l \cos \theta}{r_c} \quad (11.7)$$

With  $\Delta P_c$  the capillary pressure generated by the arteries,  $\sigma_l$  the surface tension of the liquid,  $\theta$  the wetting angle (perfect wetting assumed;  $\theta = 0$ ) and  $r_c$  the capillary radius.

$$\Delta P_{lm} = \frac{\pi r K_l Q}{A_c 2K} \quad (11.8)$$

With  $\Delta P_{lm}$  the summed pressure loss in the condenser and evaporator,  $r$  the heat pipe radius,  $K_l$  a fluid property,  $Q$  the heat,  $A_c$  the circumferential flow area for the mesh and  $K$  a mesh property. The heat pipe radius was optimised to find the highest heat transfer.

$$\Delta P_{la} = \frac{K_l l_{eff} c Q}{A_c 2K} \quad (11.9)$$

With  $\Delta P_{la}$  the pressure loss, assuming laminar flow, in a rectangular duct (as the arteries are rectangular),  $K_l$  a fluid property,  $l_{eff} c$  the effective circumferential flow length,  $Q$  the heat,  $A_c$  the circumferential flow area for the mesh and  $K$  the permeability of the mesh.

$$\Delta P_g = \rho_l g l \sin \phi \quad (11.10)$$

With  $\Delta P_g$  the gravitational pressure drop,  $\rho_l$  the fluid density,  $g$  the gravitational constant and  $\phi$  a function of channel aspect ratio.

$$\Delta P_{vl} = \frac{1}{2} \cdot \left( \frac{8K_v l_{eff} Q}{\pi r_h^4} \right) \quad (11.11)$$

With  $\Delta P_{vl}$  the vapour pressure drop,  $K_v$  a vapour property,  $l_{eff}$  the effective pipe length and  $r_{hi}$  the hydraulic radius.

$$K_l = \frac{\mu_l}{\rho_l L} \quad (11.12)$$

With  $\mu_l$  the dynamic viscosity of the fluid,  $\rho_l$  the density of the fluid and  $L$  the latent heat of the fluid.

$$K_v = \frac{\mu_v}{\rho_v L} \quad (11.13)$$

With  $\mu_v$  the dynamic viscosity of the vapour,  $\rho_v$  the density of the vapour and  $L$  the latent heat of the fluid.

$$t_{min} = \frac{Pr}{\Omega} \quad (11.14)$$

With  $t_{min}$  the minimum thickness of the wall of the heat pipe,  $P$  the pressure inside of the heat pipe and  $\Omega$  the tensile strength of the material used. All of the variables used were summarised in Table 11.2.

**Table 11.2:** Constants related to heat pipe calculations [57][56].

Constant	Value	Unit
$r$	0.002955	m
$l_{eff}$	3	m
$l_{evap}$	0.36	m
$L @ NH_3$ 313.15 K	1101	$\frac{kJ}{kg}$
$\mu_l NH_3 @ 313.15$ K	0.0020	cP
$\mu_v NH_3 @ 313.15$ K	0.000116	cP
$\rho_l NH_3 @ 313.15$ K	579.5	$\frac{kg}{m^3}$
$\rho_v NH_3 @ 313.15$ K	12	$\frac{kg}{m^3}$
$\sigma_l NH_3 @ 313.15$ K	0.01833	$\frac{N}{m}$
$r_c$	0.0015	cm
$K$	$3.14 \cdot 10^{-11}$	$m^2$
$r_h$	0.0015194	m
$\theta$	0	°

Using these values the heat flow of a heat pipe was found to equal 391.7 W. The length of the heat pipe can be varied for specific parts of the spacecraft. The length of the heat pipe has an inverse relation with the amount of heat it can transport. Meaning that the longer the heat pipe is, the less heat it can transport per second. Changing only  $l_{eff}$  to 2 m will increase to heat its able to transport to 607.2 W. In Figure 11.4 The length of the heat pipe with corresponding heat its able to transport is shown.

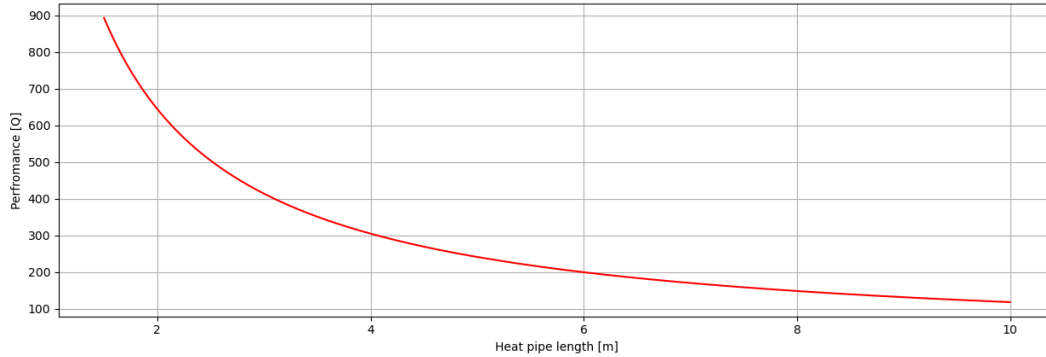


Figure 11.4: Effect of heat pipe length on total heat its able to transport.

### 11.3.3. Variable Conductance Heat Pipes Architecture

As the optimal thermal conditions differ drastically from one spacecraft component to the other, designing the heat pipe architecture is a challenging task. There are a number of factors that should be taken into account; The number of heat pipes each component requires, which, in turn, depends on the length of the heat pipes, as discussed in the previous subsection and the placing of the radiators, which also influences the length of heat pipes.

#### Heating of the Water and Hydrogen Peroxide Tanks

The water, payload oxygen and hydrogen peroxide tanks will be kept at 288.15 K, 80 K and 288.15 K, respectively. These tanks will be heated in the crater via recycling of the waste heat via heat pipes or simply by heating by a heater. The amount of heat needed to heat the tanks was estimated via the following formula:

$$Q_{heat} = \sigma \epsilon (T_{tank}^4 - T_{crater}^4) A_{tank} \quad (11.15)$$

With  $Q_{heat}$  the heat that needs to be channeled into the tanks to keep them at the required temperature,  $\sigma$  the Stefann Boltzmann's constant,  $\epsilon$  the emissivity of the tank,  $T_{tank}$  the temperature of the tank,  $T_{crater}$  the effective temperature in the crater and  $A_{tank}$  the surface area of the tank. The heat needed for the water, payload oxygen and the hydrogen peroxide tank are estimated to be 62.98 W, 67.69 W, and 1355.45 W, respectively. As the power required to heat the oxygen and water tank is quite low, it was deemed to be heated by heaters instead of by recycling waste heat. This is because the heaters will be significantly lighter than the heat pipe system.

To heat the hydrogen peroxide tank there will be a condenser where this tank is, as seen in Figure 11.4.

In Table 11.3 a preliminary configuration of the heat pipes is shown. The length was now calculated as the maximum length the heat pipe will be. This length was an estimation taking into account the geometry of the spacecraft. In Table 11.3 first the specific heat pipe is identified with an identifier, which specifies for which subsystem the heat is to be removed. In the second column is the *max* heat to be removed of the spacecraft component.



**Table 11.3:** Preliminary configuration of the heat pipes per specific spacecraft component.

Identifier	Heat to be removed [ $Q_w$ ]	Number of Heat Pipes	Max. Length in [m]	Description
HP-PUMP-1	203.1	1	5.89	Transports heat of the oxygen fuel pump directly to a radiator.
HP-CSS-(1 to 8)	1819.5	8	5.31	Transports heat of the hydrogen cryocooler directly to a radiator.
HP-CSS-9	378.0	1	3.26	Transports heat of the oxygen cryocooler directly to a radiator.
HP-CDH-1	180.0	1	6.64	Transports heat of the main computer directly to a radiator.
HP-ADCS-(1 to 4)	1561.1	4	3.17	Transports heat of the hydrogen peroxide printer directly to a radiator.
HP-EPS-(1 to 5)	2515.1	8	3.89	Transports heat of the fuel cell to the hydrogen peroxide tank and then to a radiator.
HP-ADCS-(1 to 4)	1561.1	4	3.17	Transports heat of the hydrogen peroxide printer directly to a radiator.
HP-TTC-(1 to 4)	240	4	19+	Transports heat of the antennas (one on top and three on the side of the s/c) to a radiator.

As Table 11.3 only considers the highest heat to be removed, which drastically changes between different phases of the mission, some of the heat pipes will freeze in the crater/eclipse. This is not an issue however, as freezing and thawing of the heat pipes is a possibility when using VCHP. The NCG reservoir can also be used to restrict freezing of the pipe by stopping fluid movement through the pipe<sup>4</sup>. The NCG will also increase the pressure in the heat pipe, providing an easier startup.

In Figure 11.6 a preliminary heat pipe architecture is shown. The figure shows the plumbing of the heat pipes in the spacecraft. The locations of the spacecraft components are shown at their approximate place in the spacecraft. The read box stands for an evaporator, the blue box for a condenser and the white circle stands for the NCG reservoir.

Some spacecraft components of the spacecraft that also produce heat are left out of the heat pipe system. This is because these components do not produce a significant amount of heat. The hydrogen fuel pump, for example, only produces 36.96 W of waste heat. For this low amount of power it was decided that other thermal control system are used. For example, thermal straps to connect the spacecraft component to the radiator. The architecture of the thermal straps is out of the scope of this report, however.

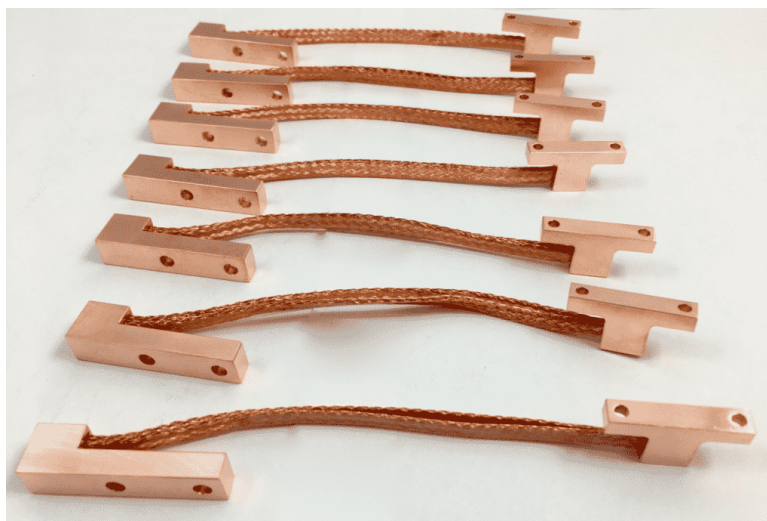


**Figure 11.5:** Thermal straps that passively move heat [URL:https://thermal-space.com/copper-thermal-straps/](https://thermal-space.com/copper-thermal-straps/).

<sup>4</sup>[URL:https://tfaws.nasa.gov/TFAWS12/Proceedings/TFAWS2012-AT-001.pdf](https://tfaws.nasa.gov/TFAWS12/Proceedings/TFAWS2012-AT-001.pdf)

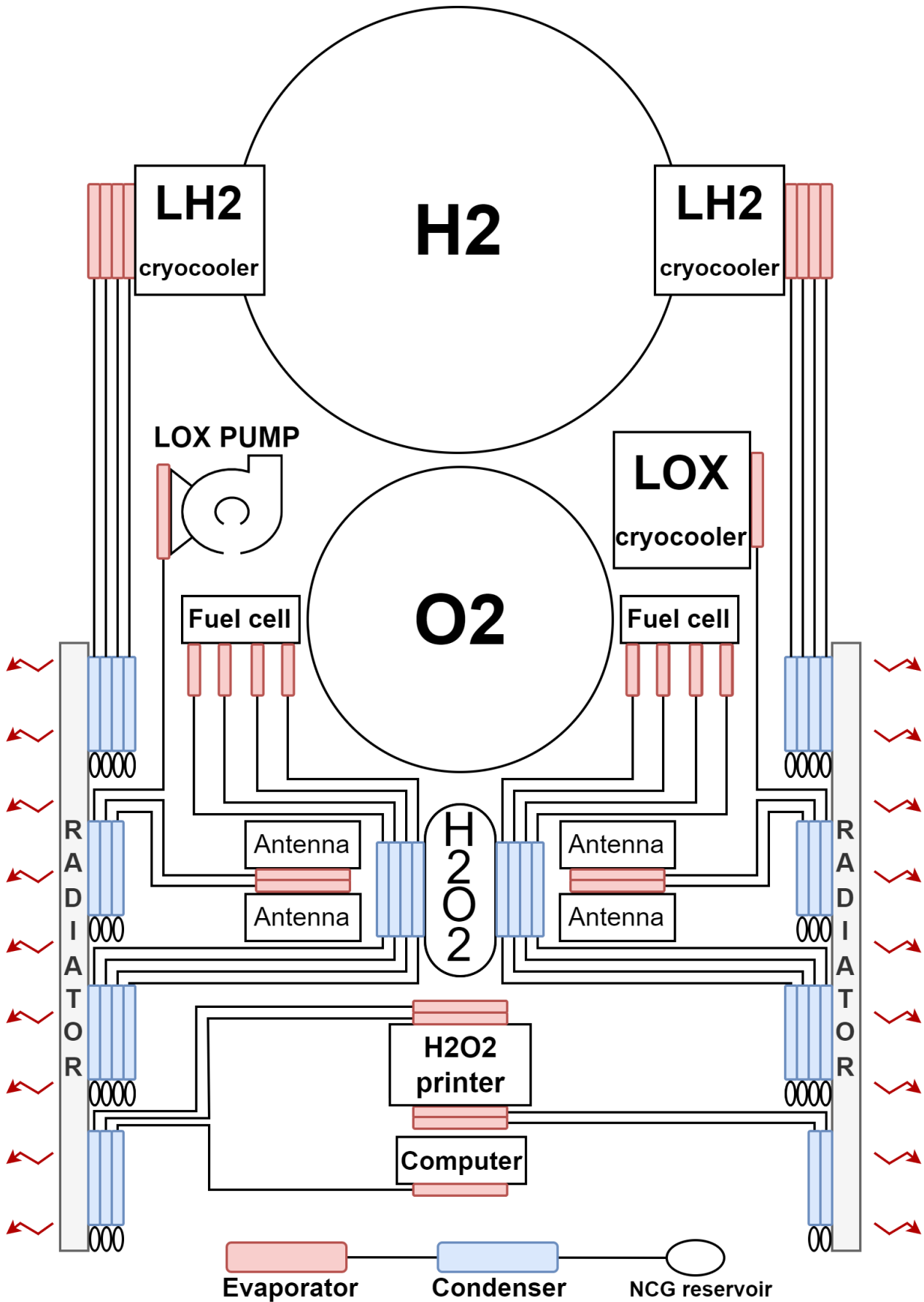


Figure 11.6: Preliminary heat pipe architecture.

### 11.3.4. Coating

To have better thermal control of the spacecraft, a thermal coating will be used. To find the optimal coating a database from NASA was utilised [35]. The coating will determine two main factors of the spacecraft surface:  $\alpha$ , the absorptivity of the spacecraft, and  $\epsilon$ , the emissivity of the spacecraft. As the critical mode for the TMS is refueling the customer in orbit, where the temperatures and thermal load are relatively high, the absorptivity should be as low as possible and the emissivity should be as high as possible.

Using Equation 4.5 and changing the absorptivity,  $\alpha$ , and the emissivity,  $\epsilon$ , the relation of these variables to the maximum variables can be seen. The absorptivity has a near linear relation with the maximum temperature while the emissivity has a hyperbolic relation with the maximum temperature. This means that a low emissivity drastically increases the maximum temperature while a high emissivity has a progressively lower effect on lowering the temperature. As the size of the coating database is considerable, a formula was set up to find the optimal coating:

$$f_{coating} = \alpha_{coating} \cdot \frac{1}{\epsilon_{coating}^2} \quad (11.16)$$

With  $f_{coating}$  a factor that can determine the best coating; the lower this factor is, the more desirable the coating is. A python code was written to find the optimal coating. The optimal coating was found to be barium sulphate with polyvinyl alcohol, with  $\alpha = 0.06$  and  $\epsilon = 0.88$ . This coating will be applied everywhere possible on the spacecraft. It was assumed that the entire spacecraft has the same absorptivity and emissivity for the calculations.

### 11.3.5. Radiator

The radiator will be sized using the Stefan–Boltzmann law (Equation 11.17), as all of the values are known except for the radiator area. Body-mounted radiators will be used. This is because deployable radiators are prone to failure<sup>5</sup> when deploying and they need to be extended and retracted during launch and flight due to launch loads.

$$Q = \epsilon \sigma A T^4 \quad (11.17)$$

As the environmental radiation also has to be taken into account, the formula to calculate the radiator area will differ from mode to mode. The higher the environmental radiation, the more surface area needed to control the temperature of the spacecraft. For the modes that are in direct sunlight Equation 11.18 holds (modes 2, 3, 5, 7 and 9):

$$A_{radiator} = \frac{Q_w}{T_{radiator}^4 \sigma \epsilon - (q_{IRorbit} + q_{albedo} + q_{solar})} \quad (11.18)$$

Where  $A_{radiator}$  is the radiator area,  $Q_w$  is the waste heat,  $T_{radiator}$  the radiator temperature,  $\sigma$  the Stefan-Boltzmann's constant,  $\epsilon$  the emissivity of the radiator,  $q_{IRorbit}$  the average infrared flux in orbit,  $q_{albedo}$  the albedo flux from the Lunar surface and  $q_{solar}$  the solar flux.

The temperature of the radiator was set to 303.15 K, as this is the limiting temperature for the outside of the spacecraft. This is because the star sensors have a maximum operating temperature of 303.15 K [81].

for modes 4, 6 and 8 Equation 11.19 holds.

$$A_{radiator} = \frac{Q_w}{T_{radiator}^4 \sigma \epsilon - (q_{IRorbit})} \quad (11.19)$$

Lastly for modes 1, 2 and 10 Equation 11.20 holds for the radiator area.

$$A_{radiator} = \frac{Q_w}{T_{radiator}^4 \sigma \epsilon - (q_{IRcrater})} \quad (11.20)$$

Where  $q_{IRcrater}$  is the infrared flux inside the crater.

For every mode the radiator area was determined. The highest surface area was found for mode 7; Refueling in the sun. Therefore the minimum radiator area is equal to the area needed for mode 7, which is equal to 41.89 m<sup>2</sup>. Using that the radiator unit mass is equal to 3.3  $\frac{\text{kg}}{\text{m}^2}$  [81] the total mass of the radiators will be 138.25 kg.

<sup>5</sup>URL:<https://esmat.su.se/esmatpapers/pastpapers/pdfs/2021/rivera.pdf>

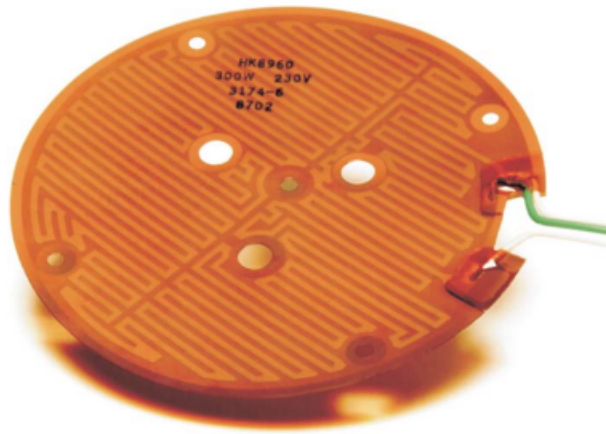


Figure 11.7: Kapton heater for space applications <http://www.temflexcontrols.com/pdf/hs202b.pdf>.

### 11.3.6. Electrical heating

As mentioned previously, for many of the applications heat pipes are to be used. However, for smaller heating requirements a complex heating pipe system may not be necessary and even unreliable. One of the systems that are required to be heated are the RCS thrusters. These require a range of  $+15C^{\circ} - +80C^{\circ}$ <sup>6</sup>. For such an application (and most other applications) electrical resistance heaters are used, in particular Kapton heaters<sup>7</sup>. Since the propellant shall arrive heated already, minimal heating of the inlet or the fuel lines would be necessary, therefore the power requirement is assumed to be negligible. A kapton heater can be seen below: Further, the  $GO_2$  &  $GH_2$  tanks are required to be heated to  $15 C^{\circ}$ . For this application Kapton is also to be used, and the power requirement is considered negligible, since the masses for  $GO_2$  and  $GH_2$  are 21 g and 751 g respectively, which is negligible (from Chapter 7).

As discussed in Section 11.3.3 the oxygen tank and water tank need to be heated in the crater. As standard kapton heaters weight  $0.05 \frac{g}{cm^2}$  with  $0.8 \frac{W}{cm^2}$ <sup>8</sup> and the power requirements of both the oxygen tank and water tank were less than 70 W. The total weight of the heater of each of the tanks would then be less than 5 g and is therefore seen as negligible for the scope of this report.

<sup>6</sup><https://www.nammo.com/product/220n-h2o2-thruster/>

<sup>7</sup><https://www.nasa.gov/smallsat-institute/sst-soa/thermal-control>

<sup>8</sup>URL:[https://www.nph-processheaters.com/assets/uploads/pdfs/flexible-heaters/Kapton\\_Insulated\\_and\\_Silicone\\_Rubber\\_Flexible\\_Heaters.pdf](https://www.nph-processheaters.com/assets/uploads/pdfs/flexible-heaters/Kapton_Insulated_and_Silicone_Rubber_Flexible_Heaters.pdf)

# 12 Structural Design & Layout

The structural design and layout (STR) is an essential design aspect of the UCM. The STR encompasses all the structural elements that hold the subsystems of the UCM together. Additionally, the STR subsystem will contain the landing gear which will be designed in Section 12.1. The landing gear is important as it ensures the entire structure of the UCM stays intact upon landing on the Lunar surface. In Section 12.3 the configuration and layout of the UCM will be discussed.

## 12.1. Landing Gear Design

**Table 12.1:** Basic structure and operations landing gear requirements [60].

Requirement ID	Requirement
REQ-TC-UCM-STR-LG-1	The landing gear shall withstand loads and conditions imposed by the natural and induced environments.
REQ-TC-UCM-STR-LG-2	The landing gear shall maintain strut loads within the LM structural design requirements
REQ-TC-UCM-STR-LG-3	The landing gear shall deploy and lock down in Lunar orbit
REQ-TC-UCM-STR-LG-4	The landing gear shall provide sufficient energy -absorption capability at touchdown
REQ-TC-UCM-STR-LG-5	The landing gear shall provide adequate toppling stability at touchdown.
REQ-TC-UCM-STR-LG-6	The landing gear shall provide sufficient clearance on Lunar surface to avoid impact of descent-stage structure, tanks, and plumbing.
REQ-TC-UCM-STR-LG-7	The landing gear absorbers shall be reusable at least 25 times.

The landing gear is one of the most essential subsystems of the UCM. It gives the lander the required stability and support during the landing. It is also responsible for absorbing the landing shocks, such that the main structure of the vehicle remains intact. In this section a preliminary design of landing gear will be performed including a stability and stress analysis. It also will include a comprehensive study on reusability of the absorbers, followed by their initial sizing.

### 12.1.1. Landing Gear Layout & Configuration

Over the past decades, a number of the planetary landers has been created, each with a unique landing gear configuration, tailored to the specific needs of the intended mission. Despite the uniqueness of their designs, the majority of these configurations can be segregated (based on their working principle and schematics) into two main categories: an inverted tripod configuration and a cantilever configuration, shown in Figure 12.1. Both configurations have been used in previous Lunar missions<sup>1</sup> [59]. Even though both were applied, there are several differences between them.

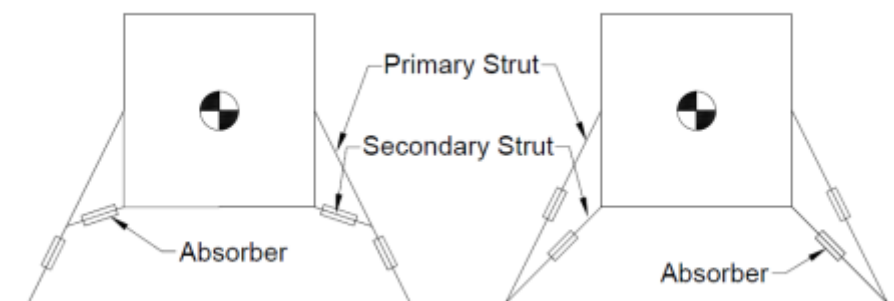


**Figure 12.1:** Cantilever design on the left, and the inverted tripod on the right [80]

The inverted tripod type consists of two types of struts or actuators: primary and secondary, which are both connected to the lander's footpad. Both struts are designed to carry axial loads and in the majority of cases,

<sup>1</sup><https://nssdc.gsfc.nasa.gov/nmc/spacecraft/display.action?id=1968-001A>

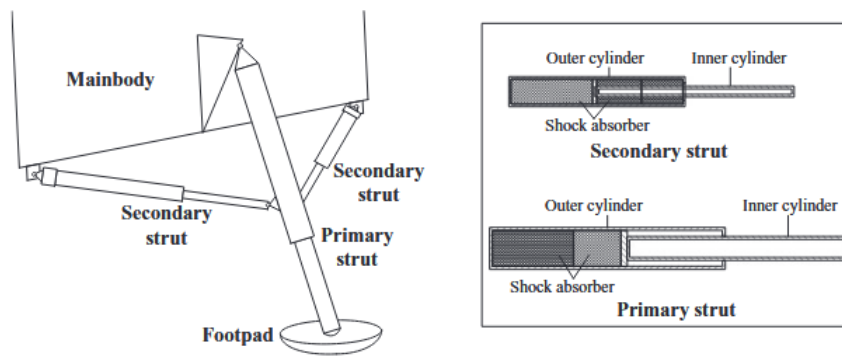


Figure 12.2: Cantilever configuration of landing gear, with strut design layout [42]

both absorb main landing shocks with adequate absorbers [80]. The inverted tripod type is more suitable for smaller landers, as the complexity of the system is less as to the other types [87].

On the other hand, the cantilever landing gear configuration only has a primary actuator coupled to the footpad. The secondary strut is connected to the upper part of the primary one, looking like a cantilever beam. In comparison to the tripod configuration, the primary strut is subjected mostly to the bending moment coming from the secondary strut, which is predominantly axially loaded. Both struts are equipped with shock absorbers, but the primary absorber is designed to tackle the vertical impact, whereas the secondary should absorb the horizontal impact [87]. The cantilever design is superior to the tripod configuration in terms of both mass and stability, but provides larger clearance requirements [80]. The increased performance of the cantilever configuration is burdened with a higher design and system complexity and a more difficult manufacturing process [87][80]. Generally, this landing gear configuration is recommended for large-scale landers [87].

Given all the advantages and disadvantages of the previously discussed configurations, the cantilever configuration was selected for the UCM. It provides higher stability and lower mass for this particular subsystem and given the high mass and height of the UCM is far more restricting than either system complexity or part manufacturability. Moreover, this exact type was used for the Apollo program, providing proof of concept and giving an opportunity to implement suggested modifications [59]. The final configuration depicted in Figure 12.2 consists of one primary strut equipped with a primary shock absorber and two secondary type actuators that are fixed at  $45^\circ$  with respect to the primary one, armed with their respective absorbers as well.

Apart from the landing gear strut configurations, the final gear configuration is decided by establishing the required amount of legs and their layout. Both parameters influence the so-called polygon of landing stability, which is an area bounding the projection of the center of gravity position vector as shown by Figure 12.3. This polygon depicts a stability region, where the S/C will not turn over [87]. The polygon vertices correspond to the positions of the landing pads. The larger the area of the polygon, the better the stability. However, larger areas result in more complex mechanical interfaces and a heavier structure [87]. The Apollo program engineers initially considered using a six leg lander to increase stability, but ultimately abandoned the idea because of the mass increase [47]. The implications of the larger stability lead to the designing of mostly three-legged or four-legged landing systems [80]. However, NASA recommends using at least four legs to limit the chance of flip overs on uneven surfaces [47]. Therefore, the four leg configuration will be adopted for the preliminary design of the UCM's landing gear, with the landing gear legs positioned at four corners of the spacecraft.

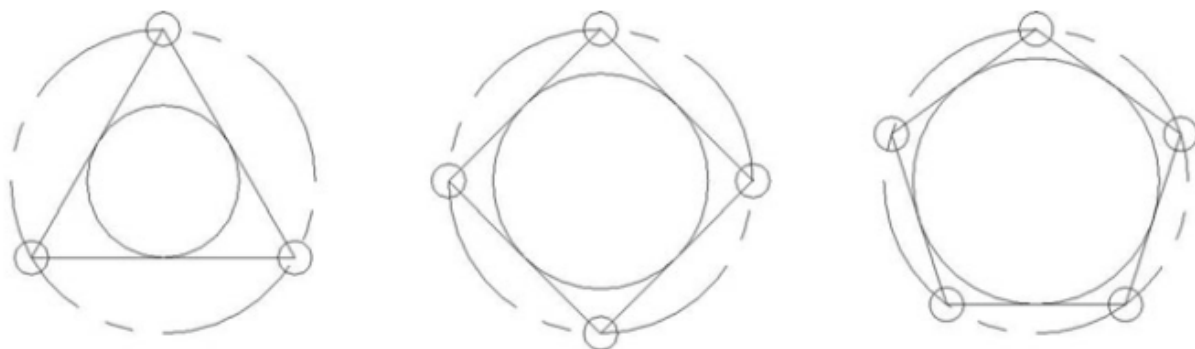


Figure 12.3: Stability polygons for different quantity of footpads [87]

### 12.1.2. Landing Gear Geometry & Stability

In order to properly size the landing gear width, a full dynamic landing stability study has to be conducted with different load cases applied. Unfortunately, given the short time frame of this project, this is not possible. Hence, only a simplified Two-Dimensional In-elastic Impact Theory will be applied for symmetrical landing conditions. Yet, the simplified model still requires input of basic geometrical parameters. These are shown in Figure 12.4 and defined as follows:

- $L_w$ : The horizontal distance between the c.g. and the top attachment of the primary strut, constrained by the faring diameter.
- $L_v$ : The vertical distance between the ground and the bottom of the lander, calculated as the sum of minimum clearance distance  $D_h$  and the maximal vertical absorber stroke (translating to the maximal allowable height decrease of the lander).
- $D_h$ : minimum clearance distance, defined as the sum of the engine's length and half its diameter [80].
- $L_{cg}$ : The vertical distance between the bottom of the lander and the center of gravity.
- $L_{fp}$ : The horizontal distance from the center of gravity to the footpad.
- $\tau_p$ : The angle between the primary strut with the body vertical reference. Assumed to be  $25^\circ$  as explained in [80].
- $\tau_t$ : The angle between the secondary strut with the body vertical reference. Assumed to be  $80^\circ$  as explained in [80].

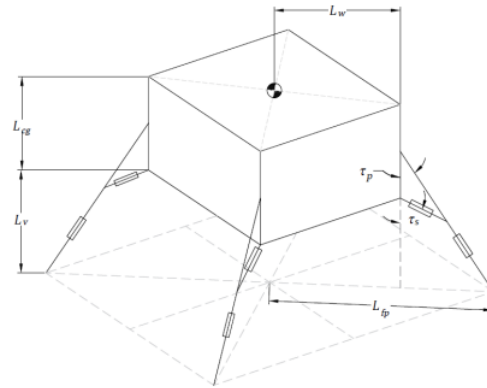


Figure 12.4: Basic geometry parameters of the lander [80]

### Two-Dimensional Inelastic Impact Theory & Tumbling modes

The stability of the vehicle at landing depends on the number of parameters including terrain slope or landing velocity, but primarily is effected by the landing orientation/modes [80]. These modes are derived based on the number of legs and the order of the pads touching the soil as shown in Figure 12.5. NASA differentiates between four critical tumbling modes [78]:

- *2 and over* : Two feet stick simultaneously; the vehicle then rotates about an axis connecting the two feet so as to carry the center of gravity over the axis of rotation.
- *2-2 and over*: Two feet stick simultaneously; the vehicle then rotates leading to a two and over impact on the remaining two feet.
- *2-1 and over*: Two feet stick simultaneously; the vehicle then rotates until a single other foot sticks. Consequently, there is a rotation about an axis through the single pinned foot carrying the center of gravity over the axis of rotation.
- *1-2-1 and over*: A single foot sticks; the vehicle then rotates about an axis through this foot leading to a two-one and over impact involving the remaining feet.

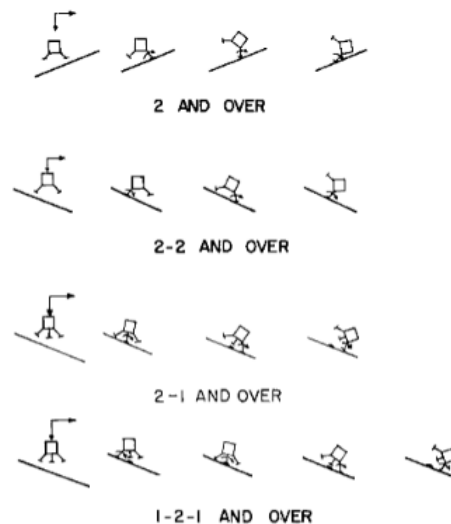


Figure 12.5: Critical modes of two-dimensional tumbling[78]

From these tumbling modes, the 2-2 and over and 1-2-1 and over are said to be the most critical ones [80][30]. The former has a larger impact on the side stability, whereas the latter on the leg loading and the maximal stroke of the absorber[80]. In this paper only the symmetrical 2-2 tumbling mode will be used for the stability analysis, as it has the largest impact on the length and consequently on the mass of the landing gear, although in some conditions the 1-2-1 may be more critical [30]. Given the selected critical landing mode and using the Two-Dimensional Inelastic Impact Theory, a critical angular velocity,  $\dot{\gamma}_{cr}$  for the lander is defined by Equation 12.1 [78]. It uses a dimensionless parameter,  $M$  which is defined by Equation 12.2, with  $\theta$  being the critical turn over angle,  $I$  the mass moment of inertia and  $l$  the distance between the center of gravity and the footpad.

$$\dot{\gamma}_{cr} = \left( \frac{2g}{l} [1 - \cos \theta] \frac{\bar{M}}{1 + \bar{M}} \right)^{1/2} \quad (12.1) \quad \bar{M} = Ml^2/I \quad (12.2)$$

Then knowing that at the turn over, the rotational kinetic energy of the body has to be smaller or equal to the increase of the potential energy gained during the motion, a stability condition can be derived as shown by Equation 12.3 [87]. The increase in potential energy is caused by increase of height of the c.g. during the turn over motion. Assuming lack of compression and sinking, the  $\Delta h$  can be calculated by Equation 12.4 [87], with  $H_0 = L_v + L_{cg}$ . Combining the two aforementioned equations yields the condition described by Equation 12.5. Equation 12.5 is the final stability equation that will be used to solve for the landing gear radius  $L_{fp}$ , with the turn over angle set at  $35^\circ$ .

$$0.5 * I * \dot{\gamma}_{cr}^2 \leq m \cdot g_{moon} \cdot \Delta h \quad (12.3) \quad \Delta h = \sqrt{H_0^2 + L_{fp}^2} - H_0 \quad (12.4)$$

$$\sqrt{H_0^2 + L_{fp}^2} [1 - \cos \theta] \frac{1}{1 + \frac{M(H_0^2 + L_{fp}^2)}{I}} \leq \sqrt{H_0^2 + L_{fp}^2} - H_0 \quad (12.5)$$

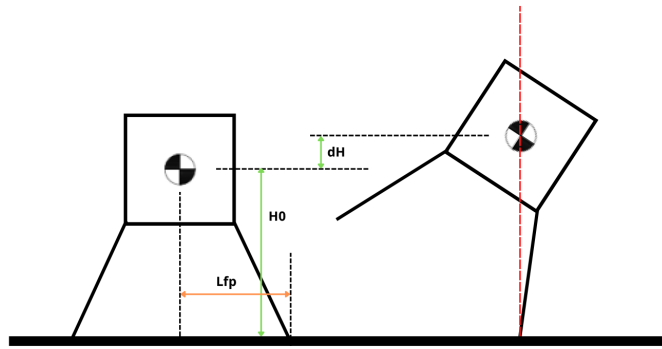


Figure 12.6: Visualization of the increase of potential energy at the turn over

### Complete Landing Gear Geometry

Given the initial geometry of the lander and the landing gear radius  $L_{fp}$  that was calculated in the previous section, the initial sizing of the struts can be performed by applying basic geometry rules. The detailed geometry of the lander is shown in Figure 12.7, where the parameters involved in the calculations include the following:

- $\tau$ : the primary strut angle.
- $\varphi$ : angle defined as  $180^\circ - \tau_s$ .
- $h_P$ : the top attachment point of the primary strut.
- $L_H$ : the vertical distance between the the soil and the  $h_P$  point.
- $L_p$ : the primary strut length.
- $L_s$ : the secondary strut length, defined as the distance between the bottom part of the lander structure and middle point of the primary strut.

$$Stroke_{max} = \frac{L_p - (L_H - drop_{allowable})}{\cos(\tau)} \quad (12.6)$$

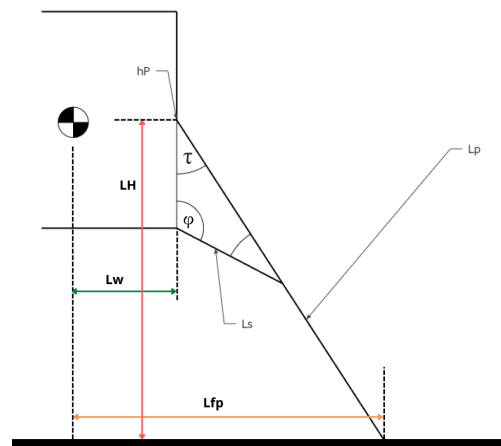


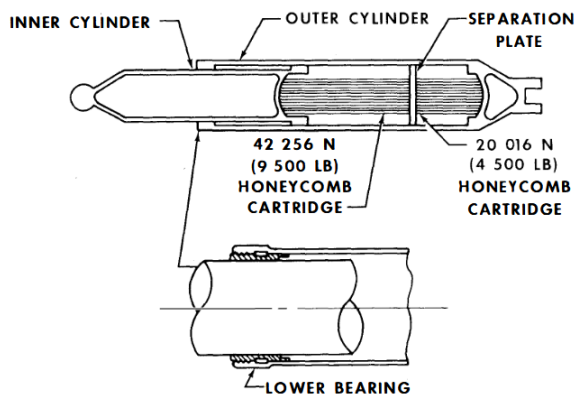
Figure 12.7: Complete geometry of the landing gear.

Through the use of basic geometric transformations and the vertical stroke limit, it is possible to calculate the lengths of both the primary and secondary struts. Moreover, knowing the maximal vertical stroke of the primary actuator (which in the preliminary design was constrained to be 1 m), the maximal stroke of the primary absorber is described by Equation 12.6. Unfortunately, it is not possible to apply a similar approach for the secondary absorber, hence the maximal stroke was manually set to be 20 % of the  $L_s$ , as it gave a good compromise between the diameter and thickness of the casing.

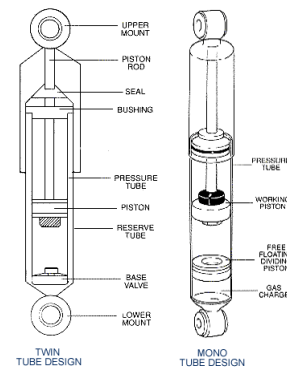


### 12.1.3. Reusable Shock Absorbers

The reusability of a shock absorber is the main challenge for the UCM's landing gear, as historically all the landing gear designs were non-reusable [80]. The majority of space landers, including the Apollo moon lander, used aluminum honeycomb cartridges, placed inside the cylindrical strut [80][30]. The working principle of this type is simple. During the impact, the honeycomb deforms plastically, absorbing the shock, until the load is insufficient to continue crushing the cartridge [80]. This solution is mechanically very simple, hence reliable, moreover it is also very mass efficient, as the honeycomb is empty inside. Unfortunately given the specifics of the UCM's mission it is not possible to apply this technology. The replacement of the cartridges would require to lift the entire spacecraft from the ground, such that the absorber would return to its uncompressed position. The amount of man-power needed and complexity of this maneuver is not achievable at the bottom of the crater, with the scarce resources available, thus other alternatives have to be explored.



(a) Apollo aluminium honeycomb absorber [60].



(b) Design of a typical hydraulic shock absorber<sup>a</sup>

<sup>a</sup><https://autoinfome.blogspot.com/p/shock-absorbers.html>

Hydraulic shock absorbers and dampers were considered, as they are a proven solution and they have been used in a number of rough terrestrial conditions under significant loads [75]. Although, their application poses a number of challenges. In order to keep the required viscosity of the liquid and prevent it from freezing [75], the leg has to be heated at all times, which means higher power consumption and larger system mass. Furthermore, as the system will receive minimal maintenance through the mission duration, the reliability of the system may become an issue. Possible leaks could lead to catastrophic consequences and lack of opportunity to refill the system with hydraulic liquid would exploit it quickly. Lastly, the Lunar dust is extremely abrasive, quickly deteriorating all the seals [75], leading to leakages and smaller cushioning forces. Therefore, this alternative was discarded as well.

An interesting idea was proposed in [28], where electromagnetic absorbers were applied. During the landing, a magnet attached to the inner cylinder, would pass through the coil changing the magnetic flux, which according to Faraday's law would induce the current. Its direction would be such that the resultant magnetic field would oppose the changing magnetic field that produced it. This opposite magnetic field creates a magnetic braking force, which slows the magnet passing through the coil, damping the oscillations. In comparison to the hydraulic absorber, this system is more reliable and requires neither heating nor seals, but the magnets and coil significantly increase the subsystem's mass. Moreover, the proposed solution was designed for a small lander with inverted tripod configuration. As the possibility of scaling of the solution is not known and no long term testing was conducted for this absorber type, it was removed from the solution list as well.

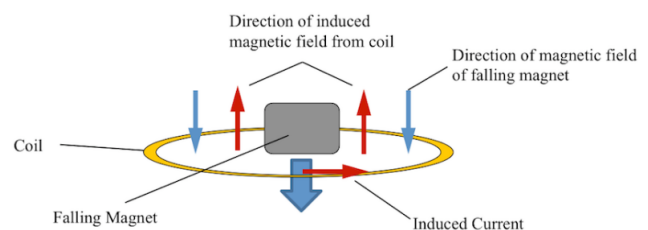
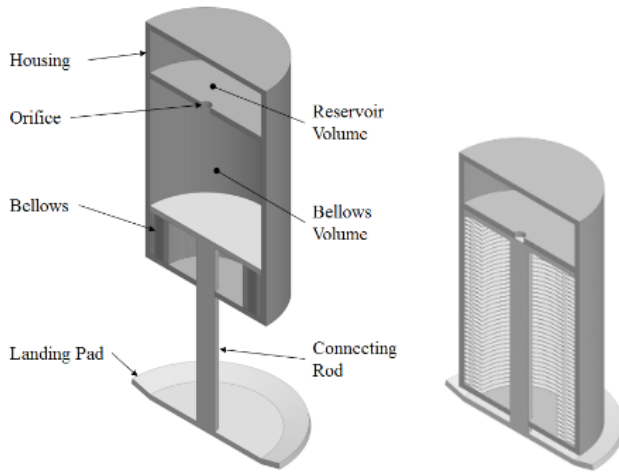


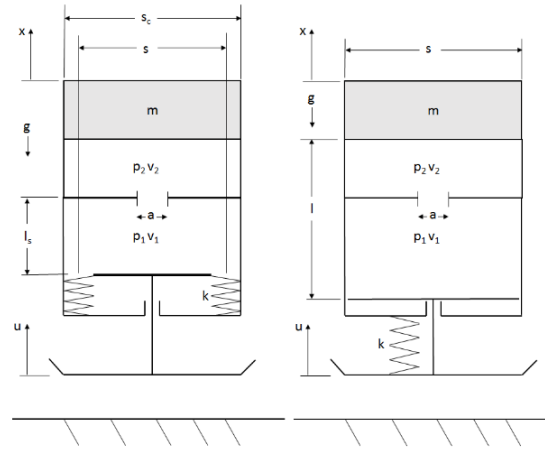
Figure 12.9: The principle of working of electromagnetic absorber [28].

The last alternative considered were pressurized metal bellows shock absorbers. A bellow is an elastic vessel

that can be compressed when pressure is applied to the outside of the vessel or extended under vacuum <sup>2</sup>. The absorber consists of two gas chambers separated by an orifice and a piston connected to the metal bellow. Both the chambers and the bellow are placed inside a housing and hermetically sealed off [80][75]. At the touchdown, the bellows extend, compressing the gas inside and pushing it through the orifice. The compression and extension of the bellows act as a spring element, whereas the flow through the orifice as a damper. In comparison to the previous ideas, stainless steel bellows are applicable in extreme temperatures ranges and vacuum environment [75]. Furthermore, as mentioned, it is hermetically sealed, consequently eliminating the issues with application of seals [75]. Lastly, the bellows have a high fatigue cycle and are mass efficient in comparison to the proposed alternatives<sup>3</sup>. The only disadvantage of the bellows is that sometimes they squirm (bellows's counterpart to buckling), but the problem can be easily resolved by the proper design of the casing [75]. Henceforth, given the overall performance, the pressurized metal bellows will be applied in both the primary and secondary actuators of the UCM's landing gear.



(a) Pressurized bellow absorber design, retracted on the right [75].



(b) Full (left) and simplified (right) model of the pressurized bellow shock absorber [75].

### Pressurized Metal Bellows Vibration Simulation and Analysis

In order to simulate the behaviour of the system, a simplified model of the absorber was created as shown in Figure 12.10a. Using the shown frame of reference, the equation of motion is given in Equation 12.7.

$$m\ddot{x} = F_{bellow} - F_{gas} - F_{orifice} - mg \quad (12.7)$$

The  $F_{bellow}$  is just a spring resistance force defined by Equation 12.8, with the effective bellow stiffness extrapolated from the available spreadsheet <sup>4</sup> as the the function of the initial chamber pressure.

$$F_{bellow} = -k_{bellow} \cdot x(t) \quad (12.8)$$

The gas pressure force, given that the gas inside the chamber is air at cryogenic temperature, follows an adiabatic process during compression [55] and is calculated via Equation 12.9, where  $n$  is the heat capacity ratio of the gas,  $p_0$  the initial pressure in chamber, and  $V_0$  the initial volume of the first chamber.

$$F_{gas} = p_0 S \left[ \left( \frac{V_0}{V_0 - S \cdot x(t)} \right)^n - 1 \right] \quad (12.9)$$

Next, assuming the length  $l$  to be the maximal stroke allowable, and the  $V_0$  as the product of cross sectional area  $S$  and  $l$ , the orifice force  $F_{orifice}$  could be derived. But before that, one has to know the orifice width  $a$ . In order to simplify the calculations and get the most conservative result [75] the width was set as:  $a = s$ , hence defining the flow of the gas through the orifice as simply the change of  $p_{gas}$  with time. Therefore, the orifice damping can be expressed by Equation 12.10.

<sup>2</sup><https://americanboa.com/blog/metal-bellows/>

<sup>3</sup><https://www.witzenmann.com/mediapool/documents/metal-bellows-manual.pdf>

<sup>4</sup><https://www.witzenmann.com/mediapool/documents/metal-bellows-manual.pdf>

$$F_{orifice} = \dot{F}_{gas} = \frac{S^2 n p_0 \cdot \left( \frac{V_0}{V_0 - Sx(t)} \right)^n \dot{x}(t)}{V_0 - Sx(t)} \quad (12.10)$$

The same model was applied for both primary and secondary struts, only with changed initial conditions acting on the actuator, including maximal allowable stroke of the actuator, the initial chamber pressure as well as the maximal vertical and horizontal descent velocities. The equation was solved analytically in Python using Scipy integrate module function *odeint*.

### Model input and output parameters

Following the recommendations from NASA, the primary actuator absorber was sized as if there were only three operational legs [47], thus taking one third of the entire axial load. The secondary actuator was constrained to take the entire side load on its own [87]. Both absorbers were assumed to be filled with air, at cryogenic temperature with the effective heat capacity ratio set at 1.7 [55]. The initial pressures were set to be 9 Bar for the primary actuator, and 6 Bar, respectively. For a given diameter  $d$ , the model then simulated the systems acceleration, velocity and position and calculated the maximum pressure inside the casing as well as the stroke compression due to the highest launch mass.

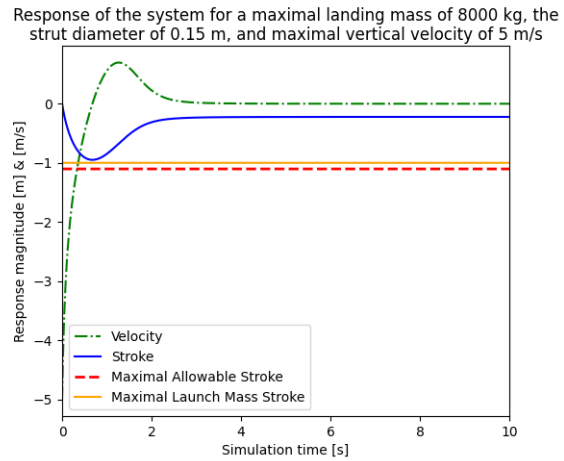


Figure 12.11: Sample simulation run results.

### 12.1.4. Landing Gear Stress Analysis

The structural sizing of the struts followed a modified procedure from [80].

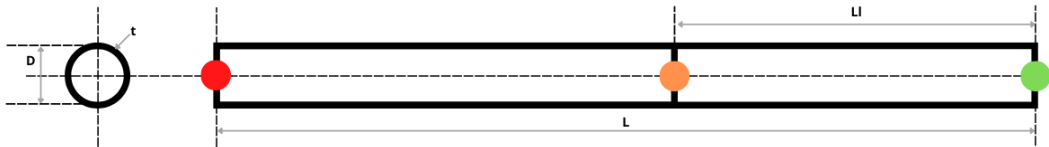


Figure 12.12: Primary strut geometry, with diameter  $D$ , thickness  $t$  and total length. The red dot is the attachment point to the lander, the orange the connection to the secondary strut and the green to the footpad

Firstly, for the given diameter  $D$  and maximal chamber pressure  $p_{max}$ , the required thickness of the cylinder was calculated with the longitudinal stress equation in Equation 12.11.

$$t_s = \frac{D \cdot p_{max} \cdot FoS}{2\sigma_{ultimate}} \quad (12.11)$$

In Equation 12.11,  $\sigma_{ultimate}$  is the ultimate strength of the material and  $FoS$  is the ultimate factor of safety equal to 1.4 taken from NASA-STD-5001B<sup>5</sup>. Then, depending on the absorber type (primary or secondary), the stress carried by the member is calculated. As mentioned, the primary strut is subjected to both axial and bending stresses. The bending stress induced by the secondary strut is calculated via Equation 12.13.

$$M_p = F_s \sin(\tau_s - \tau_p) L_l \frac{(L - L_l)}{L} \quad (12.12) \quad \sigma_m = -\frac{M_p D}{2I} \quad (12.13)$$

In Equation 12.12,  $F_s$  is the force exerted by the secondary actuator and in Equation 12.13,  $I$  is the second moment of area and  $L_l$  the distance between the secondary strut and the footpad. The axial force can be simply calculated with Equation 12.14, where  $F$  is the axial force acting on the absorber.

<sup>5</sup>[https://standards.nasa.gov/sites/default/files/standards/NASA/B-w/CHANGE-2/2/nasa-std-5001b\\_w\\_change\\_2.pdf](https://standards.nasa.gov/sites/default/files/standards/NASA/B-w/CHANGE-2/2/nasa-std-5001b_w_change_2.pdf)

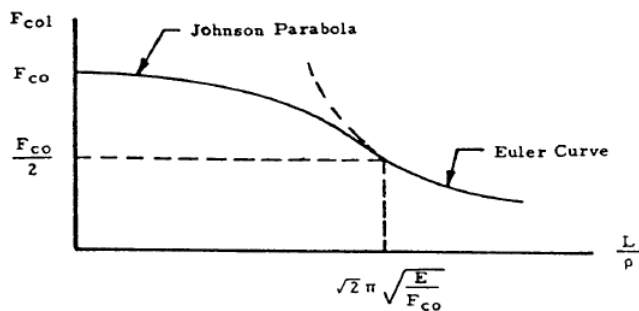
$$\sigma_{axial} = \frac{F}{A} = \frac{m_{landing_{max}} a_{max}}{\pi D t} \quad (12.14)$$

Merging these two yields the total stress in the element expressed by Equation 12.15.

$$\sigma_{total} = \sigma_{axial} + \sigma_m \quad (12.15)$$

The stress in the secondary actuator is caused by the horizontal load and can be established using Equation 12.14.

Then for both the struts, critical buckling conditions are checked. The first buckling condition that was considered was Johnson's parabolic buckling. In order to determine whether the element follows Euler's curve or the Johnson parabola<sup>6</sup>, the critical and actual ratios of the strut are calculated with Equation 12.16 and Equation 12.17. The  $L_e$  is the effective length and is a product of strut length and the boundary condition  $C$ . It was assumed that both ends of the element are fixed and thus:  $C = 0.5$  [85].



$$\left(\frac{l}{k}\right)_{cr} = \sqrt{\frac{2\pi^2 E}{\sigma_y}} \quad (12.16)$$

$$\left(\frac{l}{k}\right) = L_e \sqrt{\frac{A}{I}} \quad (12.17)$$

Figure 12.13: The Johnson-Euler curve.<sup>6</sup>

If the critical ratio is smaller than the actual ratio, the critical Euler buckling condition (Equation 12.18) is applied, otherwise the Johnson condition is employed Equation 12.19.

$$\sigma_{cr_{Euler}} = \frac{\pi^2 E}{\left(\frac{l}{k}\right)^2} \quad (12.18) \quad \sigma_{cr_{Johnson}} = \sigma_y - \frac{1}{E} \left(\frac{\sigma_y}{2\pi}\right)^2 \left(\frac{l}{k}\right)^2 \quad (12.19)$$

The second critical buckling condition was the critical local buckling, which was calculated using Equation 12.20, where  $K_c$  is a theoretical factor resulting from material imperfections and is assumed to be 0.6 [85].

$$\sigma_{cr_{local}} = \frac{K_c E}{D/t} \quad (12.20)$$

Both buckling conditions have to be satisfied for the structure to work, meaning that the total stress in either one of the struts has to be below the critical buckling stresses. If for the calculated thickness  $t$  these constraints are not met, the thickness has to be increased.

### 12.1.5. Landing Gear Footpad Design

The footpads of the lander are the only points of contact between the spacecraft and the ground, thus their design is of great importance for the landing gear. Detailed design of these is beyond the scope of this paper due to the lack of dynamic landing model of the vehicle, although by using a simplified, static method a rough preliminary sizing will be performed.

<sup>6</sup><https://engineeringlibrary.org/reference/simple-column-analysis-air-force-stress-manual>

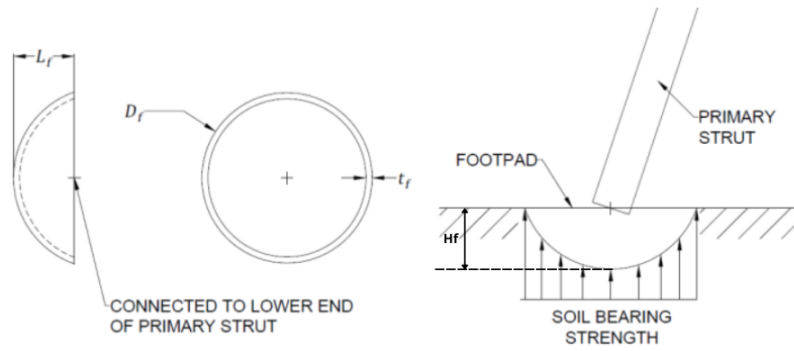


Figure 12.14: Landing footpad geometry [80].

### Footpad Surface Area

As the pad is the only element distributing the weight of the lander over the regolith, it is vital to design them such that the lander is capable of sitting on the Lunar surface without sinking further into the soil. Unfortunately, given the physical properties of the regolith, this task is particularly challenging as the bearing strength depends exponentially on the soil's bulk density. This means that even a small change in density significantly affects sinking resistance of the soil. For a density of  $1.2 \text{ g/cm}^3$ , the bearing strength is approximately  $300 \text{ Pa}$ , whereas for  $1.5 \text{ g/cm}^3$  it is as high as  $10 \text{ kPa}$  [29]. On the bottom of the mission crater, the density is estimated to be around the latter<sup>7</sup>, thus a bearing strength of  $10 \text{ kPa}$ . Meaning that the individual leg cannot exert higher pressure than this value as otherwise it would lead to sinking and possible instability of the lander. Knowing that the lander has higher mass at launch than at landing, the maximal launch mass was set as the restricting factor. Furthermore, using NASA's advise on the footpad design [47], only three legs were assumed to have contact with the ground. On top of that, a safety factor of 1.5 was applied as suggested in [80]. Lastly, the allowable sinking height, which is unavoidable during the dynamic situation, was set at  $0.18 \text{ m}$ , similarly to the Apollo lander [60]. Given all that assumptions an equation for the required footpad surface area can be written in the form of Equation 12.21.

$$A_{\text{footpad}} = \frac{m_{\text{max}} \cdot g_{\text{moon}} \cdot FoS/3}{\sigma_{\text{bearing}}} \quad (12.21)$$

### Footpad Dimensions & Mass

The shape selected for the footpad was an ellipsoidal dish. The hemisphere was considered as well but was neglected in the process. Its required radius to satisfy the bearing strength condition would result in a larger sink height, and the one satisfying the height condition would be unnecessary large. By using the required surface and set height, the necessary radius was obtained through Equation 12.22<sup>8</sup>:

$$S = 2\pi L_f^2 + \frac{\pi H_f^2}{e} \ln\left(\frac{1+e}{1-e}\right) \quad (12.22) \quad e = \sqrt{1 - \frac{H_f^2}{L_f^2}} \quad (12.23)$$

Because no data was found on the actual thickness of the footpad ( $t_f$ ), for the mass estimation purpose it was assumed to be  $2 \text{ mm}$ , allowing to calculate total footpad mass from Equation 12.24.

$$m_{\text{footpad}} = A_{\text{footpad}} \cdot t_f \cdot \rho_{\text{footpad}} \quad (12.24)$$

#### 12.1.6. Landing Gear Mass Estimation

For this paper only a simplified mass estimation will be performed with the following assumptions:

- The strut is a simple beam with a constant circular cross section.
- The thickness is constant.
- Mass of the primary type bellow is set to be  $10 \text{ kg}$  and for the secondary type at  $5 \text{ kg}$ .
- The material used for primary and secondary struts is HexTow® IM7 (HS-CP-5000) for reasons mentioned in the midterm report [5].
- The material used for the footpad is Aluminium 7075 alloy [80].

<sup>7</sup><https://curator.jsc.nasa.gov/lunar/letss/regolith.pdf>

<sup>8</sup><https://mathworld.wolfram.com/OblateSpheroid.html>

- The mass of the deployment mechanism (used for storing the mechanism in a stowed position inside the faring) is assumed to be equal to the mass of the secondary strut assembly [80].
- The mass of the thermal insulation of the system is calculated with a mass surface density of  $0.6 \text{ kg/m}^2$  [80].
- For every mass, the calculated factor of mass  $FoM$  was included to account for discrepancies as described in [80].

With the previously described assumptions in place, the mass of the struts can be calculated with Equation 12.25, where  $FoM_{strut}$  for the primary strut is 1.1 and 2.0 for the secondary strut.

$$m_{strut} = V_{strut} \cdot \rho_{strut} \cdot FoM_{strut} + A_{strut} \cdot \rho_{insulation_{thermal}} \quad (12.25)$$

Each leg assembly consists of one primary strut and two secondary struts, with two secondary type bellows and one primary. Consequently, Equation 12.26 could be derived.

$$m_{leg} = m_{strut} + 2m_{bellows_{secondary}} + m_{bellows_{primary}} \quad (12.26)$$

Finally, the entire mass of the subsystem is simply the mass of the four legs and the footpads as showed in Equation 12.27, with  $FoM_{footpad}$  being equal to 2.0 and  $FoM_{deployment}$  to 1.5.

$$m_{system} = 4m_{leg} + 4m_{footpad} \cdot FoM_{footpad} + m_{deployment} \cdot FoM_{deployment} \quad (12.27)$$

## 12.2. Landing Gear in UCM sizing

The structure of the main sizing code follows the structure of the landing gear section. First, four main inputs are loaded into the sizer: maximal landing mass, maximal launch mass, mass moment of inertia of the lander, the location of the center of gravity with respect to the bottom of the spacecraft & spacecraft width. These are first parsed into initial geometry sizer function, which calculates basic geometrical parameters, explained in detail in Section 12.1.2. Then using results it calculates the minimal landing gear width to satisfy the stability condition, and proceeds to determine the remaining geometry parameters for the strut sizing. With all parameters calculated, the program creates dictionaries consisting geometrical, physical and technical properties of both primary and secondary actuators. In the next step a list of allowable strut diameters is generated and for each diameter absorber response simulation is run. If the maximal stroke during the motion doesn't exceed 90% of maximal allowable stroke (Bottoming out condition), the diameter together with simulated maximal pressure & acceleration are stored. The saved configurations are passed through the stress analysis and thickness sizer followed by the mass calculation of the assembly consisting of a strut, thermal insulation and the absorber. If the mass of the assembly is lower than previous lowest mass, the configuration is temporarily stored. This process is repeated for all simulation approved diameters. After completion the program permanently stores the actuator properties, and repeats the steps for the second type. In the last step program goes through the footpad sizing and mass functions and creates the mass of the subassemblies: footpad, primary absorber/strut & two secondary absorbers/struts, and multiply the subassembly's mass with the number of legs to get the total mass of the subsystem.

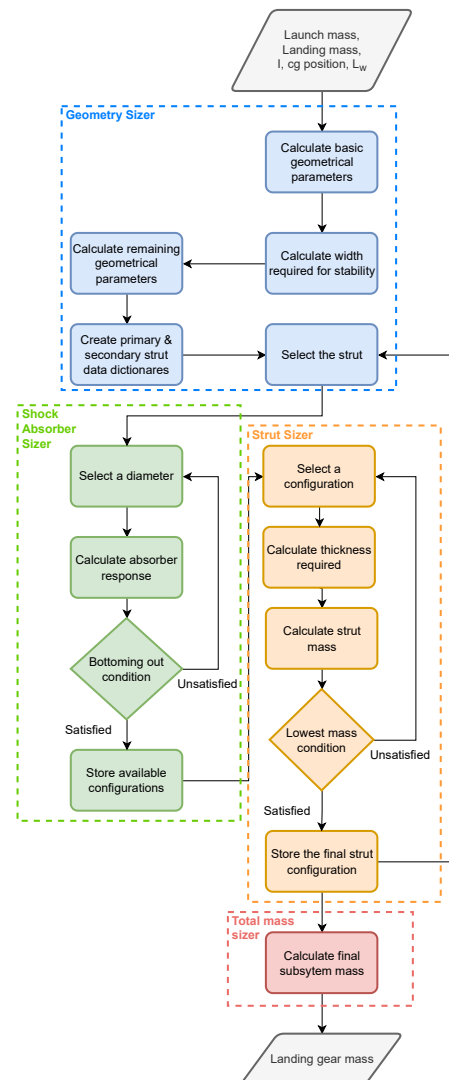


Figure 12.15: The flowchart of the landing gear sizing code

## 12.3. Architecture

In this section detail architectural considerations will be presented. They include the primary structure selection and application and layout options and guidelines. Finally, the final UCM configuration will be showed and explained in detail.

### 12.3.1. Load carrying framework

The last major element considered for the spacecraft was the main load carrying framework of the lander. Given the mass of the payload and propellant required to transport it, the mass of the structure had to be as low as possible. Thus, limiting the material selection to composites only. They combine high strength resulting in high rigidity of the structures with low density, effectively decreasing the mass of the components. The composites also allow for the structure design to be more integrated with individual components [7], decreasing the weight even further as less adapters are required.

In spacecraft design there are several techniques for designing a composite framework including use of monocoques, trusses, stiffened panels and load carrying tanks. Unfortunately, the last approach was immediately discarded, because of the application of the spherical tanks, which are not suitable for carrying launch loads [31]. The time and resources required for analysing the remaining options and performing a proper trade off were not available during the project duration, thus this trade off was left out of this paper's scope. Instead, the results from a Boeing framework study will be used [7].

In their study Boeing considered different structure variations of the same manned Lunar lander and then conducted a full trade off including three main parameters: mass of the system, stiffness of the structure and integration with components. The options included a full truss structure, a full shell and two types of variations of these combined. Full results of the trade-off are visible in Figure 12.16.

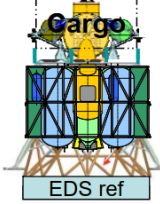
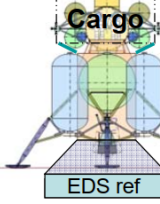
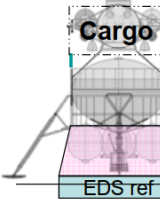
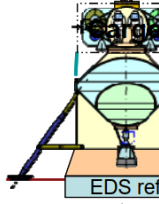
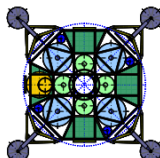
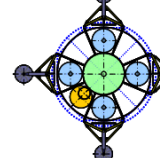
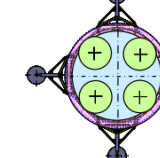
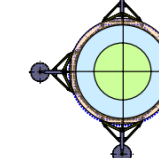
Structure Type	Truss	Truss / Shell	Shell / Truss	Shell
				
				
Integration	Low / Moderate	Moderate	High	High
Stiffness	Low	Low / Moderate	Moderate / High	High
Mass	High	Moderate	Low	Moderate

Figure 12.16: Boeing trade off results [7].

Neither the purely truss or shell (monocoque) structure provide the sufficient stiffness - the truss design, nor are lightweight - the shells. According to Boeing, the most efficient structures in terms of both stiffness and mass are the mix constructions. They provide moderate to high stiffness with low to moderate mass and can be easily suited for the mission requirements. This idea also helps with maintenance and thermal control as the shell provides additional protection from the Lunar dust, while blocking solar radiation as well. Overall, given its performance, the shell - truss was adopted for the main structure frame of the spacecraft.

### 12.3.2. Lander's layout

The layout of the spacecraft is always individually suited for the mission's requirements. There are no strict guidelines ruling the configuration of the parts within the spacecraft, leaving the architectural decisions to the mission's design team only. However, knowing the performance requirements of the lander and the environment of the mission, as well as the individual needs of the subsystem components, a set of design conventions can be derived.

The center of gravity location is one of the most important parameters affecting the design. It's placement directly influences the design of the propulsion and landing gear subsystems. If the axis of the engine thrust is misaligned with the CG vector, a moment is created, leading to the unstable flight conditions. Similarly, for the

landing gear design, the change of horizontal CG position such that it is beyond the polygon of stability may cause a lateral instability and cause the lander to fall. Furthermore, the vertical position of the center of gravity also impacts the gear design. It dictates the required span of the gear to turnover at the given angle. Lower positions are beneficial for the mass of the subsystem, because the struts can be shorter and therefore lighter. Although, the position of the center of mass can not be too low. The lander is supposed to be reusable and is required to perform launch operations numerous times. Therefore, from a control point of view, a lower CG location would worsen the steerability during the ascent phase.

The next important parameter affecting the design is the fairing dimensions. The launcher's fairing implies the slenderness ratio of the spacecraft and its maximal width and height of the configuration. Rarely, the fairings are cylindrical thus, especially for larger vehicles, it denotes a certain tempering of the upper section of the s/c.

Lastly, for the propellant transfer, the cg has to be positioned in line with the transfer feed system, otherwise an uncontrolled tumbling may occur. Furthermore, the docking port for the system should be positioned in easily accessible part of the spacecraft.

Hence, the implications on the layout are as follows:

- The center of gravity has to be aligned with the center axis of the spacecraft, thus the mass distribution has to be symmetrically distributed within the spacecraft cross sectional area.
- The vertical position of the CG has to be above the engine assembly and below the payload module, ensuring a suitable position for both the touchdown and flight stability.
- The load carrying framework is supposed to be lightweight and allow for easy attachment of remaining components.
- The packaging of the components shall be such that the lander fit inside Starship's fairing.
- The dock for the propellant transfer system shall be fixed on top of the spacecraft [24].

### 12.3.3. Moment of Inertia of the preliminary configuration

For mass moment of inertia calculation purposes, a simplified model of the lander was created with the bare minimum of components, mainly including propellants vessels. The elements were positioned with accordance to the guidelines develop in the previous section. The in-built CAD mass moment of inertia calculator tool was used to get a rough estimate of the parameters, which then were parsed to RCS and landing gear sections. An overview of the estimated mass moment of inertia for each of the three body axes is given in Table 12.2.

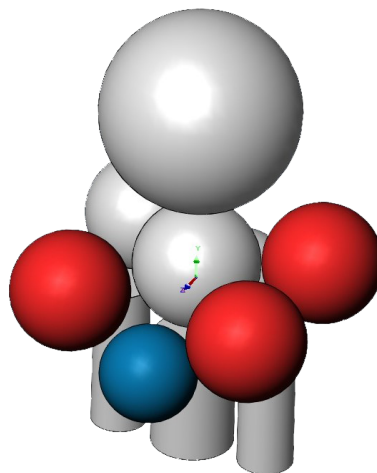


Figure 12.17: Simplified lander configuration.

Table 12.2: Mass Moments of Inertia around Body Axes

Mass Moment of Inertia	Value [ $kgm^2$ ]
$I_{xx}$	2,080,578
$I_{yy}$	261,772
$I_{zz}$	1,950,791



### 12.3.4. Final Architecture

Using the guidelines developed in the previous section and the outputs from the UCM generator, the final configuration for the preliminary design of the lander was established as visible in Figure 12.19.

#### Payload Propellant Module

On top of the lander, the docking mechanism of the propellant transfer system was installed. This position ensured the most optimal refuelling position for the system as explained in Section 5.6. The docking port was connected via a feed system with the CSS pumps, visible on the sides, and tanks. The large tank directly underneath the docking port is the CSS hydrogen tank. It is the largest tank in the assembly, however, when loaded it is relatively light. The placement of the tank in the top part of the spacecraft allowed to conserve space in the lower section, as the pure size would not allow for placement of other components next to it as it would exceed the maximal allowable diameter of the s/c. The tank was connected to the main framework by a skirt, going through the centerline. The skirt was constrained by a number of struts merged with the primary structure. This solution is quite typical for large tanks design in both satellites and lander design. It allows to save the weight of the structure system, and simultaneously allows to conserve the space inside the spacecraft.

Underneath, the CSS oxygen tank was placed. This element had the most impact on the vertical position of the center of gravity as it was the heaviest object in the entire lander. Due to higher density of the oxygen than hydrogen, the vessel was significantly smaller than its hydrogen counterpart. Therefore, it had to be positioned centrally to ensure the structural stability of the spacecraft and provide enough structural supports. This location was also suitable for both the RCS and landing gear, as it allowed to limit the required width of the gear. Thus, the final configuration differs from the one presented in the midterm report. In the previous paper [5] the configuration had a more tetrahedron look, as the heavier tank was placed on the the hydrogen one, which for the landing gear would cause excessively long and heavy lander legs.

#### RCS system

The RCS subsystem elements were spread across the spacecraft. The groups of three thrusters were placed equidistantly on the lander. There are two set of RCS lines. The first set, the top one, was installed on the skirt of the CSS  $LH_2$  tank. The second one, the lower one, on the bottom part of the landing gear shell. Unfortunately, given their small size, they are not visible on the render, Figure 12.19. The design and placement of feeding lines for the lander were beyond the scope of this paper and thus not included in the assembly. In the lower stage of the spacecraft, the hydrogen peroxide storage and distribution unit was placed. It is placed conveniently into the system, as there is enough space in this part of the lander for both system tanks ( $H_2O_2$  and water). This localization also allows to shorten the feed system to thrusters and consequently lowers the required mass.

#### EPS system

The solar panels are a secondary source of power for the UCM and thus their size is limited compared to other orbiting spacecrafts. In order to conserve the space inside the fairing and use the side area of the vehicle, the panels were fitted in between the trusses. Composite honeycomb plates were added as a secondary structure for their fitting to provide sufficient stiffness<sup>9</sup>.

#### Propulsion Tanks Module & Engines

All the propulsion tanks were set relatively low in the assembly to limit the total height of the spacecraft and ensure its fitting inside the fairing, similarly as showed on Figure 12.16. This solution also allowed to limit the center of gravity of the lander during the landing, as only propulsion tanks will include propellant at that point in operations, leading to more stable landing condition. The tanks were symmetrically put around the vertical axis of the vehicle in order to ensure alignment with the thrust axis. The heavier oxygen tanks were put slightly higher up to ensure that the center of gravity is not too low, which might have had a negative impact on the RCS. This position also provides the vertical space for storing the landing gear deployment mechanism. Further, the engines were placed centrally underneath the tanks. A simplified engine envelop was created, a mushroom looking part, to asses the amount of available free space between the inside components. In between the top oxygen and the highest engine (VINCI), a void of 0.5 m was left to accommodate the required feed system, which design was left out from the paper's scope. The engines due to their unique configuration were placed closed to each other, approximately at a distance of 0.3 m in order to satisfy the fairing conditions. The engines themselves were attached to the primary structure using trusses.

#### Landing gear system

The landing gear was positioned in the lower part of the lander. The secondary struts were directly connected to the primary structure of the lander. However their position and exact attachment method may change, depending

<sup>9</sup>[https://sci.esa.int/documents/34200/36212/1567256957247-7-1\\_Borriello\\_Aviospace-MDL-Sorrento.pdf](https://sci.esa.int/documents/34200/36212/1567256957247-7-1_Borriello_Aviospace-MDL-Sorrento.pdf)

on the final design of the landing gear deployment mechanism. The primary strut attachment point currently is not known as it solely depends on the deployment mechanism. The design of that tool is beyond the scope of this paper, however to estimate the required space, the Apollo Lunar lander mechanism was studied [60]. The possibility of reusing the mechanism was considered and the space inside the spacecraft for this element was insured as well, by analyzing current servo dimensions. However, as no previous work has been done in this area, the use of servos was assumed in this report as mentioned in Section 10.1.

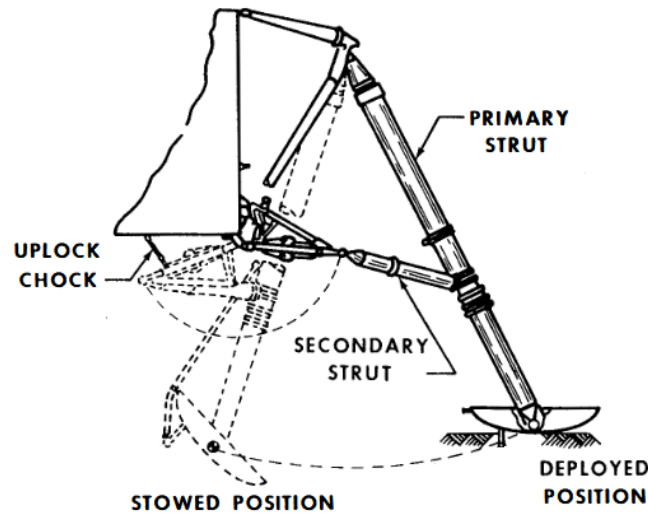


Figure 12.18: Apollo Lunar lander deployment mechanism [60].

### Structure system

As mentioned in Section 12.3.1, a load carrying structure consisting of trusses and shells will be incorporated in the design. The lower section was entirely enclosed by one shell in order to reinforce the region where the thrust load is introduced into the frame, but also to enclose all vital components and shield them from Lunar dust. It was also applied as less changes over the future iterations of the design are expected in this region, allowing for the finalization of the shells geometry. The upper part of the structure consists mostly of trusses as these are used to constrain the large propellant tank. The application of trusses also allows to easily modify this part of the spacecraft in the future iterations, which is expected.

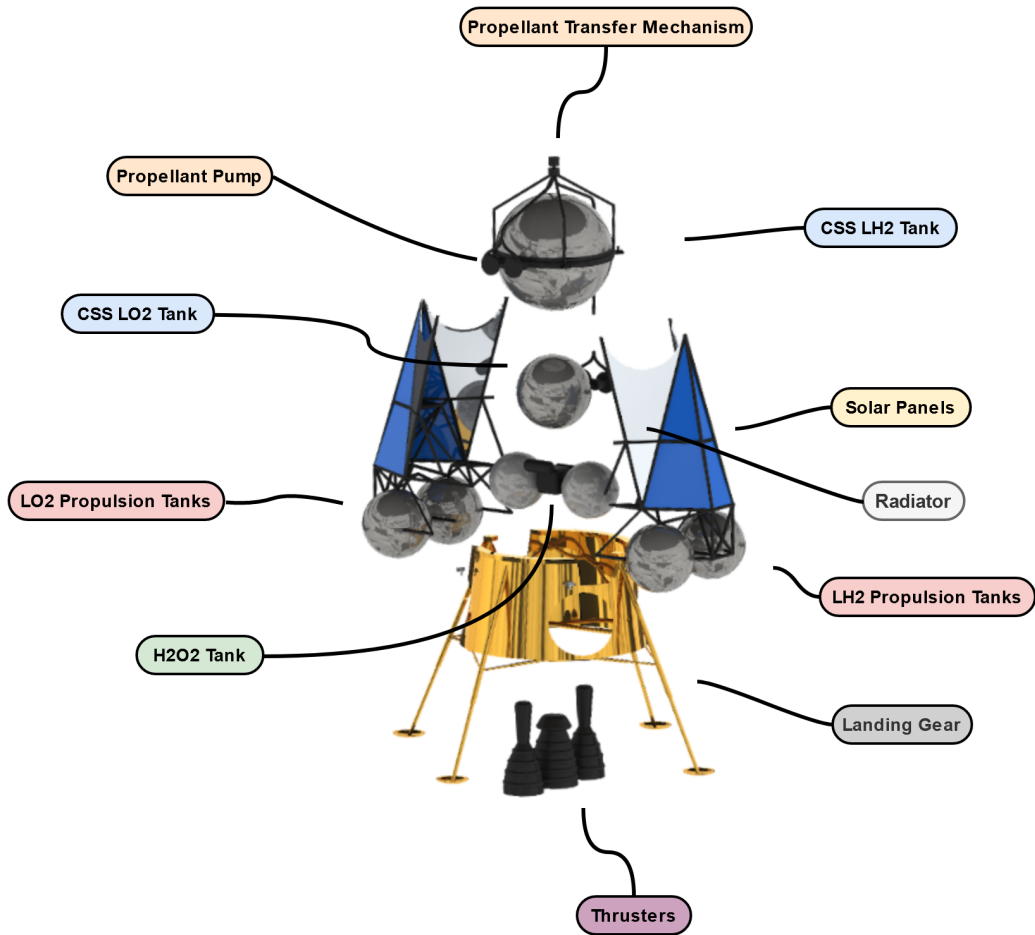


Figure 12.19: Final configuration of the UCM.

# 13 Sustainable Optimisation Results

All sizing methods have been described allowing the sustainable optimisation process described in Chapter 4 to be performed. The results of this process and the resulting UCM will be described in Section 13.1. Finally, a sensitivity analysis will be performed in Section 13.2. This analysis will investigate which subsystems and their outputs affect the optimisation criteria (P2P) and how.

## 13.1. Result

In order to obtain the optimal UCM design, the UCM generator (shown in Section 4.2) was iterated for the values shown in Table 13.1 according to the method described in Section 4.3. The  $LH_2$  and  $LO_2$  boil-off range resulted in a total of 10,210 design options (101 each). The  $LH_2$  and  $LO_2$  MLI layer number resulted in a total of 6,561 design options (81 each). In total 67 million design options were possible. It was unfeasible to evaluate all of these options using the UCM generator due to the long run time. Smaller design option sets showed that the optimal boil-off (for the highest P2P ratio) always resulted in 0% boil-off per month. Therefore, the largest number of iterations performed was 6,561 in order to account for all possible combinations of the  $LO_2$  and  $LH_2$  MLI layers.

**Table 13.1:** Overview of inputs that were iterated across

Input	Minimum Value	Maximum Value	Interval	Number of Values
$CSS\ H_2\ Boil-off\ [%/month]$	0	10	0.1	101
$CSS\ H_2\ n_{MLI}\ [-]$	20	100	1	81
$CSS\ O_2\ Boil-off\ [%/month]$	0	10	0.1	101
$CSS\ O_2\ n_{MLI}\ [-]$	20	100	1	81

The optimal UCM design resulted in having 77 MLI layers for the  $LH_2$  tank and 29 MLI layers for the  $LO_2$  tank. For this design option, an overview of the most important system parameters can be seen in Table 13.2. It can be seen that in the case of the most optimal design, the P2P ratio is 0.485. This means that for every kilogram of  $LH_2/LO_2$  propellant purchased, 486 grams can be delivered to a customer in an orbit 100km above the moon.

**Table 13.2:** Overview of UCM properties

Item	Value	Unit
$P2P$	0.485	[-]
$Dry\ Empty\ Mass\ (Landing)$	6,874	[kg]
$Dry\ Full\ Mass$	32,281	[kg]
$Wet\ Full\ Mass\ (Launch)$	56,473	[kg]

As explained in Chapter 4, each subsystem was sized in an iterative loop to ensure the design converged. Results of the entire sizing method are summarized and can be seen in Tables 13.3 through 13.9.

**Table 13.3:** Overview of the CSS

Item	Value	Unit
<i>Oxygen tank mass</i>	362	[kg]
<i>Oxygen tank structural layer thickness</i>	25.75	[mm]
<i>Oxygen tank inner face thickness</i>	2.25	[mm]
<i>Oxygen tank core thickness</i>	23	[mm]
<i>Oxygen tank outer face thickness</i>	0.5	[mm]
<i>Oxygen tank insulation thickness</i>	11.6	[mm]
<i>Oxygen tank outer radius</i>	1.72	[m]
<i>Oxygen tank cryocooler mass</i>	16.5	[kg]
<i>Peak O<sub>2</sub> cryocooler power consumption</i>	0.411	[kW]
<i>Oxygen pump power consumption</i>	5.1	[kW]
<i>Hydrogen tank mass</i>	1502	[kg]
<i>Hydrogen tank structural layer thickness</i>	40.7	[mm]
<i>Hydrogen tank inner face thickness</i>	3.8	[mm]
<i>Hydrogen tank core thickness</i>	36.4	[mm]
<i>Hydrogen tank outer face thickness</i>	0.5	[mm]
<i>Hydrogen tank insulation thickness</i>	30.8	[mm]
<i>Hydrogen tank outer radius</i>	2.71	[m]
<i>Hydrogen tank cryocooler mass</i>	137	[kg]
<i>Peak H<sub>2</sub> cryocooler power consumption</i>	1.98	[kW]
<i>Hydrogen pump power consumption</i>	0.92	[kW]
<i>Boil-off in 24h orbit</i>	0	[kg]

**Table 13.4:** Overview of the EPS

Item	Value	Unit
Fuel cell mass	3.46	[kg]
Fuel cell peak power	9.43	[kW]
Solar panel mass	2.1	[kg]
Solar Panel Area	11.2	[m <sup>2</sup> ]
Solar panel peak power	3.5	[kW]

**Table 13.5:** Overview of the ADCS

Item	Value	Unit
Sensor mass	46.7	[kg]
Peak sensor power consumption	99	[W]
Actuator mass	35.5	[kg]
Peak actuator power consumption	200	[W]
H <sub>2</sub> O <sub>2</sub> propellant mass	1032	[kg]
H <sub>2</sub> O <sub>2</sub> tank mass	85.3	[kg]
H <sub>2</sub> O <sub>2</sub> tank diameter	60	[cm]
H <sub>2</sub> O <sub>2</sub> tank cylinder length	1	[m]

**Table 13.6:** Overview of Propulsion subsystem

Item	Value	Unit
<i>Ascent Thrust</i>	360	[kN]
<i>Descent Thrust</i>	66.7	[kN]
<i>Hover Thrust (Start)</i>	10.96	[kN]
<i>Hover Thrust (End)</i>	10.48	[kN]
<i>Hover duration</i>	120	[s]
<i>Total engine mass</i>	1260	[kg]
<i>Oxygen used in mission cycle</i>	20.5	[t]
<i>Hydrogen used in mission cycle</i>	3.47	[t]
<i>Number of oxygen tanks</i>	2	[-]
<i>Oxygen tank mass</i>	176	[kg]
<i>Oxygen tank structural layer thickness</i>	20.15	[mm]
<i>Oxygen tank inner face thickness</i>	1.65	[mm]
<i>Oxygen tank core thickness</i>	18	[mm]
<i>Oxygen tank outer face thickness</i>	0.5	[mm]
<i>Oxygen tank insulation thickness</i>	10	[mm]
<i>Oxygen tank outer radius</i>	1.35	[m]
<i>Number of hydrogen tanks</i>	4	[-]
<i>Hydrogen tank mass</i>	315	[kg]
<i>Hydrogen tank structural layer thickness</i>	24.9	[mm]
<i>Hydrogen tank inner face thickness</i>	2.2	[mm]
<i>Hydrogen tank core thickness</i>	22.2	[mm]
<i>Hydrogen tank outer face thickness</i>	0.5	[mm]
<i>Hydrogen tank insulation thickness</i>	10	[mm]
<i>Hydrogen tank outer radius</i>	1.6	[m]
<i>Boil-off in 24h orbit</i>	242	[kg]

**Table 13.7:** Overview of the TT&C subsystem

Item	Value	Unit
Phased array antenna count	3	[-]
Phased array antenna area	1.3	[m <sup>2</sup> ]
Parabolic antenna count	1	[-]
Parabolic antenna area	2	[m <sup>2</sup> ]
Peak power draw	300	[W]

**Table 13.8:** Overview of the TMS

Item	Value	Unit
Radiator area	42	[m <sup>2</sup> ]
Subsystem mass	164.4	[kg]
Maximum power to radiate	2.99	[kW]
Number of heat pipes	27	[-]
Coating absorptivity	0.06	[-]
Coating emissivity	0.88	[-]
Heat pipe radius	2.955	[mm]

**Table 13.9:** Overview of landing gear

Item	Value	Unit
Number of landing legs	4	[-]
Primary strut length	10.7	[m]
Primary strut mass	180.2	[kg]
Secondary strut length	2.3	[m]
Secondary strut mass	16.2	[kg]
Foot-pad diameter	1.6	[m]
Landing gear width	8	[m]
Maximum vertical acceleration	34.2	[m/s <sup>2</sup> ]
Maximum horizontal acceleration	3.6	[m/s <sup>2</sup> ]
Total landing gear mass	1	[kg]

## 13.2. Sensitivity Analysis

The final design of the UCM was determined through an iterative process. This means that the output of one subsystem in terms of mass and power is used as the input for the next subsystem in the iteration loop. As is known, the design and sizing of a subsystem comes with a certain uncertainty on the results. Consequently, a certain uncertainty is transferred as input to the next subsystem. This means that uncertainties travel through the iterative loop of the design generator. It is therefore important to estimate the sensitivity of the final design due to changes in input of the dedicated subsystems. A disastrous example would be a case where additional payload has to be added to the mission. Consequently, more thrust would be required to lift off from the Lunar surface, which means that more propellant will be burned and a larger storage tank is therefore required that adds more mass to the structure. In such a way, one can see that this repetitive cycle will only add more mass to the proposed design solution, meaning that design diverges away and becomes unfeasible.

Therefore, a sensitivity analysis was performed with the following approach: for each subsystem, the mass and power consumption will be varied by  $\pm 30\%$  of the nominal value the UCM generator indicated. Consequently, the effects on the P2P ratio and the dry mass of the UCM were estimated. During the process, the main focus was set on looking for signs of exponential growth that could indicate the start of a growing, divergent design solution. If the output varied linearly with the input weight, it was concluded that the iterator functioned as desired, since the input was scaled linearly as well.

In Table 13.10, the results are tabulated for a percentual increase of ten percent of the nominal P2P ratio of 0.485 and a UCM dry mass of 6874 kg. As can be seen, the propulsion subsystem shows the most variances in both P2P ratio and dry mass, however this range of values is still close to the nominal value and what can be expected of the chosen approach using linear varied scale of input weights.

Table 13.10: Sensitivity analysis values.

Subsystem / Value	P2P			Dry Mass		
	-10%	0%	10%	-10%	0%	10%
Static Mass Output	0.491	<b>0.485</b>	0.482	6539	<b>6874</b>	7106
Static Power Output	0.486	<b>0.485</b>	0.485	6858	<b>6874</b>	6890
EPS Mass Output	0.485	<b>0.485</b>	0.485	6872	<b>6874</b>	6876
TMS Mass Output	0.486	<b>0.485</b>	0.485	6856	<b>6874</b>	6892
TMS Power Output	0.485	<b>0.485</b>	0.485	6874	<b>6874</b>	6874
STR Mass Output	0.487	<b>0.485</b>	0.483	6772	<b>6874</b>	7018
PROP Mass Output	0.492	<b>0.485</b>	0.481	6438	<b>6874</b>	7207
ADCS Mass Output	0.486	<b>0.485</b>	0.485	6862	<b>6874</b>	6886
ADCS Power Output	0.487	<b>0.485</b>	0.484	6871	<b>6874</b>	6877

Consequently, for the propulsion system, the output was plotted in Figure 13.1 for the UCM dry mass when the input weights were varied with the previously indicated 30 % of the nominal value. It can be seen that the dry mass scales almost perfect linearly with the input weights, ranging from the usual 6874 kg at an input weight of 1 to 8000 kg at an input weight of 1.3. This means that an increase of 10 % in the mass of the propulsion system leads to an average increase of 375 kg or 5.4 % of the original dry mass.

It could be concluded that the UCM generator design tool performs as desired by outputting the mass and power of subsystem in a linear fashion as was expected. Furthermore, no signs of exponential growth were found that could indicate the start of a divergent iterative design loop. In such a way, it was determined that the UCM generator is a robust tool for the design of a vehicle of the COLD mission.

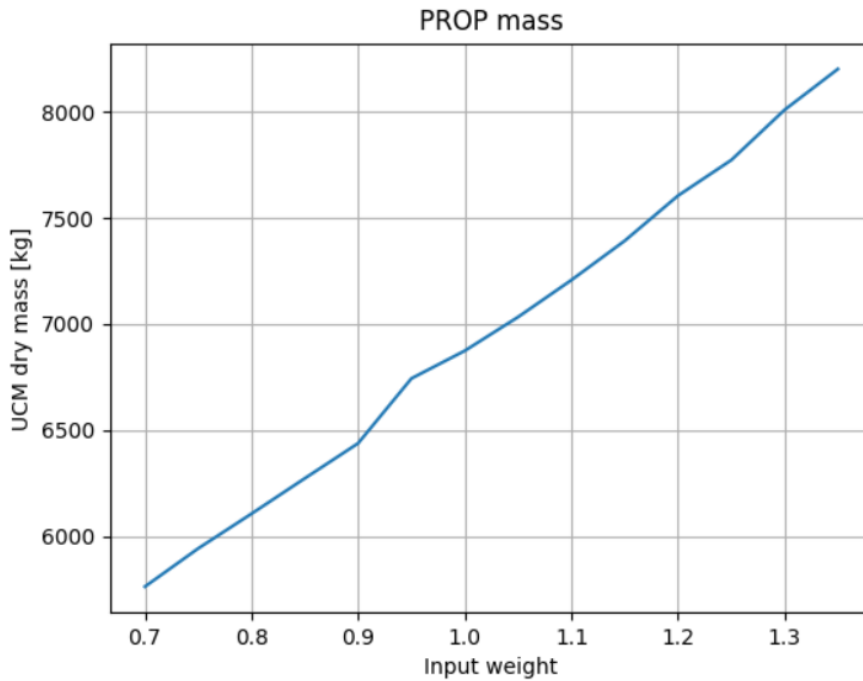


Figure 13.1: UCM dry mass as a function of input weight for the propulsion system

# 14 Universal Cryogenic Module Lifespan

The universal cryogenic module (UCM) undergoes several main phases throughout its lifetime. In this chapter, these phases are described and elaborated upon. The first phase is the manufacturing, integration and testing phase in which the UCM is created and validated for use. This phase is described in Section 14.1. The delivery of the UCM into space, the regular operations and end-of-life of the UCM are described in Section 14.2. Throughout its entire lifespan, there are risks the UCM is subjected to. These risks are assessed and described in Section 14.3 and mitigation strategies are created in case of risks that were deemed unacceptable.

## 14.1. Manufacturing, Integration & Testing

The process of manufacturing, integration and testing is an essential part of any mission. This process may take many years, even decades for some complex spacecrafts. It is therefore very important to outline a clear plan which is comprehensive and can be followed by the interested parties in order to make it easy to keep track of progress. This process may be split up into 4 main steps [81]:

1. Review of governing program documents and plans.
2. Develop spacecraft designs to implement required system functions; work with subcontractors and global supply chain.
3. Manufacture, assemble and test component-level space hardware; develop and test unique test and support equipment.
4. Perform spacecraft-level integration and testing.

### 14.1.1. Step 1: Review program documents

This step will identify subsystem and system verification procedures. The available verification procedures are the following [26]:

- **Inspection** - Inspect product to show compliance with the requirement.
- **Analysis** - Show compliance with the requirement by mathematical or other analysis technique.
- **Demonstration** - Show compliance with the requirement by operation / usage of the product.
- **Test** - Show compliance with the requirement by testing the product (or a representative model) under realistic conditions.

These tests will be developed considering a number of factors; complexity of the product to be tested, available budget and importance of the product. The more complex a product is, the more difficult the method of inspection and analysis may be due to the high number of interconnections. If the budget available is limited, a test or demonstration of a product may be prohibitively expensive since these type of tests require significant set-up operations. If a product is mission critical and its failure could lead to mission failure, it may be beneficial to verify the product using a physical test in order to fully understand all relevant aspects.

These tests are always defined in conjunction with the technical requirements. It is therefore also important to ensure the requirements are applicable and realistic. The tests will then be defined in collaboration with the hardware and software suppliers.

### 14.1.2. Step 2: Develop spacecraft designs

This step will involve creating all necessary documents in order to document the design. These documents will include technical drawings, equipment specifications, software development plans and production plans. In order to create technical drawings, a detailed CAD model shall be created. This model not only allows to check the physical placement and interaction of components, but also allows verification of previously estimated masses, mass moment of inertia and volumes.

Equipment specifications will follow from subsystem requirements and will be communicated to suppliers in order to make sure the off the shelf components are compatible with other subsystems and the system as a whole. The software development plan ensures that the software developed for the system is able to handle all functions portrayed in the software diagram shown in Figure 10.1. Furthermore the data handling block diagram (see Figure 10.2) will be incorporated in the software development plan in order to define the inputs and outputs of the various software blocks.



### 14.1.3. Step 3: Manufacture, assembly and testing of subsystems

This step will involve procuring components which have been decided to be off the shelf. Furthermore, qualified materials and products required for the production of components which have been decided to be created in-house will be purchased. Following this, the components will be assembled, tested, documented and passed on to the integration centre. This step will make use of a production plan which will outline the production process of the individual subsystems. It will include information such as the materials required, the manufacturing processes to be used and will allocate a time-span for the completion of the product.

For the to be produced parts of the subsystems in this step, a distinction can be made: parts will either be off the shelf or custom manufactured. In the latter, another distinction can be made into parts that are either fully custom or partially custom. First, the creation of the custom parts will be treated, with the main focus being the manufacturing of the tanks containing the cryogenic propellant. In Figure 14.2, it can be seen that the tanks for the payload, the main propulsion system, the reaction control system and the water storage tank will be custom manufactured. In Section 5.2, it was decided that the cryogenic propellant tanks will be made from three segments: an internal structural layer made out of fibers, a core structure and a second composite layer on the outside. For the composite structural layer of the tank, it was chosen to make use of fibers CYCOM 5320-1, as discussed in Section 5.2. Furthermore, in Section 5.3, it was decided that the structural layer will be made out of an aluminum alloy hexagonal honeycomb filled with aerogel. It has been assumed that the remaining tanks will be manufactured from the same materials and in a similar manner. However, since the hydrogen peroxide tank for the reaction control system is cylindrical instead of spherical, a different mandrel is required.

Manufacturing of the structural composite layer of the tank can be done in multiple ways, where different manufacturing processes can lead to different tank shape designs. A common method that ensures high accuracy is automated filament winding with the use of a robot, so called Robotic Automated Fiber Placement (RAFP) [44]. Additionally, hand lamination should be avoided because of the lay-up inaccuracies that might occur during the process. In case of RAFP, strings of fiber are placed around a mandrel at the wanted orientation in a consecutive manner:  $[+45^\circ, +90^\circ, 0^\circ, -45^\circ]$ . In such a way, it is ensured that all the fibers are laid up with the correct orientation. It should be noted that in this case, the mandrel will be made out of the liner that is in between the cryogenic propellant and the fibers, because it is otherwise not possible to take the mandrel out of the tank once all the fibers are laid up. This production process knows, including testing, five main steps that need to be performed as listed:

1. RAFP onto the mandrel in four different orientations
2. Creation of the aluminum honeycomb structure
3. Installation of honeycomb structure onto tank
4. Second round of RAFP and curing
5. Final assembly, integration and testing

The manufacturing process of the tank is visualized in Figure 14.1. After the first lay-up, the manufacturing of the aluminum hexagonal honeycomb structure is performed. Such a structure is typically created with the expansion method<sup>1</sup>. It starts with the printing of adhesive bond lines onto an aluminum sheet. Afterwards, the sheets are stacked onto each other and heated, such that the adhesives are cured. Consequently, a HOBE is created, a HOneycomb Before Expansion. The final step is loading the structure with a tensile forces that expands the structure into its characteristic hexagonal shape.

The next step of the process is to install the honeycomb structure onto the tank itself. At this point in the process, they honeycomb will not yet be permanently fixed, because it will be held in place by the cured resin once curing has taken place. Usually, the joining of a honeycomb and composites is performed with the use of adhesives, however due to the cryogenic temperatures that are involved, this is not possible [19]. When the honeycomb structure is installed, it can be filled with the insulative aerogel that was chosen in Section 5.2. Subsequently, the second lay-up round is performed, where the fibers are placed in the four desired directions in the same way as in the first round. Again, a liner would have to be placed onto the honeycomb structure as it is most likely not possible to perform the lay-up directly onto this structure. Afterwards, with all the structural components assembled, the structure can be cured in an autoclave since the fibers are already pre-impregnated. This process takes roughly eight to ten hours [44]. Once the curing is complete, final tank assembly is performed. This includes for example integrating the propellant transfer mechanism into the tank.

After the propellant tank has been manufactured, it will be subjected to several tests to ensure that it meets the requirements, for example the maximum design pressure. McCarville et al. (2017) states that three tests are usually conducted: an ambient pressure test, a cryogenic pressure test and a design life-cycle test. The ambient pressure test is designed to check whether there are any leaks in the tank, the piping or the joints.

<sup>1</sup>[https://www.pccomposites.com/wp-content/uploads/2015/07/PCHC4-4TY4\\_TDS.pdf](https://www.pccomposites.com/wp-content/uploads/2015/07/PCHC4-4TY4_TDS.pdf)

By pressurizing the tank and applying bubble soap to the surface, leaks can easily be spotted. Afterwards, the cryogenic pressure test is performed. The tank is again pressurized, but this time with a gas at cryogenic temperatures. The pressure is varied between ten percent and a hundred percent of the maximum design pressure. Finally, the life-cycle test was performed to demonstrate the structural adequacy of the tank, by simulating all expected loads during the lifetime of tank with load- and shear actuators. The tanks will only pass this phase if there is no evidence of catastrophic structural failure and no detrimental yielding, delamination or joint failure [44].

After the tank has been tested and certified for use, installation of the multi-layer insulation will have to be conducted. The multi-layer insulation will be purchased from an external manufacturer<sup>2</sup>. The integration of the insulation layer then concludes the tank manufacturing process.

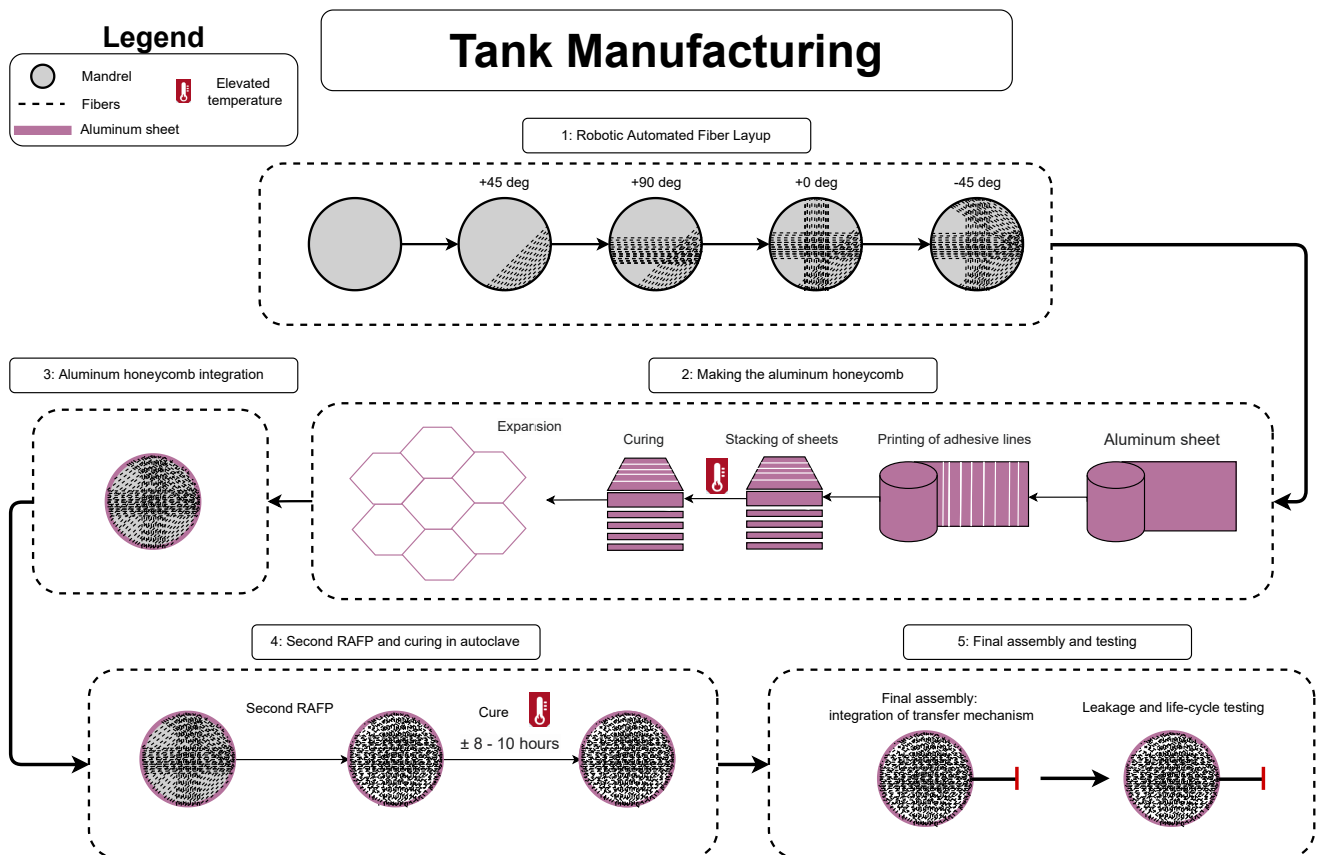


Figure 14.1: Overview of the tank manufacturing process

For the commercially available off-the-shelf parts indicated in Figure 14.2, the testing of individual components is left to the manufacturer that has to ensure that the product meets the specified requirements. This ranges from the fuel cell of the EPS, the cryocoolers of TMS to the thrusters used by propulsion and RCS and more. It should be noted that the parts are tested of course during the integral system testing. This will be more elaborated upon in Figure 14.2. If the product doesn't meet the requirements, then either the manufacturer should be contacted or replacement part should be found, which can prove difficult since the design is already finalized, leaving little room for modifications.

#### 14.1.4. Step 4: Integration and testing of complete system

Once all the individual subsystems have been built, tested and validated, integration of these subsystems into the main spacecraft bus can start. Wertz et al. (2011) states that integration normally starts with the delivery of a structural frame which can already feature an integrated propulsion subsystem, but this is not necessary. Hence, the first step should be to integrate the propulsion subsystem into the bus if this hasn't been done already. The propulsion subsystem should be first assembled into the structure, because the fields that are used to braze propulsion components together are not compatible with electronic components. The wiring harness for all the electrical components can either be implemented before or after the propulsion system. Afterwards, it is common practice to start the electronic assembly of the spacecraft by implementing power and command and

<sup>2</sup><https://frakoterm.com/cryogenics/multi-layer-insulation-mli/>

data handling subsystem components. The order of the remaining subsystems varies and is dependant on the spacecraft design [81].

In this case, it was decided to first integrate the payload tank and the propellant tank for the reaction control system once the propulsion system has been put in place, before implementing the electronic assembly into the craft. This follows the main integration philosophy of working from the inside towards the outside. Afterwards, the wiring harness can be assembled onto the frame such that all cables are in place when the remaining devices are integrated. Furthermore the fuel cell can be placed with the corresponding feeding system from the oxygen and hydrogen tanks to the fuel cell and then to the water tank. The next phase will be the integration of the thermal management system into the bus. The cryocoolers will have to be placed, alongside with heaters and radiators. Additionally, all the piping will be laid down such that all components are connected to a heat pipe that can either heat or cool certain elements. Then, the main computer that is responsible for communicating commands to all the different subsystems can be implemented, together with the coders and decoders of the TTC. Consequently, the thrusters that will be used by ADCS to propel and orient the vehicle and their corresponding sensors can be integrated into the vehicle, accompanied by the altimeters, docking sensor and mechanism. The final subsystem that will be implemented on the inside of the vehicle is the TTC, which requires the placement of the receiving and transmitting antenna and the signal amplifiers.

Next, the spacecraft can be closed of with the assembly of the outside covers, after which the outside can be coated for protection. Finally, the joining of the landing gear and the integrated vehicle can take place. The only thing that remains is the mounting of the solar panels on their respective arrays. Subsequently, the vehicle can be subjected to various system tests that check the proper integration of all the subsystems. An overview of spacecraft bus integration can be found in Figure 14.2. Furthermore, Figure 14.2 indicates whether subsystem parts are off the shelf parts, custom parts or partially custom.

Afterwards, integrated system tests can be performed to test whether all the subsystems are communicating correctly to each other and that the right data is sent at the right time to the right place. During these tests, all anomalies, discrepancies or out-of-tolerance measurements are addressed and solved. Usually, the following tests are performed in the order as listed [81]:

1. **Temperature cycling** to verify proper assembly of the mechanically integrated spacecraft
2. **Vibration and acoustic testing** to check that the vehicle can handle the specified vibratory loads and test the natural frequencies of the structure.
3. **Thermal vacuum tests** that simulate the thermal loads that are expected in the space environment.

If the integrated vehicle demonstrates that it can achieve the specified minimum number of error-free hours during the thermal vacuum tests, then the spacecraft is ready for shipment to the launch site [81].

Additionally, a manufacturing timeline was constructed if the project were to move out of the design phase and into the construction phase. This timeline is given in Figure 18.5 in the Appendix. The main assembly phases are also summarized in Table 14.1.

**Table 14.1:** System manufacturing and integration timeline

Mission phase	Description	Allocated time
Phase 0	Develop spacecraft designs	1.5 years
Phase 1	Manufacture, assembly and integration of subsystems	2 years
Phase 2	Integration and testing of complete system	2 years

### 14.1.5. Sustainability Considerations

The manufacturing of composites use significant amounts of energy as the fibers need to be cured at elevated temperature and pressure. Additionally, when the final product is trimmed down to the desired dimensions, parts of the fibers are lost and cannot be used anymore. Consequently, the sustainability of this industry is compromised and limited. Luckily, improvements are made in the recycling of carbon fibers, where currently research is done into fluidised bed pyrolysis, which has been shown to recover good quality fibres<sup>3</sup>. Although recycled fibers cannot replace virgin fibers directly, recycled fibers can be integrated into non-woven mats and thereby offer similar performances as aluminum but at a lower weight<sup>3</sup>. This opens up new ways in which end-of-life solutions can be found through the recycling of parts, thereby compensating for the less sustainable production process.

<sup>3</sup>[https://green-alliance.org.uk/wp-content/uploads/2021/11/Novel\\_Materials.pdf](https://green-alliance.org.uk/wp-content/uploads/2021/11/Novel_Materials.pdf)

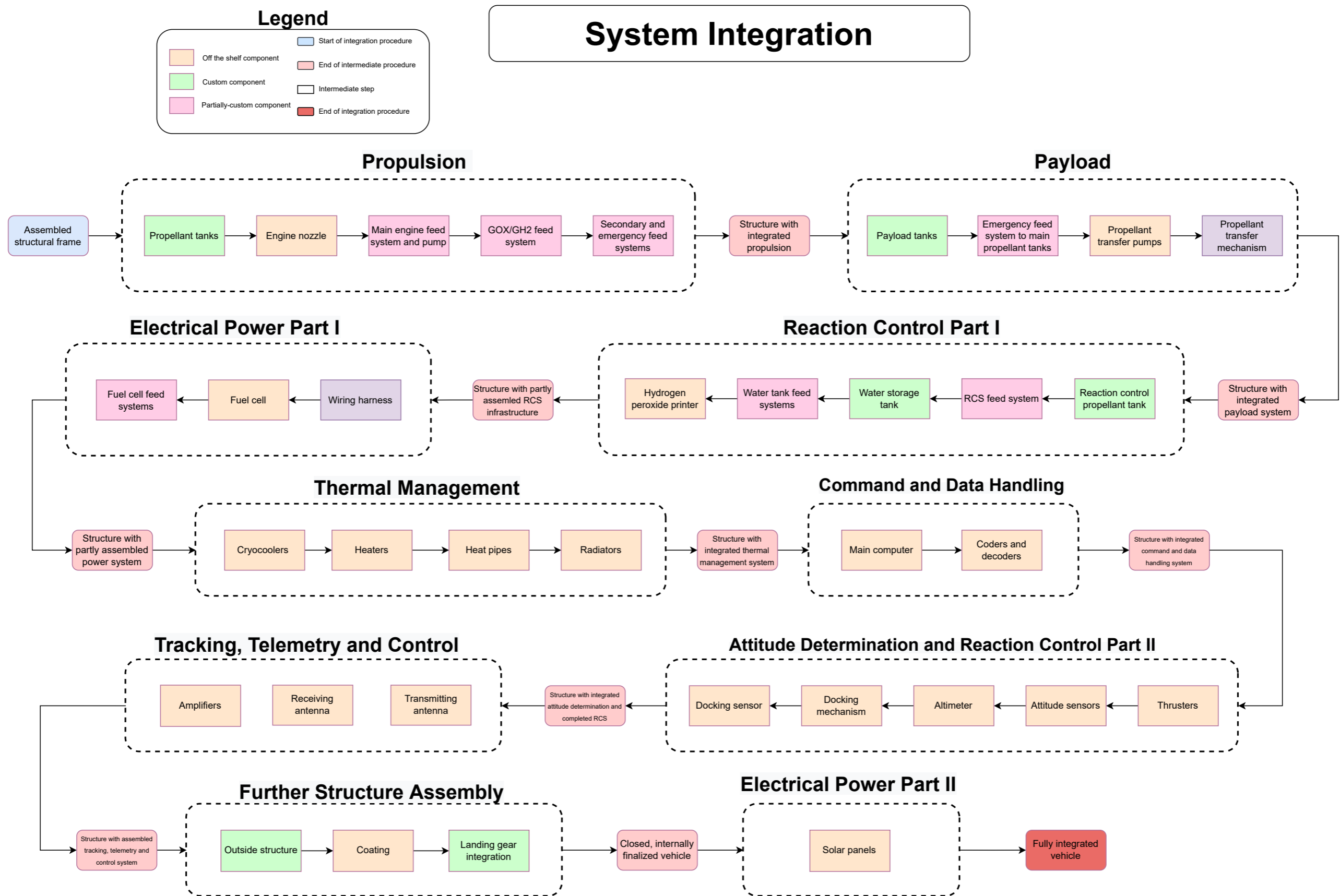


Figure 14.2: System Integration

## 14.2. Operations & End-of-life

Once the launch vehicle containing the UCM is in TLI orbit, the operational burden is passed to the UCM itself. In this section, the procedures required to begin operations are discussed, in addition to a detailed description of a mission cycle as well as possible courses of action at end-of-life.

The functionalities of the UCM are divided in three primary stages: Pre-operations, Operations and End-of-life as can be seen in figure Figure 14.3. In this figure, the most important steps of each stage are also displayed in chronological order. Further explanation of each mission step can be found in Subsections 14.2.1, 14.2.2 and 14.2.3. Finally, a detailed functional breakdown, summarizing the entire mission is presented in Section 14.2.4.

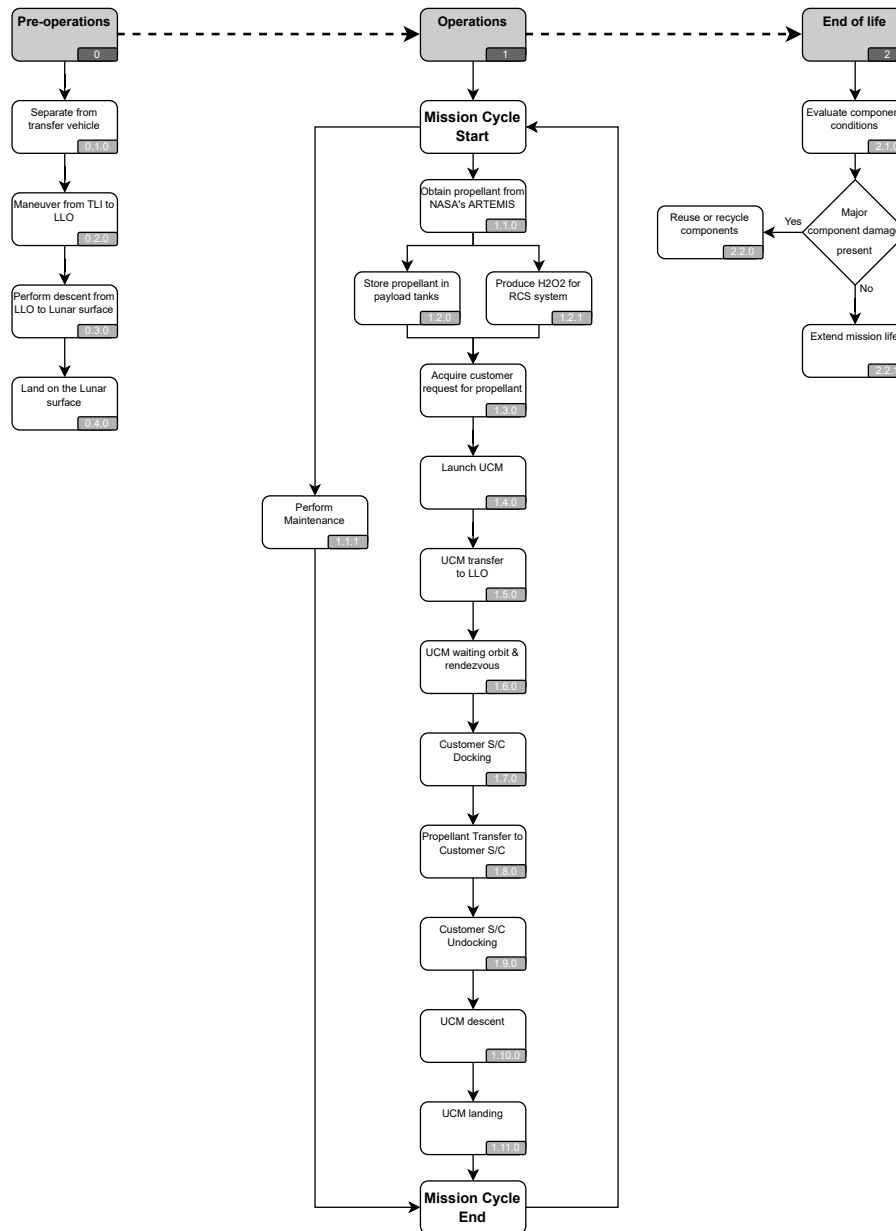


Figure 14.3: Functional flow of the UCM

### 14.2.1. Pre-operations

The pre-operations stage of the UCM encompasses all procedures from the moment of separation from transfer vehicle to the first touchdown on the Lunar surface. During this stage of the mission, the UCM must not only arrive at the  $LH_2$  and  $LO_2$  production site on the Moon, but also initialize all subsystems and provide assurance to the ground station that the mission may proceed as expected. In order to begin autonomous operation the UCM shall initialize all subsystems and detach from the payload adapter when the Starship fairing is fully open.

A flight profile for a Lunar mission of the Starship can be seen in Figure 14.4<sup>4</sup> and the UCM separation will commence once the Starship begins the Lunar flyby at point 05.

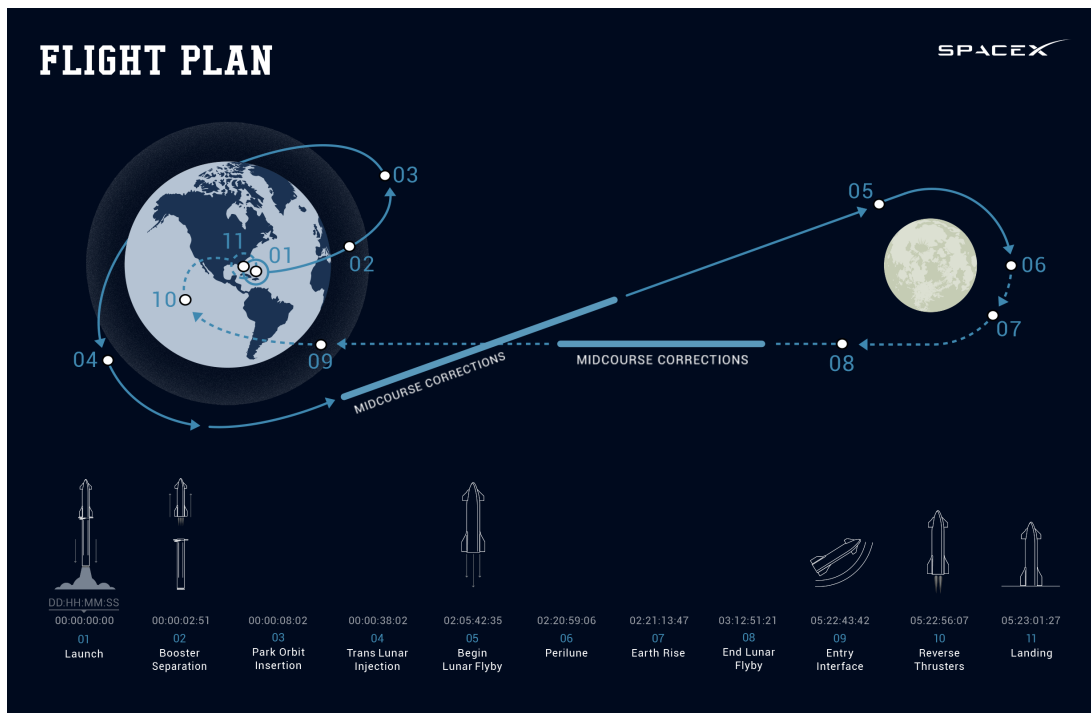


Figure 14.4: Starship TLI flightplan

At this point in time, telemetry can begin to be transmitted to operators on Earth. Should all subsystems perform as expected, the UCM will perform all necessary maneuvers to both enter LLO and begin descent to the Lunar surface. This marks the start of the final step of pre-operations. The spacecraft must now deploy landing gear for the first time, hover if necessary above the landing site and touchdown. Upon confirmation, the UCM may begin the main operations stage as described in the next subsection.

### 14.2.2. Operations

With the UCM on the Lunar surface, the operations stage of the mission may begin. As can be seen in Figure 14.3, operations consist of repeating mission cycles, each starting with the process of obtaining propellant from Artemis and ending with the UCM returning to the Lunar surface after transferring propellant to a customer spacecraft in LLO.

A single mission cycle can be divided in many steps, starting with the ones taking place on the Lunar surface. The first of which is the process of obtaining propellant from NASA's Artemis [50]. The propellant must of course be stored by methods described in Chapter 5. Furthermore,  $H_2O_2$  must be produced for the RCS system by means described in Chapter 8. As the mission is dependant on customer spacecraft approaching, the launch schedule is determined based on customer request. When such a request is received, the UCM shall determine a launch window depending on propellant availability and customer orbit and proceed to the launch sequence.

In order to ensure safe operations, the launch must be prefaced with safety procedures such as ensuring the UCM has successfully disconnected from Artemis and no critical system damage was sustained while on the surface. With the welfare of the craft confirmed, the take-off engines may be ignited and the UCM may lift-off. During ascent, the propulsion system in tandem with the flight computer and ADCS must ensure the spacecraft is successfully inserted to LLO.

The next steps of the mission cycle are performed in LLO and begin with the UCM in waiting orbit. During this time, the rendezvous time and position can be updated and maneuvers necessary for close approach should be performed. With both spacecraft in proximity, the docking procedures shall begin. The docking sensor shall monitor relative S/C velocity, position and attitude and any necessary corrections can be performed using the RCS. Once the physical connection is established and verified, the propellant transfer may begin. Propellant transfer is driven by a combination of UCM rotation and pumps. Therefore, in order to begin propellant transfer, the RCS must first be used to achieve a rotational rate of approximately 0.38 rpm. This shall settle the propellant

<sup>4</sup><https://dearmoon.earth/schedule.html>

on the walls of the spacecraft and allow the pumps to transfer it to the customer spacecraft as discussed in Section 5.6. Once the tanks have been emptied to a sufficient degree, they should be sealed and the undocking procedure may begin. This of course includes safety procedures, as well as data transfer to the customer S/C confirming the start of the decoupling process in addition to the physical separation. With both the spacecraft at a safe distance, the descent step of the mission cycle may begin.

In order to ensure the UCM may land at the desired site, the descent procedure must begin at a specific location and point in time along the orbit. The UCM must thus determine when to begin the descent and only do so after receiving the go-ahead command from Earth. The need for a go-ahead is important as it shall prevent possible collisions with other spacecraft around the Lunar mining site. With the go-ahead received, the descent burn may begin with an RCS impulse to settle the propellant. The UCM must then ignite the descent engine and ensure the center of gravity is still in line with the thrust vector before performing the main de-orbit burn. During descent, similarly to ascent, the flight computer, ADCS and propulsion subsystems must ensure the spacecraft remains at desired attitude and trajectory.

The final step of a mission cycle is landing. When approaching the Lunar surface, the first step is to deploy the landing gear. In addition, when the UCM is sufficiently low, a landing sensor mounted at the bottom of the craft may be used to take precise measurements of altitude. When altitude is sufficiently low, the hovering procedure begins in order to precisely select the landing location. Once the UCM is positioned directly above the landing site, the main landing thruster is throttled down and the UCM lands on the Lunar Surface.

It must be said that maintenance of the UCM is performed in parallel to the other steps of the mission. It is covered in more detail in Chapter 15

### 14.2.3. End-of-life

As COLD is a project with the goal of not only providing an economical solution to deep space travel, but also with the aim to ensure space exploration is as sustainable as possible, sustainability should be considered for the end-of-life procedures as well. In order to ensure COLD is as sustainable as possible, the 3R approach is used to define the end-of-life procedures. The 3R approach stands for: "Reduce, Reuse, Recycle", it forms guidelines to minimize waste and is employed in practice by some of the largest manufacturing companies in the world such as the Toshiba Group<sup>5</sup> or Samsung<sup>6</sup>.

When the ten year mark of operations is reached for a given UCM, it officially enters the end-of-life stage of the mission. However, as the first principle of the 3R approach is to "Reduce" waste, the possibility of extending the operations should be considered. If after performing health checks on all subsystems it is found that the UCM can continue operations, it shall receive a command to do so. Doing this would reduce or even effectively eliminate the need of a replacement system, resulting in less resources spent.

In the case that some components are damaged and continuing operations is a risk to either the propellant production depot or any customer spacecraft, extending the mission life is not an option. In this case, the other two principles of 3R shall be applied. Any components that are still functional shall be repurposed. An example of this would be to "Reuse" cryogenic tanks on the Lunar surface, even if they can no longer be considered fit for transport to LLO.

Finally, any components with critical damage or wear that can no longer serve a purpose should be "Recycled". The materials used for the UCM are some of the highest performing on the market. This means, even if due to wear subsystems can no longer function, the base material can still likely be reused in production or repair of other, less demanding systems. The extent to which this part of the philosophy can be applied shall vary vastly depending on the other available infrastructure on the moon when end-of-life is reached.

### 14.2.4. Detailed functional breakdown

As discussed in the previous subsections, an overview of the functionality of the UCM is presented in Figure 14.5 in the form of a functional breakdown. It should be noted, that the pre-operations and end-of-life mission stages have not been defined in as much detail as the primary operations. This is both due to the lesser importance of those functionalities on the design of the UCM, and due to less certainty in available infrastructure on the Lunar surface at EOL.

---

<sup>5</sup><https://www.global.toshiba/ww/environment/corporate/economy/resource.html>

<sup>6</sup><https://www.samsung.com/pk/sustainability/environment/resource-efficiency/>

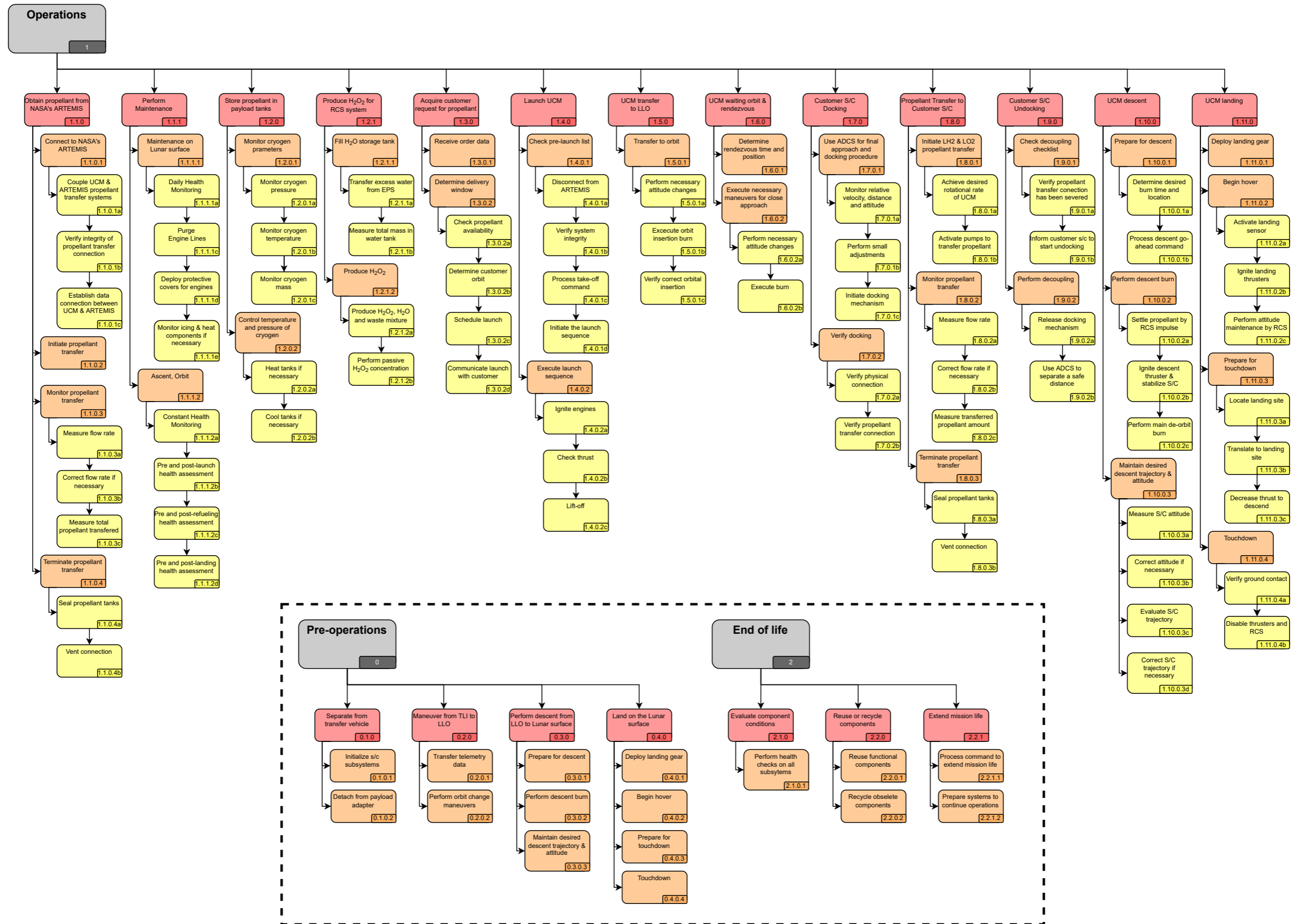


Figure 14.5: Functional breakdown of the UCM



## 14.3. Risk Management

In order to anticipate on and react appropriately to events that might occur, it is important to perform risk assessment continuously before and during the mission lifetime. Therefore, distributions of risk likelihood and impact were created to identify the severity of an event, which is described in Section 14.3.1. Afterwards, risks that were determined during earlier design phases, that might occur during operation are revisited in Section 14.3.2. Next, in Section 14.3.3, new risks are analysed and the likelihood and impact of each risk is determined and the corresponding consequence estimated. Additionally mitigation strategies are created for the risks with severe consequences that were deemed unacceptable accordingly. With that, an overview of the risks is given in Section 14.3.4, both before and after the mitigation strategies are applied.

### 14.3.1. Risk Overview

Risk is defined as the product of the likelihood of occurrence of the event and the consequence the event. In order to categorise risks, it is necessary to create different categories such that the risks can be ranked based on their occurrence and severity. In order to effectively list and describe the potential risks, the following categories were made based on the phases of the project: *Design (DES)*, *Production (PROD)*, *Launch & Mission Set-up (LMS)*, *Operations (OPS)* and *End-of-Life (EOL)*. Additionally, a naming convention was created to refer to identified risks, which follows **RISK-PHASE-NUMBER**.

For risk likelihood, five categories were found, ranging from remote for very rare events to highly likely events in the form of events that are almost certain to happen. An overview of the possible classes with a description can be found in Table 14.2. It should be noted that the scale is distributed in an uneven manner to ensure that very remote risks are of relative smaller influence than more moderate risks.

**Table 14.2:** Risk Likelihood

Class	Probability	Description
Remote	0-10%	This event is very rare, but still possible
Unlikely	10-30%	This event has a low probability of happening but shall not be overlooked
Possible	30-60%	This event has a moderate probability of happening and mitigation measures have to be taken
Likely	60-80%	This event will most likely happen and thus has to be strictly accounted for
Almost Certain	80-100%	This event will happen and mitigation measures have to be ready to counter it

Classes for the impact of a certain event on the mission were created in a similar manner. The severity of an event ranges from negligible, meaning little impact is expected on the success of the mission, to catastrophic, where mission failure will occur instantaneously. Table 14.3 elaborates further on the created classes.

**Table 14.3:** Risk Impact

Class	Probability	Description
Negligible	0-10%	This event has a negligible impact on the overall mission's success
Minor	10-30%	The impact of this event on the mission is not negligible but not mission-endangering.
Moderate	30-60%	The impact of this event can not be ignored and can lead to major issues if not mitigated
Major	60-80%	This event can end the mission prematurely and has to be taken in charge by the mitigation measures.
Catastrophic	80-100%	This event will instantaneously end the mission and has to be avoided or strongly mitigated

### 14.3.2. Previously Identified Risks

As risks are dynamic and ever changing, risks that were identified during earlier phases in the design cycle should first be updated in terms of likelihood and consequence. These risks were identified in the midterm report and the mitigation method for the risks that were deemed of unacceptable impact can be found there as well [5].

**Table 14.4:** Identified Risks, Likelihood and Impact [5]

ID	Risk	Likelihood	Impact
RISK-DES-01	One of the design budgets can not be adhered to.	Likely	Moderate
RISK-DES-02	The simulation code is not properly verified nor validated.	Possible	Major
RISK-PROD-01	A material is not available for a certain period of time.	Unlikely	Moderate
RISK-PROD-02	A material is delivered at sub-standard quality and still used in the design.	Possible	Major
RISK-PROD-03	The production of a part or assembly is delayed.	Likely	Moderate
RISK-PROD-04	A part or assembly is created at sub-standard quality and still used in the design.	Possible	Major
RISK-LMS-01	The launch system fails during launch.	Remote	Catastrophic
RISK-LMS-02	Delays in launch day due to external factors, such as hazardous weather.	Possible	Minor
RISK-LMS-03	A collision of the system with the launch vehicle's fairing or body.	Remote	Catastrophic
RISK-LMS-04	Damage is caused to the system by the loads experienced during launch.	Unlikely	Major
RISK-LMS-05	An eventual collision with space debris at any point in time during the mission.	Unlikely	Catastrophic
RISK-LMS-06	A failure in any subsystem during travel.	Remote	Major
RISK-LMS-07	The launch system fails to insert the UCM into the desired translunar injection orbit	Possible	Catastrophic
RISK-LMS-08	The Launch vehicle has not reached the desired TRL when the UCMs need to be launched.	Possible	Major
RISK-LMS-09	Maintenance proves to be too expensive to fit in the budget.	Remote	Major
RISK-OPS-01	Unforeseen circumstances lead to mission control on Earth being unavailable.	Remote	Major
RISK-OPS-02	A client cancels their propellant order unexpectedly shortly before hand-off.	Unlikely	Major
RISK-OPS-03	Hostile entities engage with the UCM.	Remote	Catastrophic
RISK-OPS-04	A solar flare occurs leading to computer failure.	Unlikely	Catastrophic
RISK-OPS-05	NASA stops or reduces its propellant production.	Unlikely	Catastrophic
RISK-OPS-06	The UCM fails for unforeseen reasons.	Unlikely	Catastrophic
RISK-OPS-07	During the mission the operational cost of the UCM turn out more expensive than expected, exceeding the budget.	Possible	Major
RISK-EOL-01	Failure in the de-orbiting of the UCM after final flight.	Unlikely	Moderate

### 14.3.3. Newly Identified Risks

During the more detailed design phase, new risks were identified that should be analysed in order to see whether they should be mitigated or not. Since resources are scarce, only the most severe risks can be mitigated down to a lower, acceptable level.

**Table 14.5:** Newly Identified Risks, Likelihood and Impact

ID	Risk	Likelihood	Impact
RISK-EOL-02	The UCM cannot sustain the harsh Lunar environment after final system shutdown.	Likely	Minor
RISK-LMS-10	The designated crater is used for a different purpose and cannot be used anymore to land the UCM.	Unlikely	Moderate
RISK-OPS-08	The reaction control system is unable to provide sufficient rotation for the propellant transfer to the customer.	Unlikely	Major
RISK-OPS-09	The landing gear cannot sustain imposed loads during landing.	Unlikely	Major
RISK-OPS-10	The propellant transfer mechanism is unable to transfer propellant to the customer vehicle.	Remote	Catastrophic
RISK-OPS-11	SolvGE's printer is unable to provide sufficient hydrogen peroxide needed for the reaction control system.	Possible	Moderate
RISK-OPS-12	Water residue created by hydrogen fuel cell exceeds storage capabilities.	Possible	Minor
RISK-OPS-13	The UCM has failed to dock with the customer spacecraft.	Unlikely	Major
RISK-OPS-14	Metals used in the assembly of the UCM suffer from metal fatigue during operation.	Possible	Catastrophic
RISK-OPS-15	Lunar dust covers the solar panels during the stationary phase on the Lunar surface.	Almost certain	Moderate

### 14.3.4. Risk Map

Based on Table 14.4 and Table 14.5, a risk map can be constructed that gives an overview of the severity of the risks, as given in Figure 14.6. As said, the highest risks can only be mitigated, since resources are scarce. Furthermore, by reducing the risk level of the highest risks, the risk of mission failure is reduced in the most effective way.

As can be seen in Figure 14.6, there are three risks of high severity that should be brought down to an acceptable level: RISK-LMS-07, RISK-OPS-14 and RISK-OPS-15. In order to reduce these risks, mitigation strategies were found and these are described in Table 14.6. When the strategies given in Table 14.6 are applied, the risk map can be updated. The result is shown in Figure 14.7, where it can be seen that there are no more risks present in the upper right corner. In such a way, all the risks are of an acceptable level.

**Table 14.6:** Mitigation strategies for Unacceptable Risks

Risk-ID	Mitigation	New Likelihood	New Impact
<i>RISK-LMS-07</i>	Ensure that the selected launcher has a high insertion accuracy and that the launcher has a high TRL.	Unlikely	Catastrophic
<i>RISK-OPS-14</i>	Minimize sudden changes in load bearing cross-section, such that stress concentrations can be minimized.	Possible	Moderate
<i>RISK-OPS-15</i>	Prepare landing site for the UCMs by tamping the Lunar surface such that less Lunar dust is stirred up during landing.	Likely	Minor

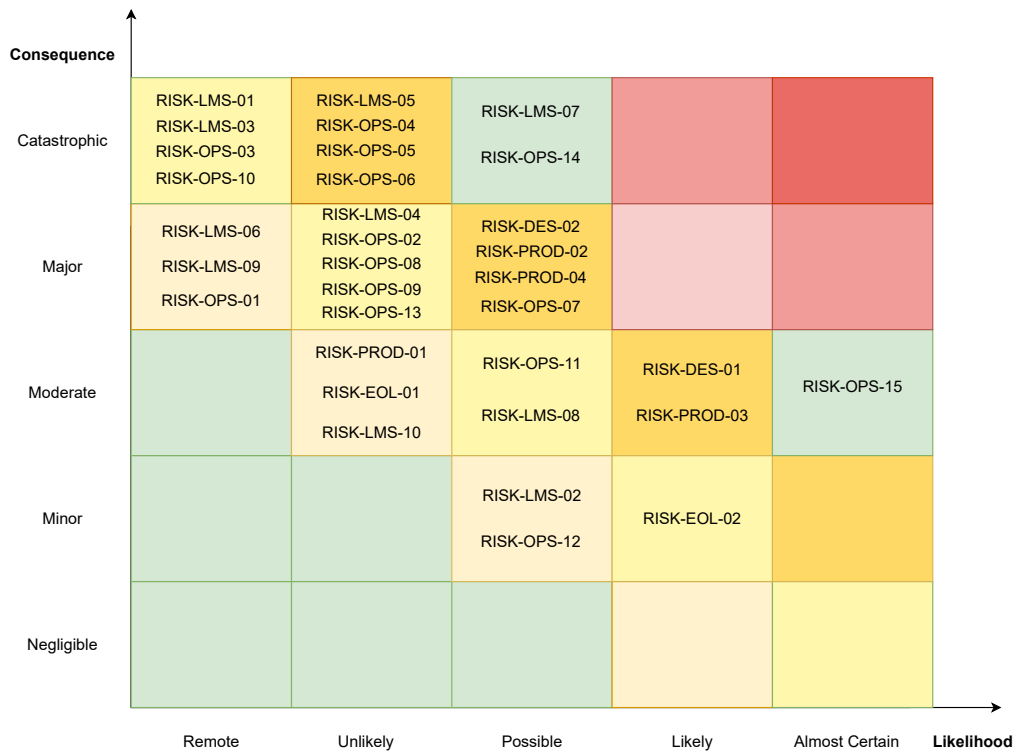


Figure 14.6: Risk map without mitigation strategies

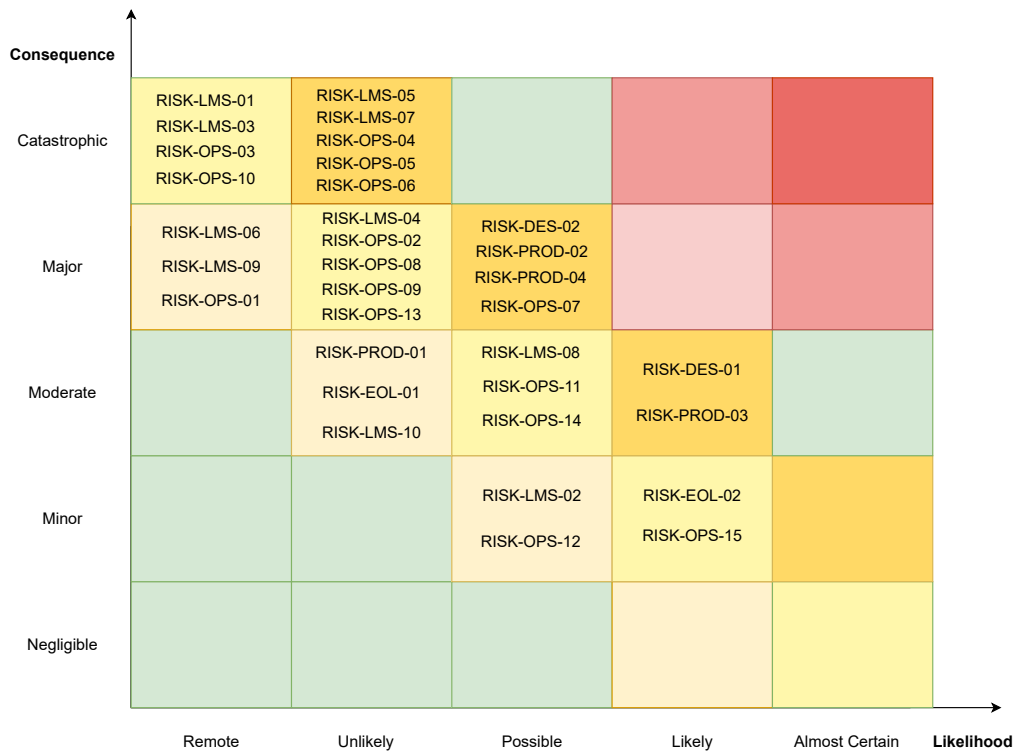


Figure 14.7: Risk map when mitigation strategies are applied

# 15 Maintenance & Supportability

Maintenance and supportability are a crucial aspect of the operations of any spacecraft. Being able to properly assess the current health state of the spacecraft, and having mitigation measures in case of damage is required to ensure a successful mission. Prof. A. Cervone of the Propulsion department of the TU Delft and Dr. M. Dinesh, Propulsion expert of SolvGE have been contacted for external help regarding maintenance of spacecraft, especially the propulsion subsystem. The following sections show the methods and processes the C.O.L.D. mission will undergo to provide maintenance & supportability of the system throughout its lifespan.

## 15.1. Maintenance Philosophy

Telerobotic maintenance on the Lunar surface/orbit has to date, never been done. Additionally, all other telerobotic maintenance performed until now has been very superficial. Literature on this topic is very restricted, and most spotlights lie on the assembly and not the repair of spacecraft. In fact, most autonomous repair robots that are currently under development focus on servicing mechanically simple parts such as fixing damaged truss structures of the International Space Station, and not complex parts such as the turbopumps of an engine or the wiring of the power bus. For this reason, the philosophy followed in the maintenance of the spacecraft will differ from usual maintenance of other engineering systems. The main philosophy is simple; prevention instead of repair. To reduce the need for active maintenance, the system will have to undergo many different processes before the mission starts, starting from monitoring, simulation, and identification methods, to passive maintenance techniques. Once these are set-up, the possibility of active telerobotic maintenance techniques will be analysed.

## 15.2. Digital Twin Technology

As the industry grows ever more digital, new technologies to simulate the real world more accurately are being developed. At the core of these new technologies lies the Digital Twin Technology, which offers a consistent computational model that predicts a product's life cycle. This is not necessarily restricted to one or few systems, entire cities can be modelled in this way. As stated by Zongyan Wang [79], *"It is the simulation technology that integrates multidisciplinary, multiphysical quantity, multiscale and multi probability by making full use of physical model, sensor update, operation history and other data. It is the mapping technology for the whole lifecycle process of physical equipment in virtual space"*. Shortly phrased, this technology creates a digital version of a physical system which is then tested and monitored in many different scenarios. The input for the virtual model is real-world data, and it outputs information of high value to the engineers. Having such a model is a great asset for risk analysis and mission simulations, in which possible failure modes are detected. As failures in space missions are immensely costly, implementation of DTT would greatly reduce these risks, making the mission more reliable and increasing the chance of reaching ROI. This implementation would be done after the design phase in order to identify possible inherent design flaws and most simulations are expected to be performed before the start of the mission.

## 15.3. Health Monitoring

Once the mission is started, the ability to track each individual part's state is required in order to determine the state of the spacecraft as a whole. This is done to determine whether the spacecraft is able to perform its planned operations beforehand. Systems for health monitoring involve two parts, telemetry detectors/sensors and monitors. These systems are called FDIR systems, and previous FDIR consisted of automatic monitoring of key parameters of specific parts. Here, the user manually inputs an acceptable threshold and if the sensors on the part output a value outside this acceptable nominal range, an alarm is sent to the control board to notify the operational team. This method works, but is inherently insufficient if used as only method as faults can be overlooked by the surveillance system if they were to still lie in the acceptable range. Especially, since these ranges are manually set by the user, they might not be accurate enough and leave some faults undetected. However, seeing this lack in monitoring techniques, Fuertes et al. developed a new software called NOSTRADAMUS which relies mainly on the OC-SVM method that is able to automatically monitor and process a large amount of house-keeping telemetry parameters [23]. This method OC-SVM method is illustrated in Figure 15.1 below: Once the outliers are identified, the spacecraft operation engineers have to manually look at them and qualify them either as anomaly or false alarm. NOSTRADAMUS has implemented machine learning, and every time the engineers perform a decision, the software learns and the false alarms become less and less frequent, to reduce manual work. Furthermore, these systems can be used in combination with the DTT for

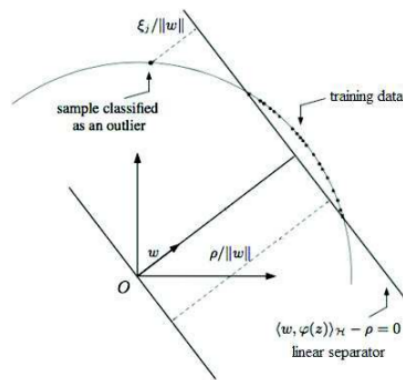


Figure 15.1: OC-SVM principle: finding a linear separator to identify outliers from nominal data [23].

comparison and analysis.

There are many other methods to treat the raw data from the spacecraft's sensors. For example, NASA's Mission Control Centers uses a standard suite of tools for monitoring. Information Sharing Protocol is a tool that acts as primary data feed for the other tools, such as Real Time Plotting, MSK-view, or ELOG which automatically shows telemetry change events in real time [32]. These certified methods can be used in combination with the NOSTRADAMUS method, which will work concurrently with the Information Sharing Protocol, and will be implemented in the spacecraft's operation systems and in the ground control centers to ensure permanently available health monitoring.

Health monitoring will be performed at different levels of intensity throughout an operational cycle. The operation starts when the UCM is landed on the Lunar surface, with its payload and own propellant tanks empty. Before refueling from NASA's Artemis [50], a health check protocol will be run in order to assess the current state of the spacecraft. If it is ready for refueling, refueling begins and the transfer is monitored to identify possible issues. This is not a full-scale monitoring of the UCM, but only the tanks & fuel transfer mechanisms. Post-refueling health checks protocol follow the fuel transfer. After this, the UCM will be idling for a rather long period on the Lunar surface. During this time, communication and health monitoring has to be possible at any given instant, but will nominally only be performed daily. This will be a full-scale UCM health monitoring including camera footage. The camera is the same camera that was used for landing, and in this case can be used to visually inspect the landing gear as it is hard to have housekeeping telemetry on mechanical parts such as the landing gear. This phase is the least monitoring intensive phase of the operational cycle. The next phase is the refueling operation with the customer and the return to the Lunar surface. Similarly as for the other phases, health check protocols will be run before and after the operation to ensure no major damage was dealt to the UCM during operations. During the operations, health monitoring will be the most intense, offering constant real-time tracking of every subsystem's health. This allows for quick reaction of the ground station in case of a preventable malfunction or if manual remote override is necessary. A flow diagram of the health monitoring routine is shown in Figure 15.2 below:

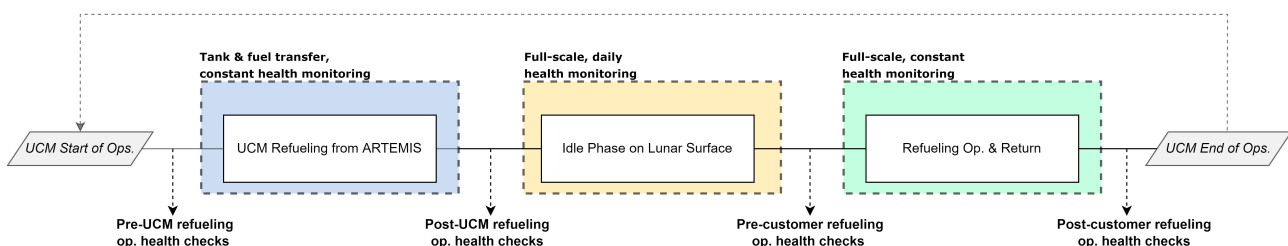


Figure 15.2: Health Monitoring levels throughout an Operational cycle

## 15.4. Replacement

Having the ability to replace parts from a spacecraft allows for greatly enhanced mission lifetime and reduces the risk of total mission failure. However, this ability requires various difficult features. It requires the specific part to be modular, or at least to have the possibility of being disattached from the spacecraft's core body without compromising the body itself. This often leads to higher structural masses, and in general, most critical subsystems such as the propulsion systems simply cannot be replaced. Moreover, due to the mission's nature, it inherently needs to be automated and remotely controlled from the Earth command center. The engineering

team, in accordance with a NASA report about the supportability of Lunar systems [51] has concluded that this is unfeasible in the scope of this project and budget. Having modular tanks was one of the first concepts for the UCM, however, it was ruled out by Dr. Atli-Veltin, cryogenic expert at the TU Delft, mostly due to the danger those operations would induce. Another big factor is that telerobotic replacement of parts has never been performed and the research costs that follow such technology would overcome the allocated budget for maintenance and supportability by a large margin.

## 15.5. Threat of Lunar Dust

The Lunar surface is a very hazardous and hostile environment. Lunar dust, which is very small fragments of moon rock that has been pulverized by meteorites millennia by meteorites, is the main threat. There are many complications because of Lunar dust. The main issue is that it is highly abrasive, and will completely wear out and destroy weak parts of structures such as joints of robotic arms or retractable parts [71]. On top of that, it has been negatively charged by the sun's radiation [1] which leads to very serious issues: the dust levitates because dust particles repel each other, greatly increasing the range of these particles. Furthermore, because of their electrostatic charge, these dust particles tend to stick on surfaces they adhered on firmly, complicating the removal of dust. The most critical risks caused by Lunar dust are listed below:

- **Landing Gear:** being the closest part to the surface, the landing gear inherently is prone to Lunar dust damage. The seals in the pistons, the damping mechanisms and the hinges between the struts and the footpad are the most vulnerable parts.
- **Engines:** Lunar dust that enters the nozzles right after landing is an issue to be addressed. The abrasive dust could damage the nozzle, lowering the thrust performance of the engines. However, as great thrust margins have been taken, this small loss in performance will not be of great importance, especially as possible agglomerations of Lunar dust will be expelled every time the engines are turned on. The bigger issue is if the Lunar dust finds a way to the combustion chamber, where it can inflict critical damage to the fuel injectors.
- **Tanks:** tank inlets are very susceptible to Lunar dust. The presence of Lunar dust in these inlets can lead to leaks in the tanks which are critically endangering to the UCM.
- **Docking Adaptors:** the docking adaptor, which is located at the top of the spacecraft, is very susceptible to Lunar dust. The presence of dust in this part can make the UCM unable to dock, rendering it unusable and resulting in major mission drawbacks.

The following subsections of Section 15.5 address measures to tackle these listed threats.

### 15.5.1. Protective Shell & Port Covers

The most straightforward measure that will be taken is a protective, thin-walled lightweight sandwich structure shell around the spacecraft. It is not only needed for Lunar dust, but mostly for thermal control. It physically impedes Lunar dust to reach susceptible parts, as well as facilitating coating for Lunar dust and thermal control.

### 15.5.2. Mechanical Iris Valve

As there will be no rover to clean the engines' dust on the Lunar surface, another measure has to be implemented to take care of this issue. During the landing sequence, the Lunar dust will be stirred up and if nothing is done dust will most likely get into the nozzle, endangering the system, despite the relatively big clearance between engine and ground. However, this damage to the nozzle has proven to be non-lethal, as it would only reduce the thrust performance by a bit which already has quite high margins. The great damage would be dealt if dust could find its way up in the combustion chamber, damaging fuel injectors leading to UCM failure. For this, and for the docking adaptors, mechanical iris valves will be implemented, which themselves will be coated in Indium Tin Oxide. A picture of such valves is found below:

### 15.5.3. Indium Tin Oxide Coatings

The adhesion of Lunar dust causes many problems to the spacecraft's health, and the team has come up with many options to counter this. First, since the dust particles are negatively charged, applying a negative electrostatic charge to the spacecraft was considered but quickly discarded as there are very strict requirements on spacecraft conductivity due to passage through the Earth's magnetosphere. Sacrificial rods that would attract the dust away from the critical parts were then considered. The idea consists of attracting the dust by positively charging long rods around the spacecraft, and then reverse the polarity in orbit to release the caught rods. However, this has not been considered by any space agency as it is a solution that can be counterproductive as the spacecraft would be attracting more dust and some can land in places other than the sacrificial rod. Thus,

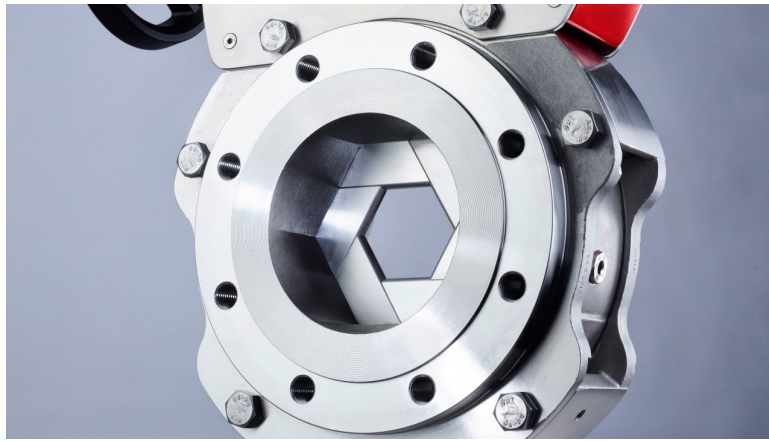


**Figure 15.3:** Mechanical Iris Valve

existing methods were looked into. To overcome the issue of Lunar dust particles adhering to the spacecraft's body, NASA has come up with a possible solution over the last decades [18][2]. More recent studies have confirmed that this proposed solution might be the most viable solution for NASA's Artemis systems [21]. This consists of a thin coating of the susceptible surfaces or parts with Indium Tin Oxide. Such coatings would prevent the build-up of electrical charges that could destroy on-board electronics as well as impeding the dust to stick to the surface.

This coating would be applied in the landing gear and the lowest part of the spacecraft's casing as they are the parts that are the most exposed Lunar dust. The landing gear is especially prone to Lunar dust damage because it is right on the surface and because it has susceptible mechanical parts. These parts are the hinges which connect the struts to the footpads, as well as the footpads and the struts themselves. The lowest ends of the UCM's shell will also be coated in indium tin oxide paint to aid the prevention of Lunar dust in the propulsive system.

## 15.6. Possible Manned Intervention

Knowing the presence of NASA's Artemis mission [50] specific part repair could be entrusted to NASA if a certain set of conditions are met. First, a thorough budget analysis has to assess the cost of the repair, and see if it is worth it to repair. Second, the budget has to allow for it without needing extra investments: in other words, this repair has to be paid purely by profit money after the mission reaches the break-even point. Third, NASA has to have the infrastructure necessary for such repair. This means that, if for example the UCM needs specific electron showers to repel Lunar dust in one specific port, or to weld a part that has cracked, NASA has to have the capability of doing such repairs. This possibility could increase the mission life by a good margin as well as decreasing the impact of UCM part failure, proving to be a beneficial asset to the mission.

## 15.7. Discarded Cleaning & Maintenance Rover

In the previous stages of the design, part of the budget was allocated for a maintenance rover that would perform cleaning of the spacecraft, especially to prevent dust agglomerations and icing in the engines. However, the impact of Lunar dust was underestimated at that point in time. It is impossible to have a maintenance rover that stays exposed to the Lunar environment without intense maintenance, as the Lunar dust would damage the mechanical functions of the rover faster than the spacecraft itself due to its large amount of dynamic parts. Removing the maintenance rover from the allocated budget resulted in having 400 M\$USD extra for alternate maintenance processes.



# 16 Business Case

The reasons for evaluating COLD's business case are relatively straightforward. First, It explains the reasoning behind the project in terms of its economic benefits. Additionally, the evaluated business characteristics serve to convince potential investors of the projects profit value and persuade them to invest their money in it.

The general approach in evaluating the economic characteristics of COLD is explained in Section 16.1. This is followed by the cost breakdown of the whole mission including the costs of different subsystems, presented in Section 16.2. Section 16.3 displays the motivation and approach used in determining the different propellant price characteristics. The other economic parameters, as well as different metrics used in the projects economic performance evaluation were described in Section 16.4. Finally a sensitivity analysis, as presented in Table 13.10, was performed to evaluate the effects of marginal changes to the economic parameters on the overall performance. The results of the financial analysis can be seen in Section 16.5.

## 16.1. Analysis Approach

The proposed COLD mission, as is the case for almost any space mission at the conceptual stage of development, has a lot of inherent uncertainty in regards to its details. The cost of different mission elements is especially difficult to estimate. This is due to some individual components having to be designed and produced specifically for this mission leading to large uncertainties in the final mission cost. For example, this would be the case for the cryocoolers described in Section 5.5, components rarely historically used in space missions. This phenomenon of uncertainty is by no means unique to the COLD mission. The NASA cost estimation handbook also mentions this difficulty in precise estimations during the conceptual design stage [48].

As such, for a financial analysis of COLD it is important to take these uncertainties into account. The most frequently used method do so is to make use of Monte Carlo simulations. These serve to create models based on sampling multiple values from the distribution of each individual parameter, such as the cost of development of the spacecraft. These are then used to calculate the final outcome given the drawn numbers. Here, the desired outcome is the total cost of the mission. This process is repeated millions of times to create a distribution for the searched value. This process is illustrated in greater detail in Section 16.2.

An important factor to mention is that not all different cost parameters used in the simulations follow normal distributions. This is for example the case of development cost of the spacecraft. This value was estimated using a NASA paper describing conceptual Lunar lander design, where it was mentioned that after consultation with multiple experts, the value produced by the method was expected to be an overestimation [47]. Additionally, for COLD estimations a safety factor of 1.2 was used for the development cost. As such, an uncertainty of -25% and +10% of the cost was used in the Monte Carlo simulations.

In order to deal with the asymmetric distributions of different financial parameters, a special distribution called the split normal distribution, also called a two piece distribution, was used to model these variables. This method was chosen, because such distributions are often used when modelling asymmetric distributions in financial analysis [76]. Furthermore, as to model the total costs, a python script was used to perform Monte Carlo simulations, using a specific library<sup>1</sup> that enabled the implementation of the two piece distribution model. The parameters defining such a distribution are two separate deviations,  $\sigma_1$  and  $\sigma_2$ , one for the left and one for the right side of the plot respectively, with a mode in the center  $\mu$ . The general formulation of such distributions can be seen in Equation 16.1, where  $A$  represents the normalising constant. This is best illustrated in Figure 16.1b in Section 16.2.3. Before continuing on further with the economic analysis, it is worth to point out that when referring to any value which originates from a distribution, the distributions mode is meant.

$$\begin{aligned} f(x; \mu, \sigma_1, \sigma_2) &= A \exp\left(-\frac{(x-\mu)^2}{2\sigma_1^2}\right) && \text{if } x < \mu \\ f(x; \mu, \sigma_1, \sigma_2) &= A \exp\left(-\frac{(x-\mu)^2}{2\sigma_2^2}\right) && \text{otherwise} \end{aligned} \quad (16.1)$$

## 16.2. Cost Breakdown

Before calculating the profits of the project, it is first crucial to determine its costs. This is done in this section, with the development and production costs split into specific subsystem costs in Section 16.2.1. Furthermore,

---

<sup>1</sup>URL:<https://quantgirl.blog/two-piece-normal/>

the other total cost elements and their uncertainties are presented in Section 16.2.2. The results of the total cost calculations, estimated using Monte Carlo methods, can finally be seen in Section 16.2.3.

### 16.2.1. Subsystem Cost Breakdown

In order to obtain estimates for the development and production costs for the Universal Cryogenic Module, it is necessary to first look at its individual subsystems. All of them were described in great detail in the previous parts of this report. However, the cost characteristics of these subsystems have not yet been evaluated explicitly, apart from some preliminary estimates for the EPS. This is because it is extremely difficult to obtain any economic information about state-of-the-art spacecraft components. For example, there is almost no information regarding the phased array antennas used on the NASA's Orion capsule mentioned in Chapter 9 because the manufacturer deliberately conceals this data. The only spacecraft components which have financial information publicly available are those for small satellites, and these are not relevant for the UCM. They are not relevant as the UCM is orders of magnitude larger and does not conform to a typical satellite mission profile. Therefore, in estimating the costs of different subsystems of the UCM, relevant methods and values presented in various literature sources were used [8] [47] [81] [88].

In the subsystem cost breakdown, different specific subsystems are sometimes combined together for calculation purposes. For example, the cryogenic storage system is assumed to be split between "tanks" and "thermal control" based on its application. In this fashion tank coating would belong to the former while radiators to the latter. Additionally, the "Communications and Data Handling" subsystem includes both C&DH as well as TT&C from chapters 10 and 9 respectively.

Guidance, Navigation, and Control (GNC) refers to the whole software and hardware architecture required to control the spacecraft. Landing and docking procedures require large precision as any mistake could result in catastrophic failure of the vehicle. As such extensive software as well as hardware attitude determination systems and sensors have to be set in place, resulting in the relatively large price tag of this category. However, the reaction control system of the ADCS is not included in GNC costs. This is because the reaction control system requires additional infrastructure: the monopropellant production unit described in Section 8.3.

**Table 16.1:** Breakdown of separate subsystem costs for the UCM Lunar lander. Production costs are recurring for each individual unit produced, while the development costs remain constant regardless. The safety factors (SF) employed for the development and production costs are 1.2 and 1.1 respectively.

Subsystem	Development costs F2022M\$	Production Costs F2022M\$
Structures	288	20
Tanks	195	24
Separation System/Launcher compatibility	2	1
Thermal Control	78	12
Payload/Docking Adapter	46	5
Landing Gear	60	27
Guidance, Navigation, and Control	400	115
Communications and Data Handling	146	27
Electrical Power System	161	31
Reaction Control System	159	20
Propulsion	0	60
System Engineering and Integration	300	34
<b>Total</b>	<b>1,835</b>	<b>376</b>
<b>Total(SF)(Dev - 1.2, Prod - 1.1 )</b>	<b>2,202</b>	<b>414</b>

For the propulsion subsystem off-the-shelf components will be used: two Vinci engines worth approximately 15M\$ each, and one larger RL engine worth 25M\$. The last 5M\$ encompass the ignition, feed system and other miscellaneous parts of the propulsion subsystem. As off-the-shelf components are used for this subsystem, no development costs are involved for these parts.

The propulsion subsystem does not involve development costs as off the shelf components are used in this case: two Vinci engines worth approximately 15M\$ each, and one larger RL engine worth 25M\$. The last 5M\$

encompass the ignition, feed system and other miscellaneous parts of the propulsion subsystem.

The final element of the cost breakdown is the system engineering and integration, and while not explicitly a subsystem, it is nonetheless a vital part of design process of the UCM. Its costs were also estimated using the NASA's conceptual Lunar lander design paper[47]. As not all subsystems covered in this paper are applicable to the UCM, several covered subsystems costs were removed. These included: Atmosphere Management and Crew Accommodations which are not applicable to the unmanned UCM mission. Following these reductions, the systems engineering and integration costs were scaled down accordingly.

All of these findings were corroborated by the specific subsystems engineers and their order of magnitude were confirmed. It is important to mention that the main source of the subsystem cost information states, that the estimated values are most likely an overestimation [47]. This fact will be elaborated upon in the following section 16.2.2. The values of different subsystem costs are presented in Table 16.1. It is important to not that the development costs are one time expenses, while the production costs rise with the number of units (UCMs) fabricated.

It is important to place emphasis on the fact that the values represented in Table 16.1 are rough estimates. However, as there are no other possibilities to determine more accurate costs without access to more elaborate estimation tools such as PRICE, NAFCOM, or MOCET, the estimations presentable in the table are the only viable option. From this it may follow that different subsystem costs might differ substantially from what is presented in Table 16.1. Despite this, the total calculated costs should remain somewhat accurate as one subsystem may have a lower than expected cost whilst another might have a higher cost resulting in approximately the same total cost [47].

### 16.2.2. Uncertainties of Total Cost Elements

Given the production and development costs, it is possible to continue the financial analysis of the COLD mission. Here different cost parameters were used, each describing a different aspect of the mission. Most of these were again determined using an already mentioned paper from NASA describing conceptual lander design [47]. These were then compared to literature values presented in different research papers mentioning Lunar landers [8]<sup>2</sup>. The uncertainties in these parameters were determined in a similar fashion: they were based on NASA estimates [48] as well as via comparison to other literature values [8] [47]. The results of these estimations can be seen in tab:costbreakdown, where the different total cost elements and their respective uncertainties are depicted.

In terms of the specific cost elements, the total development and production costs of the Lunar lander used in COLD, described in the previous subsection made up a large part of the total mission costs at 57.4% of the total estimated mission cost. Their uncertainties were estimated at -25% and +10% of their costs both. This is because, as briefly mentioned in Section 16.1, the estimation approach presented in [47] already predicts that these estimates are most likely overestimating the total cost. On top of that, a safety factor of 1.2 added on top of the estimated value, as prescribed by COST ANALYSIS, additionally shifts the total costs to the higher range of the estimates. Even though, it is still possible that these costs are below what would be necessary in reality, as the COLD lander will be completely distinct from any other vehicle flown in space so far, and unknown variables might come into play. Even though the team agrees that by using these specific uncertainty values, the most realistic pricing range is achieved.

Another large factor for the financial analysis of the mission are the costs for testing and certification, at 27.7% of the total mission cost. These costs include costs of system test hardware, operations (i.e. technicians salaries) and support equipment. These were obtained from [47], and were corroborated using [22]. An often mentioned disclaimer when it comes to testing and certification was that it is very difficult to estimate these costs, as for example sometimes dedicated facilities have to be built, as to test the necessary mission components. Should this be the case, a two billion price tag seems reasonable, and might even be substantially higher. Should available testing facilities be well suited, this is a rather large overestimation. As very little information can be found on how much these costs vary, a large uncertainty of -40% and +20% was applied to these costs. While not extremely informative on its own, this accommodates the vast range of possible values for the testing costs for COLD. Otherwise, vast underestimation of the total costs could be made, resulting in the mission going above the allocated budget or vastly increasing risk mission failure by skipping certain testing elements, both of which are undesirable.

The COLD mission also includes recurring expenses in the form of operational costs. These include but are not limited to: funding support teams, payments for usage of ground stations and frequencies/bandwidth, program management, software maintenance etc. Here these costs are given as the total costs, however in reality these

---

<sup>2</sup>URL:<https://www2.deloitte.com/content/dam/Deloitte/fr/Documents/energie-et-ressources/Publications/fueling-the-future-of-mobility-spaciaux.pdf>

are spread throughout the total mission duration. They were estimated using reference literature values [47] [8] [81] [14], as well as a NASA's mission costs estimation guidelines for confirming the magnitude of these costs<sup>3</sup>. These costs were estimated to be equal to 40 million USD a year. As for their uncertainty, while these costs can be higher, it is possible that the autonomous/remote nature of COLD may result in large cost savings. This is because the number of technicians and engineers working with the mission can be minimised, and because their salaries make up the bulk of operational costs<sup>4</sup>, the total yearly expenses would decrease substantially. For this reason an uncertainty of +20% and -20% was determined to reflect this possibility the most. An important thing to mention is that the propellant spent while idling on the Lunar surface is not considered in operational costs. This is because it is already a factor in the P2P ratio described in Section 4.3, which is the main metric for determining the amounts of bought and sold propellant.

The two last factors describing the financial aspect of the mission are the insurance and launch costs. The latter were taken directly from SpaceX, with the price of a single launch being priced at 20 million USD<sup>5</sup>. SpaceX mentions 10 million, however that was deemed unreasonably low, and as such a safety factor of 2 was added on top of it. The uncertainty follows the same logic: -10% and +30% of total costs were selected as the launch costs uncertainty because the Starship launch vehicle is still in development and cost increase is likely, while a decrease is not something that experts predict would happen<sup>6</sup>.

Finally, the insurance costs were estimated using Transcost methods [40], which mention that the insurance costs are typically in the range of 30% of the cost of production of a single unit and 30% of the launch costs. The COLD includes four Lunar landers and four launch vehicles, and as such, the insurance costs were adapted accordingly by multiplying these numbers by 4. The insurance might be higher because this is a new and perhaps risky venture, but they could also be lower by insuring in bulk all four launchers, the so called wholesale insurance. As not much additional information could be found regarding the insurance, apart from brief mentions in the SMAD book [81] corroborating the Transcost model values, the uncertainty in the insurance was determined to be  $\pm 30\%$ .

**Table 16.2:** Different cost parameters and their uncertainties used in the financial analysis of the COLD mission. The different values were obtained from [47] with corroboration from different subsystem departments

Item	Value	Units	Uncertainty
Total Development (safety margin 1.2)	2202	F2022M\$	-25%/+10%
Total Production (safety margin 1.1)	4x414	F2022M\$	-25%/+10%
Testing and Certification	1860	F2022M\$	-40%/+20%
Operational Costs	400	F2022M\$	-30%/+15%
Launch Costs	4x20	F2022M\$	-10%/+30%
Insurance Costs	521	F2022M\$	-15%/+15%
Total Mission Cost	6,719	F2022M\$	

### 16.2.3. Total Costs

In order to create an analysis of the total costs incurred by the mission, it is important to take into account the uncertainties in the different total cost elements, described in Section 16.2.2. This was done by following the Monte Carlo analysis approach described in Section 16.1. After creating split normal (two piece) distributions for each of the cost elements, random samples from each of them were taken, which were then summed up as to obtain a value for the total cost. This process was repeated for a million different samples, creating in the process a distribution for a given cost estimate. This procedure was done for the total cost of initial investment, as well as for the recurring costs and the total costs, comprising of the sum of the previous two.

The total cost was further evaluated as to find the percentage chance of reaching a budget of over 7 billion USD. While the initial investment cost almost never reaches this amount, the recurring costs are also included in this evaluation. This is because it might be possible that for example employee salaries and/or frequency bands usage would have to be guaranteed before the project would begin operations. The initial costs of the mission, including all the cost elements from Table 16.2 apart from the operational costs are displayed in Figure 16.1a.

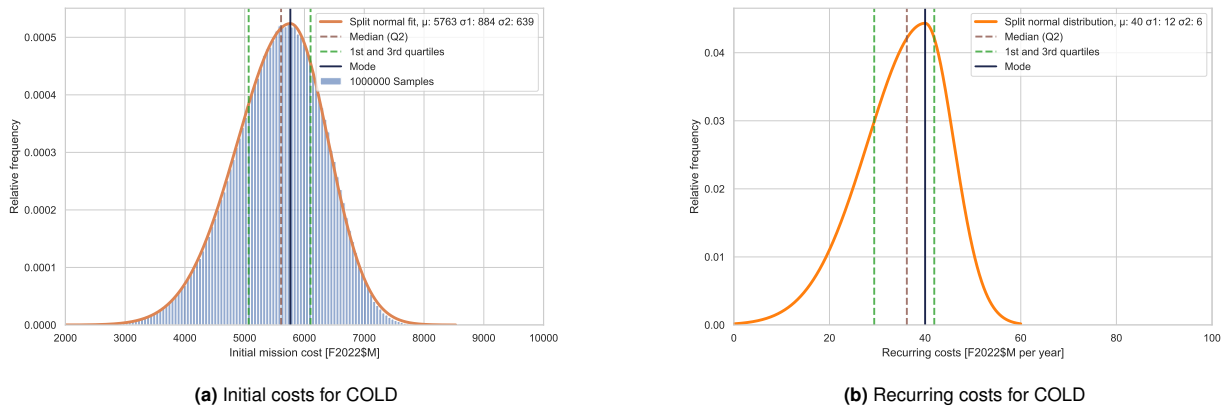
<sup>3</sup>URL:[https://www.nasa.gov/sites/default/files/files/20\\_MOCET\\_NASA\\_Cost\\_Symposium\\_Briefing\\_2015-08-21\\_tagged.pdf](https://www.nasa.gov/sites/default/files/files/20_MOCET_NASA_Cost_Symposium_Briefing_2015-08-21_tagged.pdf)

<sup>4</sup>URL:[http://www.yorku.ca/bquine/pages/mission\\_costs\\_and\\_reliability.htm](http://www.yorku.ca/bquine/pages/mission_costs_and_reliability.htm)

<sup>5</sup>URL:<https://www.science.org/content/article/spacex-now-dominates-rocket-flight-bringing-big-benefits-and-risks-nasa>

<sup>6</sup>URL:<https://www.space.com/spacex-starship-flight-passenger-cost-elon-musk.html>

The operational costs per year are depicted in Figure 16.1b, and as they only include one parameter, are a good indicator of how the split normal distribution works.



Here the describing parameters are displayed in the figures, with the initial costs distribution being described with a mode of 5763 (-884, + 639), or alternatively 5763 -15.3% + 11.2% M\$. The recurring costs remain unchanged from Table 16.2 at 40 +12/-6 M\$ per year (40 +30%/-15% M\$ per year). Additionally, the first and third quartiles, as well as the median are shown in the figure, as to give an idea of probability concentration around the mode. The mean is omitted as it is not a very descriptive characteristic for skewed distributions.

Finally, by performing a secondary Monte Carlo analysis on these two distributions, the total costs and its uncertainty can be estimated. The results of this simulation can be seen in Figure 16.2, where the red solid line represents the 7 billion USD budget limit. The total cost of the mission was determined to be equal to 6111 M\$ -885/+650 M\$. This translates to 6111 M\$ -14.5%/+10.6%. Such a result is surprising at first as it does not match the value predicted by summing the values from Table 16.2 by around 600 million USD. However after closer inspection, it can be seen that this result is indeed correct. This is because the maximal uncertainties for the left side of the different parameters - negative uncertainties, are larger than those on the right side. This results in rather large skew to the left of the total cost estimate. Additionally, percentage uncertainties of the distribution are comparatively small, compared to the ones in Table 16.2.

Based on these simulations, COLD's business venture was estimated to have a 93.1 % chance of remaining within the prescribed 7 billion USD budget. As such it is reasonable to expect that the project will not run into cost overruns, given that the assumptions from Section 16.4.1 and Section 16.2.2 are correct.

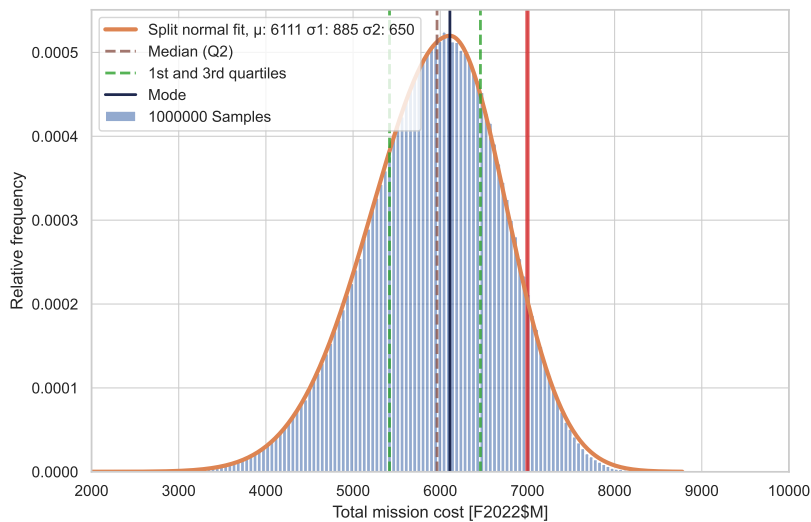


**Figure 16.2:** Total cost of the Cryogenic Orbital Lunar Depot mission. Red line represents the 7 billion USD budget limit.

## 16.3. Propellant Pricing

This section presents the evaluation of the price of propellant purchased on Lunar surface, as well as the setting of the price at which propellant will be sold in low Lunar orbit. The former has to be estimated as precisely as possible, as the success of COLD depends on the ability to turn a profit. The setting of the sell price has to be done with the same goal in mind, with customers and their willingness to pay in mind.

### 16.3.1. NASA Sale Price

One of the most important factors in creation of the business model of COLD is the price at which the propellant will be procured from the supplier on the Lunar surface. In this case, the supplier will be NASA, producing hydrogen and oxygen by electrolysing water from Lunar ice deposits. The correct setting of this parameter is crucial, as a too high price will lead to an unprofitable venture. On the other hand, financial analysis with the propellant purchase price set too low will not be a reliable source of information as it will not match reality and can lead to the project going through based on false assumptions. It is not a far stretch to say that this factor is one of the deciding factors deciding the success or failure of COLD as an economic project.

For this reason a great effort has been made in estimating this value as realistically as possible. Different reports and scientific articles mention a value of 500\$ per kilogram of propellant sold on the Lunar surface [14] [69] [64]. This value was based on assumptions of propellant delivery to LEO at 3000\$/kg, and will serve as the basis for financial analysis in the further sections of this chapter. While the price of propellant sold by COLD might not follow the same pricing strategy as outlined in literature [14], it was determined that the 500\$ price tag is within reasonable range. This is because NASA, COLD's supplier, will produce propellant at a rather low price as it is a governmental agency, not interested in profit but rather results. With the help of COLD, it will deliver propellant to the orbit for its own spacecraft missions and as such will not strive to financially depreciate COLD, its main partner. Additionally, since COLD's mission duration is 10 years, perhaps a bulk propellant purchase agreement could be made in advance, further bringing down the price per kilogram.

In the financial analysis purchase prices of 500, 600 and 700 \$/kg will be considered, as to evaluate how COLD's financial performance will be affected with changes to propellant purchase prices. However the 500\$/kg will remain the main base for different calculations as it is the value most often quoted and it seems to be a generally agreed to assumption [69].

### 16.3.2. Setting Price Point

In order to determine the best price at which to sell the propellant in the low Lunar orbit, it is necessary to look at the potential customers of COLD's business venture. As long as it is interesting for them to buy the propellant, then the mission has a chance of being profitable, with the only alternative option is to compare it to the price of propellant from Earth. Both customer identification and the determination of price of Earth produced propellant was done in Chapter 3. As it was mentioned in that chapter, one of the most interesting customers for COLD is the propellant transfer industry, which would deliver propellant to customers within different Earth as well as high Moon orbits. As these are out of range for the UCM's, this would effectively become a business partnership as the two would have to cooperate in a symbiotic relationship. The most important factor for such customers would be the  $\Delta V$  required to move within the different orbits, as it defines the amount of propellant that would have to be used to get to their potential customers in the first place. The sale of the remaining propellant would make up for the costs incurred when purchasing from COLD. Table 16.3 presents the necessary pricing for the partnered entity assuming a space tanker with a weight of 5 tonnes and maximal capacity of 50 tonnes including the tanks with fuel for travel. The three different evaluated scenarios for pricing of the propellant by COLD are 5000, 5500 and 6000 \$ per kilogram. Such pricing results from preliminary economical analysis showing that this is the price range required for a large enough internal rate of return to attract investors, something that will be discussed in greater detail in Section 16.4. This pricing is also required based on the total costs of the mission and the predicted demand of 250 tonnes per year, as throughout 10 years of operations the venture should prove profitable.

As can be seen from Table 16.3, the economic partner specialising in propellant transfer to different orbits can still deliver prices to most of the locations around Earth rather profitably, with the exception of low Earth orbit. There the costs become rather large, preventing any competition with the substantially cheaper propellant delivered from Earth. One solution to this problem is presented by Kornuta in his paper [14], in which he mentions the possibility of aerobraking slashing the required  $\Delta V$  requirement, effectively lowering the prices. However at this stage the price of propellant offered by COLD is still higher at LLO than propellant made on Earth at LEO. Should the yearly demand be higher, the price of propellant offered by COLD could be lowered, translating to larger cost savings. The same would occur if the mission lifespan would be longer, as the total investment costs would spread out more thinly, allowing for lower pricing.

**Table 16.3:** Cost of propellant at different locations. The first column refers to the cost of bringing propellant from Earth, while the other three refer to an external party selling its propellant in different locations after buying it from COLD (external party transfer vehicle assumptions: 5tonnes dry mass, 50 tonnes max capacity including payload and functional propellant)

Location	Cost of propellant from Earth	Sell price: 5000\$	Sell price: 5500\$	Sell price: 6000\$
Earth's surface	1 \$/kg	-	-	-
LEO	3000 \$/kg	14150 \$/kg	15565\$/kg	16980\$/kg
GTO	6000 \$/kg	-	-	-
GEO	12000 \$/kg	8334 \$/kg	9168 \$/kg	10001\$/kg
EML1	9000 \$/kg	5851 \$/kg	6436\$/kg	7021 \$/kg
LLO	16000 \$/kg	5000 \$/kg	5500 \$/kg	6000 \$/kg
Lunar surface	27000 \$/kg	500 \$/kg	500 \$/kg	500 \$/kg

It is also important to remember that the cost of propellant as delivered from Earth is not exactly the price of propellant, but rather how much it costs to deliver one kilogram of mass to the orbit. This pricing however does not reflect the need for a specialised vehicle to deliver propellant (which would be difficult to make reusable due to reentry requirement), as well as profit margins. All of these elements have a significant impact of the refueling industry business model, effectively making the cost of delivery higher. This is because it would lower the total amount propellant that could be brought to orbit each individual launch.

## 16.4. Economic Analysis

After selecting the basic financial parameters - the buy and sell price of the propellant, as well as determining the probability distributions of initial and recurring costs of the mission, the financial analysis of COLD's business venture was performed. Once gain a Monte Carlo approach was followed, as to simulate the probability based on the different cost element distributions. In doing so however one important assumption was made. Notably, it was assumed that COLD is the only customer of NASA's Lunar propellant production plant, and the negative consequences of diminishing market share are not be considered in this study. This is a rather realistic strategy, as the COLD's venture is very risky as it is very expensive and unproven. As such, competitors would not invest large sums of money into their respective programs, should this business model not be demonstrated to turn a profit first. Additionally, there is no real indication whether the propellant delivery market is large enough to support competition, or whether the different economic actors would starve themselves out.

### 16.4.1. Financial Analysis Metrics

In order to evaluate the economic performance of COLD's venture, different indicators reflecting its separate elements were considered. Out of these, four separate metrics were determined to be of greatest influence and value for this evaluation. These are (from [11]):

- **Cash Flow:** The summed flow of cash for a period.
- **Present Value:** This is the required amount of money that if invested for a specific return today, would yield a specified future value. This concept is very fundamental to all finance and it mainly describes that a dollar in the future is less valuable than today due to risk. The total present value (for all cashflows) is defined as:

$$PV = \sum_{t=1}^T \frac{C_t}{(1+r)^t} \quad (16.2)$$

This is also known as the discounted cash flow (DCF).

- **Net Present Value:** The net present value (NPV) is the present value with the initial investment (usually the initial cash flow that is negative) summed up. It is defined as:

$$NPV = C_0 + \sum_{t=1}^T \frac{C_t}{(1+r)^t} \quad (16.3)$$

The NPV reflects the net value of all discounted cashflows, which of course includes the initial investment. Evidently, if the NPV is below 0, then value is not created by the venture, but lost. Moreover, the larger the NPV the better and for an investor this is a fairly universal metric for comparing the value of investments. For this reason the NPV is one of the main parameters used to analyse the COLD's economic characteristics.

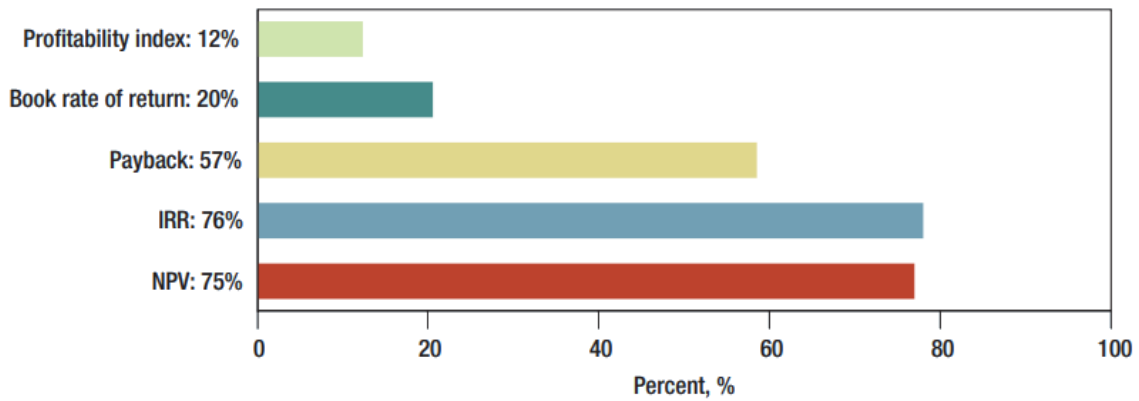


Figure 16.3: Percentage of CFOs who choose a particular investment evaluation technique [11]

- **Internal Rate of Return:** The internal rate of return (IRR) is yet another useful financial metric. This metric is the discount rate for the project for an NPV of 0. The IRR allows for different investments to be compared, as well as, the investment can then be also compared to the market return (if one were to invest and take the returns of the market average). If the IRR is lower than the return of the market, then the investor has no reason to invest since he or she could diversify, take a loan, or simply invest elsewhere and obtain superior returns. Therefore this metric is to be higher than the average return of the market, to be attractive to the average investor.
- **Return on Investment:** The return on investment (ROI) here is defined simply by taking the net of the cash flows and then dividing it by the cost of the initial investment:

$$ROI = \frac{\text{Current Value} - \text{Initial Investment}}{\text{Initial Investment}} \quad (16.4)$$

- **Discounted Break-even Point (Payback):** The break-even point is the point in time at which total cost and total revenue are equal. This is a good metric as to evaluate how fast would COLD become a profitable venture. The discounted version is even a more conservative option of the payback. Here it is evaluated based on how many years will it take for the total revenue to overtake the total costs.

In the figure below survey evidence can be seen on the percentage of CFOs who always, or almost always, use a particular technique for evaluating investment projects in Figure 16.3:

Additionally, a few very important assumptions were made when determining the economic parameters:

- The nominal discount rate ( $r$ ) was set as equal to 10%, as mentioned by a similar economic study[14].
- The average inflation ( $i$ ) over the 10 years was set as 5%, based on the average inflation rate in the US <sup>7</sup>
- The real discount rate was calculated as follows:  $r_{real} = \frac{(1+r)}{(1+i)} - 1$
- The UCM was assumed to make 10 launches per year, each time selling 25 tonnes of propellant

### 16.4.2. Net Present Value

The net present value was evaluated for the three different prices as presented in Section 16.3.2. For the 5000 USD per kilogram, the results of the Monte Carlo analysis based on the initial and recurring costs, as well as the assumptions from the previous subsection, can be seen in Figure 16.4. Similar plots for the price set at 5500 and 6000 USD per kilogram can be seen in Figure 16.5a and 16.5b respectively. The results of the net present value simulation are summarised as follows:

- **NPV** for a sell price of 5000\$/kg; 1707M\$ -642M\$/+886M\$ (1707M\$ -37.6%/+51.9%)
- **NPV** for a sell price of 5500\$/kg; 2680M\$ -640M\$/+890M\$ (2681M\$ -23.9%/+33.2%)
- **NPV** for a sell price of 6000\$/kg; 3360M\$ -638M\$/+892M\$ (2681M\$ -19%/+26.5%)

<sup>7</sup>URL:<https://www.worlddata.info/america/usa/inflation-rates.php>



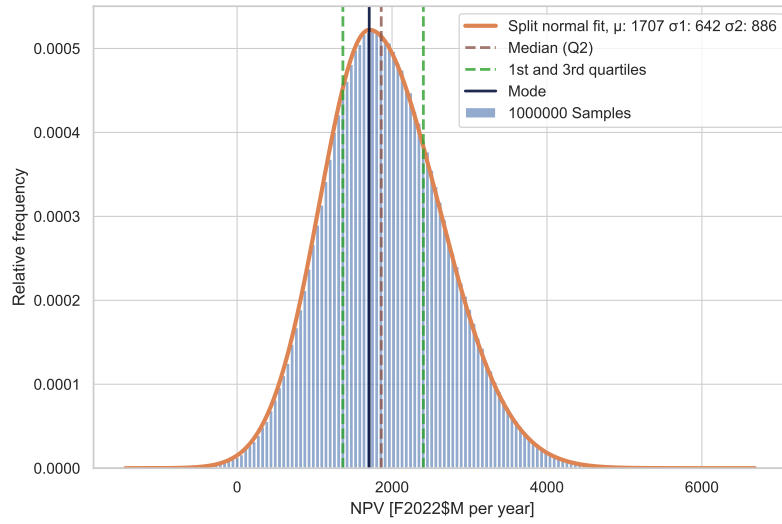
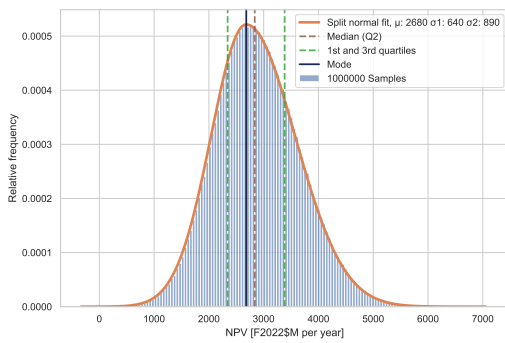
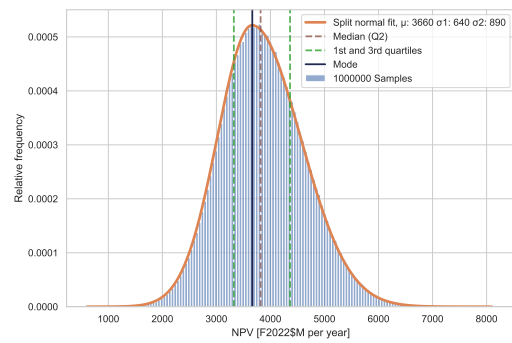


**Figure 16.4:** The plot of the net present value economic parameter, for a 5000\$/kg sell price setting



**(a)** NPV plot, for a 5500\$/kg sell price setting



**(b)** NPV plot, for a 6000\$/kg sell price setting

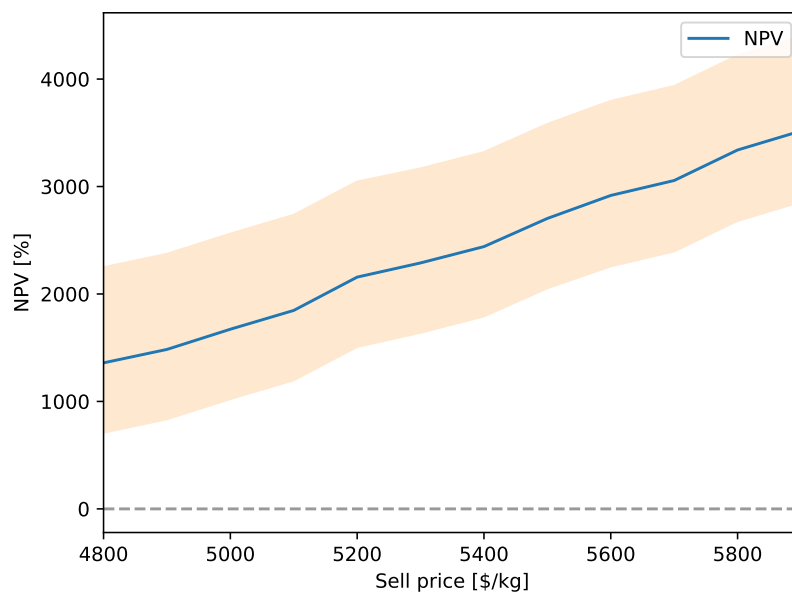


**Figure 16.6:** The plot of NPV values against the sell price of propellant, including uncertainties

It can be seen that in all three cases the net present value stays well above zero - for all three the probability of the NPV being below 0 remains below 0.5%. As such, it is expected that the project will produce more income than could be otherwise gained by earning the discount rate by investing in "safer" projects or funds. Such a result proves that COLD is an interesting venture for investors, as it demonstrates the profitability of COLD's mission. The general relation between the sale price and the net present value, including the uncertainties is presented in Figure 16.6.

### 16.4.3. Internal Rate of Return

In a similar fashion as for the NPV, the evaluation of the internal rate of return was also done for the three selected price scenarios. Here the term internal refers to the fact that the calculation excludes external factors such as inflation or the financial risk. As mentioned in Section 16.4.1, the IRR should remain above the discount rate, according to the "IRR rule" <sup>8</sup>, as otherwise the investors would be more inclined to invest in the market instead, as this would lead to larger profits. This is because IRR describes the performance of an investment; if its below the discount rate, the investment performs worse than the market. Alternatively, if the IRR is higher than the discount rate, it performs better. For this analysis, as mentioned in the assumptions from Section 16.4, the discount rate was set at 10%.

The IRR for the three different evaluated scenarios can be seen below in the figures. Figure 16.7 presents the results of IRR analysis for the 5000\$/kg scenario. The 5500\$/kg and 6000\$/kg scenarios can be seen in Figure 16.8a and Figure 16.8b respectively. The findings regarding the internal rate of return are summarised below:

- **IRR** for a sell price of 5000\$/kg; 9.50 -1.95/+4.35 percent (9.5 -20.5%/+45.8%). The IRR was higher than the discount rate in 64% of cases.
- **IRR** for a sell price of 5500\$/kg; 12.40 -2.10/+4.70 percent (12.4 -16.9%/+37.9%). The IRR was higher than the discount rate in 92.2% of cases.
- **IRR** for a sell price of 6000\$/kg; 15.30 -2.30/+4.90 percent (15.3 -15%/+32%). The IRR was higher than the discount rate in 99.3% of cases.

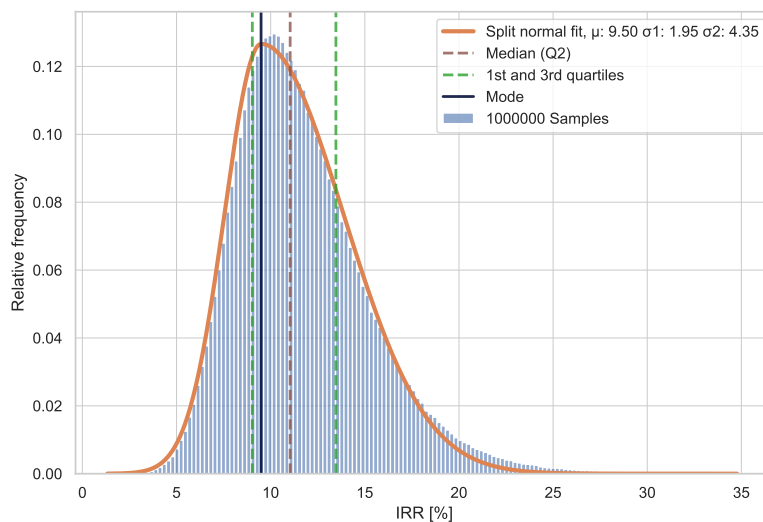
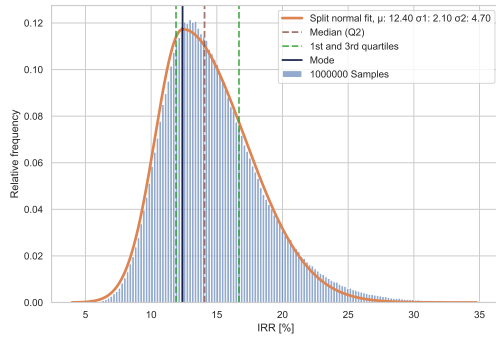
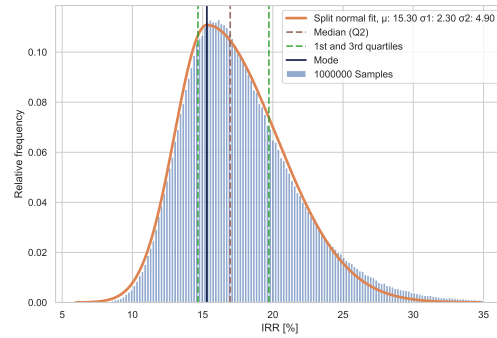


**Figure 16.7:** The plot of the internal rate of return economic parameter, for a 5000\$/kg sell price setting

<sup>8</sup>URL:<https://www.investopedia.com/terms/i/internal-rate-of-return-rule.asp>



(a) IRR plot, for a 5500\$/kg sell price setting



(b) IRR plot, for a 6000\$/kg sell price setting

For the internal rate of return, the general relation linking it to the sale price of the propellant is presented in Figure 16.9.

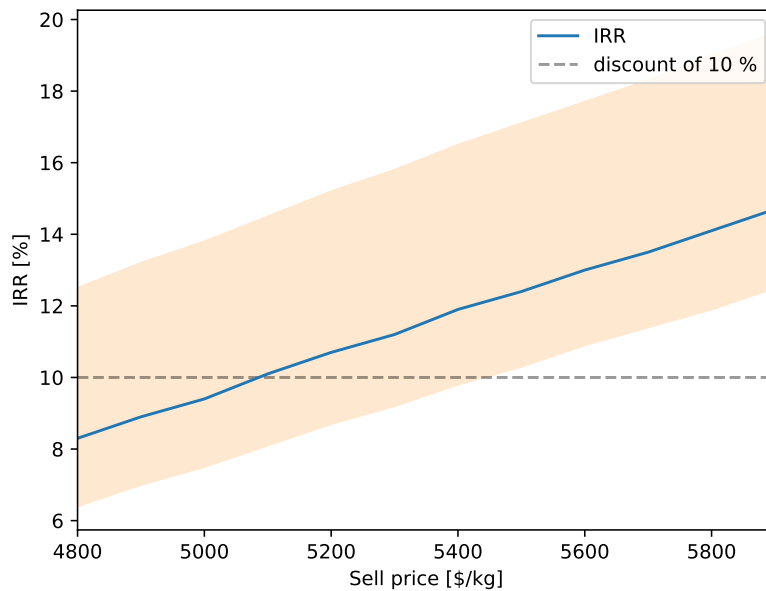


Figure 16.9: The plot of IRR values against the sell price of propellant, including uncertainties

#### 16.4.4. Break-even price and the return on investment

The time to break-even is one of the most important elements of any economic analysis for a given investment. For COLD there is no pressure to break-even as fast as possible, as it is the type of ventures that does not turn a profit for quite some time. Regardless, it has to break even before the end of mission, that is before "year 11" as it is presented in the plots. The only case in which this has a probability of happening based on a million cases is the case at which the propellant is priced at 5000\$ per kg. Even then, the probability of the project not turning a profit after 10 years of operation is around only 2%. The break-even charts depicting the frequency of sample breaking even in a given year are presented below. The chart depicting the break even frequency for the 5000\$/kg of propellant is shown in Figure 16.10. Likewise, for the 5500\$/kg and 6000\$/kg scenarios, the frequency plots can be seen in Figure 16.11a and Figure 16.11b.

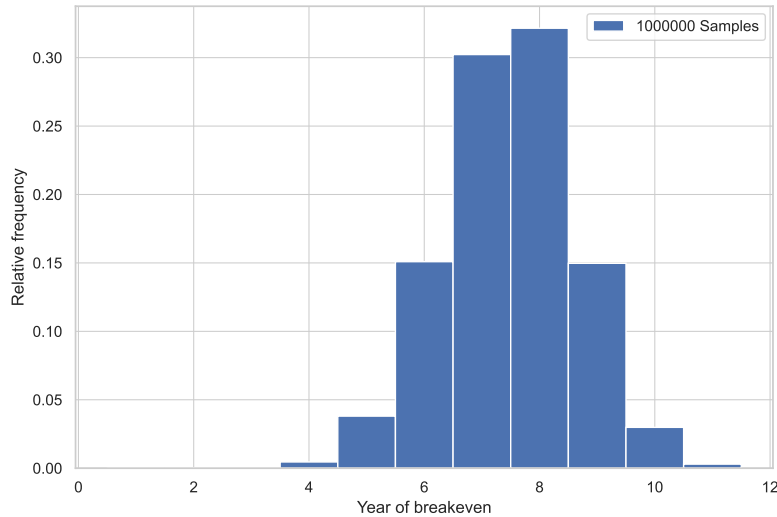
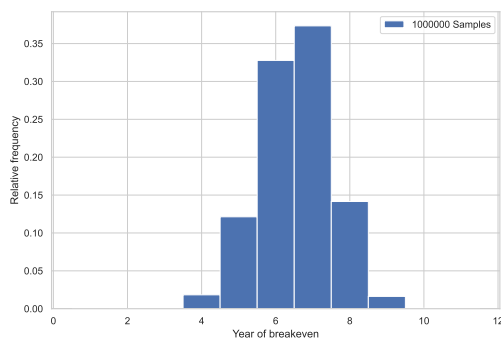
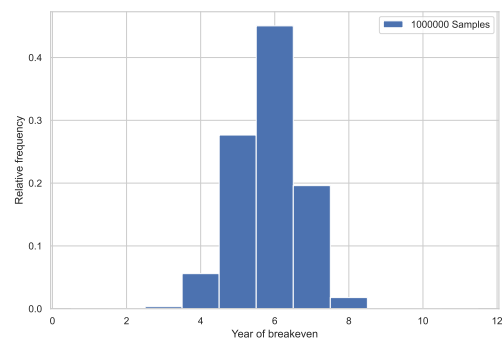


Figure 16.10: Break-even time probability distribution for the 5000\$/kg sell price



(a) Break-even time probability distribution for the 5500\$/kg sell price



(b) Break-even time probability distribution for the 6000\$/kg sell price

As for the return on investment value, it was deemed to not be a very informative metric, as long term investments returns typically are not evaluated using ROI<sup>9</sup>. This is because money loses its value over time due to inflation, and as such, the ROI becomes less and less descriptive of the economic model, at least in isolation. For COLD, the ROI is equal to 46%, 72% and 92% for the 5000\$/kg, 5500\$/kg, and 6000\$/kg pricing scenarios. These numbers are very high, way higher than the 20% ROI necessary to attract investors [14], yet due to the long lifespan of the mission, these values are not representative of real profits made. If profits are to be evaluated, the NPV should be used instead, as it accounts for yearly discounting. Nevertheless the ROI is an interesting parameter to complement the other economic metrics used in analysis of the business case of the COLD.

## 16.5. Financial Analysis Results

Thanks to the economic analysis of the project, it was determined to set at a propellant sale price of 5400 \$/kg. This price is still high enough for COLD to make a significant profit, as well as assure that the internal rate of revenue is attractive enough to attract investors. It simultaneously low enough to allow for profitable deliveries to most places in the cislunar space by potential partnered entities. The net present value created in this scenario was around 2.5 billion dollars, while the IRR remained above the discount rate in 90% of cases, something deemed satisfactory by the team. Also, with such pricing, the project would break even on average around the 7th year of operation. The detailed results of the price choice are listed below:

- **NPV** for a sell price of 5400\$/kg; 2508M\$ -649M\$/+881M\$ percent (2508M\$ -25.9%/+35.1%)
- **IRR** for a sell price of 5400\$/kg; 11.9 -2.1/+4.6 percent (11.9 -17.6%/+38.7%). The IRR was higher than the discount rate in 88.5% of cases.

<sup>9</sup><https://www.investopedia.com/articles/investing/111715/return-investment-roi-vs-internal-rate-return-irr.asp>

- In 90% of cases the project broke even after 8 or less years, as visible in Figure 16.12

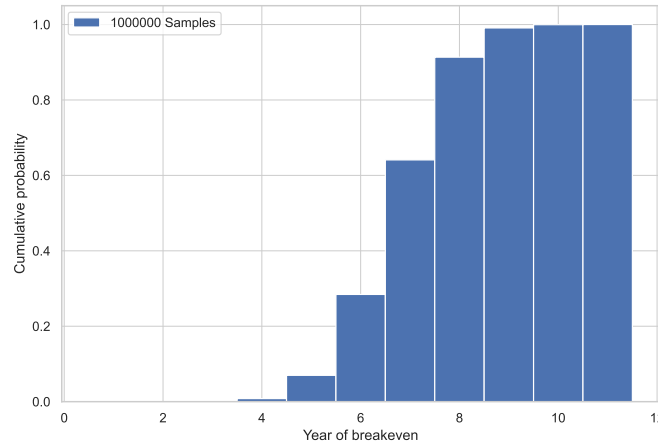
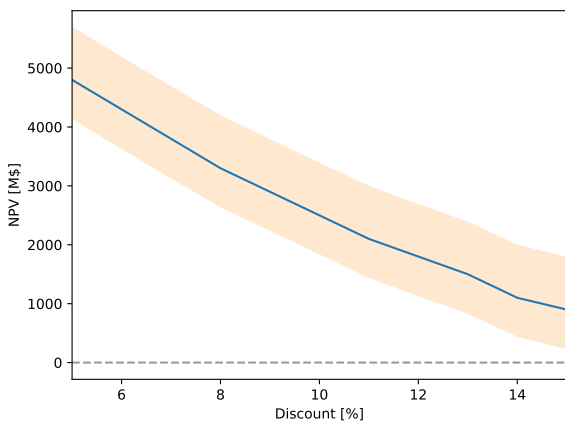


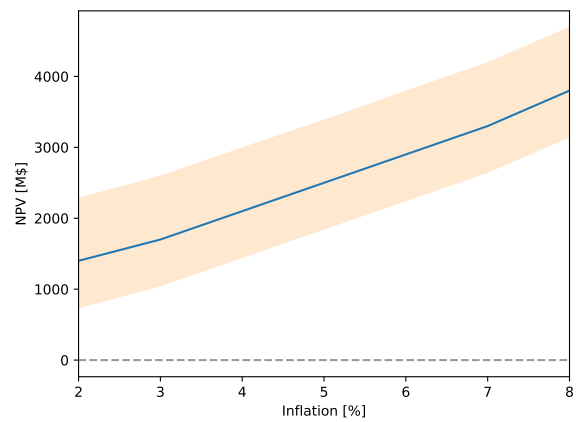
Figure 16.12: Break-even time cumulative probability distribution for a sell price of 5400\$/kg

### 16.6. Sensitivity Analysis

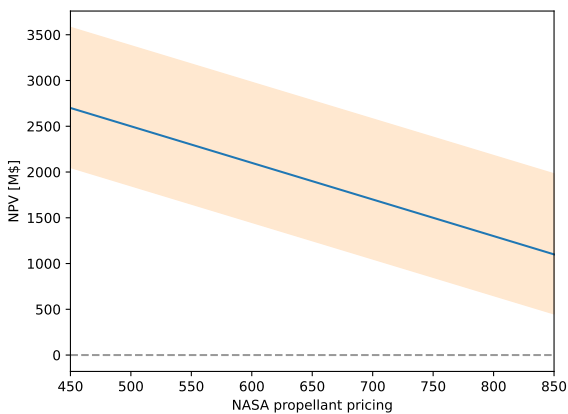
It is important to remember that some of the assumed economic parameters, such as the discount or inflation rate are just predictions of the future. As such, it is important to evaluate how the project would perform economically should these parameters vary. Its financial performance was thus evaluated for a range of values for the discount and inflation rate, as well as differing prices of the purchase the propellant on the Lunar surface from NASA. The results of these sensitivity analysis procedure can be seen in the figures below. The



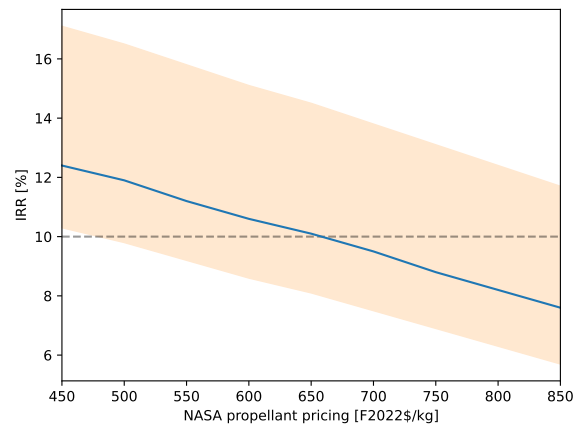
(a) NPV as a function of the discount rate, for the 5400\$/kg sell price



(b) NPV as a function of the inflation rate, for the 5400\$/kg sell price



(a) NPV as a function of buy price of propellant, for the 5400\$/kg sell price



(b) IRR as a function of buy price of propellant, for the 5400\$/kg sell price

Figure 16.13a show the effects of a changing discount rate. It can be seen that with an increasing discount rate, the net present value of the investment, as it is inversely proportional to the discount rate. It can be seen that the NPV is rather sensitive to the discount rate. Since the latter represents how risky<sup>10</sup> a given venture is, perhaps it could be higher than the assumed 10%, a standard value in the investment industry<sup>11</sup>. Nonetheless, the NPV remains on average positive until around a discount rate of 15%, value which is 50% higher than the rate assumed by experts in a very similar study [14].

Figure 16.13b shows the effect of changing inflation rate. The higher the inflation, the larger the NPV. The net present value remains positive with inflation rate above 1%, something almost guaranteed, as long as the economy is growing<sup>12</sup>.

For the changing purchase price the effects are as expected negative, as the propellant resell profit margins will be smaller. The effect on the NPV are rather small, as the price of the bought propellant would have to increase 2.5 fold in order for it to become negative. While small changes, in the hundreds of dollars per kg can be expected, a 2.5 increase in costs seems unlikely due to the non profit nature of NASA's endeavour. The effects on the IRR are more noticeable: the IRR remains above the assumed discount rate of 10% in only 70% of cases for a sale price of 650\$/kg of propellant sold. While this is still acceptable by some standards, the fact that a 28% increase in price results in a considerable loss of IRR certainty should not be disregarded. As such, the considerable negotiation effort should be made as to keep the purchase price of the propellant around 500 \$/kg or lower, possibly via long term contracts or special agreements. Alternatively, should the price of purchased propellant increase by for example 200\$, the price at which COLD will sell its propellant should increase accordingly by 200\$ divided by the P2P ratio.

---

<sup>10</sup>URL:<https://yourbusiness.azcentral.com/net-present-value-future-cash-flows-increase-decrease-discount-rate-increases-12255.html>

<sup>11</sup>URL:<https://www.globest.com/2019/08/08/the-cap-rate-and-discount-rate>

<sup>12</sup>URL:<https://www.investopedia.com/articles/06/gdpinflation.asp>

# 17 Design Evaluation

Now that all elements of the mission have been discussed it is important to discuss whether the initial requirements set has been met. Section 17.1 will cover all stakeholder requirements and state whether the designed UCM complies with them or not. In addition, the methods of verification and validation that can be used to verify these requirements will be listed. Following the requirement compliance, self-reflection will be performed. Recommendations for a future team picking up this project will be made and the design process will be evaluated in Section 17.2.

## 17.1. Requirement Compliance

In order to provide a comprehensive overview of the stakeholder requirements, a compliance matrix was created. It can be seen in Table 17.1. In the compliance matrix, every stakeholder requirement is mentioned along with the relevant requirement identification number and an indication whether the design is compliant with the requirement at this stage of the design. Furthermore, the verification methods for each stakeholder requirement are also displayed in this section. There are four primary verification methods considered: Test, Demonstration, Analysis and Inspection. In the compliance matrix, the verification method for a requirement is indicated by the first letter (T, D, A or I).

**Table 17.1:** Stakeholder requirement compliance matrix

Requirement ID	Requirement	Design Compliant	Verification Method
REQ-SH-01	The infrastructure shall be delivered at a cost of \$36k/kg	✓	A
REQ-SH-02	The overall project budget shall not exceed \$7B	✓	A
REQ-SH-03	Launch vehicle that transfers spacecraft shall use green propellants for launch or $LH_2$ & $LO_2$	✓	A
REQ-SH-04	All spacecraft infrastructure shall be transported from earth to moon through heavy launch vehicles	✓	I
REQ-SH-05	Launch vehicle that transfers propellant storage tanks shall use green propellants for launch or $LH_2$ & $LO_2$	✓	A
REQ-SH-06	The propellant transfer spacecraft shall be powered by solar panels or a hydrogen fuel cell	✓	I
REQ-SH-07	The propellant transfer system shall be powered by solar panels or a hydrogen fuel cell	✓	I
REQ-SH-08	Propellant transfer spacecraft shall be able to transfer 25 tonne of propellant per one trip to orbit	✓	A
REQ-SH-09	COLD shall be able to deliver 50 tonnes of $LH_2$ and $LO_2$ propellant to a single spacecraft in LLO	✓	A
REQ-SH-10	$LH_2$ shall be stored in a storage tank for 1 month with less than 10% boiloff	✓	A
REQ-SH-11	$LO_2$ shall be stored in a storage tank for 1 month with less than 10% boiloff	✓	A
REQ-SH-12	COLD shall be able to facilitate the transfer of 250 tonnes of propellant per year	✓	A
REQ-SH-13	COLD shall be able to store 50 tonnes of $LO_2$ and $LH_2$ at the Lunar surface	✓	I
REQ-SH-14	The propellant transfer spacecraft (Lunar surface to LLO and vice versa) shall have $\Delta V$	✓	I

<i>REQ-SH-15</i>	The propellant transfer spacecraft shall use a cryogenic propulsion system	✓	I
<i>REQ-SH-16</i>	The propellant transfer spacecraft shall be operable in space conditions	✓	A
<i>REQ-SH-17</i>	The propellant transfer spacecraft shall be able to be re-used for multiple refuelling missions	✓	A
<i>REQ-SH-18</i>	The propellant transfer spacecraft shall be remotely controllable from Earth	✓	A
<i>REQ-SH-19</i>	The propellant transfer mechanism shall be remotely controllable from Earth	✓	A

As seen from Table 17.1, all stakeholder requirements at this stage of the project have been met. However, the verification can only be done through inspection and analysis, since only theoretical models, and no prototype exist at this moment. Therefore, in future design the compliance matrix should be closely monitored and updated, to ensure that the design will always meet the requirements even with more sophisticated methods as testing or demonstration.

## 17.2. Recommendations

Over the course of the design process many decisions have been made and many decisions remain to be made before COLD touches down on the Lunar surface. With the designated 10 week design period coming to an end, the team behind COLD would like to provide recommendations on any further steps to be taken in the design process, in addition to any considerations that should be made given more time or leniency in requirements. In this section, additional concepts that may be treated in the future will be covered in Section 17.2.1 and further advice on analytical models that may be employed to improve the design will be presented in Section 17.2.2. Finally, numerical simulations to verify the performance of the design will be discussed in Section 17.2.3.

### 17.2.1. Alternate System Concepts

First of all, when considering mission concepts and more specifically methods of electrical power generation on the Lunar surface, one option was dismissed after conversation with the stakeholders. The option is discussed in Section 6.7.2 and involves directly purchasing power from Artemis, rather than using an onboard hydrogen fuel cell while on the Lunar surface. This option was dismissed on the basis that COLD should produce its own power. However, should this requirement be omitted, cost savings in the range of \$96-\$125 million are possible. This is of course only the monetary savings, there are sustainability arguments that can be made due to less consumption of hydrogen and oxygen. Therefore, it is strongly recommended to reconsider the necessity of the power requirement in the future.

Next, during the design of the landing gear, the electro-magnetic absorber based design was dismissed due to lack of information on scalability and long term testing as discussed in Section 12.1.3. However, should the concept be investigated further with the necessary time and resources, there are possible gains when it comes to landing gear reliability.

The prospect of repairs on the UCM performed by astronauts onboard NASA's Artemis was mentioned in Section 15.6. As discussed in the relevant section, the possibility of on site maintenance may extend the mission life and substantially reduce risk. However, as part replacement or other manned maintenance procedures have not been defined in detail, the costs and feasibility remains unknown and should be investigated.

Finally, the end of life procedures of the UCM should be investigated further. As mentioned in Section 14.2.3 the process of retiring a UCM shall follow the 3R philosophy, aiming to "Reduce, Reuse and Recycle". However, as there is high uncertainty in the available infrastructure on the Lunar surface, the extent to which recycling can be applied is unknown. Determining the necessary processes to recycle components of the UCM and cross referencing this with expected available infrastructure from projects such as Artemis shall provide the means to quantify the benefits of such a design philosophy.

### 17.2.2. Further Analytical Modelling

In further phases, a noise temperature model for TT&C should be drawn. This is to be done to obtain more reliable link budget results. Further, for the structures an analytical model and vibrations simulations should be carried out to analyse the fatigue properties of the design. In particular, the S/C truss structure should be addressed.



For attitude control, further investigation should be performed in the creation of a Proportional Integral Derivative (PID) control model. The control design task here is to determine the controller gains such that the performance and stability requirements can be met [84]. In such a way, the reaction of the spacecraft on disturbances can be modeled more accurately, leading to a closer  $\Delta V$  budget. Additionally, the full Euler rotational equations of motion for a rigid body can be used for the propellant transfer instead of the simplified version, taking into account the influence of the mass moments of inertia of the other two body axes onto the rotating body axis [84].

### 17.2.3. Numerical Simulations

Over the course of the design process up to this point in time, all sizing methods used were either empirical, analytical or iterative in nature. This means that no real numerical simulations were performed, primarily due to time constraints. With most analytical methods, simplifications have to be made in order to find a solution and these simplifications may lead to skewed and unrealistic results if applied improperly. Thus, using numerical simulations that are based on the full, governing physics equations is a good method to verify the design and in some cases even optimize it. The following numerical simulations are recommended to be given priority should the resources be available:

1. Finite element analysis for truss design
2. Finite element analysis for tank structural layer
3. Numerical flight trajectory modelling for propellant consumption rates
4. Numerical thermal modelling for UCM

First of all, finite element analysis of the truss structure of the UCM is recommended. This part of the S/C has not been sized in detail due to time constraints and a numerical method may be used to ensure the structure is able to withstand launch and landing loads. Next, finite element analysis of the cryogenic tank's structural layer should be considered. This is because the structural layer is very complex, consisting of two carbon fibre reinforced face sheets and an aerogel filled aluminium honeycomb as described in Section 5.2. A complex structure as such, may not behave exactly as expected under load thus additional verification by numerical means is desired.

Thirdly, the current  $\Delta V$  budget is based off simplifications explained in Section 7.3 and does not include detailed treatment of the UCM's trajectory during ascent or descent. Developing a numerical model for detailed trajectory calculations and optimization would allow to more precisely find necessary  $\Delta V$  (and by extent propellant) requirements. Lastly, as the thermal state of the UCM is critical for both the functionality of all subsystems and the propellant payload itself, the TMS design should be thoroughly verified. By means of numerical analysis and modelling, more detailed results on heat input, transfer and leakage can be found and used in order to confirm if the analytical sizing methods will result in desired performance.

# 18 Conclusion

The aim of this report was to present the preliminary detailed design of an in-space cryogenic  $LH_2$  and  $LO_2$  propellant transfer and refuelling station infrastructure that was designed over the course of ten weeks by a team of ten engineering students of TU Delft's Aerospace Faculty. This chapter serves purpose as the conclusion of the report. The main findings lead to concise preliminary detailed design of the universal Lunar refuelling depot that can provide new ways of transportation to the space community, while improving sustainability.

Firstly, a market analysis was performed in Chapter 3 in order to assess the economic sustainability of the mission. The potential market was found to be between 0.5 and 4 trillion US\$. Therefore, the COLD mission was considered to be large enough to prove to be a successful business venture, based on carried out market size estimations and market growth predictions. In order to measure the sustainability and profitability of the operation, the propellant sold to propellant bought ratio was defined in Chapter 4. This ratio should be optimised as much as possible as providing a sustainable design is of vital importance for mission success. The driving optimisation variables were found to be the storage of liquid hydrogen and oxygen at temperatures of 30 K and 80 K at pressures of 1 MPa and 0.1 MPa respectively. Additionally, the full cycle for a single universal cryogenic module was found to be 41 days: 40 days idling time on the Lunar surface and an active refueling mission of an additional 24 hours.

With this in mind and the main design focus laying on the payload tank design, Chapter 5 concluded that the  $LH_2$  tank mass comes in at 1503.28 kg and the  $LO_2$  tank at 361.82 kg, at inner radii of 2.71 m and 1.68 m, respectively. This was found through an iterative process that sought to minimize mass and maximise stiffness for different boil-off conditions. Additionally, single stage cryocoolers were selected for the  $LO_2$  tanks and multi stage cryocoolers for the  $LH_2$  tanks; a decision dictated by the respective temperature differences to be achieved (of which the required for  $LH_2$  cooling was larger). In addition, a propellant transfer method was selected. This is to be achieved by rotating the spacecraft at 0.4 RPM to settle the propellant, which is then pumped to the receiving spacecraft, connected through a docking port with an integrated bearing. This concept allows to transfer the entire payload of 25 tonnes in four hours to the customer.

Then, in Chapter 6, a solar panel and fuel cell combination for power generation was selected. The hydrogen fuel cell is to operate in eclipse and when at idle in the crater, while the solar panel is to be used in sun exposed orbit. The maximum power consumption for the fuel cell was found to be 9353 W and 3524 W in these conditions. Further, in Chapter 7, the propulsive system was defined to have two Vinci engines for ascent and one RL-10 CECE engine for descent, where all engines will be ignited by a  $GO_2/GH_2$  spark plug torch. Additionally, the ignition sequence along with plumbing diagram were defined and a total  $\Delta V$  for operations was found to be 4092 m/s.

Next, in Chapter 8, sensors were selected for the attitude determination and control system. This selection included: two sun sensors, two star sensors, an inertial measurement unit and an altimeter along with a LIDAR sensor for docking. For the reaction control system, a hydrogen peroxide thruster system was selected with 8 clusters of 3 thrusters coming in at 24 thrusters total, providing 220 N each. In such a way, rendezvous and docking with the customer can be performed in 6 min, after which the propellant transfer can start by slewing the UCM to the desired rate of 0.4 RPM in just under 6 s. In addition, a self-pressurised piston tank was selected for  $H_2O_2$  storage, with a teflon lining to prevent propellant degradation. The total  $H_2O_2$  monopropellant mass comes in at 1032 kg for all attitude maneuvers.

Furthermore, for the TT&C, it was determined that the communications will be done mostly through external relay satellites. In terms of onboard equipment, the spacecraft itself will be outfitted with three medium gain phased array antennas, as well as a single high gain parabolic antenna. Moreover, the control and data handling was discussed in Chapter 10, where a detailed software diagram describing the functionality of each software element was drawn up.

Afterwards, in Chapter 11, the thermal management system was designed. It features the modelling of the thermal balance, which allowed for the design and sizing of the radiators and heaters. It was decided for heat transfer through the UCM, to make use of variable conductance heat pipes that are connected to all the components in need of thermal management. Furthermore, coating of the spacecraft was researched and it was found that barium sulphate with polyvinyl alcohol would be the best option.

An important aspect of the UCM is the structure that incorporates all of the designed subsystems, which is described in Chapter 12. One of the main considerations was the landing gear. A reusable systems consisting

of four legs was designed that satisfies basic stability conditions, using pressurized metal bellows as shock absorbers. In addition, a design for the UCM was found having a height of over 22 meter and a width of 16 meter when the landing gear is extended. The structural mass of one UCM is roughly 7 tonnes and a wet mass of 56 tonnes was found when fully loaded with both cryogenic propellant for the customer and propulsion.

All sizing of the subsystems leads to one discussed parameter indicating the design sustainability: the propellant sold to propellant bought ratio, which is discussed in Chapter 13. After serious effort, this ratio was able to be pushed up to 0.485, meaning that nearly half of the bought propellant is sold back to customers.

As the UCM undergoes several phases throughout its lifetime, it is important to consider all of them: from manufacturing to operations to end-of-life. This was researched in Chapter 14. Therefore, manufacturing of the subsystems and integration into the main bus was researched. Additionally, the operations were planned and end-of-life solutions and procedures were determined to ensure that the UCM's sustainability is not compromised post-operations. Finally, potential risks during all of the mission phases were analyzed and mitigation strategies created to lower the unacceptable risks. Furthermore, due to the long mission lifetime of ten years, maintenance will be unavoidable to ensure proper operation of the UCM. The main philosophy that was pursued was to prevent potential failures instead of repairing them as was determined in Chapter 15.

Moreover, the business case was examined in Chapter 16. Through Monte Carlo analysis it was found that in 93% of cases the project does not overrun the given 7 billion USD budget. With a sale price 5000 US\$ per kilogram, the project was found to break even in 98% of simulated cases in lifetime of 10 years. The internal rate of return was found to be higher than the discount rate in 63% of cases.

With sustainability as a key concept during the design phase, maximizing recyclability was applied wherever possible. The reaction control system makes use of hydrogen peroxide, which can be created from water, the residue of the fuel cell that is used to generate power. Additional left over water can be sold back to NASA after the mission is complete, which can then be transformed back into the hydrogen and oxygen needed for propulsion or the customer. In such a way, the waste stream on board is minimized and all resources are used up to their best extent.

All in all, the design was found to be sustainable, profitable and a lucrative investment, soon to change the ways of conventional space travel and exploration.

# Task Division

<b>Executive Overview</b>	<b>Author (text writing)</b>	<b>Contributing Engineers</b>
<i>Executive Overview</i>	Neil, Mattias, Luc, Matas	-
<b>Introduction</b>	<b>Author (text writing)</b>	<b>Contributing Engineers</b>
<i>Introduction</i>	Neil, Matas	-
<b>Market Analysis</b>	<b>Author (text writing)</b>	<b>Contributing Engineers</b>
<i>Motivation</i>	Jarek	Jarek
<i>Market Identification</i>	Jarek	Jarek
<i>Cislunar Markets</i>	Jarek	Jarek
<i>Interplanetary Markets</i>	Jarek	Jarek
<i>Customer Summary</i>	Jarek	Jarek
<b>System Description &amp; Optimisation Method</b>	<b>Author (text writing)</b>	<b>Contributing Engineers</b>
<i>Concept</i>	Teun	Teun, Augustas, Adrian
<i>Sizing Process</i>	Teun, Mattias	Teun, Augustas, Adrian
<i>Sustainable Optimisation Method</i>	Teun	Teun, Augustas, Adrian
<b>Cryogenic Storage System</b>	<b>Author (text writing)</b>	<b>Contributing Engineers</b>
<i>Trade-off Summary &amp; Requirements</i>	Teun	Teun
<i>Composite Structural Layer</i>	Adrian, Augustas	Teun, Augustas, Adrian, Marcel, Jonah
<i>Insulation Layer</i>	Adrian	Teun, Augustas, Adrian
<i>Heat Flow Calculation Method</i>	Adrian	Teun, Augustas, Adrian
<i>Cryocoolers</i>	Luc, Adrian	Augustas, Luc, Adrian
<i>Propellant Transfer Mechanism</i>	Jonah	Jonah, Augustas
<i>Complete Sizing Method</i>	Teun, Adrian	Teun, Adrian, Augustas
<b>Electrical Power System</b>	<b>Author (text writing)</b>	<b>Contributing Engineers</b>
<i>Requirements &amp; Trade-off Summary</i>	Jonah, Teun	Jonah, Mattias
<i>Power Consumption Profiles</i>	Jonah	Jonah, Mattias
<i>Solar Panel Selection, Configuration, &amp; Sizing</i>	Mattias, Jonah	Jonah, Mattias
<i>Fuel Cell Sizing</i>	Jonah	Jonah, Mattias
<i>EPS System Profiles</i>	Jonah	Jonah, Mattias
<i>System Overview</i>	Jonah	Jonah, Mattias
<i>EPS Budget Analysis</i>	Jonah	Jonah, Mattias
<b>Propulsion System</b>	<b>Author (text writing)</b>	<b>Contributing Engineers</b>
<i>Requirements &amp; Trade-off Summary</i>	Matas, Neil	Matas, Neil
<i>Engine Selection &amp; Tank Design</i>	Neil, Augustas	Matas, Neil, Augustas
<i><math>\Delta V</math> Budget &amp; Thrust Level</i>	Neil	Neil
<i>Operations Profile</i>	Neil	Neil
<i>Engine Ignition</i>	Matas	Matas
<i>Plumbing</i>	Matas	Matas
<b>Attitude Determination &amp; Control System</b>	<b>Author (text writing)</b>	<b>Contributing Engineers</b>
<i>Requirements &amp; Trade-off Summary</i>	Luc	Luc
<i>Attitude Determination</i>	Luc	Luc
<i>Reaction Control System</i>	Matas, Luc, Mattias	Matas, Luc, Mattias
<b>Telemetry, Tracking, &amp; Command</b>	<b>Author (text writing)</b>	<b>Contributing Engineers</b>
<i>Requirements</i>	Jarek, Teun	Jarek
<i>Concept</i>	Jarek, Teun	Jarek
<i>Antenna selection</i>	Jarek, Teun	Jarek

Figure 18.1: Task distribution

<b>Command &amp; Data Handling</b>	<b>Author (text writing)</b>	<b>Contributing Engineers</b>
<i>Functionality &amp; Software</i>	Augustas, Adrian	Augustas, Adrian
<i>Configuration &amp; Data Handling</i>	Augustas, Adrian	Augustas, Adrian
<i>Power consumption estimation</i>	Augustas	Augustas, Jonah
<b>Thermal Management System</b>	<b>Author (text writing)</b>	<b>Contributing Engineers</b>
<i>Requirements</i>	Mattias	Mattias
<i>Mission Profiles</i>	Mattias	Mattias
<i>Thermal Control System</i>	Mattias, Matas	Luc, Matas, Mattias
<b>Structural Design &amp; Layout</b>	<b>Author (text writing)</b>	<b>Contributing Engineers</b>
<i>Landing Gear Design</i>	Marcel	Marcel, Adrian, Jarek
<i>Landing Gear in UCM sizing</i>	Marcel	Marcel
<i>Architecture</i>	Marcel	Marcel
<b>Sustainable Optimisation Results</b>	<b>Author (text writing)</b>	<b>Contributing Engineers</b>
<i>Result</i>	Teun, Augustas, Adrian, Luc	Teun, Augustas, Adrian
<i>Sensitivity Analysis</i>	Luc	Adrian, Teun, Luc
<b>Universal Cryogenic Module Lifespan</b>	<b>Author (text writing)</b>	<b>Contributing Engineers</b>
<i>Manufacturing, Integration &amp; Testing</i>	Luc, Adrian	Luc, Adrian, Jonah
<i>Operations &amp; End-of-life</i>	Augustas, Adrian	Augustas, Adrian
<i>Risk Management</i>	Luc	Luc
<b>Maintenance &amp; Supportability</b>	<b>Author (text writing)</b>	<b>Contributing Engineers</b>
<i>Maintenance Philosophy</i>	Neil	Neil
<i>Digital Twin Technology</i>	Neil	Neil
<i>Health Monitoring</i>	Neil	Neil
<i>Replacement</i>	Neil	Neil
<i>Threat of Lunar Dust</i>	Neil	Neil, Matas, Marcel
<i>Possible Manned Intervention</i>	Neil	Neil
<b>Business Case</b>	<b>Author (text writing)</b>	<b>Contributing Engineers</b>
<i>Analysis Approach</i>	Jarek	Jarek
<i>Cost Breakdown</i>	Jarek	Jarek, Jonah, Marcel
<i>Propellant Pricing</i>	Jarek	Jarek
<i>Economic Analysis</i>	Jarek	Jarek, Matas, Teun
<i>Financial outlook</i>	Jarek	Jarek
<i>Sensitivity Analysis</i>	Jarek	Jarek
<b>Design Evaluation</b>	<b>Author (text writing)</b>	<b>Contributing Engineers</b>
<i>Requirement Compliance</i>	Augustas, Matas	-
<i>Recommendations</i>	Augustas, Matas	-
<b>Conclusion</b>	<b>Author (text writing)</b>	<b>Contributing Engineers</b>
<i>Conclusion</i>	Matas, Luc	-

Figure 18.2: Task distribution continued





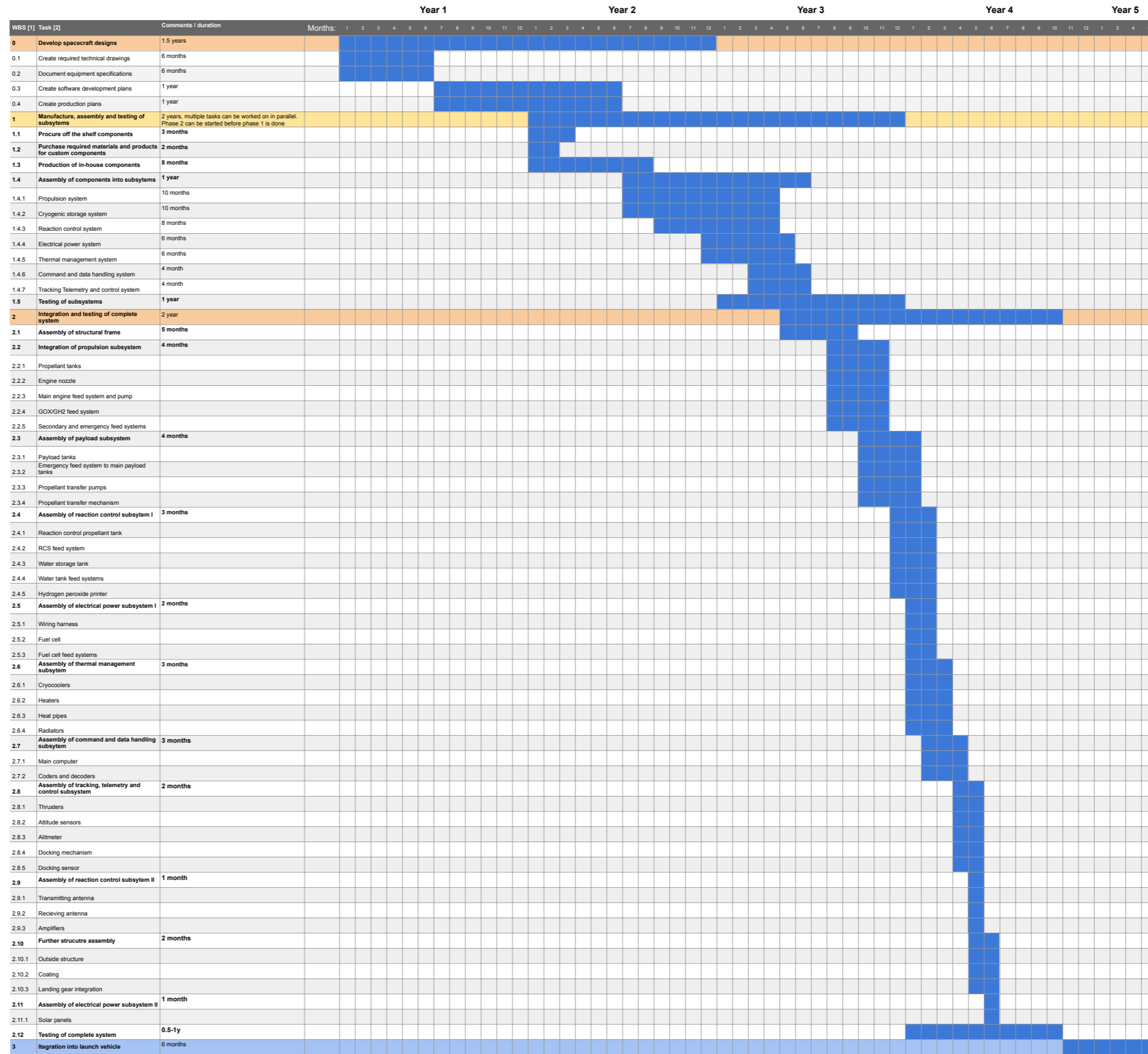


Figure 18.5: Gantt chart showing required tasks to be completed if the COLD mission is to move forward



# References

- [1] M.M. Abbas et al. "Lunar dust charging by photoelectric emissions". In: *Planetary and Space Science* 55 (7-8 May 2007), pp. 953–965. ISSN: 00320633. DOI: 10.1016/j.pss.2006.12.007.
- [2] Juan Agui, John Griffin, and Paul Hambourger. *Durable Coating Technology for Lunar Dust Protection and Mitigation*. 2006.
- [3] David Akin. "Launch and Entry Vehicle Design Mass Estimating Relations (MERs)". 2016.
- [4] F. Barbir, T. Molter, and L. Dalton. "Efficiency and weight trade-off analysis of regenerative fuel cells as energy storage for aerospace applications". In: *International Journal of Hydrogen Energy* 30 (4 Mar. 2005), pp. 351–357. ISSN: 0360-3199. DOI: 10.1016/J.IJHYDENE.2004.08.004.
- [5] A. Barysas et al. "Midterm Report - C.O.L.D: Cryogenic Orbital Lunar Depot". 2022.
- [6] Joseph Baumeister. *RL10 Engine Ability to Transition From Atlas to Shuttle/Centaur Program*. NASA Glenn Research Center, 2015.
- [7] Mark G. Benton et al. "Boeing design trades in support of the NASA Altair lunar lander concept definition". In: *Space 2008 Conference* (2008).
- [8] Brad Blair et al. "Space Resource Economic Analysis Toolkit: The Case for Commercial Lunar Ice Mining". In: (Apr. 2022).
- [9] Stephanie L Booth and Michael A Marsden. "Radio Frequency and Optical Communication Link Trade Studies Between Earth, Deep Space Gateway, and Lunar Surface". In: (2019).
- [10] Hermanus JM ter Brake and GFM Wiegerinck. "Low-power cryocooler survey". In: *Cryogenics* 42.11 (2002), pp. 705–718.
- [11] Richard Brealey and Stewart Myers. *Principles of corporate finance*. 12th ed. Columbus, OH: McGraw-Hill Education, Jan. 2016.
- [12] Pablo Calla, Dan Fries, and Chris Welch. "Asteroid mining with small spacecraft and its economic feasibility". In: (Aug. 2018).
- [13] D. Cardwell et al. "Very High Specific Power ELO Solar Cells (>3 kW/kg) for UAV, Space, and Portable Power Applications". In: *2017 IEEE 44th Photovoltaic Specialist Conference (PVSC)*. 2017, pp. 3511–3513. DOI: 10.1109/PVSC.2017.8366552.
- [14] "Commercial lunar propellant architecture: A collaborative study of lunar propellant production". In: *REACH* 13 (Mar. 2019), p. 100026. ISSN: 2352-3093. DOI: 10.1016/J.REACH.2019.100026.
- [15] *Cryogenics Industry | Specialist Bearings Tools | Carter Manufacturing*. URL: <https://www.carterbearings.co.uk/industries/cryogenics>.
- [16] Roger Dendy, Daniel J Zeleznikar, and Michael J Zemba. "NASA LUNAR EXPLORATION-GATEWAY'S POWER AND PROPULSION ELEMENT COMMUNICATIONS LINKS". In: (2021).
- [17] Leslie J. Deutsch, Frank J. Stocklin, and John J. Rush. "Modulation and Coding for NASA's New Space Communications Architecture". In: (2008).
- [18] Joyce Dever, Sharon Rutledge, and Paul Hambourger. *Indium Tin Oxide-Magnesium Fluoride Co-Deposited Films for Spacecraft Applications*. 1998.
- [19] Prof. C.A. (Clemens) Dransfeld. *Consultation with Expert*. 2022.
- [20] *Dry Lubricant Smooths the Way for Space Travel, Industry | NASA Spinoff*. URL: [https://spinoff.nasa.gov/Spinoff2015/ip\\_7.html](https://spinoff.nasa.gov/Spinoff2015/ip_7.html).
- [21] Bill Farrell. "Busting the Dust". In: *Goddard* (2019).
- [22] Bernard Fox, Kevin Brancato, and Brien Alkire. *Guidelines and Metrics for Assessing Space System Cost Estimates*. Santa Monica, CA: RAND Corporation, 2008.
- [23] Sylvain Fuertes et al. *Improving Spacecraft Health Monitoring with Automatic Anomaly Detection Techniques*. SpaceOps, 2016.
- [24] F. Gampe, K. Priesett, and R. H. Bentall. *A Modular Docking Mechanism For In-Orbit Assembly and Spacecraft Servicing*. Aug. 1985.
- [25] Thomas S. Gates et al. "Facesheet delamination of composite sandwich materials at cryogenic temperatures". In: *Composites Science and Technology* 66 (14 Nov. 2006), pp. 2423–2435. ISSN: 0266-3538. DOI: 10.1016/J.COMPOSITECH.2006.01.028.
- [26] Prof. Dr. Eberhard Gill. "Systems Engineering and Aerospace Design (AE3211-I) - Verification and Validation for the Attitude and Orbit Control System". In: (Feb. 2022).
- [27] Victor Giuliano. *CECE: A Deep Throttling Demonstrator Cryogenic Engine for NASA's Lunar Lander*.
- [28] William Gullotta et al. "Resettable Landing Gear For Mars Hopper". In: 2014. DOI: 10.13140/2.1.1840.3524.
- [29] DAVID T. VANIMANBEVAN M. FRENCH GRANT H. HEIKEN. *Lunar Sourcebook*. Cambridge University Press, 1991. ISBN: 0-521-33444-6.
- [30] Robert W. Herr and H. Wayne Leonard. *Dynamic Model Investigation Of Touchdown Stability of Lunar-landing Vehicles*. Langley Research Center.
- [31] Dieter K Huzel and David H Huang. *DESIGN OF LIQUID PROPELLANT ROCKET ENGINES*. NASA, 1967.
- [32] David L. Iverson. "System Health Monitoring for Space Mission Operations". In: *IEEE*, Mar. 2008, pp. 1–8. ISBN: 978-1-4244-1487-1. DOI: 10.1109/AERO.2008.4526646.
- [33] Harry W. Jones. "The Recent Large Reduction in Space Launch Cost". In: *48th International Conference on Environmental System* (2018).

- [34] Christos Kassapoglou. *Design and Analysis of Composite Structures : With Applications to Aerospace Structures*. en. ProQuest Ebook Central. 2013.
- [35] Lonny Kauder. *Spacecraft thermal control coatings references*. Tech. rep. 2005.
- [36] Col John E Keesee. "Spacecraft Thermal Control Systems". In: *Lecture taught by Col. John E. Keesee, undated; Course 16-851, Satellite Engineering, School of Engineering, Massachusetts Institute of Technology* (2003).
- [37] C. W. Keller. *Thermal performance of a customized multilayer insulation (MLI)*. 1974.
- [38] Thomas W Kerslake. "Lunar Surface-to-Surface Power Transfer". In: (2007). URL: <http://www.sti.nasa.gov>.
- [39] Peter Kittel. "Cryocooler performance estimator". In: International Cryocooler Conference. 2007.
- [40] Dietrich Koelle. *Handbook of cost engineering for space transportation systems : with TRANSCOST 7.2 ; statistical-analytical model for cost estimation and economical optimization of launch vehicles*. Rev. 2. TCS TransCostSystems, 2007.
- [41] Bernard F Kutter et al. *Settled Cryogenic Propellant Transfer*. 2006.
- [42] Yuanyuan Liu et al. "Landing stability analysis for lunar landers using computer simulation experiments". In: *International Journal of Advanced Robotic Systems* (2017). DOI: 10.1177/1729881417748441.
- [43] "Lunar Reconnaissance Orbiter Mission and Spacecraft Design". In: *Space Sci Rev* 150 (2010), pp. 23–62. DOI: 10.1007/s11214-009-9624-4.
- [44] Douglas A Mccarville and Justin R Jackson. "Chapter 09958 - Design, Manufacture and Test of Cryotank Components". In: (2017). DOI: 10.1016/B978-0-12-803581-8.09958-6.
- [45] Subodh K. Mital. "Review of Current State of the Art and Key Design Issues With Potential Solutions for Liquid Hydrogen Cryogenic Storage Tank Structures for Aircraft Applications". In: (2006).
- [46] NASA. *Heat Pipe Design Handbook: Volume I: June 1, 1979*. VOL. 1. National Aeronautics and Space Administration, 1979.
- [47] NASA. "Lunar Lander Conceptual Design". In: (1988).
- [48] NASA. *NASA Cost Estimating Handbook, Version 4.0*. Feb. 2015.
- [49] "NASA Office of Inspector General Office of Audits". In: (2022). URL: <https://oig.nasa.gov/hotline.html>.
- [50] *NASA's Lunar Exploration Program Overview*. National Aeronautics and Space Administration, 2020.
- [51] Richard Oeftering, Peter Struk, and Jennifer Green. *Lunar Surface Systems Supportability Technology Development Roadmap*. NASA, 2012.
- [52] DA Paige et al. "The Lunar Reconnaissance Orbiter Diviner Lunar Radiometer Experiment". In: *Space Sci Rev* 150 (Jan. 2009), pp. 125–160. DOI: 10.1007/s11214-009-9529-2.
- [53] G.P. Peterson. *An Introduction to Heat Pipes: Modeling, Testing, and Applications*. 1st ed. Wiley-Interscience, 1994.
- [54] D. A. Petti et al. "Triso-coated particle fuel performance". In: *Comprehensive Nuclear Materials* 3 (2012), pp. 151–213. DOI: 10.1016/B978-0-08-056033-5.00055-0.
- [55] Malin Presthus. "Derivation of Air Spring Model Parameters for Train Simulation MALIN PRESTHUS". Lulea University of Technology, 2002.
- [56] D.A. Reay, P.A. Kew, and R.J. McGlen. "Chapter 3 - Heat pipe components and materials". In: *Heat Pipes (Sixth Edition)*. Ed. by D.A. Reay, P.A. Kew, and R.J. McGlen. Sixth Edition. Oxford: Butterworth-Heinemann, 2014, pp. 65–94. ISBN: 978-0-08-098266-3. DOI: <https://doi.org/10.1016/B978-0-08-098266-3.00003-0>.
- [57] D.A. Reay, P.A. Kew, and R.J. McGlen. "Chapter 3 - Heat pipe components and materials". In: *Heat Pipes (Sixth Edition)*. Ed. by D.A. Reay, P.A. Kew, and R.J. McGlen. Sixth Edition. Oxford: Butterworth-Heinemann, 2014, pp. 65–94. ISBN: 978-0-08-098266-3. DOI: <https://doi.org/10.1016/B978-0-08-098266-3.00003-0>.
- [58] George A Repas. "NASA Technical Memorandum 106493". In: (1994).
- [59] William F. Rogers. *Apollo Experience Report - Lunar Module Landing Gear Subsystem*. 1972.
- [60] William F. Rogers. *Apollo Lunar Module Landing Gear*.
- [61] K Schäfer and C Böhm. *Development of Altitude Simulation for Vinci Engines*. DLR, 2007.
- [62] Scott H Schaire and David L Carter. "Near Earth Network (NEN) Users' Guide Date NEN Wallops Manager, Near Earth Network Project, Code 453 NASA Wallops Flight Facility Date Project Manager Near Earth Network Project, Code 453 NASA Goddard Space Flight Center". In: (2019).
- [63] Eckart Schmidt, Gerald Brewster, and George Cain. "Mars Lander Retro Propulsion". In: (Oct. 1999).
- [64] Robert Shisko. "A comparison of previously published papers on the economics of lunar In Situ Resource Utilization (ISRU)". In: (Nov. 2019).
- [65] *SICERA@ Ultra KV-08 Cryopump - SHI Cryogenics Group*. URL: <https://www.shicryogenics.com/product/sicera-ultra-kv-08-cryopump/>.
- [66] Bruno Siciliano and Oussama Khatib. *Springer Handbook of Robotics*. 2nd. Springer International Publishing Ag, May 2008, p. 484. ISBN: 9783319325507.
- [67] "SKF hybrid bearings for extreme application conditions". In: (). URL: [https://www.skf.com/binaries/pub12/Images/0901d19680805572-16651\\_1-EN---SKF-hybrid-bearings-for-extreme-applications\\_tcm\\_12-455708.pdf](https://www.skf.com/binaries/pub12/Images/0901d19680805572-16651_1-EN---SKF-hybrid-bearings-for-extreme-applications_tcm_12-455708.pdf).
- [68] Ruslan S. Skomorohov, Andreas M. Hein, and Chris Welch. "In-orbit Spacecraft Manufacturing: Near-term Business Cases". In: *67th International Astronautical Congress (IAC)* (2016).
- [69] George F. Sowers. "The Business Case for Lunar Ice Mining". In: *New Space* 9.2 (2021), pp. 77–94. DOI: 10.1089/space.2020.0045.
- [70] S. Speretta et al. "Designing the Radio Link for a Lunar CubeSat: the LUMIO Case". English. In: 72nd International Astronautical Conference, 2021.
- [71] Stubbs T., Vondrak R., and Farrell W. *Impact of dust on lunar exploration*. 2007.

- [72] Mak Tafazoli. "A study of on-orbit spacecraft failures". In: *Acta Astronautica* 64 (2-3 Jan. 2009), pp. 195–205. ISSN: 00945765. DOI: 10.1016/J.ACTAASTRD.2008.07.019.
- [73] "Thermal performance of multilayer insulation: A review". In: *IOP Conference Series: Materials Science and Engineering* 396 (1 Aug. 2018), p. 012061. ISSN: 1757-899X. DOI: 10.1088/1757-899X/396/1/012061.
- [74] Thomas M Tomsik and Michael L Meyer. *Liquid Oxygen Propellant Densification Production and Performance Test Results With a Large-Scale Flight-Weight Propellant Tank for the X33 RLV*. 2010.
- [75] J. Trautwein. "Pressurized Metal Bellows Shock Absorber for Space Applications." University of Central Florida, 2015.
- [76] Mattias Villani and Rolf Larsson. *The Multivariate Split Normal Distribution and Asymmetric Principal Components Analysis*. Working Paper Series 175. Sveriges Riksbank (Central Bank of Sweden), Dec. 2004.
- [77] *Vinci Engine - Space Propulsion*. ArianeGroup, 2020.
- [78] W. C. Walton, R. W. Here, and H. W. Leonard. "Studies of Touchdown Stability for Lunar Landing Vehicles". In: *J. Spacecraft* 1 (5 May 2012), pp. 552–556. ISSN: 00224650. DOI: 10.2514/3.27696.
- [79] Zongyan Wang. *Digital Twin Technology*. 2020. DOI: 10.5772/intechopen.80974.
- [80] Rusty Goh Weixiong. "Preliminary Design Of Reusable Lunar Lander Landing System". Lulea University of Technology, 2017.
- [81] J.R. Wertz, D.F. Everett, and J.J. Puschell. *Space Mission Engineering: The New SMAD*. Space technology library. Microcosm Press, 2011. ISBN: 9781881883159.
- [82] John C Whitehead, Michael D Dittman, and Arno G Ledebuhr. "SSC99-XII-5 Progress Toward Hydrogen Peroxide Micropropulsion". In: (1999).
- [83] Bong Wie. "Space vehicle dynamics and control". In: (2008), p. 950.
- [84] Bong Wie, Vaios Lappas, and Jesús Gil-Fernández. "Attitude and orbit control systems". In: *The International Handbook of Space Technology* (Jan. 2014), pp. 323–369. DOI: 10.1007/978-3-642-41101-4\_12.
- [85] Jacob Job Wijker. *Spacecraft Structures*. Springer-Verlag Berlin Heidelberg, 2008. ISBN: 9783540755524. DOI: 10.1007/978-3-540-75553-1.
- [86] Yi Yang et al. "Failure analysis of deployment mechanism of a satellite solar array". In: *The Proceedings of 2011 9th International Conference on Reliability, Maintainability and Safety*. 2011, pp. 931–937. DOI: 10.1109/ICRMS.2011.5979419.
- [87] Deng-Yun Yu, Ze-Zhou Sun, and He Zhang. *Technology of Lunar Soft Lander*. Vol. 38. Space Technology Library, National Defense Industry Press, 2014. ISBN: 978-981-15-6579-3. DOI: 10.1007/978-981-15-6580-9.
- [88] B.T.C. Zandbergen. "AE1222-II: Aerospace Design & Systems Engineering Elements I, Part: Spacecraft (bus) design and sizing". In: (2020).
- [89] B.T.C. Zandbergen. *Delta-V required for launch from planet surface*. TU Delft, 2018.